NUREG/CR-4174

Rock Mass Sealing -- Experimental Assessment of Borehole Plug Performance

Annual Report
June 1983 - May 1984

Prepared by J. J. K. Daemen, W. B. Greer, G. S. Adisoma, K. Fuenkajorn,
W. D. Sawyer, Jr., A. Yazdandoost, H. Akgun, B. Kousari

Department of Mining and Geological Engineering
University of Arizona

Prepared for
U.S. Nuclear Regulatory
Commission

NUREG/CR-4174
RW

Rock Mass Sealing -- Experimental Assessment of Borehole Plug Performance

Annual Report
June 1983 - May 1984

Manuscript Completed: December 1984
Date Published: March 1985

Prepared by
J. J. K. Daemen, W. B. Greer, G. S. Adisoma, K. Fuenkajorn,
W. D. Sawyer, Jr., A. Yazdandoost, H. Akgun, B. Kousari

Department of Mining and Geological Engineering
University of Arizona
Tucson, AZ 85721

Prepared for
Division of Radiation Programs and Earth Sciences
Office of Nuclear Regulatory Research
U.S. Nuclear Regulatory Commission
Washington, D.C. 20555
NRC FIN B6627
Under Contract No. NRC-04-78-271

ABSTRACT

This report describes experimental field and laboratory borehole plugging performance assessment studies that have been performed, completed, started, or planned during the period June 1, 1983 - May 31, 1984.

Results are given from field flow tests on three cement plugs installed in vertical boreholes in basalt and on one nearly horizontal cement plug. The horizontal plug seals the borehole very well, as does one of the vertical plugs. The initial hydraulic conductivity of the other two vertical field plugs has been relatively high, and remedial action is described.

Laboratory simulations have been performed to study the influence of dynamic loading on cement plug performance, and no detrimental effects have been detected. Conversely, drying of cement plugs, especially over extended periods of time and at elevated temperatures does increase the hydraulic conductivity of the plugs severely, as well as reducing their bond strength along the plug-rock interface.

Microscopic inspection, strength and flow tests on boreholes in basalt have been used to identify the characteristics of a drilling-induced damaged zone in basalt. While such a damaged zone exists, and has typical features (e.g. fracture density, size, location, orientation) determined by the drilling method and the rock characteristics, it is thin and not likely to be a preferential flowpath.

A comprehensive suite of standard engineering characterization tests has been performed on seven commercial bentonites, complemented by flow tests on bentonite plugs, chemical analysis and swelling tests.

Experimental designs are given for the study of size and of thermal effects on plug performance, and a few preliminary results are presented.

Results are included from ongoing cement push-out tests and swelling measurements.

TABLE OF CONTENTS

TABLE OF CONTENTS--Continued

Page

TABLE OF CONTENTS--Continued

TABLE OF CONTENTS--Continued

TABLE OF CONTENTS--Continued

LIST OF FIGURES

LIST OF FIGURES--Continued

LIST OF FIGURES--Continued

LIST OF FIGURES--Continued

LIST OF FIGURES--Continued

LIST OF FIGURES--Continued

LIST OF FIGURES--Continued

LIST OF TABLES

LIST OF TABLES--Continued

LIST OF TABLES--Continued

LIST OF TABLES--Continued

LIST OF TABLES--Continued

LIST OF TABLES--Continued

ACKNOWLEDGMENTS

The research covered by this report was performed by the University of Arizona, Department of Mining and Geological Engineering, for the U.S. Nuclear Regulatory Commission (NRC). Project monitor for the NRC has been Dr. F.L. Doyle during the period reported on, and presently is Mr. J. Philip. The project is under Mr. Leon L. Beratan, Chief, Earth Sciences Branch, Division of Health, Siting and Waste Management, Office of Nuclear Regulatory Research.

Jaak J.K. Daemen, Associate Professor, Department of Mining and Geological Engineering, University of Arizona, was the Principal Investigator. Dr. James G. McCray, Acting Director, Nuclear Fuel Cycle Research Program, Department of Nuclear and Energy Enginering, University of Arizona, provided project management assistance. During the period reported on here research was performed by graduate students William B. Greer, Gatut S. Adisoma, Kittitep Fuenkajorn, Willis D. Sawyer, Arash Yazdandoost, and Haluk Akgun. Nora I. Colburn, Research Associate, provided geological expertise. Behrooz Kousari, David F. Miles, and Robert S. Armstrong, laboratory technicians, provided instrumentation and experimental assistance. Mike Porter assembled, typed and produced the report.

We wish to express our sincerest gratitude to Mr. Richard C. Laird, Union Mines Inc., for permission to work at the Oracle Ridge Mine, as well as for the continual assistance in performing the field work.

We gratefully acknowledge the U.S. Army Corps of Engineers, Walla Walla District, Washington, for permission to drill holes and perform sealing tests in the area of the proposed Second Powerhouse, McNary Lock and Dam, Columbia River, Oregon and Washington. Special thanks is given to Dale Munger and Ken Hutchinson for providing geological data and to Larry Labonte, Foreman, McNary Lock and Dam, for his on-site help.

We gratefully acknowledge the assistance of Dowell Division of Dow Chemical U.S.A. in providing cement and additives, and especially the technical help provided by Erik B. Nelson.

American Colloid Company provided precompressed Volclay® bentonite tablets and C/S Granular bentonite. Valuable technical assistance and discussions with Chris Jepsen, Mark Bertane and Todd Harriet of American Colloid are gratefully acknowledged. Bentonite samples also have been donated by Dresser Minerals, Federal Bentonite, Georgia Kaolin, International Minerals & Chemical Corp., and Whitaker, Clark & Daniels.

ROCK MASS SEALING
EXPERIMENTAL ASSESSMENT OF BOREHOLE PLUG PERFORMANCE
Annual Report, June 1, 1983 - May 31, 1984

EXECUTIVE SUMMARY

This Annual Report describes the work performed on the Rock Mass Sealing Contract No. NRC-04-78-271 during the period June 1, 1983 - May 31, 1984 by the Department of Mining and Geological Engineering, University of Arizona, Tucson, Arizona, for the U.S. Nuclear Regulatory Commission, Division of Health, Safety, and Waste Management.

The objective of this research project is to provide an experimental performance assessment of existing technology for sealing boreholes. This assessment will provide a factual data basis on the acceptability of using presently available technology to reduce waterflow (and, indirectly, radionuclide migration) through boreholes near a High Level Waste (HLW) Repository. Although HLW repositories will be located at sites with highly favorable isolation characteristics, two aspects that could create a concern with respect to radionuclide release, for any site, are manmade penetrations of the rock mass within or near a repository, and local, e.g. geologically disturbed, rock zones with reduced isolation capabilities.

The research reported on here adresses primarily the sealing of manmade penetrations, and experimentally directly the sealing of boreholes. To some extent the experimental work performed can be considered as scaled down work on the sealing of manmade penetrations in general (e.g. including shafts and drifts). It can be expected, for example, that interface flow between cement grout behind a shaft liner and the surrounding rock should be very similar to interface flow observed in experiments described here, i.e. should be very minimal if high quality cement and installation procedures are used, but could show significant piping or channeling with some installation procedures (e.g Chapter 2). Attempts at explicitly scaling up have had mixed results, at best. Further work in this area is planned and in progress, but it appears highly probable that testing on a considerably larger scale will be necessary to permit a widely valid and reliable determination of size effects.

1. Introduction

The first chapter of this report introduces the work performed this year. It gives a brief justification for the research - primarily the lack of available, quantitative experimental verification of borehole plug performance. Such an independently developed factual data basis will assist NRC in making findings about sealing procedures proposed in HLW repository license applications. The chapter summarizes the scope as well as the limitations of work performed and planned. It concludes with a list of reports issued previously on this contract, putting the present progress report within the general framework of the ongoing research.

2. Field Testing of Borehole Plug Performance

2.1 Introduction

The second chapter describes field plug installation procedures and results of field testing of borehole plug performance at the McNary Dam site (Columbia River, Oregon) and at the Oracle Ridge Mine site. Also presented are results of laboratory tests performed in support of field testing. The prime objective of these lab tests is to try to identify potential field installation problems by simulating field installation procedures. Particularly of concern in this context are the frequently observed channeling or piping along the rock-plug interface.

2.2 McNary Dam Site

Twenty cm long, 10 cm diameter plugs have been placed in three vertical holes in basalt at depths of approximately 45 to 50 m below the surface. One of these plugs has sealed very effectively. Two plugs that have not sealed effectively have been capped with an additional 20 cm cement. After this remedial work one of the capped plugs has shown very low hydraulic conductivity, while the third plug continues to allow relatively large waterflows.

The site, borehole configuration, etc., have been described in detail in the previous annual report. Instrumentation used for hole and plug testing includes a straddle packer assembly, remote tracer injectors, pressure-temperature recorders and a plug tester, as well as supporting equipment.

Borehole photography and core logging have been used to select plug locations, based on rock competence, low fracture density and sufficient depth below the water table. Packer testing has been performed in the intervals selected on the basis of the results from the preliminary surveys as being the most promising for plug installation and testing. The packer tests provide the hydraulic conductivity of the formation.

Plug emplacement is preceded by installation of the tracer injector and of the below-plug instrumentation package. These instruments are covered with gravel, sand and foam rubber, on top of which cement is placed with a bailer. In one case bailer emplacement has been noticeably unsuccessful, in another case probably so.

Plug testing is performed with a plug test packer installed directly above the plug, and consists of tracer travel time tests, fluid inflow tests and pressure build-up tests. Results are presented for all three plugs, but comprehensive data analysis is still in progress.

2.3 Oracle Ridge Mine Site

A cement plug has been installed in a nearly horizontal borehole connecting two mine drifts, thus allowing access to both ends of the plug, and greatly facilitating testing. Constant pressure injection tests have been performed on the plug since May 1983. An extensive discussion of the results is presented, and further testing and analysis are in progress. It can be concluded already, with some qualifications, that effective sealing of horizontal holes appears quite feasible with a swelling cement.

2.4 Laboratory Testing in Support of Field Tests

The objective of this laboratory testing is to try to resolve the frequently observed channeling or piping along the interface between a cement plug and the surrounding wall (e.g. acrylic tube in many lab tests) when plugs are installed within a water column. Such channeling (piping) has major detrimental consequences, i.e. drastic increases in hydraulic conductivity. Several alternatives have been tried in order to prevent such channeling, but none has proved fully successful. It is probable that this type of channeling might be less severe for plugs or grouts installed in a high density drilling mud (as compared to installations in water), but that it nevertheless should be of concern for all grouting and cementing in fluid-filled holes.

Two radial permeameter tests have been performed on rock from the Oracle Ridge Mine, both with rock bridges and with cement plugs.

3. Effects of Dynamic Loading and of Drying on Cement Borehole Plug Performance

This chapter is the executive summary of a topical report to be issued within the near future.

Flow testing has been conducted on cement borehole plugs installed in granite cylinders. The effect of dynamic loading on the hydraulic conductivity of the seals has been studied by subjecting the sealed rock samples to dynamic loading, i.e. controlled shaking on a shaking table. The influence of cement drying has been evaluated by comparing water flow through cement seals that have been maintained saturated since initial curing through all tests with results obtained on seals which have been allowed to dry out (typically for many months, either at room temperature, or in a laboratory oven).

It can be stated conclusively that dynamic loading, at accelerations up to 2 g for applications up to 5 minutes, i.e. considerably more severe testing conditions than would be encountered during any expected earthquake loading, does not have a measurable detrimental effect on cement borehole plug performance. Even after such loading the hydraulic conductivity of the plug remains at or below that of the (low permeability) granite in which it has been installed, i.e. no preferential flowpath develops along or through the plug.

It can be stated equally conclusively that drying of the cement tested here shows severe detrimental effects. The swelling is reversed, and the resulting net shrinkage first induces a strongly preferential flowpath (i.e. a partially open gap) between the plug and the rock, next shrinkage cracks within the cement itself, and a further increase in hydraulic conductivity. Upon saturating dried-out cement plugs, a partial performance recovery does take place (see also Chapter 9), but the hydraulic conductivity of the system is never reduced to values of the same order of magnitude as those for the cement plugs that are never dried out. Clearly, it would be highly desirable to complement this work by performing an experimental assessment of cement mixes designed specifically to minimize shrinkage during drying, including determination of the swelling and hydraulic conductivity behavior of such plugs, as well as of the rock-plug interface strength.

4. Experimental Assessment of Borehole Drilling Damage in Basalt

Chapter 4 consists of two parts, the executive summary of a topical report to be issued shortly, and a description of ongoing work.

The objective of this drilling damage study is to identify whether the damage induced by drilling in a rock annulus surrounding a plug, i.e. in the borehole walls, might be sufficient to allow a significant by-pass flow through this damaged zone. Experimental studies include ring tension tests, permeability (flow) measurements, and microscopic fracture studies.

The ring tension test study includes an extensive laboratory investigation of the tensile strength and stiffness of the rock around drillholes. The experimental work is complemented by a comprehensive numerical and analytical interpretation of the results. In the permeability tests an attempt has been made to identify the flow component through the damaged zone. (In a generalized sense all flow tests performed as part of this contract are tests of this type.) In the microscopic fracture studies a detailed study has been made of fractures, their density, orientation, size, etc., around boreholes both by petrographic and by electron microscopy. Three types of basalt have been used for the experimental work.

The main conclusions reached from this investigation can be summarized as follows:

- the damaged zone induced by drilling is very unlikely to be a significant flowpath.
- a damaged zone can be induced by drilling. Its thickness, in the samples tested (hole diameters ranging from 25 mm to 159 mm) does not exceed 1.7 mm, and usually is smaller.
- different drilling methods (e.g. diamond coring, rotary or percussion drilling) induce different and very characteristic types of damage (i.e. fracture density, distribution, orientation and size).

- the damaged zone depends on rock characteristics (e.g. grain size, grain orientation) as well as drilling parameters (e.g. bit size, energy input, weight on bit, rotational speed).

Probably the main remaining uncertainty in this area is whether the conclusions can be extrapolated to much larger diameters. In order to resolve this uncertainty, it is recommended that tests be performed on samples with borehole diameters from about 225 mm (9") up to 600 mm (24").

5. Experimental Assessment of Bentonite Borehole Sealing

This chapter is the executive summary of a topical report to be issued shortly. Seven commercially available bentonites have been studied.

Chemical analysis of the products confirms that commercially the name bentonite refers to products that can be significantly different, particularly with regard to impurities. This suggests the need for bentonite sealing specifications to include limits on acceptable impurity content, and for experimental verification of the influence, if any, of the impurities on sealing performance.

Conventional (soil mechanics) engineering properties have been determined for the bentonites. This includes shrinkage limit, plastic limit, liquid limit, specific gravity of solids and moisture-density. Serious difficulties and large differences in experimental results have been encountered during this testing.

Permeability testing of bentonites has confirmed the low permeability of all products. Some particle migration (piping) has been observed. Saturation is difficult to obtain and to assure. The permeability results depend strongly on a large number of parameters (e.g. pressure gradient across the sample, lateral boundary conditions, compacting method and energy, water chemistry, volume changes during testing, etc.).

Direct shear tests have been performed for bentonite on bentonite and for bentonite on basalt contacts, in both cases for saturated and for unsaturated conditions. The basalt-bentonite interface always has been weaker than a bentonite-bentonite contact. A complex multiple-plane slip zone develops in the benonite tests.

Swelling tests have been performed, on one product only, with ranges of water content from 19 to 41%, and with distilled water and NaCl solutions. Swelling pressures vary widely depending upon test conditions, and easily can reach magnitudes where they could have a significant detrimental effect (e.g. by opening rock fractures in an unfavorable orientation).

Bentonite is a highly complex material. Although there are very strong arguments in its favor as a repository sealing material, it also is certain that considerably more experimental work is needed in order to provide reasonable assurance about the predictability of virtually all detailed aspects of its behavior.

6. The Effect of Temperature on Cement Plug Sealing Performance

Testing the influence of temperatures above room temperature (up to 95°C) has been initiated. For the present series of experiments, the temperature range has been selected to simulate temperatures up to a distance from the actual waste (distance determined by waste age, configuration, etc.) where steam generation is unlikely, as steam is likely to induce significant complicating effects. Results are presented from scouting experiments on one dried-out cement sample and two saturated plugs.

A detailed description is given of the experimental apparatus, including pressure intensifier, flowmeter, permeameter, heating unit, temperature control system and bladder accumulator, and of the experimental procedures.

The prelimimary experiments reported on are primarily debugging experiments for equipment and instrumentation, and it would be premature to draw conclusions from these initial results.

7. Size Effects on Cement Borehole Plug Performance

Most of the sealing studies performed as part of this contract have been performed on relatively small diameter boreholes (typically 1" to 4"). Because the properties of both rock and sealing materials (e.g. cement) are size-dependent, this introduces uncertainty in the extrapolation of the results to larger size plugs. An assessment of the uncertainty involved will be made on the basis of results obtained from experiments on larger diameter boreholes.

This chapter describes primarily laboratory equipment and instrumentation being assembled to perform the experiments.

A scouting preliminary test has been initiated, and has resulted in a revealing and potentially very significant observation. A 20 cm diameter, 20 cm long swelling cement plug has been poured in a Pomona basalt block. The basalt block had been inspected carefully prior to the test, and no obvious cracks had been observed along the hole wall. Yet, during cement curing (swelling), a nearly radial hairline fracture running almost parallel to the hole axis opened up to an aperture sufficiently wide to allow the crack to become a dominant flowpath.

Additional tests described include instrument tests.

8. Cement Swelling Experiments

Cement swelling is desirable in order to minimize the development of interface flowpaths (e.g. between plug and rock, or between grout and casing or liner) and to maximize interface strength, although excessive swelling can have detrimental effects, e.g. as described in Chapter 7.

In Chapter 8 ongoing tests are described and results are tabulated.

9. Push-out Strength of Dried and Resaturated Cement Plugs

The work described in Chapter 9 includes long-term continuation of experiments reported on previously, as well as results obtained with a modified push-out testing system which provides somewhat more detailed experimental results.

Experiments on cement plugs that have been allowed to dry out and then have been resaturated confirm the flow test results (Chapter 3): drying causes significant performance deterioration (in this case, strength loss), while partial recovery does take place upon resaturation. Repeated loading to failure of these samples virtually certainly contributes to the deterioration, but, even so, significant strength (i.e. sufficient to maintain an even short repository plug in place under expected loading) is maintained by the plugs.

An interesting, but not entirely explained, observation is that during resaturation of the cement plugs, four basalt cylinders fractured, clearly displaying a diametrical tension crack as would be expected from an internal stress (e.g. swelling pressure).

CHAPTER ONE

INTRODUCTION

1.1 Objectives

The fundamental objective of this "Rock Mass Sealing" research project is to assess experimentally the performance of existing products and methods for sealing rock masses, in the current phase of the project to conduct an experimental evaluation of borehole plug performance. This work is aimed at determining the feasibility of sealing boreholes intersecting a repository rock mass to a level where it can reasonably be assured that the plugged boreholes will not become preferential radionuclide migration paths. This project studies experimentally the likelihood of preventing such migrations by sufficiently reducing the hydraulic conductivity of the plugged borehole (including the plug-rock interface and the rock directly around the plug).

The study is being conducted primarily in order to establish a factual data basis on borehole sealing performance. Although some types of borehole sealing have been performed for many years, relatively little testing and sealing verification has been done.

Concern about boreholes and their potential influence on the isolation performance of the rock mass surrounding repositories has been expressed in a number of basic reviews on underground HLW disposal (e.g. Kocher et al., 1983, p. 54; Bredehoeft et al., 1978, p. 8; U.S. Department of Energy, 1982, p. 29; U.S. Department of Energy, 1983, p. 25; Barbreau et al., 1980, p. 528; Committee on Radioactive Waste Management, 1978, pp. 5,10; Atomic Energy of Canada Limited, 1978, p. 72; Heineman et al, 1978, p. 4; U.S. Department of Energy, 1979, p. 3.1.328; OECD, 1980, Foreword; Burkholder, 1980, p.15; Irish, 1980, p. 42; Arnett et al., 1980, p. 139; Pedersen and Lindstrom-Jensen, 1980, p. 195; Deju, 1983, p. 4).

It deserves pointing out that the need for borehole plugging, and particularly for very high performance (e.g. very low hydraulic conductivity), is not universally accepted, nor obvious, and certainly might be a somewhat site dependent requirement, as shown by consequence assessments (e.g. Pedersen and Lindstrom-Jensen, 1980, p. 195; Klingsberg and Duguid, 1980, p. 43; Intera Environmental Consultants, Inc., 1981). These authors do recognize that borehole seals will provide " ... an important redundant barrier ... " or " ... will satisfy the concept of multiple barriers ... ".

General guidelines for the separation of radioactive waste from the physical environment, and in particular for the acceptable radionuclide releases following repository closure, have been proposed by EPA (1982; 40 CFR 191). Detailed implementation of the requirements is governed by 10 CFR 60 (NRC, 1983). The research performed as part of this ongoing contract addresses specifically some of the remaining uncertainties associated with the sealing requirements specified in 10 CFR 60, including §60.51,(a),4; §60.102,b(2),e(1),(2); §60.113; §60.133,(h), §60.142,(c), but particularly §60.134, Design of seals for shafts and boreholes.

1.2 Scope and Limitations

The scope of the work performed during the subject period centers primarily on experimental assessment of borehole plug performance. Rock types used for borehole plug performance testing during this year include basalt, granite, and limestone. Borehole sealing materials include cement and bentonite. The experimental performance assessment is accomplished through field and laboratory testing.

Laboratory testing includes water flow and strength testing of plugs installed in boreholes drilled coaxially in rock cylinders. Laboratory flow testing of plugs is performed on unloaded and on stressed rock samples (confining and axial stresses up to 3,000 psi). Testing of unconfined samples is considerably easier, requires less sophisticated equipment and instrumentation, and results in higher flow rates, so that a larger data basis can be obtained in a shorter time. Testing of confined samples provides a more realistic simulation of at-depth in situ conditions, allows a higher differential pressure to be applied across the plug without risking rock fracture, and allows a severe performance test, particularly for the rock-plug interface, upon reduction of the confinement.

Testing is performed at temperatures ranging from room temperatures up to 95°C. This temperature range is selected in order to represent conditions at likely repository depths and at some distance from actual waste.

Most laboratory testing is performed on relatively small boreholes (1" to 4"). Because both rock and cement have size-dependent properties, this limits the applicability of the results. Experiments on plugs in larger diameter holes (certainly 7 3/4", possibly up to 13") are in progress, and should allow more reliable assessment of size influence on plug performance.

Laboratory and field testing is performed on a relatively limited number of materials. The rocks used in the experiments are generically representative of potential repository formations, and the sealing materials used are existing and readily available products that have a high potential for being used as actual sealing materials.

Laboratory water flow testing typically is performed under stress gradients that are considerably higher than gradients likely to be encountered near repositories. Because of the test configurations used, this should result in testing conditions imposed on the interface and on the rock surrounding the plug that are considerably more severe than those likely to be encountered in situ. It is unknown whether the pressure gradient has an effect on the cement plugs (but generally accepted conventional assumptions do not consider this to be the case), while they certainly have a significant effect on bentonite plug behavior. Field testing is performed at relatively low pressure gradients, possibly more representative for short plugs at typical repository depths.

Testing, of necessity, is limited to time lengths that are short relative to those for permanent sealing requirements. Even so, testing is continued for time lengths that exceed considerably those of most laboratory testing. Moreover, tests are repeated on plugs installed earlier, and such repetition of tests is planned to be continued in the future.

Most experiments are performed on saturated rock-plug samples. Usually experiments are started after a relatively short curing period (7-8 days) at atmospheric pressure. Further curing proceeds under whatever pressure is applied (to one end of) the plug for the particular experiment under consideration. Some experiments have been performed on cement plugs allowed to dry out in a laboratory environment, or forced to dry out in an oven, as well as on samples that have been resaturated after drying.

All axial strength testing to date has been performed on plugs in unconfined rock samples. This should provide a lower bound of the plug-rock interface as any confinement beyond that supplied by the presently used rock cylinders would increase the normal stress across the interface, and hence the frictional strength.

Dynamic testing of plugged borehole samples is performed on 6" diameter samples with 1" diameter coaxial hole. The earthquake simulation loads are increased in a series of sequentially more severe experiments until the maximum shaking table capacity is reached.

Drilling damage studies are conducted on holes ranging from 1" to 4" diameter. All drilling is performed on unconfined unloaded samples. Considering the very high strength of the basalts tested, it is believed that the in-situ stresses would have to be extremely high before the differential between stress concentration around the hole and in-hole fluid pressure would cause significantly different effects from those observed. Conversely, significant differences in drilling energy induced to the rock are more likely to induce different intensities of drilling damage.

In sum, a considerable experimental data basis, covering a wide range of sealing performance aspects is being developed. It is believed that a very good reference basis is being established to define an upper bound on the performance of existing products and methods for sealing boreholes, i.e. performance under laboratory conditions. This includes evidence on the plug material performance, on the plug-rock interface, and on the rock surrounding the plug. Qualitative and quantiative evidence also is being gathered on some potentially detrimental influences on borehole plug performance, in particular drying, field installation and stress relaxation in the rock mass. Work on scaling up experiments, results and conclusions to larger sizes has been initiated.

1.3 Organization

Each chapter of this report deals with a distinct aspect of the ongoing rock mass sealing studies. A brief summary of each chapter is given in the Executive Summary, which follows directly, chapter by chapter, the outline of the report itself.

1.4 References

Arnett, R.C., R.G. Baca, J.A. Caggiano, and D.J. Carrel, 1980, "Radionuclide Release Scenario Selection Process for a Possible Basalt Repository," pp. 131-140, Radionuclide Release Scenarios for Geologic Repositories, Proceedings of the NEA Workshop, Paris, September 1980. Published by OECD, Paris, 1981.

Atomic Energy of Canada Limited, 1978, Management of Radioactive Fuel Wastes: the Canadian Disposal Program, AECL-6314, J. Boulton (Editor), Atomic Energy of Canada Research Company, Whiteshell Nuclear Research Establishment, Pinawa, Manitoba, Canada, October.

Barbreau, A., R. Heremans, and B. Skytte Jensen, 1980, "Radionuclide Migration in Geological Formations," pp. 515-530, Radioactive Waste Management in Geological Formations, Proceedings of the First European Community Conference, Luxemburg, May 20-23.

Bredehoeft, J.D., A.W. England, D.B. Stewart, N.J. Trask, and I.J. Winograd, 1978, Geologic Disposal of High-Level Radioactive Wastes - Earth-Science Perspectives, Geological Survey Circular 779, 15 + v pp., U.S. Geological Survey.

Burkholder, H.C., 1980, "The Development of Release Scenarios for Geologic Nuclear Waste Repositories", pp. 13-20, Radionuclide Release Scenarios for Geologic Repositories, Proceedings of the NEA Workshop, Paris, September 1980. Published by OECD, Paris, 1981.

Committee on Radioactive Waste Management, 1978, Geological Criteria for Repositories for High-Level Radioactive Wastes, 19 + vii pp., National Academy of Sciences, Washington, DC, August 3.

Deju, R.A., 1983, Testimony by Dr. Raul A. Deju, Basalt Waste Isolation Project, before the Subcommittee on Energy Research and Production, Committee on Science and Technology, United States House of Representatives, Washington, D.C., March 2, 9:30 am. RHO-BW-SA-293 P, Rockwell Hanford Operations, Hanford, Washington.

Heineman, R.E., W.A. Carbiener, and S.J. Basham, 1978, "The Technical Program for Establishing the Scientific Basis for Geologic Disposal," DOE Environmental Control Symposium, Washington, DC, November 28-30.

Intera Environmental Consultants, Inc., 1981, Consequence Assessment of Hydrological Communications Through Borehole Plugs, Contractor Report SAND 81-7 164, Prepared for Sandia National Laboratories, Albuquerque, NM.

Irish, E.R., 1980, "Safety Assessment for the Underground Disposal of Radioactive Waste - The IAEA Programme," pp. 39-43, Radionuclide Release Scenarios for Geologic Repositories, Proceedings of the NEA Workshop, Paris, September 1980. Published by OECD, Paris, 1981.

Klingsberg, C. and J. Duguid, 1980, Status of Technology for Isolating High-Level Radioactive Wastes in Geologic Repositories, DOE/TIC 11207 (Draft), U.S. Department of Energy, Office of Waste Isolation, Washington, DC, October.

Kocher, D.C., A.L. Sjoreen, and C.S. Bard, 1983, Uncertainties in Geologic Disposal of High-level Wastes - Groundwater Transport of Radionuclides and Radiological Consequences, NUREG/CR-2506; ONRL-5838; 214 + xiv pp., prepared for the U.S. Nuclear Regulatory Commission by Oak Ridge National Laboratory, Oak Ridge, Tennessee, July.

Pedersen, A. and K.E. Lindstrom-Jensen, 1980, "Selection of Release Scenarios for a Danish Waste Repository in a Salt Dome, pp. 181-196, Radionuclide Release Scenarios for Geologic Repositories, Proceedings of the NEA Workshop, Paris, September 1980. Published by OECD, Paris, 1981.

OECD, 1980, Borehole and Shaft Plugging, Proceedings Workshop organized by the OECD Nuclear Energy Agency and the U.S. Department of Energy, Published by OECD, Paris

U.S. Department of Energy, 1979, Management of Commercially Generated Radioactive Waste, DOE/EIS-0046-D, Vol. 1 of 2, Draft Environmental Impact Statement, Washington, DC, April

U.S. Department of Energy, 1982, NWTS Program Criteria for Mined Geologic Disposal of Nuclear Waste: Repository Performance and Development Criteria, DOE/NWTS-33(3), Office of NWTS Integration, Battelle Memorial Institute, Columbus, OH, July, Public Draft.

U.S. Department of Energy, 1983, Summary of the Results of the Evaluation of the WIPP Site and Preliminary Design Validation Program, WIPP-DOE-161, Waste Isolation Pilot Plant, Albuquerque, NM, March.

U.S. Environmental Protection Agency, 1982, "Environmental Standards and Federal Radiation Protection Guidance for Management and Disposal of Spent Nuclear Fuel, High-Level and Transuranic Radioactive Wastes," 40 CFR 191, Draft 20, Federal Register, Vol. 47, p. 58196.

U.S. Nuclear Regulatory Commission, 1983, "Disposal of High-Level Radioactive Wastes in Geologic Repositories," Final Rule 10 CFR 60, Federal Register, Vol. 48, No. 120, June 30.

1.5 Rock Mass Sealing Contract No. NRC 04-78-271 - Reports Issued

This Annual Report describing research performed during the period June 1, 1983 - May 31, 1984, is the latest in a series of reports issued for the subject contract. A complete list of reports issued (to be issued for South and Daemen, 1985) is given below, to facilitate a general overview of work performed to date and of the overall context of ongoing work.
The first four reports, as well as the seventh, are literature surveys.

The fifth report is primarily a description of planning, experimental design and some preliminary tests.

The topical report by Jeffrey (1980) gives a comprehensive theoretical (analytical) discussion of transverse plug-rock interaction, based on elastic and viscoelastic calculations. This is complemented by the axial interaction discussed in Stormont and Daemen (1983), which is primarily experimentally oriented, but includes extensive analytical discussions.

The topical report by Mathis and Daemen (1982) presents a detailed experimental assessment of drilling damage in granites, work being continued in basalts, as described in Chapter Seven of the present Annual Report. It is expected that a topical report on drilling damage in basalt will be issued in 1985.

Experimental flow studies under polyaxial stress conditions are described in Cobb and Daemen (1982), under radially symmetric external loading in South and Daemen (1985), and on unloaded samples in Chapter Six of the present report. Additional data on plug performance under stressed and unstressed conditions will be reported in the future.

All annual reports subsequent to (5) include a combination of experiments, results, conclusions, and plans for future work, similar to the present annual report.

Quarterly progress reports are not listed as all information contained therein also is included in the annual reports.

1. South, D.L., R.G. Jeffrey, L.W. Klejbuk, and J.J.K. Daemen, 1979, "Rock Mass Sealing - Annual Report, October 1, 1978 - September 30, 1979," prepared for the U.S. Nuclear Regulatory Commission, SAFER Division, for Contract NRC-04-78-271, by the Department of Mining and Geological Engineering, University of Arizona, Tucson.

2. Daemen, J.J.K., 1979, "Rock Mass Sealing (Research in Europe)," 48 pp., Foreign Travel Trip Report to the U.S. Nuclear Regulatory

Commission, SAFER Division, for Contract NRC-04-78-271, by the Department of Mining and Geological Engineering, University of Arizona, Tucson.

3. South, D.L., 1979, "Well Cementing," 75 + vii pp., Topical Report to the U.S. Nuclear Regulatory Commission, SAFER Division, for Contract NRC-04-78-271, by the Department of Mining and Geological Engineering, University of Arizona, Tucson.

4. Sultan, H.A., 1979, "Chemical Grouting for Rock Mass Sealing - a Literature Review," 45 + iv pp., Topical Report to the U.S. Nuclear Regulatory Commission, SAFER Division, for Contract NRC-04-78-271, by the Department of Mining and Geological Engineering, University of Arizona, Tucson.

5. South, D.L., R.G. Jeffrey, S.L. Cobb, S.P. Mathis, and J.J.K. Daemen, 1979, "Rock Mass Sealing - Annual Report, October 1, 1978 - September 30, 1980," prepared for the U.S. Nuclear Regulatory Commission, SAFER Division, for Contract NRC-04-78-271, by the Department of Mining and Geological Engineering, University of Arizona, Tucson.

6. Jeffrey, R.G., 1980, "Shaft or Borehole Plug-Rock Mechanical Interaction," 145 + xi pp., Topical Report to the U.S. Nuclear Regulatory Commission, SAFER Division, for Contract NRC-04-78-271, by the Department of Mining and Geological Engineering, University of Arizona, Tucson.

7. South, D.L., 1980, "Borehole Sealing with Clay (Part A). Considerations in Clay Mineral Stability (Part B)," 50 + iv pp.; 25 + ii pp., Topical Report to the U.S. Nuclear Regulatory Commission, SAFER Division, for Contract NRC-04-78-271, by the Department of Mining and Geological Engineering, University of Arizona, Tucson.

8. Cobb, S.L., W.B. Greer, R.G. Jeffrey, S.P. Mathis, D.L. South, and J.J.K. Daemen, 1981, "Rock Mass Sealing - Annual Report, September 1, 1980 - May 31, 1981," prepared for the U.S. Nuclear Regulatory Commission, SAFER Division, for Contract NRC-04-78-271, by the Department of Mining and Geological Engineering, University of Arizona, Tucson.

9. South, D.L., W.B. Greer, N.I. Colburn, S.L. Cobb, B. Kousari, S.P. Mathis, R.G. Jeffrey, C.A. Wakely, and J.J.K. Daemen, 1982, "Rock Mass Sealing - Annual Report, June 1, 1981 - May 31, 1982," prepared for the U.S. Nuclear Regulatory Commission, SAFER Division, for Contract NRC-04-78-271, by the Department of Mining and Geological Engineering, University of Arizona, Tucson.

10. Mathis, S.P. and J.J.K. Daemen, 1982, "Borehole Wall Damage Induced by Drilling: An Assessment of Diamond and Percussion Drilling Effects," 171 + xii pp., Topical Report to the U.S. Nuclear

Regulatory Commission, SAFER Division, for Contract NRC-04-78-271, by the Department of Mining and Geological Engineering, University of Arizona, Tucson.

11. Cobb, S.L. and J.J.K. Daemen, 1982, "Polyaxial Testing of Borehole Plug Performance," 180 + xi pp., Topical Report to the U.S. Nuclear Regulatory Commission, SAFER Division, for Contract NRC-04-78-271, by the Department of Mining and Geological Engineering, University of Arizona, Tucson.

12. Daemen, J.J.K., D.L. South, W.B. Greer, J.C. Stormont, S.A. Dischler, G.S. Adisoma, N.I. Colburn, K. Fuenkajorn, D.E. Miles, B. Kousari, J. Bertucca, 1983, "Rock Mass Sealing - Annual Report, June 1, 1982 - May 31, 1983," NUREG/CR-3473, prepared for the U.S. Nuclear Regulatory Commission, Division of Health, Siting and Waste Management, for Contract NRC-04-78-271, by the Department of Mining and Geological Engineering, University of Arizona, Tucson.

13. Stormont, J.C. and J.J.K. Daemen, 1983, "Axial Strength of cement Borehole Plugs in Granite and Basalt," NUREG/CR-3594, Topical Report to the U.S. Nuclear Regulatory Commission, Division of Health, Siting and Waste Management, for Contract NRC-04-78-271, by the Department of Mining and Geological Engineering, University of Arizona, Tucson.

14. South, D.L., and J.J.K. Daemen, 1985, "Permeameter Studies of Water Flow through Cement and Clay Borehole Seals in Granite, Basalt and Tuff," Topical Report to the U.S. Nuclear Regulatory Commission, Division of Health, Siting and Waste Management, for Contract NRC-04-78-271, by the Department of Mining and Geological Engineering, University of Arizona, Tucson.

CHAPTER TWO

FIELD TESTING OF BOREHOLE PLUG PERFORMANCE

2.1 Introduction

This chapter describes procedures and results of field testing at the McNary Dam and Oracle Ridge Mine sites. Also presented are results of laboratory tests performed in support of field testing.

2.2 McNary Dam Site

2.2.1 Summary

A cement plug, about 20 cm (8 in) long, was placed in each of the following boreholes on the indicated dates: borehole no. UA-CB-1 on 9/22/83, no. UA-CB-4 on 2/15/84, and no. UA-CB-3 on 2/22/84.

Pressure build-up and extensive fluid build-up tests have been performed on the plug in UA-CB-1. Fluid build-up inflow rates for UA-CB-1 averaged 6 ml/day for the period October, 1983 through February, 1984. Initial fluid build-up tests on the plugs in UA-CB-4 and UA-CB-3 yielded much higher inflow rates, indicating that the plugs were not sealing effectively. On May 2, 1984, a cement cap 18-20 cm (7-8 in) long was placed directly on top of the plugs in holes UA-CB-4 and UA-CB-3. Preliminary fluid build-up testing indicates that the plug and cap in UA-CB-4 are sealing as effectively as the plug in UA-CB-1. In UA-CB-3 the cap has improved sealing; however, fluid build-up inflow rates are still three orders of magnitude greater than in UA-CB-1.

2.2.2 Site Description

The site consists of six experimental boreholes in basalt. The holes, which were drilled in the summer of 1982, are vertical, 10 cm (4 in) in diameter and range in depth from 46.6 m (153 ft) to 71.0 m (233 ft). The water table in the area is about 3 m (9 ft) below ground surface. A full description of the site can be found in the '82-'83 Annual Report (Daemen et al., 1983)

2.2.3 Equipment

2.2.3.1 Instrumentation

2.2.3.1.1 Packer Testing. The primary items of instrumentation for packer pressure testing are a straddle packer assembly and a water injection pump. A microcomputer is used for data recording and analysis. The straddle packer assembly utilizes two pneumatic packers having a deflated diameter of 7.6 cm (3.0 in) and a gland length of 150 cm (59 in). Electronic pressure transducers monitor the pressure in the test zone between the packers as well as above and below the packers. Digital pressure indicators provide a continuous reading proportional to the pressures measured by the transducers. A strip-chart recorder gives a graphical display of the test zone pressure. A normally-open, gas-operated valve is positioned at the injection line inlet to the test zone. The test zone length is normally 60 cm (24 in), but may be expanded easily to 150 cm (59 in) or 302 cm (9 ft 11 in). The gas-over-water injection pump delivers water to the packer test zone over a wide range of pressures and flow rates. It also permits a precise flow rate measurement. The microcomputer is an Apple II+ with two disk drives, a monitor and a printer.

2.2.3.1.2 Plug Testing. Instrumentation developed for testing of borehole plugs consists of a remote tracer injector, a remote pressure-temperature recorder and a plug tester unit. The three equipment items were built by the University of Arizona Instrument Shop.

Remote tracer injector. The tracer injector has been developed to release two different tracer volumes at staggered times beneath a borehole plug. The liquid tracers are contained in two spring-powered piston injectors. Tracer release is accomplished by opening a solenoid valve at the outlet port of each injector. A crystal-controlled digital timer opens the solenoid valve at any of a range of pre-set times up to 32 days after activation. The tracer volume per piston injector is approximately 47 cc (2.86 cu in). The tracer injector is enclosed in a stainless steel canister and is positioned in a borehole just below plug depth prior to emplacement of the plug.

Remote pressure-temperature recorder. The recorder is capable of reading and storing below-plug pressure and temperature once every four hours for more than 300 days. The instrument consists of a temperature sensor and a strain-gauge pressure transducer which are connected to a non-volatile semiconductor memory circuit. The recorder is enclosed in a stainless steel container and is positioned immediately below the tracer injector.

Plug tester. The plug tester, positioned above a borehole plug, is used to create a hydraulic gradient across the plug and to perform hydraulic tests of plug performance. The plug tester is described in detail in Section 2.2.7.1.

2.2.3.2 Other Equipment Items

The University of Arizona has an equipment trailer, a 2.7 x 3.0 m (9 x 10 ft) portable storage building and a lifting derrick on site (Figures 2.1 and 2.2). The U.S. Army Corps of Engineers, which operates McNary Lock and Dam, has provided a second portable building (1.2 x 2.1 m or 4 x 7 ft).

2.2.4 Preliminary Surveys

Preliminary surveys, consisting of core logging and borehole photography, were conducted to determine the most favorable sites for placing plugs. Core was obtained for nearly the full length of all six boreholes at the site. Core logs and above-ground color photographs of all core have been made. Also, the Corps of Engineers, Walla Walla

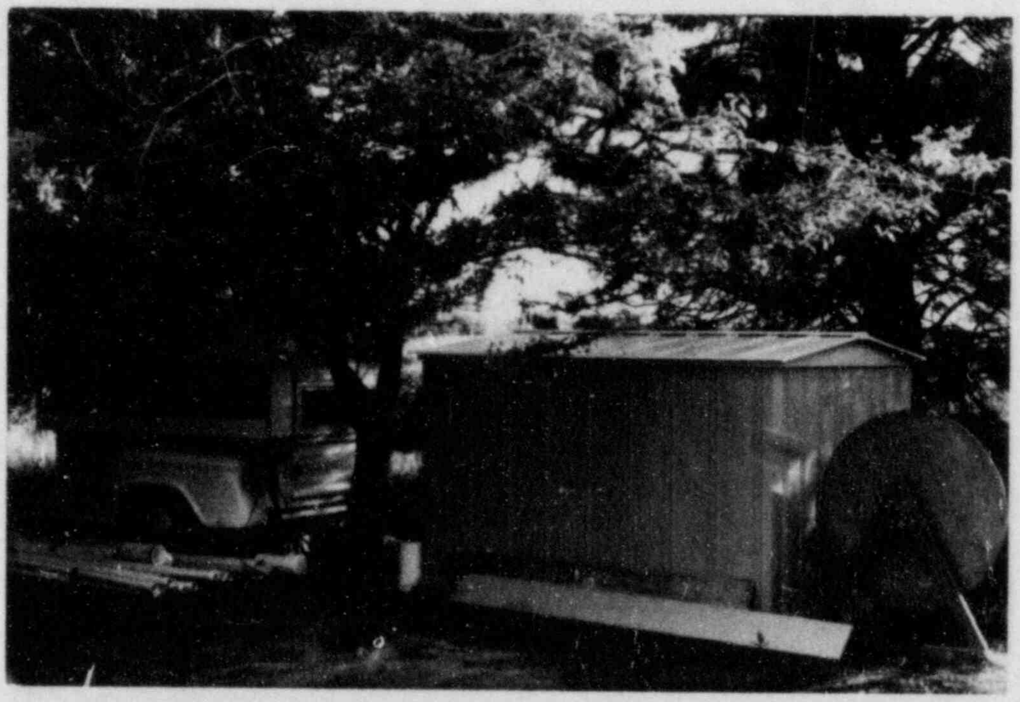

Figure 2.1 McNary Dam site: equipment trailer and portable storage building. Microcomputer and pressure monitoring equipment are housed in trailer.

Figure 2.2 McNary Dam site: lifting derrick. Derrick features an electric winch and a hand-operated winch for raising/lowering borehole instruments.

District, has taken color photographs of each of the boreholes using a specially-designed still-picture camera. Using techniques and equipment developed by the Corps of Engineers, an analysis of fractures intersecting the boreholes between about 15 and 46 m (50 and 150 feet) has been accomplished. The analysis provides depth, orientation, width estimate and general visual description of in-situ fractures. Based on the preliminary surveys, an interval in each of three of the boreholes was selected for plug placement. The intervals were selected based on the following criteria: (1) competence of rock, (2) low density of fractures, and (3) adequate depth below water table for hydraulic testing of plug.

Figures 2.3 - 2.5 show the three selected intervals. The geologic logs are based on analysis of core and the photographic logs on analysis of the Corps of Engineers borehole photographs. The logs show actual plug position within the intervals.

2.2.5 Packer Testing

Packer testing was concentrated in the intervals selected based on the preliminary surveys. Constant pressure injection tests of 24 to 186 hours duration using the straddle packer assembly were performed. Tables 2.1-2.3, 2.4-2.8 and 2.9-2.12 summarize the results of these tests.* Figures 2.6-2.8, 2.9-2.13 and 2.14-2.17 are plots of average injection flow rate vs. time for the tests. Assuming that approximately steady-state injection is achieved during the latter hours of each test, equivalent hydraulic conductivity may be calculated from the packer test results using the steady-state flow rate and the following steady-state expression for equivalent hydraulic conductivity (Ziegler, 1976):

$$k_e = \frac{Q}{\ell H_0}\left[\frac{1}{2\pi}\ln(R/r_0)\right]$$

where k_e = equivalent hydraulic conductivity [L/T],

ℓ = length of test zone [L],

H_0 = excess pressure head [L],

Q = steady-state injection flow rate [L^3/T],

R = effective radius of influence (use $R = \ell^{**}$) [L], and

r_0 = radius of borehole [L].

---

*Upon conclusion of the tests in UA-CB-4, a minute gas leak was found at the intersection of the membrane and the fixed head of the upper packer. In very tight rock, it appears that an effect of this leak is to cause the test zone pressure to equilibrate at erroneous and extremely high pressures in tests to determine ambient pressure (see Tables 2.4 - 2.7). The effect of the leaked gas on the water injection rate is being studied.

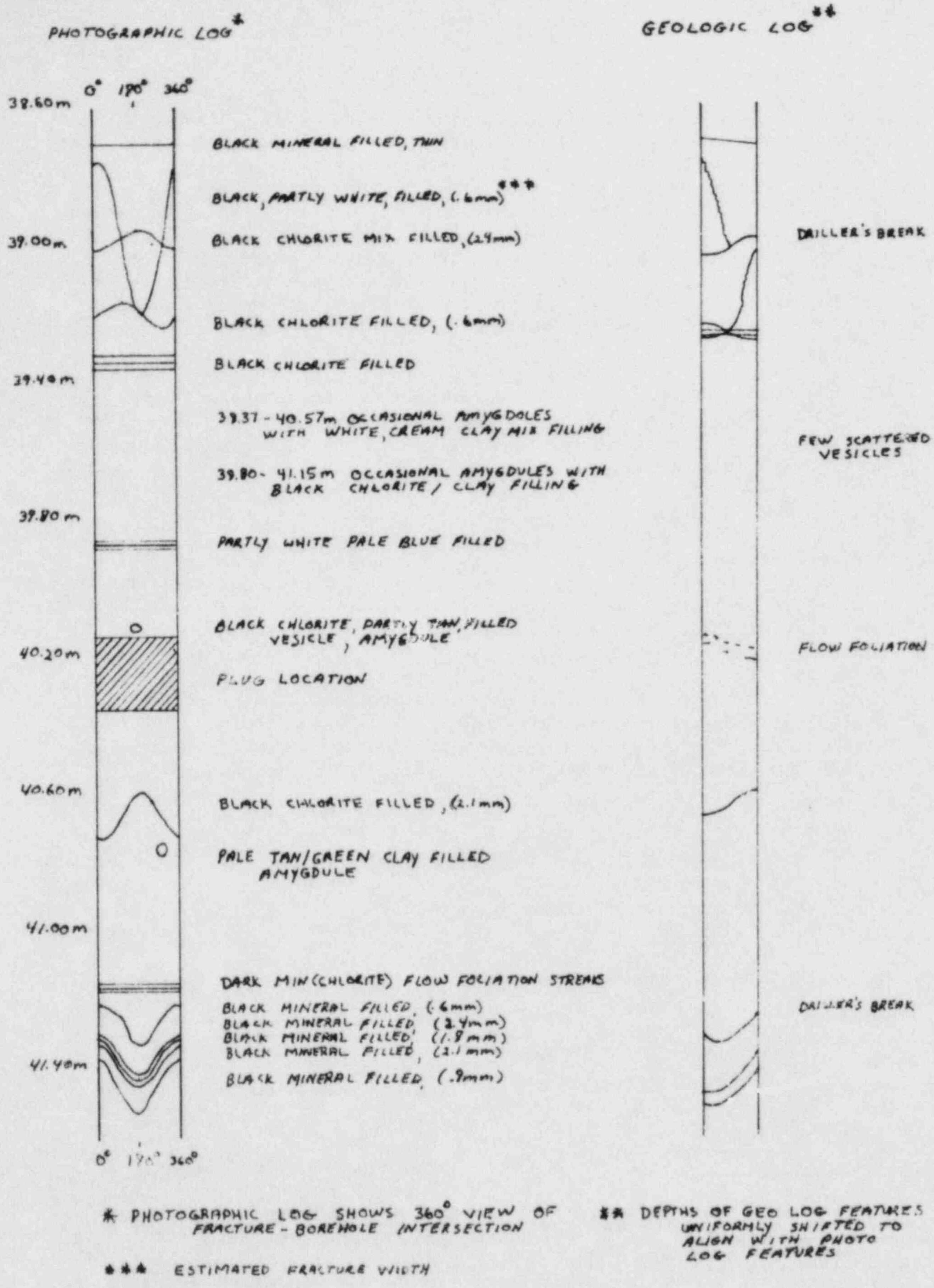

Figure 2.3 Photographic and geologic logs showing fractures/features, vicinity of borehole plug UA-CB-1.

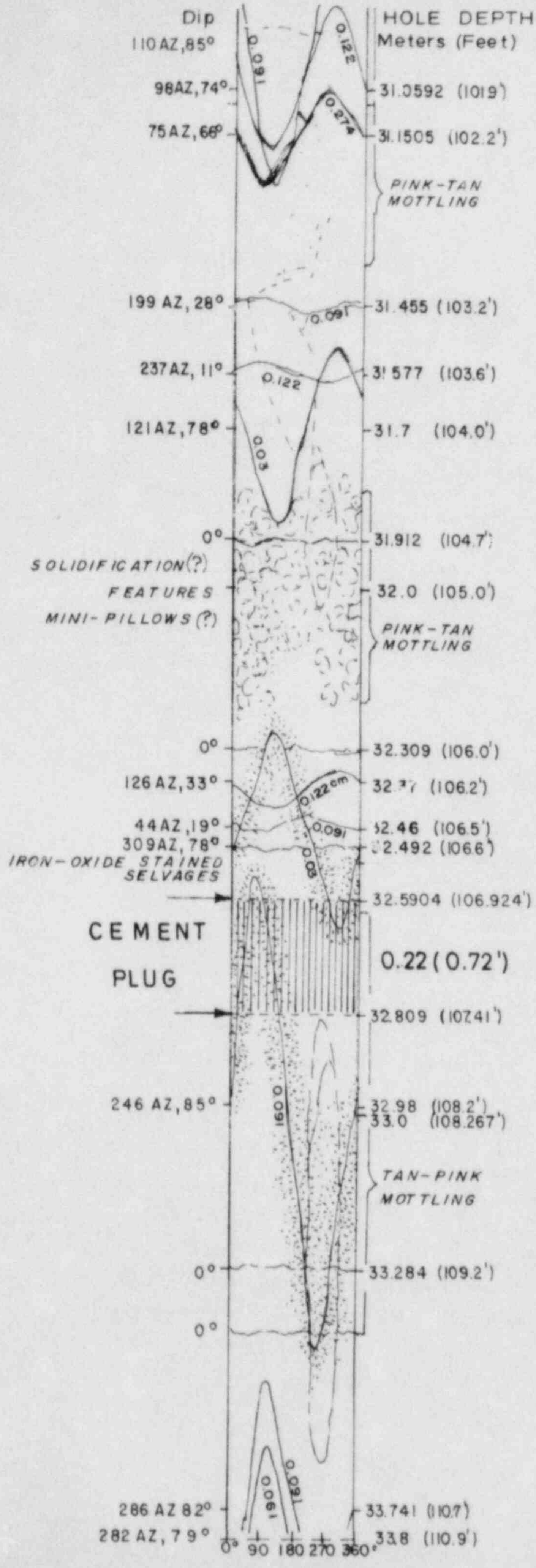

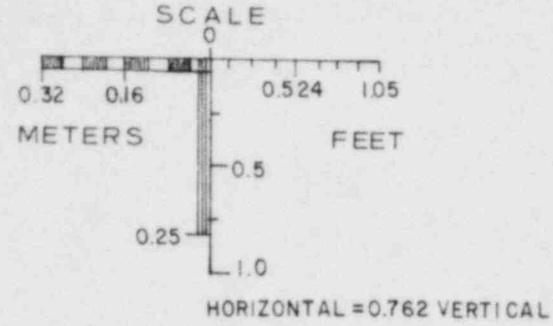

Borehole Diameter: 0.1016 m (0.333')
Borehole Circumference: 0.32 m (1.05')

Each fracture is shown as a trace of the intersection of its plane and the side of the cylindrical borehole, with the down-dip azimuth given in degrees from true north (0°).

Most fractures or joints contain a black chloritic - dark green to pale blue clay filling. Minimum normal width of a fracture shown in centimeters.

Umatilla basalt, member of Saddle Mountains basalt subgroup of the Columbia River Basalts.

Figure 2.4 Combined photographic and geologic logs showing fractures/features, vicinity of borehole plug UA-CB-3.

FRACTURE LOG UA-CB-3

McNary Dam Drill Site Umatilla, Oregon

11/84

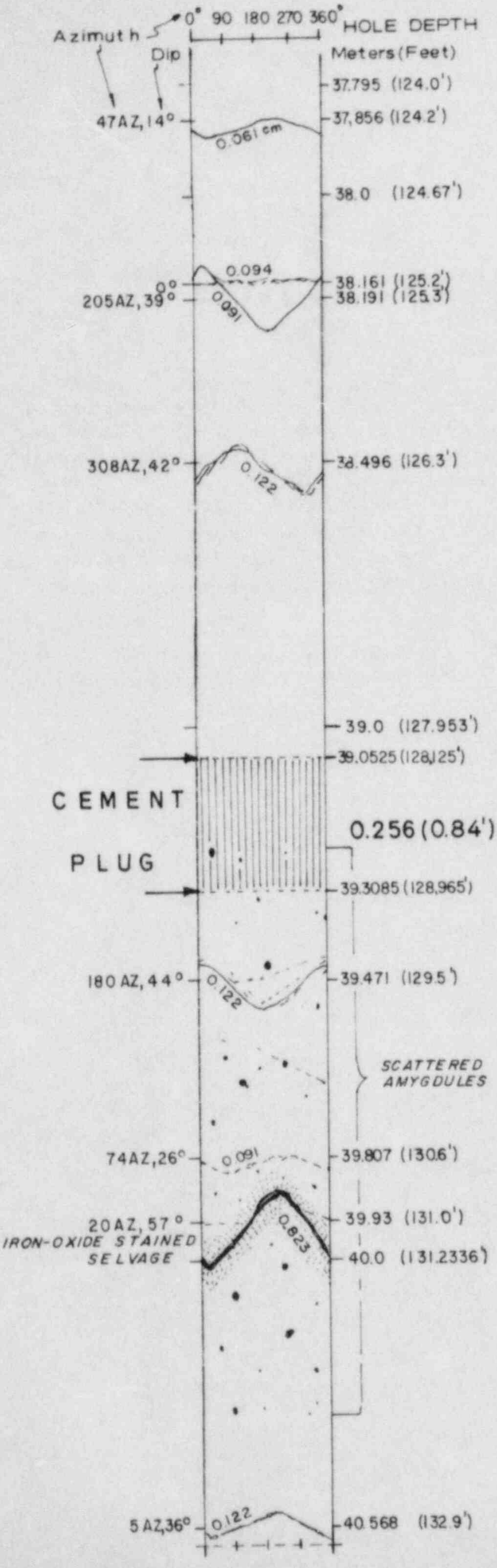

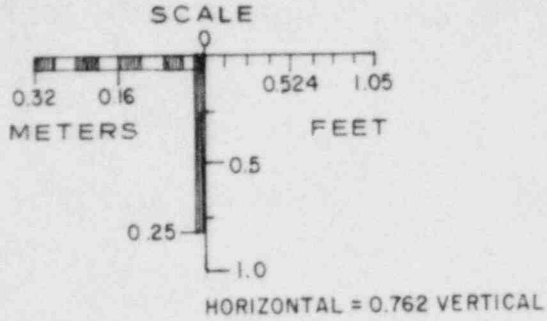

Borehole Diameter: 0.1016m (0.333')
Borehole Circumference: 0.32m (1.05')

Each fracture is shown as a trace of the intersection of its plane and the side of the cylindrical borehole.

The down dip azimuth is in degrees from true north (0°).

Minimum normal width of filled fractures is given in centimeters.

Unless noted, the Umatilla flow is a dense, dark gray basalt, uniformly fine grained, often almost aphanitic.

Figure 2.5 Combined photographic and geologic logs showing fractures/features, vicinity of borehole plug UA-CB-4.

FRACTURE LOG UA - CB - 4

McNary Dam Drill Site Umatilla, Oregon

11/84

Table 2.1 Constant Pressure Injection Test Results. Borehole UA-CB-1; test started 9-4-83; depth to top of test zone: 39.592 m; length of test zone: 60.6 cm; ambient test zone pressure: 355 kPa (51.5 psig).

Date/Time	t, Elapsed time (min)	t, Elapsed time (hours)	Δt (min)	$P_E(\Delta t)$ (psig)	$P_E(\Delta t)$ (kPa)	$V(\Delta t)$ (cm^3)	$Q_A(\Delta t) = \frac{V(\Delta t)}{(60)(\Delta t)}$ $\times 10^3$ (cm^3/sec)
9-4/0943	0	0					
			264	30.5	210	19.53	1.23
1407	264	4.40					
			199	29.8	206	14.03	1.18
1726	463	7.72					
			265	30.0	207	20.14	1.27
2151	728	12.1					
			518	30.2	208	33.56	1.08
9-5/0629	1246	20.8					
			213	30.2	208	10.98	.859
1002	1459	24.3					
			252	30.2	208	10.37	.686
1414	1711	28.5					
			139	30.0	207	7.93	.951
1633	1850	30.8					
			306	29.8	206	19.53	1.06
2139	2156	35.9					
			704	30.0	207	41.49	.982
9-6/0923	2860	47.7					
			202	30.0	207	7.93	.654
1245	3062	51.0					
			129	30.2	208	4.88	.631
1454	3191	53.2					
			36	29.8	206	1.83	.845
1530	3227	53.8					

Table 2.1 Constant Pressure Injection Test Results - NOTES

$P_E(\Delta t)$ = average pressure (in excess of ambient pressure) in the test zone between the packers over the time period Δt.

$V(\Delta t)$ = volume of water injected into the test zone during the time period Δt.

$Q_A(\Delta t)$ = average injection flow rate during the period Δt.

Table 2.2 Constant Pressure Injection Test Results. Borehole UA-CB-1; test started 9-9-83; depth to top of test zone: 39.929 m; length of test zone: 60.6 cm; ambient test zone pressure: 348 kPa (50.5 psig).

Date/Time	t, Elapsed time (min)	t, Elapsed time (hours)	Δt (min)	$P_E(\Delta t)$ (psig)	$P_E(\Delta t)$ (kPa)	$V(\Delta t)$ (cm^3)	$Q_A(\Delta t) = \frac{V(\Delta t)}{(60)\Delta t}$ x 10^3 (cm^3/sec)
9-9/1050	0	0					
			237	30.2	208	21.36	1.50
1447	237	3.95					
			98	30.2	208	7.93	1.35
1625	335	5.58					
			343	29.7	205	18.92	.919
2208	678	11.3					
			559	30.3	209	25.63	.764
9-10/0727	1237	20.6					
			435	30.3	209	14.64	.561
1442	1672	27.9					
			396	30.2	206	11.59	.488
2118	2068	34.5					
			567	29.8	206	17.70	.520
9-11/0645	2635	43.9					
			414	30.7	211	9.76	.393
1339	3049	50.8					

$P_E(\Delta t)$ = average pressure (in excess of ambient pressure) in the test zone between the packers over the time period Δt.

$V(\Delta t)$ = volume of water injected into the test zone during the time period Δt.

$Q_A(\Delta t)$ = average injection flow rate during the period Δt.

Table 2.3 Constant Pressure Injection Test Results. Borehole UA-CB-1; test started 9-12-83; depth to top of test zone: 40.437 m; length of test zone: 60.6 cm; ambient test zone pressure: 332 kPa (48.2 psig).

Date/Time	t, Elapsed time (min)	t, Elapsed time (hours)	Δt (min)	$P_E(\Delta t)$ (psig)	$P_E(\Delta t)$ (kPa)	$V(\Delta t)$ (cm^3)	$Q_A(\Delta t) = \frac{V(\Delta t)}{(60)(\Delta t)}$ x 10^3 (cm^3/sec)
9-12/1509	0	0					
			94	30.0	207	26.85	4.76
1643	94	1.57					
			323	30.0	207	64.07	3.31
2206	417	6.95					
			618	30.2	208	86.04	2.32
9-13/0824	1035	17.3					
			211	30.3	209	20.14	1.59
1155	1246	20.8					
			401	30.2	208	36.61	1.52
1836	1647	27.5					

$P_E(\Delta t)$ = average pressure (in excess of ambient pressure) in the test zone between the packers over the time period Δt.

$V(\Delta t)$ = volume of water injected into the test zone during the time period Δt.

$Q_A(\Delta t)$ = average injection flow rate during the period Δt.

Table 2.4 Constant Pressure Injection Test Results for Borehole UA-CB-4. Depth to Top of Test Zone: 37.586 m (123.31 ft); Length of Test Zone: 60.3 cm (1.98 ft); Ambient Test Zone Pressure: 600 kPa (87.0 psig)*

Date/Time	t, Elapsed time (min)	t, Elapsed time (hours)	Δt (min)	$P_E(\Delta t)$ (psig)	$P_E(\Delta t)$ (kPa)	$V(\Delta t)$ (cm^3)	$Q_A(\Delta t) = \frac{V(\Delta t)}{(60)(\Delta t)}$ x 10^3 (cm^3/sec)
12-29/0838	0	0					
			469	30.3	209	34.8	1.24
12-29/1627	469	7.82					
			1301	30.8	213	83.6	1.07
12-30/1408	1770	29.50					
			356	30.7	211	17.7	.828
12-30/2004	2126	35.43					
			864	30.0	207	44.5	.859
12-31/1028	2990	49.83					
			586	29.8	206	27.5	.781
12-31/2014	3576	59.60					
			1102	29.8	206	50.0	.757
1-01/1436	4678	77.97					

*High ambient test zone pressure is believed due to minute gas leak from packer into the tight-rock test zone of this interval (see Section 2.2.5).

$P_E(\Delta t)$ = average pressure (in excess of ambient pressure) in the test zone between the packers over the time period Δt.

$V(\Delta t)$ = volume of water injected into the test zone during the time period Δt.

$Q_A(\Delta t)$ = average injection flow rate during the period Δt.

Table 2.5 Constant Pressure Injection Test Results for Borehole UA-CB-4. Depth to Top of Test Zone: 38.094 m (124.98 ft); Length of Test Zone: 60.3 cm (1.98 ft); Ambient Test Zone Pressure: 581 kPa (84.3 psig)*

Date/Time	t, Elapsed time (min)	t, Elapsed time (hours)	Δt (min)	$P_E(\Delta t)$ (psig)	$P_E(\Delta t)$ (kPa)	$V(\Delta t)$ (cm^3)	$Q_A(\Delta t) = \frac{V(\Delta t)}{(60)(\Delta t)}$ $\times 10^3$ (cm^3/sec)
12-24/1543	0	0					
			326	30.2	208	31.1	1.59
12-24/2109	326	5.43					
			938	30.3	209	67.1	1.19
12-25/1247	1264	21.07					
			425	30.3	209	28.1	1.10
12-25/1952	1689	28.15					
			901	30.0	207	53.1	0.982
12-26/1053	2590	43.17					
			426	30.0	207	23.8	0.931
12-26/1759	3016	50.27					
			855	29.8	206	45.2	0.880
12-27/0814	3871	64.52					
			282	30.2	208	15.9	0.938
12-27/1256	4153	69.22					

*High ambient test zone pressure is believed due to minute gas leak from packer into the tight-rock test zone of this interval (see Section 2.2.2.2).

$P_E(\Delta t)$ = average pressure (in excess of ambient pressure) in the test zone between the packers over the time period Δt.

$V(\Delta t)$ = volume of water injected into the test zone during the time period Δt.

$Q_A(\Delta t)$ = average injection flow rate during the period Δt.

Table 2.6 Constant Pressure Injection Test Results for Borehole UA-CB-4. Depth to Top of Test Zone: 38.602 m (126.65 ft); Length of Test Zone: 60.3 cm (1.98 ft); Ambient Test Zone Pressure: 1090 kPa (158 psig)*

Date/Time	t, Elapsed time (min)	t, Elapsed time (hours)	Δt (min)	$P_E(\Delta t)$ (psig)	$P_E(\Delta t)$ (kPa)	$V(\Delta t)$ (cm^3)	$Q_A(\Delta t) = \frac{V(\Delta t)}{(60)(\Delta t)}$ $\times 10^3$ (cm^3/sec)
1-31/0826	0	0					
			414	30.8	213	7.32	0.295
1-31/1520	414	6.90					
			413	31.3	216	6.10	0.246
1-31/2213	827	13.78					
			596	31.3	216	0.610	0.0171
2-1/0809	1423	23.72					
			351	31.3	216	0.610	0.0290
2-1/1400	1774	29.57					
			419	31.3	216	1.83	0.0728
2-1/2059	2193	36.55					
			673	31.2	215	1.83	0.0453
2-2/0812	2866	47.77					
			398	31.2	215	1.22	0.0511
2-2/1450	3264	54.40					
			356	31.2	215	1.83	0.0857
2-2/2046	3620	60.33					
			699	30.8	213	1.83	0.0436
2-3/0825	4319	71.98					
			440	30.8	213	0.915	0.0347
2-3/1545	4759	79.32					
			391	31.0	214	0.915	0.0390
2-3/2216	5150	85.83					
			743	30.8	213	1.83	0.0411
2-4/1039	5893	98.22					
			520	31.5	217	1.22	0.0391

Table 2.6 Constant Pressure Injection Test Results for Borehole UA-CB-4. Depth to Top of Test Zone: 38.602 m (126.65 ft); Length of Test Zone: 60.3 cm (1.98 ft); Ambient Test Zone Pressure: 1090 kPa (158 psig)* --Continued

Date/Time	t, Elapsed time (min)	t, Elapsed time (hours)	Δt (min)	$P_E(\Delta t)$ (psig)	$P_E(\Delta t)$ (kPa)	$V(\Delta t)$ (cm^3)	$Q_A(\Delta t) = \frac{V(\Delta t)}{(60)(\Delta t)}$ x 10^3 (cm^3/sec)
2-4/1919	6413	106.88					
			716	31.7	218	1.83	0.0426
2-5/0715	7129	118.82					
			396	31.5	217	0.610	0.0257
2-5/1351	7525	125.42					

*High ambient test zone pressure is believed due to minute gas leak from packer into the tight-rock test zone of this interval (see Section 2.2.2.2).

$P_E(\Delta t)$ = average pressure (in excess of ambient pressure) in the test zone between the packers over the time period Δt.

$V(\Delta t)$ = volume of water injected into the test zone during the time period Δt.

$Q_A(\Delta t)$ = average injection flow rate during the period Δt.

Table 2.7 Constant Pressure Injection Test Results for Borehole UA-CB-4. Depth to Top of Test Zone: 39.110 m (128.31 ft); Length of Test Zone: 60.3 cm (1.98 ft); Ambient Test Zone Pressure: 1160 kPa (169 psig)*

Date/Time	t, Elapsed time (min)	t, Elapsed time (hours)	Δt (min)	$P_E(\Delta t)$ (psig)	$P_E(\Delta t)$ (kPa)	$V(\Delta t)$ (cm^3)	$Q_A(\Delta t) = \frac{V(\Delta t)}{(60)(\Delta t)}$ $\times 10^3$ (cm^3/sec)
1-24/1250	0	0					
			142	31.0	214	4.88	0.573
1-24/1512	142	2.37					
			375	31.0	214	5.49	0.244
1-24/2127	517	8.62					
			635	30.7	211	4.27	0.112
1-25/0802	1152	19.20					
			299	30.3	209	1.83	0.102
1-25/1301	1451	24.18					
			462	31.0	214	3.66	0.132
1-25/2043	1913	31.88					
			715	31.2	215	2.44	0.0569
1-26/0838	2628	43.80					
			331	31.3	216	1.83	0.0922
1-26/1409	2959	49.32					
			356	31.5	217	1.53	0.0714
1-26/2005	3315	55.25					

*High ambient test zone pressure is believed due to minute gas leak from packer into the tight-rock test zone of this interval (see Section 2.2.2.2).

$P_E(\Delta t)$ = average pressure (in excess of ambient pressure) in the test zone between the packers over the time period Δt.

$V(\Delta t)$ = volume of water injected into the test zone during the time period Δt.

$Q_A(\Delta t)$ = average injection flow rate during the period Δt.

Table 2.8 Constant Pressure Injection Test Results for Borehole UA-CB-4. Depth to Top of Test Zone: 37.618 m (129.98 ft); Length of Test Zone: 60.3 cm (1.98 ft); Ambient Test Zone Pressure: 350 kPa (50.8 psig)

Date/Time	t, Elapsed time (min)	t, Elapsed time (hours)	Δt (min)	$P_E(\Delta t)$ (psig)	$P_E(\Delta t)$ (kPa)	$V(\Delta t)$ (cm^3)	$Q_A(\Delta t) = \frac{V(\Delta t)}{(60)(\Delta t)}$ x 10^3 (cm^3/sec)
1-9/2054	0	0					
			671	28.8	199	1680	41.7
1-10/0805	671	11.18					
			410	27.2	187	885	36.0
1-10/1455	1081	18.02					
			324	29.3	202	777	40.0
1-10/2019	1405	23.42					
			727	30.0	207	1670	38.3
1-11/0826	2132	35.53					

$P_E(\Delta t)$ = average pressure (in excess of ambient pressure) in the test zone between the packers over the time period Δt.

$V(\Delta t)$ = volume of water injected into the test zone during the time period Δt.

$Q_A(\Delta t)$ = average injection flow rate during the period Δt.

Table 2.9 Constant Pressure Injection Test Results for Borehole UA-CB-3. Depth to Top of Test Zone: 32.099 m (105.31 ft); Length of Test Zone: 60.0 cm (1.97 ft); Ambient Test Zone Pressure: 296 kPa (43.0 psig)

Date/Time	t, Elapsed time (min)	t, Elapsed time (hours)	Δt (min)	$P_E(\Delta t)$ (psig)	$P_E(\Delta t)$ (kPa)	$V(\Delta t)$ (cm^3)	$Q_A(\Delta t) = \frac{V(\Delta t)}{(60)(\Delta t)}$ x 10^3 (cm^3/sec)
2-13/1404	0	0					
			270	30.3	209	81.8	5.05
2-13/1834	270	4.50					
			820	30.2	208	212	4.30
2-14/0814	1090	18.17					
			666	30.2	208	151	3.79
2-14/1920	1756	29.27					
			206	30.0	207	45.2	3.65
2-14/2246	1962	32.70					
			Injection pump reset during this interval				
2-14/2249	1962	32.70					
			599	30.8	213	126	3.50
2-15/0848	2561	42.68					
			899	30.7	211	171	3.18
2-15/2347	3460	57.67					
			636	30.5	210	104	2.73
2-16/1023	4096	68.27					
			724	30.2	208	112	2.57
2-16/2227	4820	80.33					
			583	30.0	207	79.3	2.27
2-17/0810	5403	90.05					
			Injection pump reset during this interval				
2-17/0825	5403	90.05					
			555	30.7	211	59.8	1.80
2-17/1740	5958	99.30					
			187	30.5	210	20.7	1.85

Table 2.9 Constant Pressure Injection Test Results for Borehole UA-CB-3. Depth to Top of Test Zone: 32.099 m (105.31 ft); Length of Test Zone: 60.0 cm (1.97 ft); Ambient Test Zone Pressure: 296 kPa (43.0 psig)--Continued

Date/Time	t, Elapsed time (min)	t, Elapsed time (hours)	Δt (min)	$P_E(\Delta t)$ (psig)	$P_E(\Delta t)$ (kPa)	$V(\Delta t)$ (cm^3)	$Q_A(\Delta t) = \frac{V(\Delta t)}{(60)(\Delta t)}$ x 10^3 (cm^3/sec)
2-17/2047	6145	102.42					
			770	30.3	209	95.1	2.06
2-18/0937	6915	115.25					
			752	30.3	209	83.6	1.85
2-18/2209	7667	127.78					
			557	30.0	207	52.5	1.57
2-19/0726	8224	137.07					
			825	30.0	207	79.3	1.60
2-19/2111	9049	150.82					
			786	29.8	206	65.9	1.40
2-20/1017	9835	163.92					
			1326	30.0	207	124	1.56
2-21/0823	11,161	186.02					

$P_E(\Delta t)$ = average pressure (in excess of ambient pressure) in the test zone between the packers over the time period Δt.

$V(\Delta t)$ = volume of water injected into the test zone during the time period Δt.

$Q_A(\Delta t)$ = average injection flow rate during the period Δt.

Table 2.10 Constant Pressure Injection Test Results for Borehole UA-CB-3. Depth to Top of Test Zone: 32.582 m (106.90 ft); Length of Test Zone: 60.3 cm (1.98 ft); Ambient Test Zone Pressure: 373 kPa (54.2 psig)

Date/Time	t, Elapsed time (min)	t, Elapsed time (hours)	Δt (min)	$P_E(\Delta t)$ (psig)	$P_E(\Delta t)$ (kPa)	$V(\Delta t)$ (cm^3)	$Q_A(\Delta t) = \frac{V(\Delta t)}{(60)(\Delta t)}$ $\times 10^3$ (cm^3/sec)
10-26/0839	0	0					
			259	30.5	210	20.7	1.34
10-26/1258	259	4.32					
			348	30.3	209	25.6	1.23
10-26/1846	607	10.12					
			797	29.7	205	54.9	1.15
10-27/0803	1404	23.40					
			292	30.5	210	17.7	1.01
10-27/1255	1696	28.27					
			199	30.2	208	12.8	1.07
10-27/1614	1895	31.58					
			274	29.8	206	17.1	1.04
10-27/2048	2169	36.15					
			677	29.8	206	42.7	1.05
10-28/0805	2846	47.43					

$P_E(\Delta t)$ = average pressure (in excess of ambient pressure) in the test zone between the packers over the time period Δt.

$V(\Delta t)$ = volume of water injected into the test zone during the time period Δt.

$Q_A(\Delta t)$ = average injection flow rate during the period Δt.

Table 2.11 Constant Pressure Injection Test Results for Borehole UA-CB-3. Depth to Top of Test Zone: 32.709 m (107.31 ft); Length of Test Zone: 60.3 cm (1.98 ft); Ambient Test Zone Pressure: 345 kPa (50.0 psig)

Date/Time	t, Elapsed time (min)	t, Elapsed time (hours)	Δt (min)	$P_E(\Delta t)$ (psig)	$P_E(\Delta t)$ (kPa)	$V(\Delta t)$ (cm^3)	$Q_A(\Delta t) = \frac{V(\Delta t)}{(60)(\Delta t)}$ x 10^3 (cm^3/sec)
10-5/0838	0	0					
			115	30.3	209	4.88	.707
10-5/1033	115	1.92					
			71	30.3	209	1.83	.430
10-5/1144	186	3.10					
			241	30.2	208	7.93	.549
10-5/1545	427	7.12					
			392	30.0	207	14.0	.597
10-5/2217	819	13.65					
			593	29.7	205	15.3	.429
10-6/0810	1412	23.53					

$P_E(\Delta t)$ = average pressure (in excess of ambient pressure) in the test zone between the packers over the time period Δt.

$V(\Delta t)$ = volume of water injected into the test zone during the time period Δt.

$Q_A(\Delta t)$ = average injection flow rate during the period Δt.

Table 2.12 Constant Pressure Injection Test Results for Borehole UA-CB-3. Depth to Top of Test Zone: 33.090 m (108.56 ft); Length of Test Zone: 60.3 cm (1.98 ft); Ambient Test Zone Pressure: 379 kPa (55.0 psig)

Date/Time	t, Elapsed time (min)	t, Elapsed time (hours)	Δt (min)	$P_E(\Delta t)$ (psig)	$P_E(\Delta t)$ (kPa)	$V(\Delta t)$ (cm^3)	$Q_A(\Delta t) = \frac{V(\Delta t)}{(60)(\Delta t)}$ x 10^3 (cm^3/sec)
11-4/1358	0	0					
			415	30.0	207	69.6	2.79
11-4/2053	415	6.92					
			613	29.8	206	88.5	2.41
11-5/0706	1028	17.13					
			393	30.0	207	53.1	2.25
11-5/1339	1421	23.68					
			519	30.0	207	59.8	1.92
11-5/2218	1940	32.33					
			534	29.5	203	40.9	1.28
11-6/0712	2474	41.23					
			431	29.3	202	29.9	1.16
11-6/1423	2905	48.42					
			464	30.2	208	33.0	1.18
11-6/2207	3369	56.15					
			599	30.3	209	41.5	1.15
11-7/0806	3968	66.13					

$P_E(\Delta t)$ = average pressure (in excess of ambient pressure) in the test zone between the packers over the time period Δt.

$V(\Delta t)$ = volume of water injected into the test zone during the time period Δt.

$Q_A(\Delta t)$ = average injection flow rate during the period Δt.

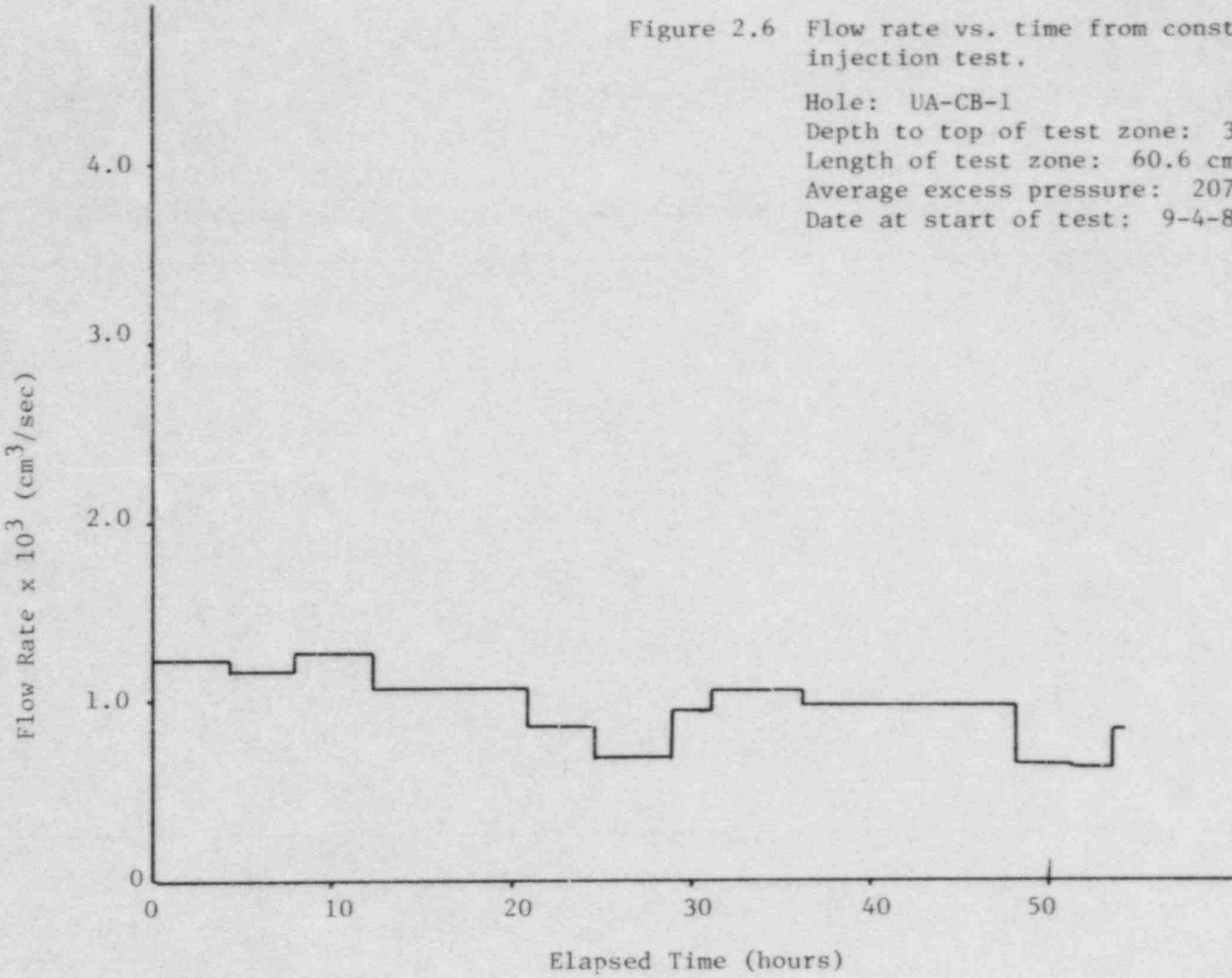

Figure 2.6 Flow rate vs. time from constant pressure injection test.

Hole: UA-CB-1
Depth to top of test zone: 39.592 m
Length of test zone: 60.6 cm
Average excess pressure: 207 kPa
Date at start of test: 9-4-83

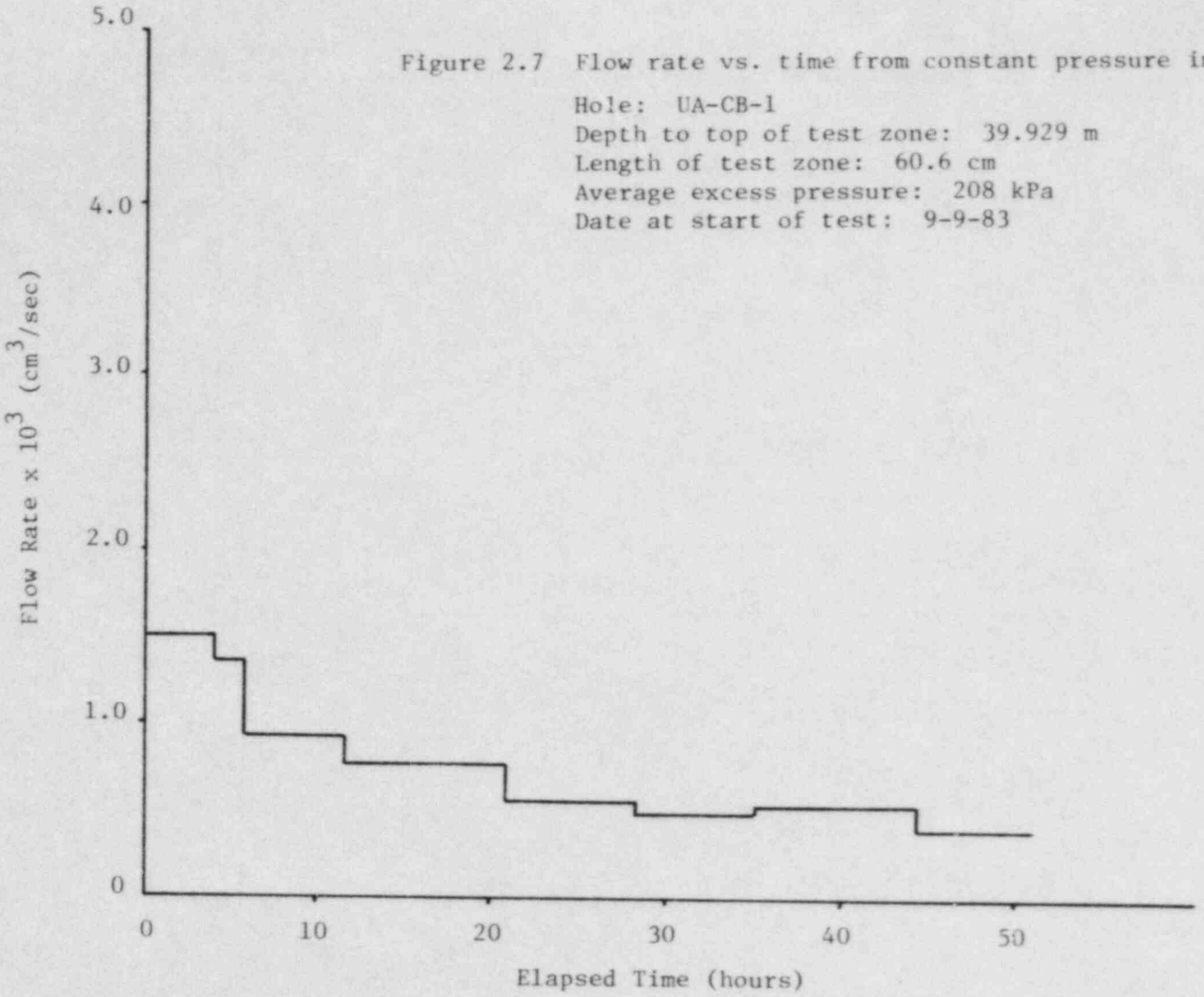

Figure 2.7 Flow rate vs. time from constant pressure injection test.

Hole: UA-CB-1
Depth to top of test zone: 39.929 m
Length of test zone: 60.6 cm
Average excess pressure: 208 kPa
Date at start of test: 9-9-83

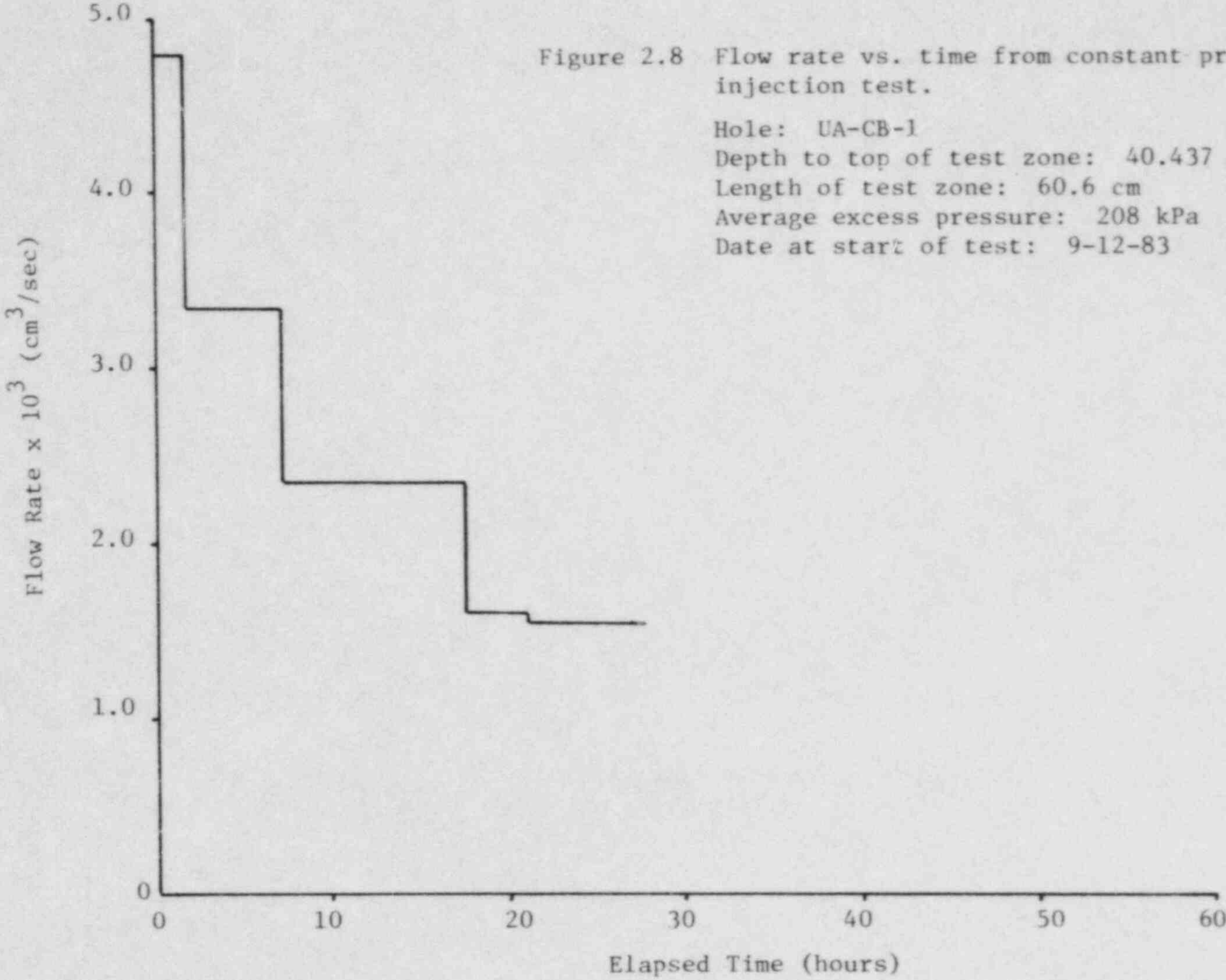

Figure 2.8 Flow rate vs. time from constant pressure injection test.

Hole: UA-CB-1
Depth to top of test zone: 40.437 m
Length of test zone: 60.6 cm
Average excess pressure: 208 kPa
Date at start of test: 9-12-83

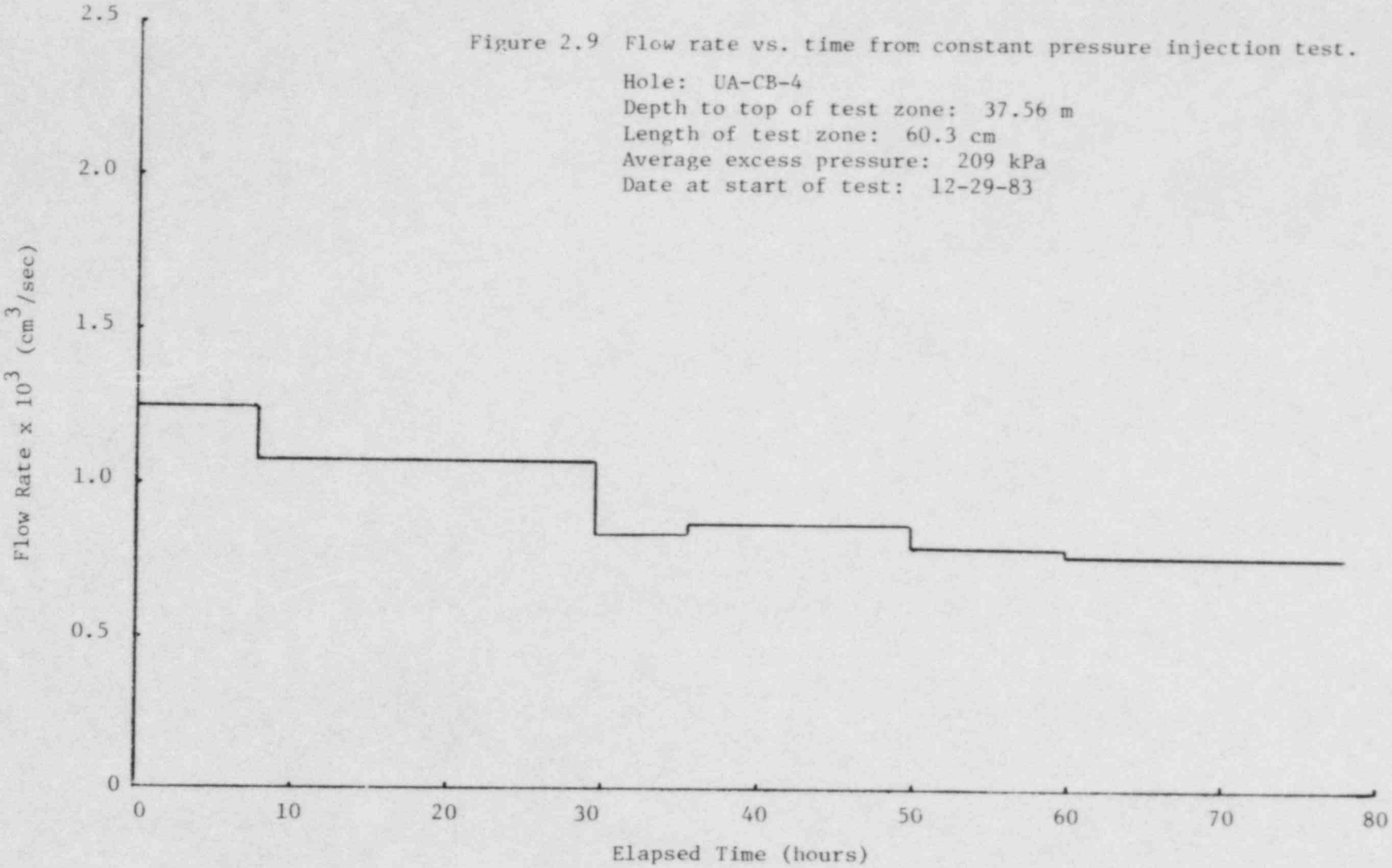

Figure 2.9 Flow rate vs. time from constant pressure injection test.

Hole: UA-CB-4
Depth to top of test zone: 37.56 m
Length of test zone: 60.3 cm
Average excess pressure: 209 kPa
Date at start of test: 12-29-83

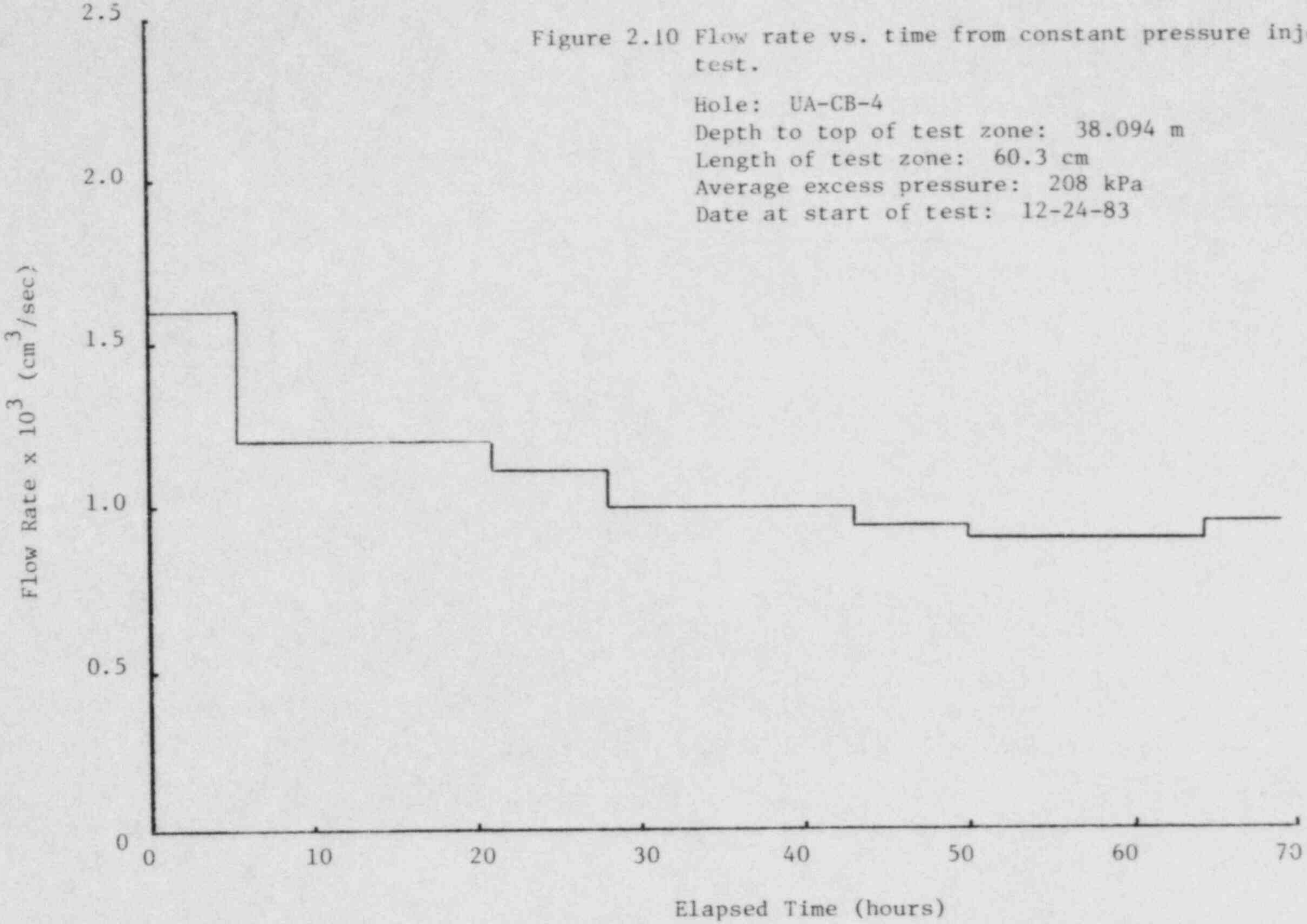

Figure 2.10 Flow rate vs. time from constant pressure injection test.

Hole: UA-CB-4
Depth to top of test zone: 38.094 m
Length of test zone: 60.3 cm
Average excess pressure: 208 kPa
Date at start of test: 12-24-83

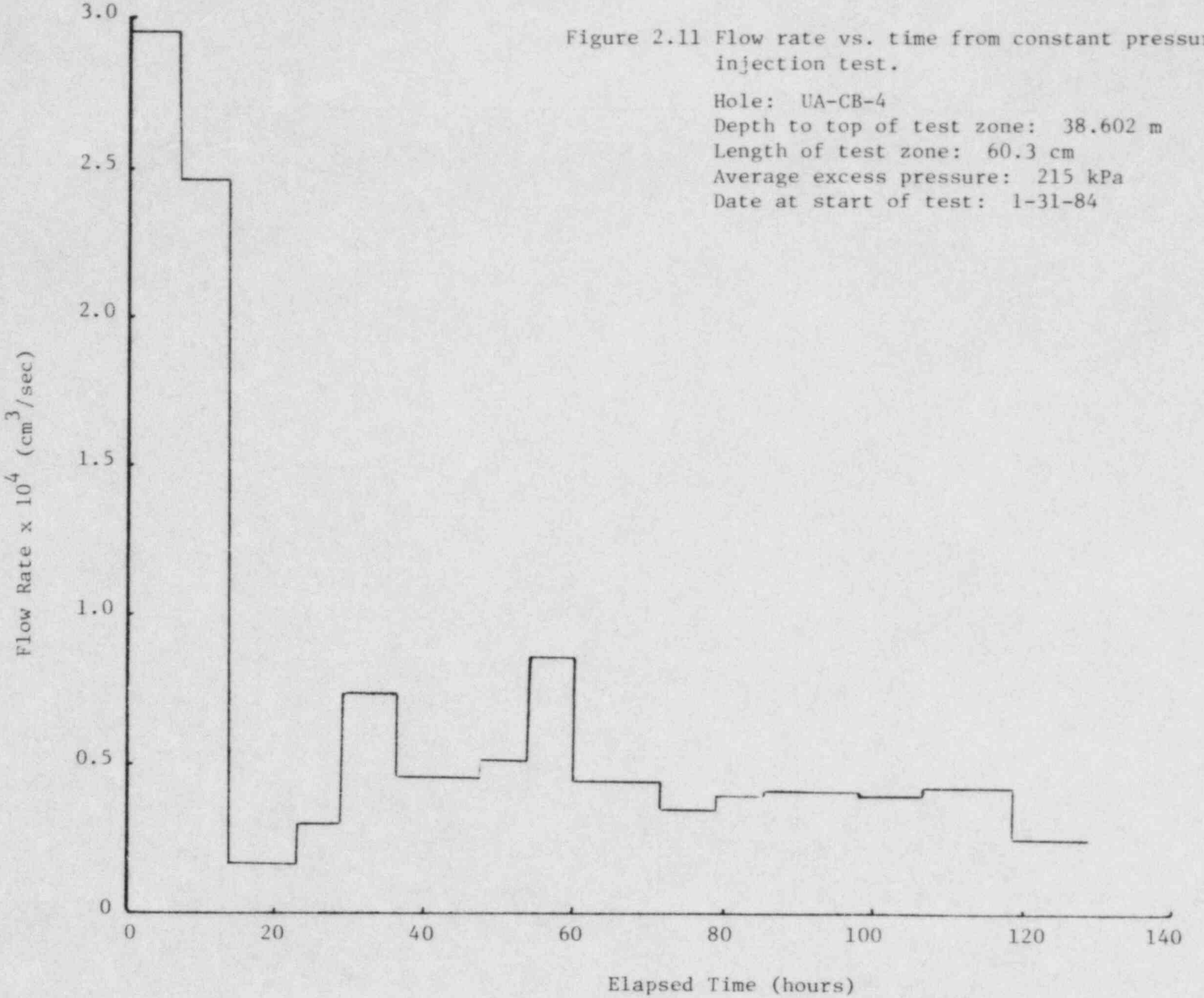

Figure 2.11 Flow rate vs. time from constant pressure injection test.

Hole: UA-CB-4
Depth to top of test zone: 38.602 m
Length of test zone: 60.3 cm
Average excess pressure: 215 kPa
Date at start of test: 1-31-84

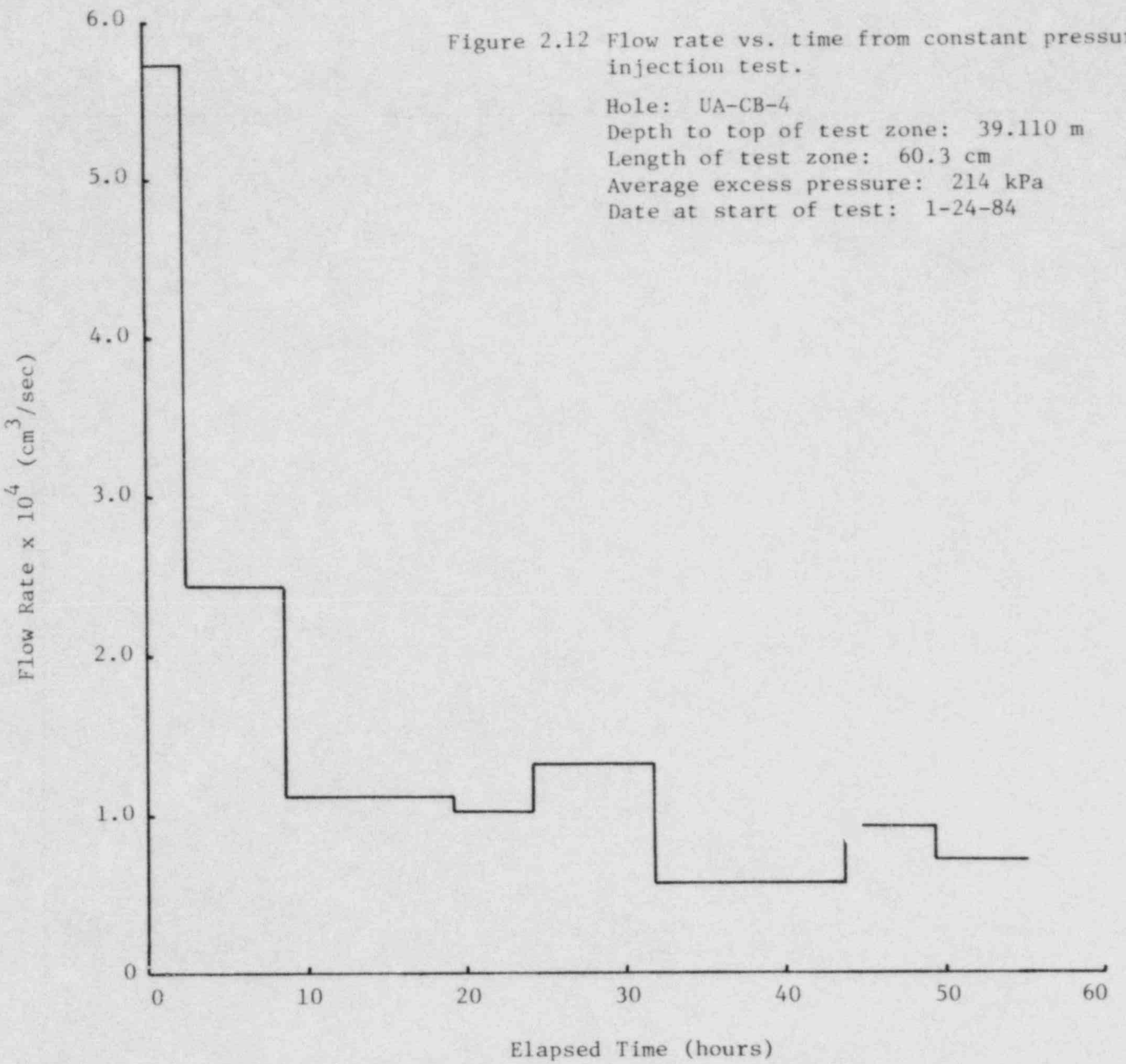

Figure 2.12 Flow rate vs. time from constant pressure injection test.

Hole: UA-CB-4
Depth to top of test zone: 39.110 m
Length of test zone: 60.3 cm
Average excess pressure: 214 kPa
Date at start of test: 1-24-84

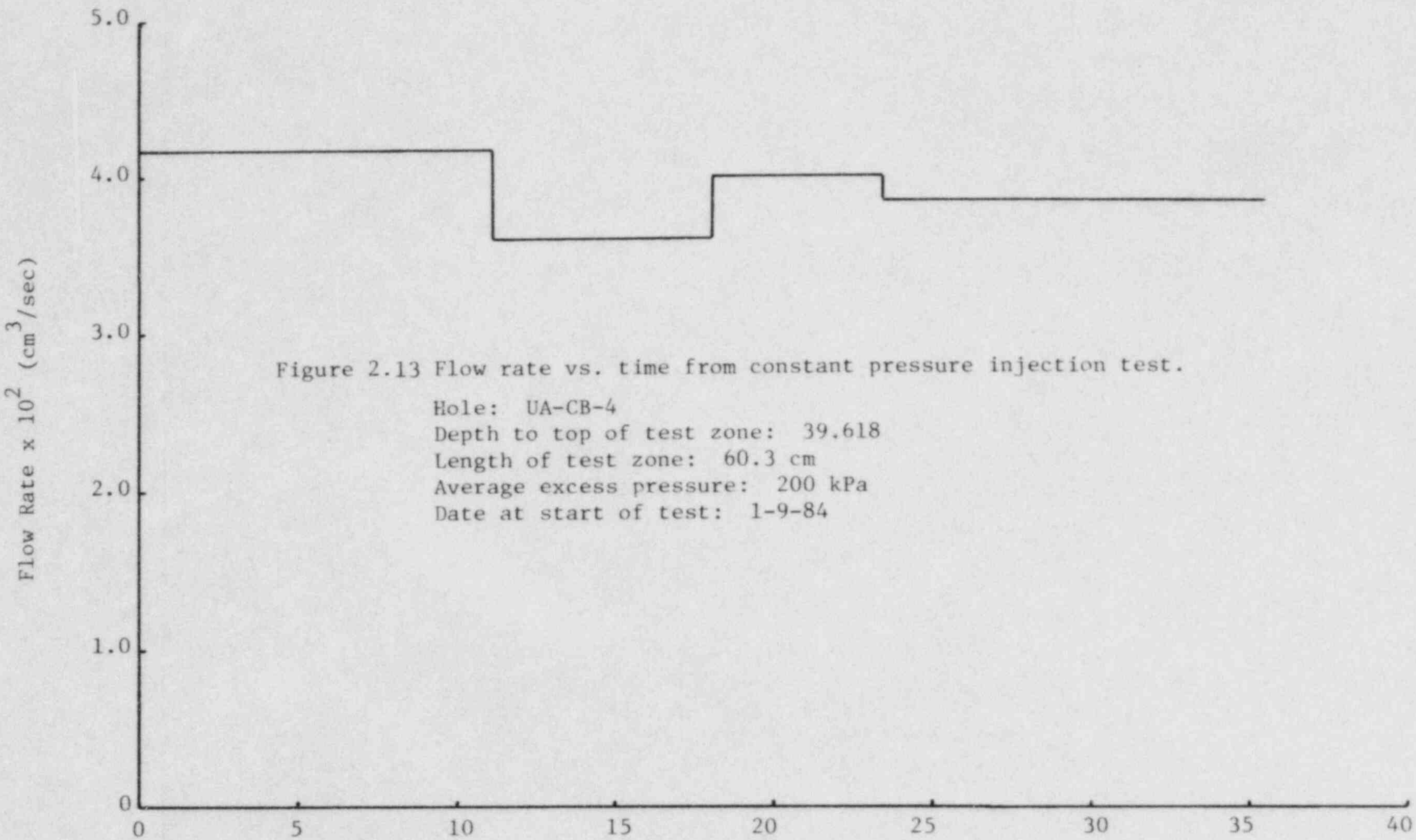

Figure 2.13 Flow rate vs. time from constant pressure injection test.

Hole: UA-CB-4
Depth to top of test zone: 39.618
Length of test zone: 60.3 cm
Average excess pressure: 200 kPa
Date at start of test: 1-9-84

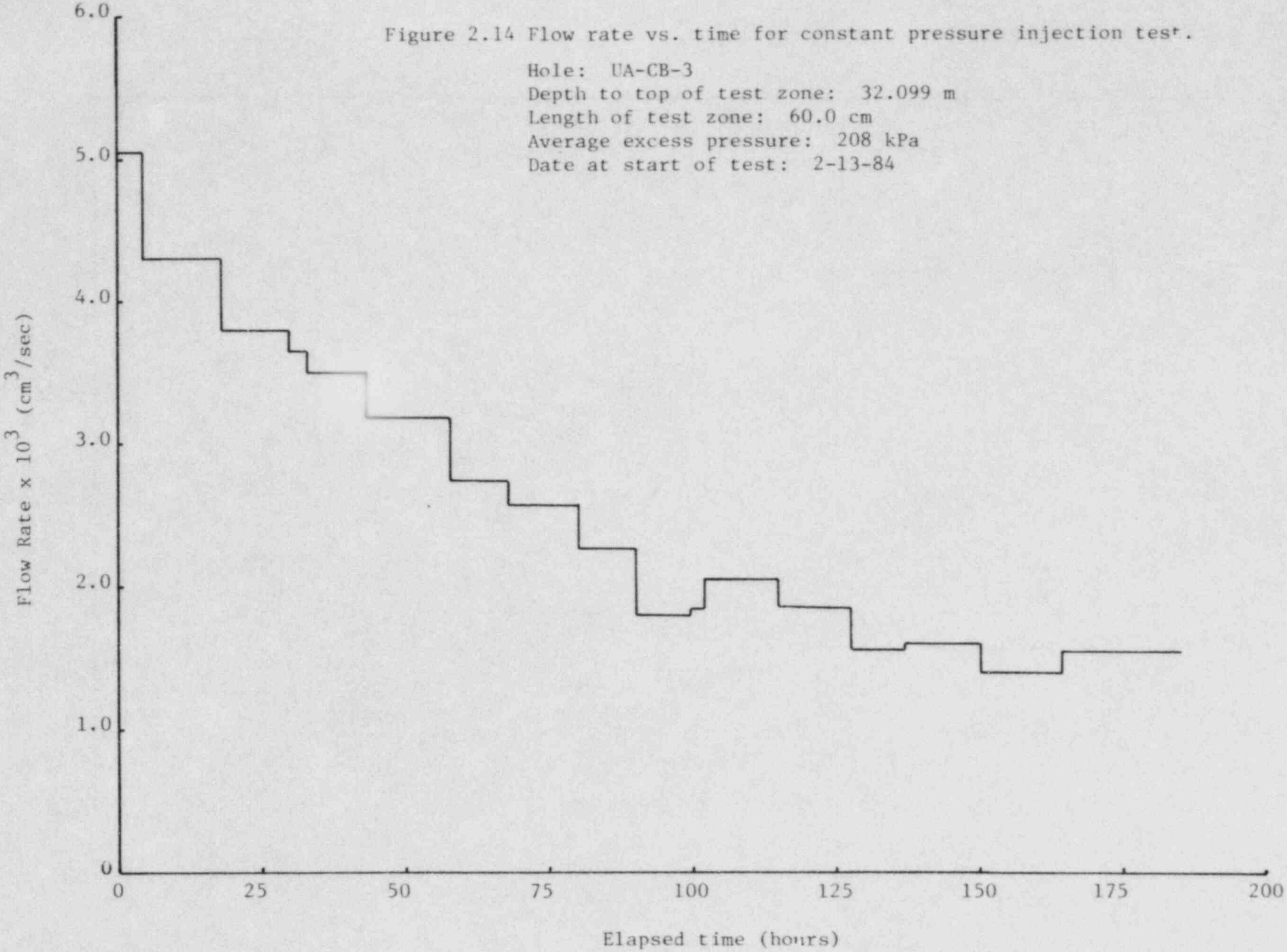

Figure 2.14 Flow rate vs. time for constant pressure injection test.

Hole: UA-CB-3
Depth to top of test zone: 32.099 m
Length of test zone: 60.0 cm
Average excess pressure: 208 kPa
Date at start of test: 2-13-84

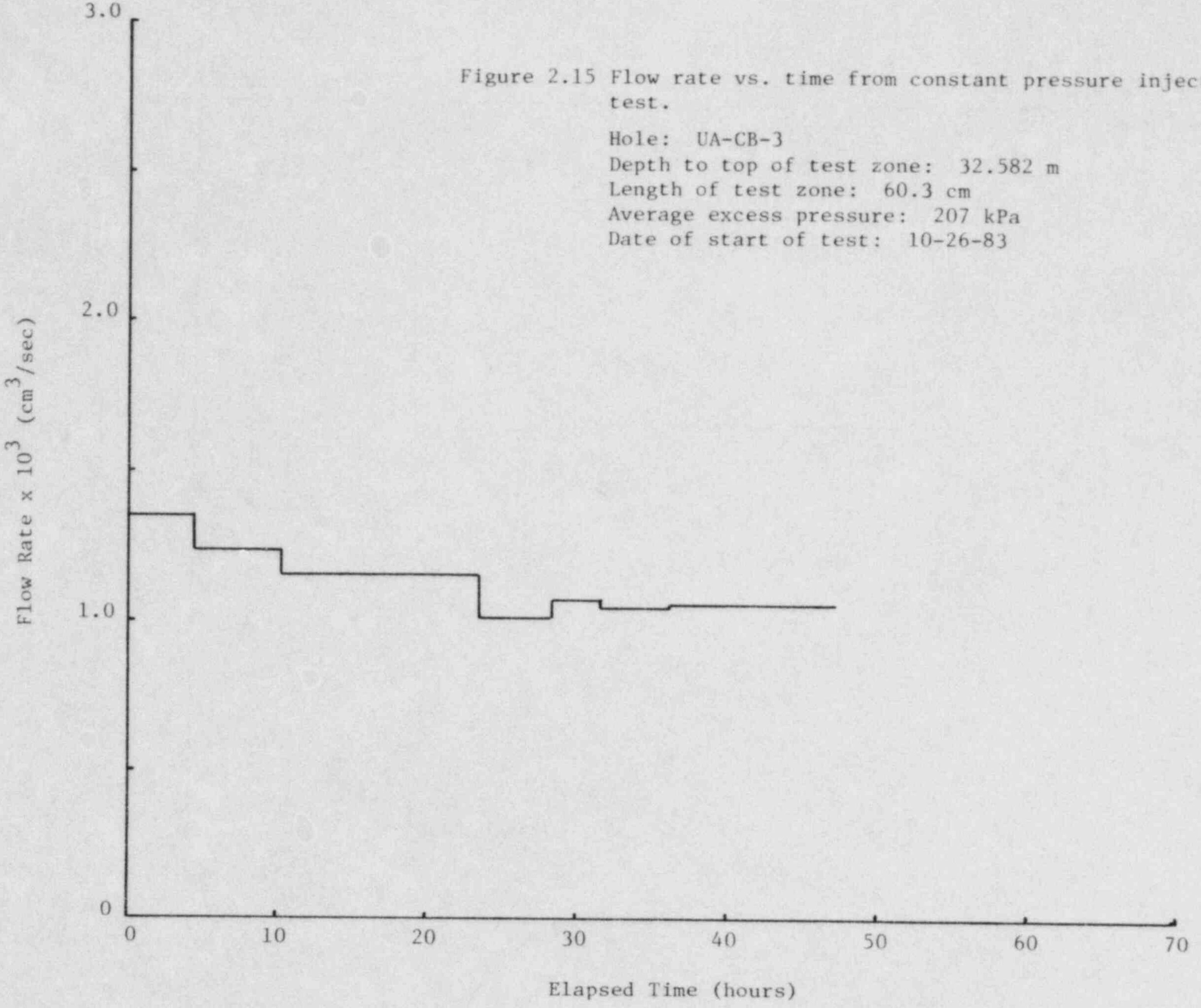

Figure 2.15 Flow rate vs. time from constant pressure injection test.

Hole: UA-CB-3
Depth to top of test zone: 32.582 m
Length of test zone: 60.3 cm
Average excess pressure: 207 kPa
Date of start of test: 10-26-83

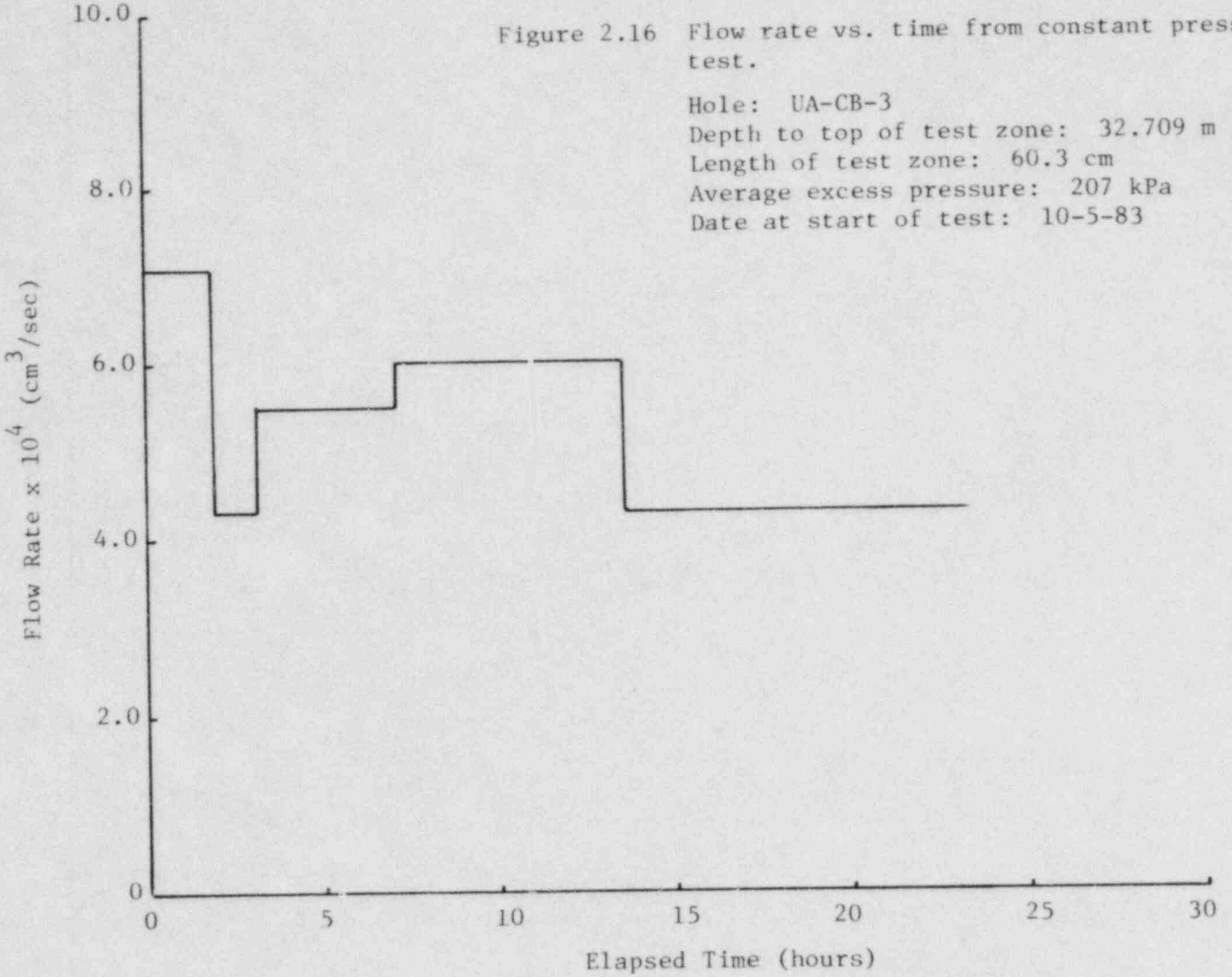

Figure 2.16 Flow rate vs. time from constant pressure injection test.

Hole: UA-CB-3
Depth to top of test zone: 32.709 m
Length of test zone: 60.3 cm
Average excess pressure: 207 kPa
Date at start of test: 10-5-83

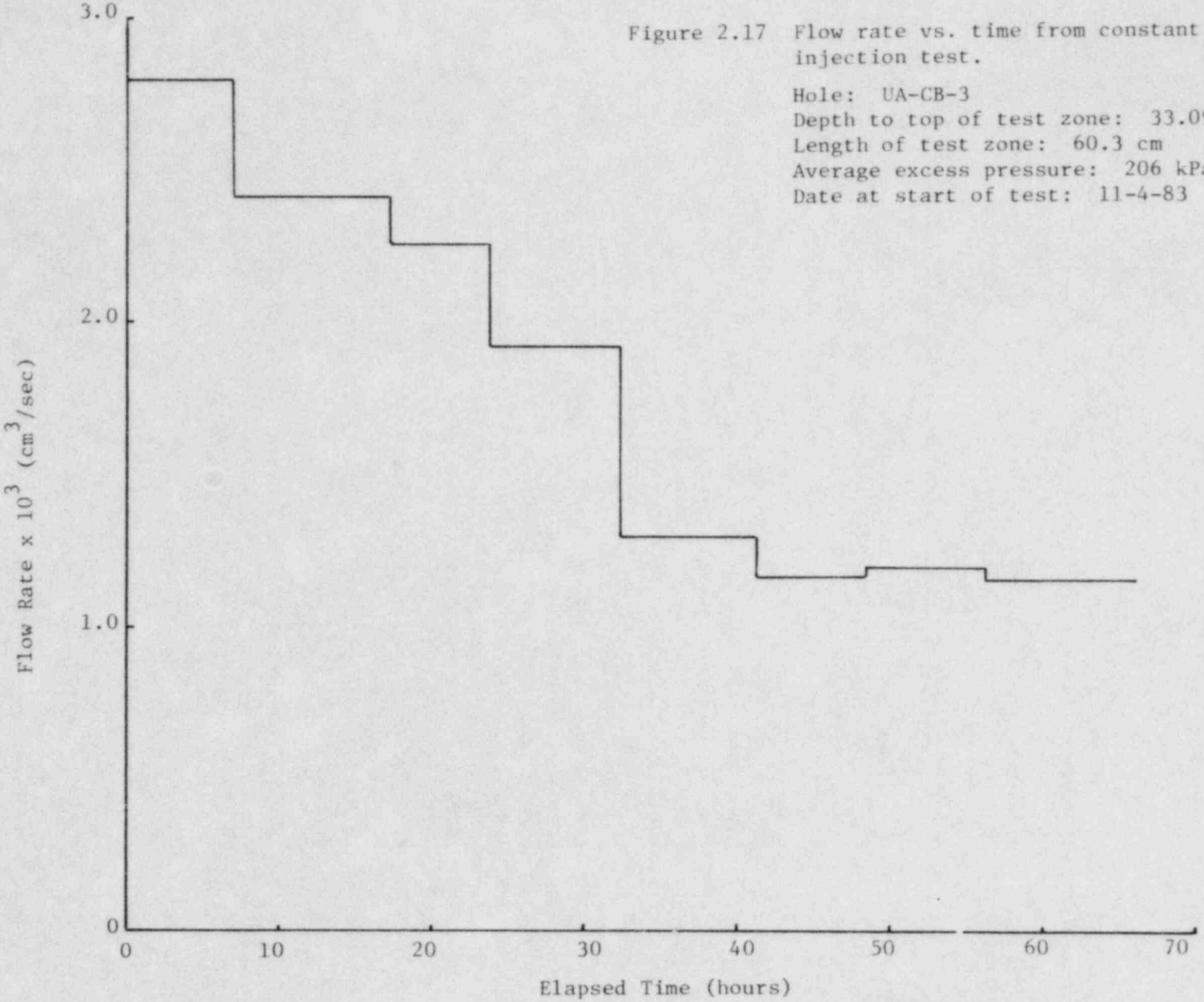

Figure 2.17 Flow rate vs. time from constant pressure injection test.

Hole: UA-CB-3
Depth to top of test zone: 33.090 m
Length of test zone: 60.3 cm
Average excess pressure: 206 kPa
Date at start of test: 11-4-83

Equivalent hydraulic conductivity values based on the packer test results are presented in Tables 2.13 - 2.15.

2.2.6 Plug Emplacement

2.2.6.1 Borehole UA-CB-1

Placement of the plug took place on September 20 and 22, 1983. On the first day, PVC bracing and a below-plug instrument package were placed. On the second day, gravel, sand and foam rubber layers were placed on top of the instrument package to form a bed for the cement, which was then placed using a dump bailer. Finally, a pneumatic packer was inflated just above the curing cement; the packer remained in place during an eight day curing period.

2.2.6.1.1 Below Plug Instrumentation Package and PVC Pipe Support

An instrument package placed below the plug consisted of a remote tracer injector and a remote pressure-temperature recorder (Figure 2.18). Both instruments are described in Section 2.2.3.1.2. The tracer injector is capable of releasing two different tracer volumes at staggered times. The first tracer, m-trifluoromethylbenzoate (m-TFMBA), was set for discharge at 4:00 am on October 1 (256 hours after arming) and the second, trifluoroacetate (TFA), at 8:00 pm on October 10 (512 hours after arming). A gravel and sand retaining collar was attached to the upper end of the tracer injector canister. The tracer injector and pressure-temperature recorder were supported in the borehole by 2-inch schedule 40 PVC pipe which, in turn, rested on the bottom of the hole.

2.2.6.1.2 Gravel, Sand and Foam Rubber Layers. To form a suitable bed upon which to place the cement plug, approximately 21 cm (8.3 in) of pea gravel and sand were placed above the tracer canister and gravel-sand retainer. The gravel and sand layers are highly permeable and permit rapid dispersion of the tracers. A layer of foam rubber with a compressed thickness of about 5 cm (2 in) was placed above the gravel and sand layers. The foam layer was used because it was found in laboratory experimentation to largely eliminate the upward channeling of minute water streams through the plug. This effect is described in Daemen et al. (1983) (see also Section 2.4.1). Figure 2.18 shows the gravel, sand and foam layers.

2.2.6.1.3 Cement Preparation. Dowell System 1 cement (Cobb et al., 1981) was used for the plug. The cement was prepared in four separate batches, each batch consisting of the following:

**R, radius of influence, is not usually known precisely. However, Ziegler recommends use of a length between $\ell/2$ and ℓ. Since k_e depends on log R, even large errors in R will not significantly affect the computed value of k_e.

Table 2.13 Calculation of Equivalent Hydraulic Conductivity.[a] Borehole UA-CB-1.

Interval[b]		t_s*	Average Excess Pressure (H_0)**		$Q^{\#}$ ($\times 10^3$)	K_e† ($\times 10^9$)
Top (m)	Bottom (m)	(hours)	(kPa)	(cm of water)	(cm^3/sec)	(cm/sec)
39.592	40.198	24	207	2111	.884	2.7
39.929	40.536	24	208	2121	.485	1.5
40.437	41.043	24	208	2121	1.52	4.7

[a]Assuming homogeneous, isotropic porous medium and steady, laminar flow.

[b]Measured from top of borehole casing.

*Time after which it is assumed injection rate is steady.

**Average pressure above ambient for elapsed time > t_s.

#Average flow rate for elapsed time > t_s.

†Equivalent hydraulic conductivity = $\left[\frac{\ln(R/r_0)}{2\pi\ell}\right]\left(\frac{Q}{H_0}\right)$, where $R = \ell = 60.6$ cm and $r_0 = 5.0$ cm.

Table 2.14 Calculation of Equivalent Hydraulic Conductivity.[a] Borehole UA-CB-4.

Interval[b] Top (m)	Interval[b] Bottom (m)	t_s[™] (hours)	Average Excess Pressure* (kPa)	Average Excess Pressure* (H_0, cm of water)	$Q^{\#}$ ($\times 10^3$) (cm^3/sec)	K_e[†] ($\times 10^9$) (cm/sec)
37.586	38.189	30	206.9	2110	.801	2.5
38.094	38.697	30	206.8	2110	.930	2.9
38.602	39.205	65	215.1	2190	.0387	0.12
39.110	39.713	35	215.9	2200	.0708	0.21
39.618	40.221	15	202.7	2070	38.4	120

[a] Assuming homogeneous, isotropic porous medium and steady, laminar flow.

[b] Measured from top of borehole casing.

[™] Time after which it is assumed injection rate is steady.

* Average pressure above ambient for elapsed time > t_s.

\# Average flow rate for elapsed time > t_s.

[†] Equivalent hydraulic conductivity = $\left[\frac{\ln(R/r_0)}{2\pi \ell}\right]\left(\frac{Q}{H_0}\right)$, where $R = \ell = 60.3$ cm and $r_0 = 5.0$ cm.

Table 2.15 Calculation of Equivalent Hydraulic Conductivity.[a] Borehole UA-CB-3.

Interval[b] Top (m)	Interval[b] Bottom (m)	t_s[**] (hours)	Average Excess Pressure[*] (kPa)	Average Excess Pressure[*] (H_0, cm of water)	Q[#] ($\times 10^3$) (cm^3/sec)	K_e[†] ($\times 10^9$) (cm/sec)
32.099	32.699	130	206.8	2110	1.53	4.8[¶]
32.582	33.185	25	206.9	2110	1.05	3.3
32.709	33.312	15	205.0	2090	.429	1.3
33.090	33.693	35	205.9	2100	1.19	3.7

[a]Assuming homogeneous, isotropic porous medium and steady, laminar flow.

[b]Measured from top of borehole casing.

[**]Time after which it is assumed injection rate is steady.

[*]Average pressure above ambient for elapsed time > t_s.

[#]Average flow rate for elapsed time > t_s.

[†]Equivalent hydraulic conductivity = $\left[\frac{\ln(R/r_0)}{2\pi\ell}\right]\left(\frac{Q}{H_0}\right)$, where $R = \ell = 60.3$ cm and $r_0 = 5.0$ cm.

[¶]Based on $R = \ell = 60.0$ cm.

Figure 2.18 Schematic of borehole UA-CB-1 with cement plug, below-plug instrumentation and support bracing.

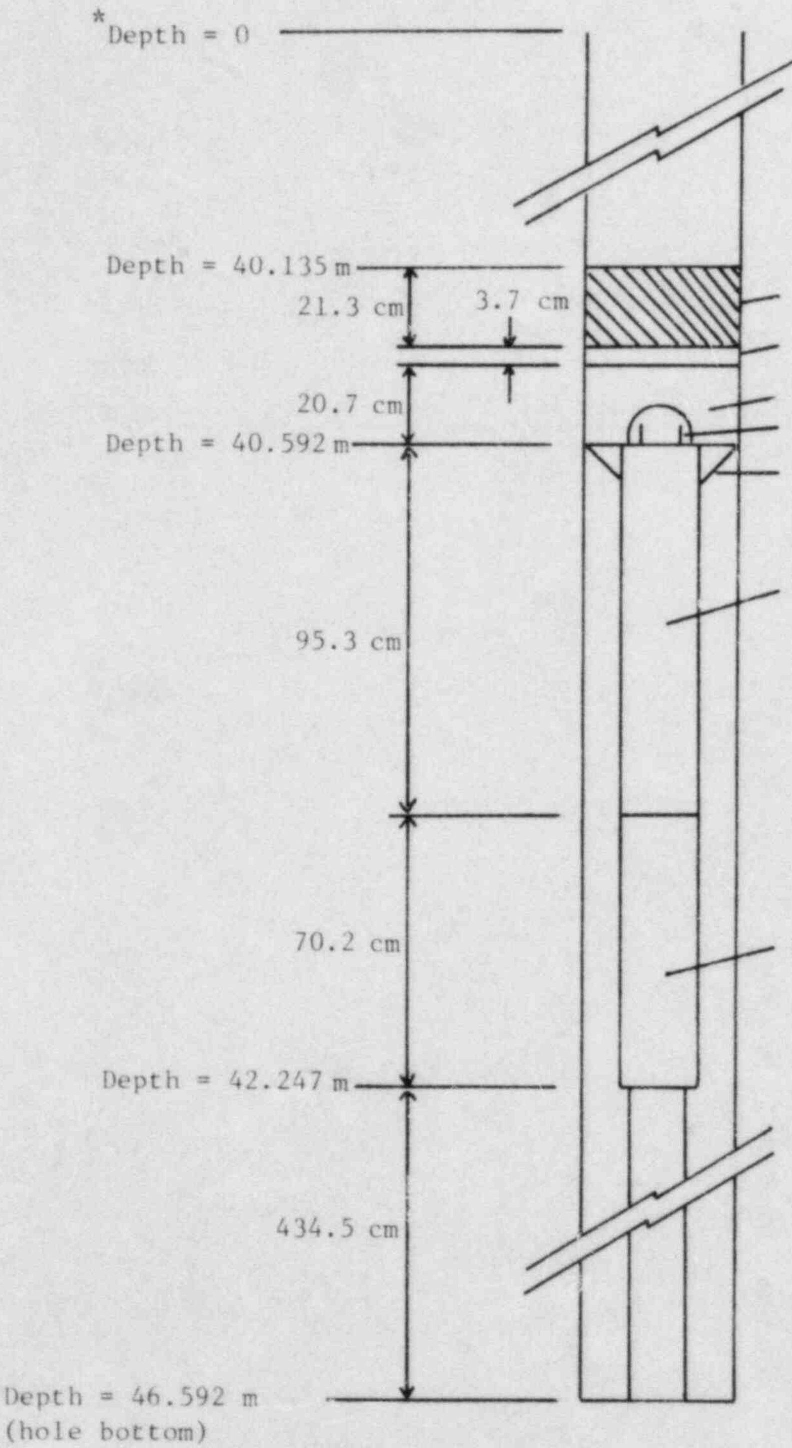

*Depths measured from top of casing

Vertical scale: 1 in = 50 cm
Not to scale horizontally

(1) 555 gm (1.22 lbs) of System 1 cement,
(2) 250 ml (8.45 fl oz) of distilled water, and
(3) 18 drops of D-47 antifoaming agent.

The ingredients of each batch were mixed in accord with established laboratory procedures for System 1 cement preparation (Daemen et al., 1981), except that a different blender model was used. As each batch was prepared, it was poured into a clean rubber bucket and stirred. After the four batches were prepared and added to the bucket the entire mix was stirred for two minutes. The mix was then slowly poured into the dump bailer. The bailer is a 1.57 m (5.15 ft) length of 7.6 cm (3.0 in) i.d. stainless steel pipe. The upper end of the bailer has a handle for attachment of a lowering cable. The lower end has a 3.3 cm (1.30 in) opening which is plugged by a rubber stopper. The stopper may be removed to release the cement by pulling on a cord attached to the stopper. The upper end of the bailer is open. After placing the mixed cement slurry into the bailer, the remainder of the bailer volume was slowly filled with distilled water.

2.2.6.1.4 Plug Emplacement with Bailer Using a hand winch, the filled bailer was lowered slowly into the borehole until it rested upon the foam layer. To release the cement, the plug at the lower end of the bailer was pulled and the bailer then very slowly raised to the surface. Finally, about four hours after the cement was placed, a packer with open mandrel was inflated just above the plug in order to duplicate stress conditions within the borehole during curing that would be encountered during later plug testing. The packer was left in place for eight days.

2.2.6.2 Borehole UA-CB-4

Placement of the plug took place on February 13, 14 and 15, 1984. On the first day the timer of the tracer injector was set and the canister enclosing the injector sealed. On February 14 the tracer injector with its PVC pipe support was placed. Next, layers of gravel, sand and, finally, foam rubber were placed above the tracer injector to form a bed for the cement. Cement was mixed and lowered into the hole in a dump bailer. When the bailer came to rest on the foam bedding surface, the cord attached to the stopper at the base of the bailer was pulled. As virtually no resistance to the pull was encountered it was evident that the cement had been released prematurely. Water samples were taken at depths of 15, 23 and 30 m (50, 75 and 100 ft) and each was found to contain significant cement residue. It was decided to flush the hole to remove as much cement as possible. The hole was pumped vigorously for about 1 hour on February 14. It was pumped again for 1 hour on February 15. Following the second pumping, additional foam was placed in the hole, cement was mixed, lowered down the hole in the bailer and properly released. On February 16, a pneumatic packer with open mandrel was inflated just above the curing cement. The packer remained in place during a 7 day curing period.

2.2.6.2.1 Below-plug Instrumentation Package and PVC Pipe Support. The instrumentation package placed below the plug in UA-CB-4 consisted of only a tracer injector. The tracer injector is described in Section

2.2.3.1.2. The tracer injector is capable of discharging two tracer samples at staggered times. The first tracer, heptaflurobutyric acid (HFBA), was set for discharge at 4:00 am on February 24 (256 hours after arming) and the second, pentafluorobenzoic acid (PFB), at 8:00 pm on March 5 (512 hours after arming).

The tracer injector used in UA-CB-4 (and also the unit used in UA-CB-3) had several improvements over the injector used in UA-CB-1, which apparently fired or leaked prematurely (Section 2.2.7.3.1). The improvements were as follows: (1) A check valve requiring 69 kPa (10 psi) to open (in direction of tracer flow) was added outside each solenoid valve. The check valve should reduce the likelihood that tracer leaking through a closed solenoid valve will contact the water environment. (2) Separate battery packs to operate each of the solenoid valves and the timer were utilized. In UA-CB-1, a single battery pack operated both valves and the timer. (3) Several improvements in the procedure used to load the tracers were also made which should reduce the likelihood for accidental contamination of the exterior of the injection device during loading. A gravel-and-sand retaining collar was attached to the upper end of the tracer injector canister. Figure 2.19 shows the tracer injector with its PVC pipe support.

<u>2.2.6.2.2 Gravel, Sand and Foam Layers</u>. A total thickness of about 21 cm (8.3 in) of pea gravel and sand were placed above the tracer injector canister and gravel-sand retaining collar. During plug placement it is likely that some sand and gravel were lost due to the flushing of the borehole and to slippage past the gravel-sand retainer. A layer of foam rubber with a compressed thickness of about 5 cm (2 in) was placed above the sand and gravel layers. After the borehole was flushed and before the second cement placement was made, an additional 5 cm (2 in) of foam was placed. Figure 2.19 shows the gravel, sand and foam layers after the second placement of cement.

<u>2.2.6.2.3 Cement Preparation</u>. The same procedure for cement preparation and filling of the bailer as used in borehole UA-CB-1 (Section 2.2.6.1.3) was followed in both attempts to place the plug in UA-CB-4.

<u>2.2.6.2.4 Plug Emplacement with Bailer</u>. Using an electric winch, the filled bailer was lowered slowly into the borehole until it rested upon the foam layer. On the first attempt, when the stopper cord was pulled there was little or no resistance, suggesting strongly that the stopper had pulled free prematurely. On the second attempt, resistance was felt before the stopper suddenly pulled free. After pulling the stopper the bailer was raised very slowly to the surface. Approximately 20 hours after the second cement placement, a packer with open mandrel was inflated just above the plug. The packer remained in place for 7 days.

2.2.6.3 Borehole UA-CB-3

Placement of the plug occurred on February 20-22, 1984. Instrumentation placed beneath the plug consisted of a remote pressure-temperature recorder as well as a tracer injector. On February 20, the timer of the pressure-temperature recorder was set and the canister enclosing the recorder sealed. On February 21, the tracer injector timer was

Figure 2.19 Schematic of borehole UA-CB-4 with cement plug, below-plug instrumentation and support bracing.

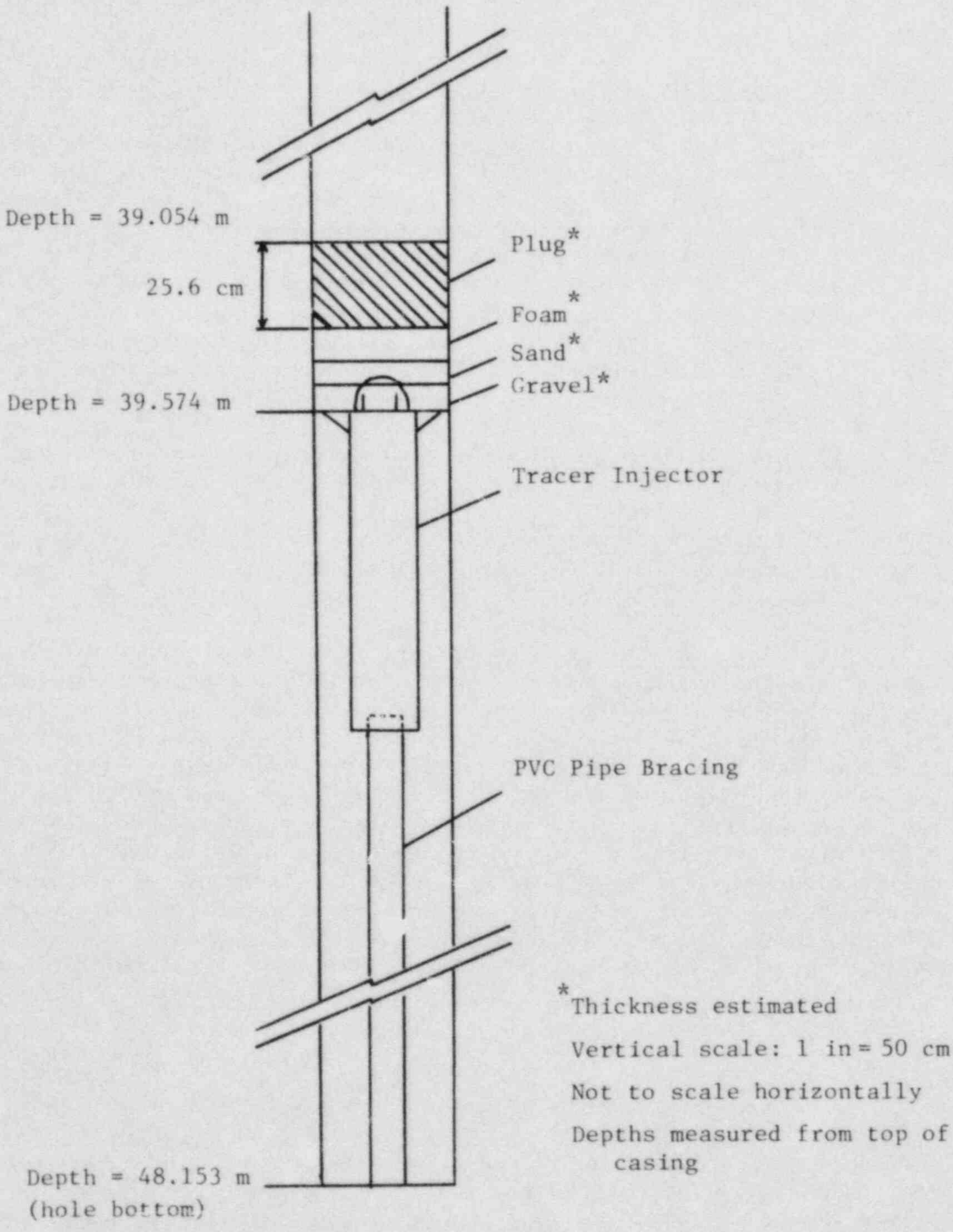

activated and the injection unit was sealed in its canister. Also on February 21, the pressure-temperature recorder and tracer injector, along with PVC pipe to support the instruments, were positioned in the borehole. On February 22, the layers of gravel, sand and foam were placed, followed by placement of the cement. Placement of the cement proceeded smoothly until withdrawal of the bailer . Considerable upward force using a hand winch was required before the bailer could be moved from the foam bedding surface. As increasing force was applied to the bailer it suddenly broke free. It was then raised slowly and easily to the surface. About 18 hours after removal of the bailer a packer with open mandrel was inflated just above the plug. The packer remained in place for 6 days as the plug cured.

2.2.6.3.1 Below-plug Instrumentation Package and PVC Pipe Support. The below-plug instrumentation consisted of a remote tracer injector and a remote pressure-temperature recorder. Both instruments are described in Section 2.2.3.1.2. The tracers used in the injector were sodium thiocyanate (to be released at 5:26 pm on March 2, 256 hours after arming) and pentafluoropropionic acid (to be released at 9:26 am on March 13, 512 hours after arming). About 10 ml of the sodium thiocyanate tracer were released during preparation procedures. All parts of the injector apparatus and canister which were exposed to the tracer were washed as thoroughly as possible. The tracer injector, pressure-temperature recorder and PVC pipe support are shown in Figure 2.20.

2.2.6.3.2 Gravel, Sand and Foam Layers. The gravel, sand and foam layers are shown in Figure 2.20. (See also Section 2.2.6.1.2.).

2.2.6.3.3 Cement Preparation. The same procedures for preparing the cement and filling the bailer were followed in borehole UA-CB-3 as in UA-CB-1 (see Section 2.2.6.1.3).

2.2.6.3.4 Plug Emplacement with Bailer. The filled bailer was lowered slowly into the borehole using a hand winch. When the bailer came to rest on the foam layer the stopper cord was pulled. Resistance to pulling was felt until the stopper suddenly pulled free. The winch was then used to raise the bailer. Upward force considerably in excess of the submerged weight of the bailer and winch cable was applied before the bailer suddenly broke free and began to move upward. Once free, the bailer was raised very slowly to the surface. It appears that foam may have become wedged between the outside of the bailer and the borehole wall so that a vacuum was created when the bailer was pulled upward. Approximately 18 hours after removing the bailer a pneumatic packer was inflated just above the curing cement. The packer remained in place for 6 days.

2.2.7 Plug Testing

2.2.7.1 Instrumentation

Testing is accomplished using the plug tester unit shown schematically in Figure 2.21. The unit is lowered into the borehole so as to be within 1 cm (0.4 in) of the top of the plug. With the gas-operated

Figure 2.20 Schematic of borehole UA-CB-3 with cement plug, below-plug instrumentation and support bracing.

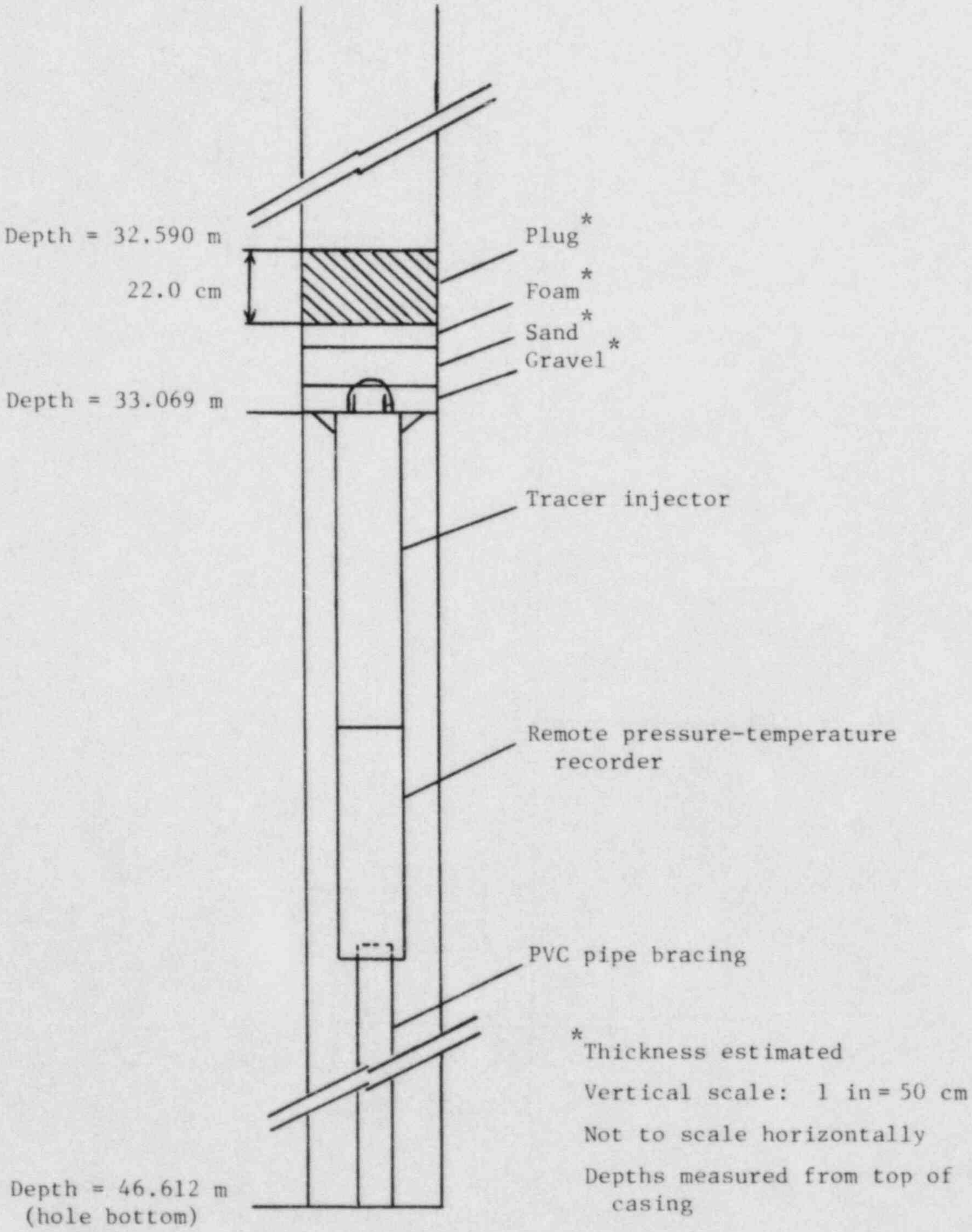

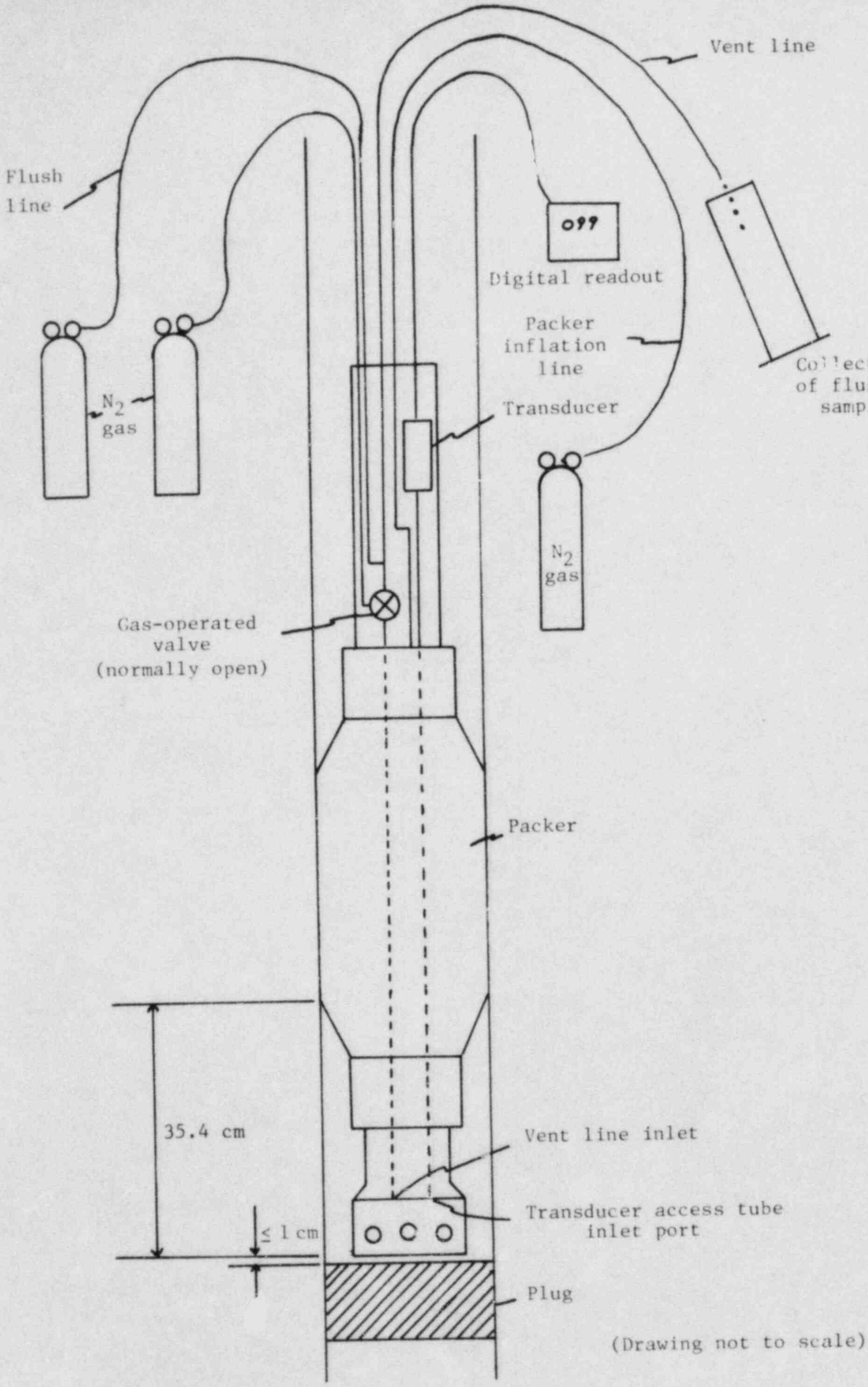

Figure 2.21 Schematic of plug tester unit.

valve on the vent line open, the packer is inflated. The zone between the packer membrane and the top of the plug is the test zone. The test zone is completely filled with water and is initially at hydrostatic pressure equal to the depth of the test zone below the water level in the hole. Next, the gas-operated valve is closed and the flush line is pressurized using compressed nitrogen gas. The pressurization flushes water from both the flush and vent lines above the gas-operated valve. The gas-operated valve is then opened and the pressure in the test zone is immediately reduced to approximately that of a column of water of height equal to the height of the gas-operated valve above the test zone. At this point, the test zone is at a lower pressure than the surrounding formation.* It also is at a pressure lower than that in the borehole below the plug.** Water flow is thus induced into the test zone from both the formation adjacent to the test zone and through the plug and plug/formation interface. With the gas-operated valve open and assuming there is negligible compression of water, the inflow volume to the test zone is simply that which fills the flush and vent lines above the gas-operated valve.

2.2.7.2 Test Procedure

The plug tester unit is used to perform three basic tests: tracer travel time, fluid build-up and pressure build-up tests. These tests are the same as those used in the Bell Canyon Test conducted by Sandia National Laboratories (Christensen and Peterson, 1981). The tests, as applied to University of Arizona plug experiments, are discussed in South et al. (1982).

2.2.7.2.1 Tracer Travel Time Test. The purpose of this test is to determine the time of first arrival of a tracer (released below the plug) to the test zone. The test is scheduled so that tracer release (release times are known) and detection occur during a period of fluid build-up testing. The test is performed by removing water samples from the test zone on a regular basis and having them analyzed for the concentration of the tracers. Samples are obtained when water is flushed in the fluid build-up test.

2.2.7.2.2 Fluid Build-up Test. The purpose of the fluid build-up test is to determine the volumetric inflow rate to the test zone under relatively steady pressure conditions. The test is initiated by closing the gas-operated valve, flushing the flush and vent lines, opening the gas-operated valve and monitoring the rise in test zone pressure. The rise in test zone pressure is directly proportional to the rise of water

---

*The ambient pressure in the formation at any depth below the water table is usually, but not always, equal to hydrostatic pressure for that depth.

**Pressure on the lower side of the plug is generally equal to hydrostatic pressure for the depth of the plug's lower side below the water table.

level in the vent and flush lines and hence proportional to the volumetric inflow to the test zone. After a sufficient* rise in test zone pressure (ΔP_R), the gas-operated valve is again closed, the lines flushed, the expelled water collected and its volume measured. The gas-operated valve is re-opened and the drop in test zone pressure (ΔP_D) is noted. The volume flushed is proportional to ΔP_D. The inflow rate over the period of rise in test zone pressure (Δt) may then be estimated using the volume flushed, ΔP_R, ΔP_D and Δt (see Section 2.2.7.3.2). With the gas-operated valve re-opened, test zone pressure again begins to rise and the procedure may be repeated.

2.2.7.2.3 Pressure Build-up Test. This test is performed as follows:

(1) close the gas-operated valve

(2) flush the flush and vent lines

(3) open the gas-operated valve briefly to reduce test zone pressure

(4) close gas-operated valve and monitor the rise in pressure.

Pressure rise will continue until the ambient pressure for the test zone depth is reached.

2.2.7.3 Plug Test Results

2.2.7.3.1 Tracer Travel Time Test. Results of the tracer test for the plug in UA-CB-1 were inconclusive. It appears that the injection device fired or leaked prematurely. It is also possible that contamination of the outside of the canister, especially the exterior of the solenoid valve ports, may have occurred during loading of the tracer. Results of the tracer tests in boreholes UA-CB-4 and UA-CB-3 have not yet been fully analyzed.

2.2.7.3.2 Fluid Build-up Test

Borehole UA-CB-1. Table 2.16 summarizes the results of fluid build-up testing for the period September 30, 1983 - February 24, 1984. In the table, an estimate is made of the average test zone inflow rate for each time period of pressure rise Δt between successive flushings. The inflow occurring between any two successive flushings is estimated by multiplying the volume of the second flushing by the pressure rise (ΔP_R) between the flushings and dividing by the pressure drop (ΔP_D) which occurred when the gas-operated valve was opened after the second flushing. The estimated inflow rate is then equal to the inflow volume divided by the time period Δt. Figures 2.22 and 2.23 are

---

*The rise in pressure should be large enough to allow collection of an adequate sample for tracer analysis and to allow a convenient time interval between flushings. ΔP_R should also be small enough so that the pressure gradient causing flow into the test zone is relatively constant.

Table 2.16 Estimated Average Test Zone Inflow Rate for Borehole UA-CB-1

Date/Time	Elapsed Time (days)	Action[a]	Δt^b (days)	$P_{TEST}{}^c$ (units)	$P_{TEST}{}^c$ (kPa)	$\Delta P_R{}^d$ (units)	$\Delta P_D{}^e$ (units)	$V_F{}^f$ (ml)	$V^g = \frac{V_F \Delta P_R}{\Delta P_D}$ (ml)	$Q^h = \frac{V}{\Delta t}$ (ml/days)
9-30/2339	0			75	17.2					
		R	.43			10			10.7	25
10-1/1000	.43			85	19.5					
		D					15	16		
10-1/1005	.43			70	16.1					
		R	1.30			11			11.0	8.5
10-2/1723	1.74			81	18.6					
		D					10	10		
10-2/1723	1.75			71	16.3					
		R	1.19			13			18.2	15
10-3/2200	2.93			84	19.3					
		D					5	7		
10-3/2210	2.93			79	18.2					
		R	1.48			13			14.9	10
10-5/0934	4.41			92	21.1					
		D					7	8		
10-5/0940	4.42			85	19.5					
		R	3.93			29			30.9	7.9
10-9/0805	8.35			114	26.2					
		D					15	16		
10-9/0810	8.36			99	22.8					
		/								
10-9/0840	8.38									
		H								
10-9/0910	8.40									

Table 2.16 Estimated Average Test Zone Inflow Rate for Borehole UA-CB-1--Continued

Date/Time	Elapsed Time (days)	Action[a]	Δt[b] (days)	P_{TEST}[c] (units)	P_{TEST}[c] (kPa)	ΔP_R[d] (units)	ΔP_D[e] (units)	V_F[f] (ml)	$V^g = \frac{V_F \Delta P_R}{\Delta P_D}$ (ml)	$Q^h = \frac{V}{\Delta t}$ (ml/days)
10-9/0910	8.40			129	29.6					
		R	.993			32			32.5	33
10-10/0900	9.39			161	37.0					
		D					62	63		
10-10/0908	9.40			99	22.8					
		R	2.99			10			11.9	4.0
10-13/0848	12.38			109	25.1					
		D					16	19		
10-13/0852	12.38			93	21.4					
		R	3.98			19			16.9	4.2
10-17/0830	16.37			112	25.7					
		D					18	16		
10-17/0834	16.37			94	21.6					
		R	3.27			13			11.1	3.4
10-20/1503	19.64			107	24.6					
		D					14	12		
10-20/1524	19.66			93	21.4					
		R	3.71			22			23.7	6.4
10-24/0829	23.37			115	26.4					
		D					13	14		
10-24/0836	23.37			102	23.4					
		/								
10-24/1214	23.52									
		H								
10-24/1538	23.67									

Table 2.16 Estimated Average Test Zone Inflow Rate for Borehole UA-CB-1--Continued

Date/Time	Elapsed Time (days)	Action[a]	Δt^{b} (days)	$P_{TEST}{}^{c}$ (units)	$P_{TEST}{}^{c}$ (kPa)	$\Delta P_R{}^{d}$ (units)	$\Delta P_D{}^{e}$ (units)	$V_F{}^{f}$ (ml)	$V^{g} = \frac{V_F \; P_R}{\Delta P_D}$ (ml)	$Q^{h} = \frac{V}{\Delta t}$ (ml/days)
10-24/1538	23.67			88	20.2					
		R	3.72			22			18.2	4.9
10-28/0859	27.39			110	25.3					
		D					29	24		
10-28/0907	27.39			81	18.6					
		R	6.98			29			24.2	3.5
11-4/0836	34.37			110	25.3					
		D					24	20		
11-4/0842	34.38			86	19.8					
		R	4.01			19			16.6	4.1
11-8/0903	38.39			105	24.1					
		D					16	14		
11-8/0913	38.40			89	20.5					
		R	5.95			22			18.9	3.2
11-14/0757	44.35			111	25.5					
		D					21	18		
11-14/0806	44.35			90	20.7					
		R	1.04			2			1.75	1.7
11-15/0907	45.39			92	21.1					
		D					8	7		
11-15/0910	45.40			84	19.3					
		/								
11-15/1022	45.45									
		H								
11-15/1856	45.80									

Table 2.16 Estimated Average Test Zone Inflow Rate for Borehole UA-CB-1--Continued

Date/Time	Elapsed Time (days)	Action[a]	Δt[b] (days)	P_{TEST}[c] (units)	P_{TEST}[c] (kPa)	ΔP_R[d] (units)	ΔP_D[e] (units)	V_F[f] (ml)	$V^g = \frac{V_F \Delta P_R}{\Delta P_D}$ (ml)	$Q^h = \frac{V}{\Delta t}$ (ml/days)
11-15/1856	45.80			88	20.2					
		R	6.61			21			17.8	2.7
11-22/0938	52.42			109	25.1					
		D					26	22		
11-22/0944	52.42			83	19.1					
		R	6.95			25			22.5	3.2
11-29/0835	59.37			108	24.8					
		D					20	18		
11-29/0839	59.38			88	20.2					
		R	8.00			23			22.0	2.7
12-7/0844	67.38			111	25.5					
		D					22	21		
12-7/0851	67.38			89	20.5					
		R	7.01			21			21.0	3.0
12-14/0907	74.39			110	25.3					
		D					21	21		
12-14/0913	74.40			89	20.5					
		R	4.98			25			22.5	4.5
12-19/0849	79.38			114	26.2					
		D					20	18		
12-19/0855	79.39			94	21.6					
		R	4.99			26			20.8	4.2
12-24/0847	84.38			120	27.6					
		D					20	16		
12-24/0857	84.39			100	23.0					
		R	5.01			25			25.0	5.0
12-29/0909	89.40			125	28.7					
		D					26	26		

Table 2.16 Estimated Average Test Zone Inflow Rate for Borehole UA-CB-1--Continued

Date/Time	Elapsed Time (days)	Action[a]	Δt[b] (days)	P_{TEST}[c] (units)	P_{TEST}[c] (kPa)	ΔP_R[d] (units)	ΔP_D[e] (units)	V_F[f] (ml)	$V^g = \frac{V_F \Delta P_R}{\Delta P_D}$ (ml)	$Q^h = \frac{V}{\Delta t}$ (ml/days)
12-29/0915	89.40			99	22.8					
		R	6.97			53			65.6	9.4
1-5-84/0836	96.37			152	34.9					
		D					42	52		
1-5/0840	96.38			110	25.3					
		R	-			-			-	-
1-5/1013	96.44									
		H								
1-5/1815	96.78			140	32.2					
		R	0.64			13			22.2	35
1-6/0937	97.42			153	35.2					
		D					76	130		
1-6/1005	97.43			77	17.7					
		R	6.94			26			52.0	7.5
1-13/0835	104.37			103	23.7					
		D					16	32		
1-13/0842	104.38			87	20.0					
		R	9.98			25			47.5	4.8
1-23/0818	114.36			112	25.7					
		D					20	38		
1-23/0823	114.36			92	21.1					
		R	7.30			19			32.3	4.4
1-30/1533	121.66			111	25.5					
		D					20	34		
1-30/1538	121.67			91	20.9					
		R	7.70			20			37.8	4.9
2-7/0822	129.36			111	25.5					
		D					18	34		

Table 2.16 Estimated Average Test Zone Inflow Rate for Borehole UA-CB-1--Continued

Date/Time	Elapsed Time (days)	Action[a]	Δt^b (days)	P_{TEST}^c (units)	P_{TEST}^c (kPa)	ΔP_R^d (units)	ΔP_D^e (units)	V_F^f (ml)	$V^g = \frac{V_F \Delta P_R}{\Delta P_D}$ (ml)	$Q^h = \frac{V}{\Delta t}$ (ml/days)
2-7/0834	129.37			93	21.4					
		R	10.07			29			66.3	6.6
2-17/1018	139.44			122	28.0					
		D					21	48		
2-17/1023	139.45			101	23.2					
		R	7.39			24			50.1	6.8
2-24/1943	146.84			125	28.7					
		D					23	48		
2-24/1951	146.84			102	23.4					
2-24/2330	146.99			102	23.4					
		H								
2-24/2335	147.00									
		D								
2-24/2340	147.00			74	17.0					
		R								
2-25/2125	147.91			115	26.4					
		D								
2-25/2129	147.91			70	16.1					
2-25/2133	147.91			70	16.1					
		P								
3-12/0815	163.36			1022	235					
		DP								
3-12/0815	163.36			110	25.3					
3-12/0836	163.37			110	25.3					
		D						33		
3-12/0858	163.39			67	15.4					

Table 2.16 Estimated Average Test Zone Inflow Rate for Borehole UA-CB-1--Continued

Date/Time	Elapsed Time (days)	Action[a]	Δt[b] (days)	P_{TEST}[c] (units)	P_{TEST}[c] (kPa)	ΔP_R[d] (units)	ΔP_D[e] (units)	V_F[f] (ml)	$V^g = \frac{V_F \Delta P_R}{\Delta P_D}$ (ml)	$Q^h = \frac{V}{\Delta t}$ (ml/days)
		P*								
5-10/1737	222.75									
		D								
5-10/1741	222.75			44	10.1					
		R	1.70			48			35.7	21
5-12/1021	224.45			92	21.1					
		D					43	32		
5-12/1025	224.45			49	11.3					
		R	2.14			51			38.0	18
5-14/1342	226.59			100	23.0					
		D					51	38		
5-14/1346	226.59			49	11.3					
		R	1.99			48			38.8	19
5-16/1327	228.58			97	22.3					
		D					47	38		
5-16/1331	228.58			50	11.5					
		R	2.02			54			57.2	28
5-18/1358	230.60			104	23.9					
		D					51	54		
5-18/1402	230.60			53	12.2					
		R	3.01			70			60.6	20
5-21/1419	233.61			123	28.3					
		D					67	58		
5-21/1423	233.61			56	12.9					
		R	2.02			52			44.0	22
5-23/1451	235.63			108	24.8					
		D					52	44		
5-23/1455	235.64			56	12.9					
		R	1.95			51			40.8	21

Table 2.16 Estimated Average Test Zone Inflow Rate for Borehole UA-CB-1--Continued

Date/Time	Elapsed Time (days)	Action[a]	Δt[b] (days)	P_{TEST}[c] (units)	P_{TEST}[c] (kPa)	ΔP_R[d] (units)	ΔP_D[e] (units)	V_F[f] (ml)	$V^g = \frac{V_F \Delta P_R}{\Delta P_D}$ (ml)	$Q^h = \frac{V}{\Delta t}$ (ml/days)
5-25/1355	237.59			107	24.6					
		D					50	40		
5-25/1359	237.60			57	13.1					
		R	4.10			95			86.0	21
5-29/1632	241.70			152	34.9					
		D					84	76		
5-29/1636	241.71			68	15.6					
		R	1.87			49			48.0	26
5-31/1339	243.58			117	26.9					
		D					51	50		
5-31/1343	243.59			66	15.2					
		R	1.89			43			41.0	22
6-2/1104	245.48			109	25.1					
		D					44	42		
6-2/1108	245.48			65	14.9					
		R	2.14			42			37.4	17
6-4/1437	247.62			107	24.6					
		D					46	41		
6-4/1441	247.63			61	14.0					
		R	1.98			40			39.0	20
6-6/1414	249.61			101	23.2					
		D					41	40		
6-6/1418	249.61			60	13.8					
		R	1.99			43			48.7	24
6-8/1400	251.60			103	23.7					
		D					38	43		
6-8/1404	251.60			65	14.9					
		R	2.99			56			56.0	19
6-11/1346	254.59			121	27.8					

Table 2.16 Estimated Average Test Zone Inflow Rate for Borehole UA-CB-1--Continued

Date/Time	Elapsed Time (days)	Action[a]	Δt[b] (days)	P_{TEST}[c] (units)	P_{TEST}[c] (kPa)	ΔP_R[d] (units)	ΔP_D[e] (units)	V_F[f] (ml)	$V^g = \frac{V_F \Delta P_R}{\Delta P_D}$ (ml)	$Q^h = \frac{V}{\Delta t}$ (ml/days)
		D					48	48		
6-11/1350	254.59			73	16.8					
		R	2.00			37			39.7	20
6-13/1346	256.59			110	25.3					
		D					41	44		
6-13/1350	256.59			69	15.9					
		R	2.01			36				
6-15/1400	258.60			105	24.1			42		
		D								
6-15/1404	258.60									
		R								
6-16/0935	259.41									
		H								
6-16/1624	259.70									

NOTES:

[a]Action: R = test zone pressure rise; D = test zone pressure drop due to flushing; H = test zone at hydrostatic pressure equal to its depth below water table (about 360 kPa); P = pressure build-up test conducted (gas-operated valve closed); DP = pressure drop due to opening gas-operated valve after pressure build-up test; P* = inconclusive pressure build-up tests conducted (complications due to power outage and erratic transducer performance).

[b]Δt: Time period (between flushings) over which pressure rise occurs and over which average inflow rate is estimated.

[c]P_{TEST}: Test zone pressure (gage). Pressure expressed in digital readout units and kPa.

[d]ΔP_R: Pressure rise over period Δt.

Table 2.16 Estimated Average Test Zone Inflow Rate for Borehole UA-CB-1-- <u>Notes - Continued</u>

[e] ΔP_D: Pressure drop due to flushing.

[f] V_F: Volume expelled from flush and vent lines during flushing.

[g] V: Estimated inflow volume for period Δt.

[h] Q: Estimated average inflow rate over period Δt.

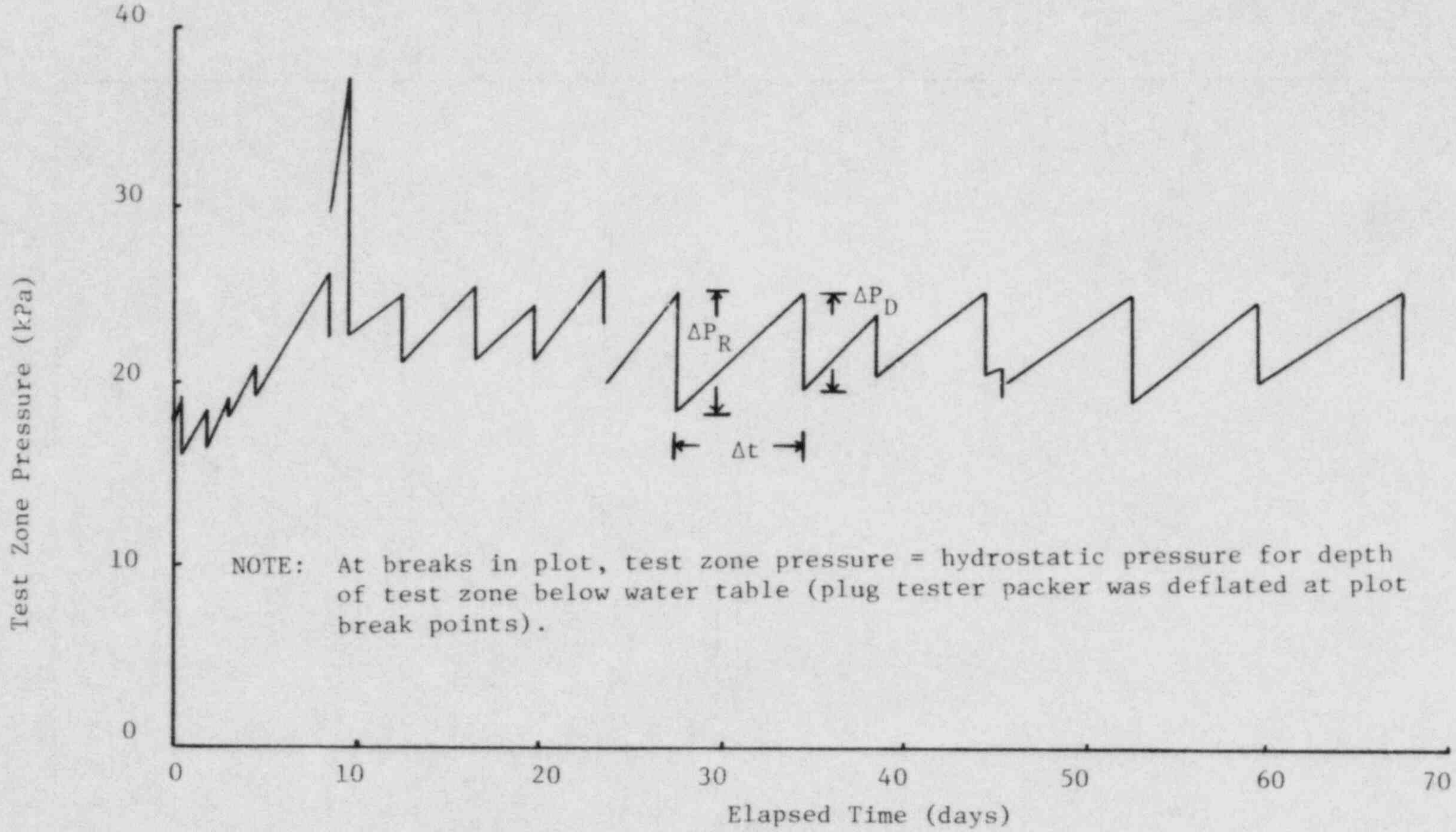

Figure 2.22 Test zone pressure vs. elapsed time for plug testing in borehole UA-CB-1. Date at start of testing: 9-30-83.

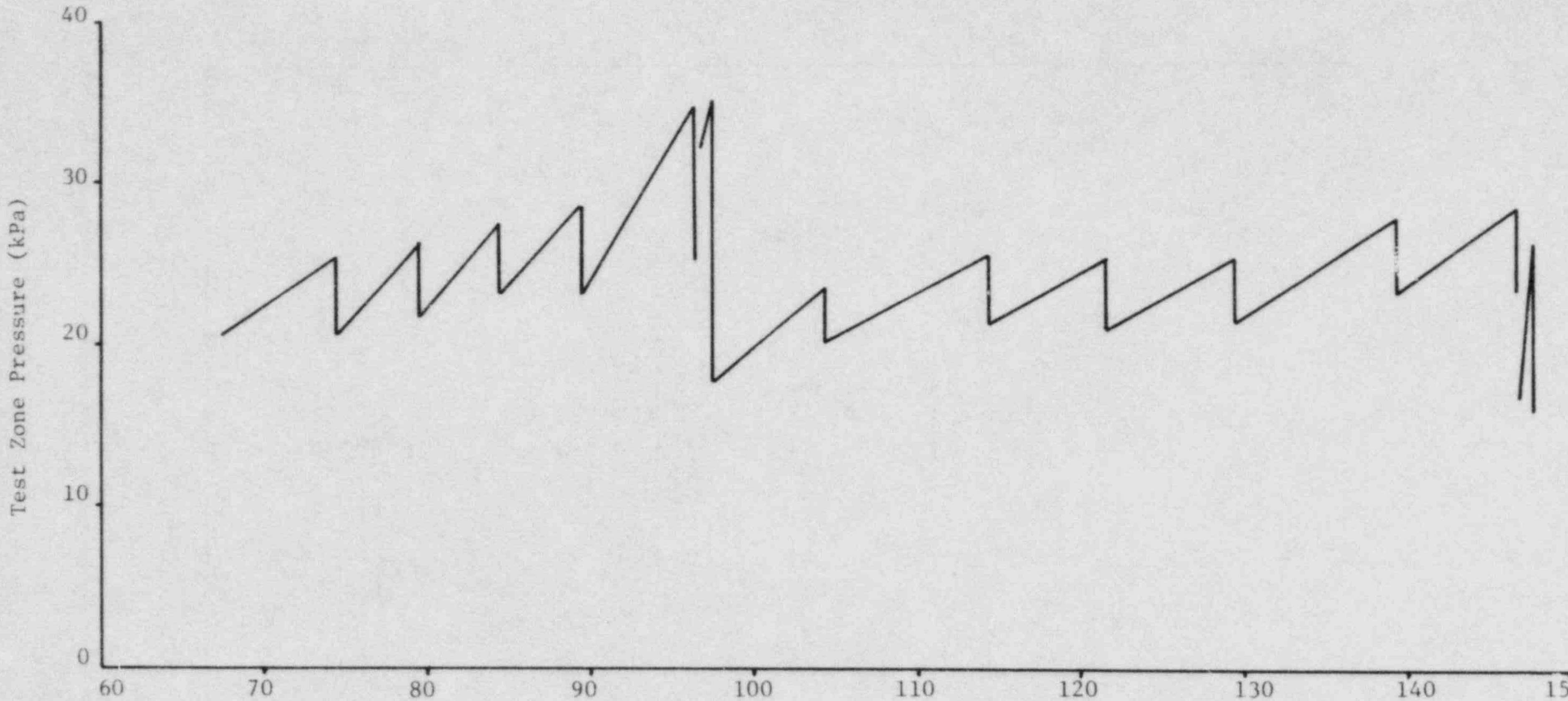

Figure 2.22 (cont.)

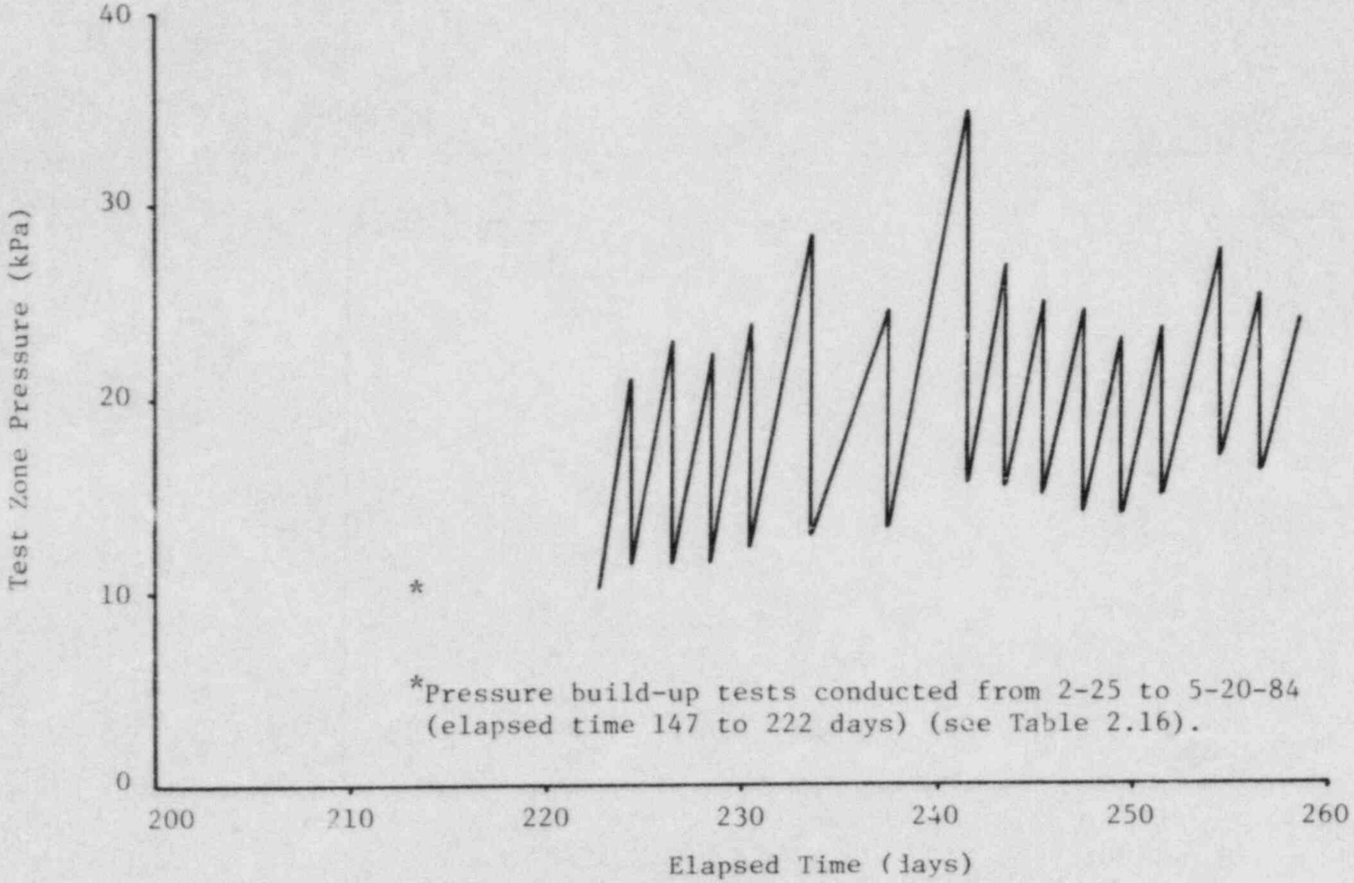

Figure 2.22 (cont.)

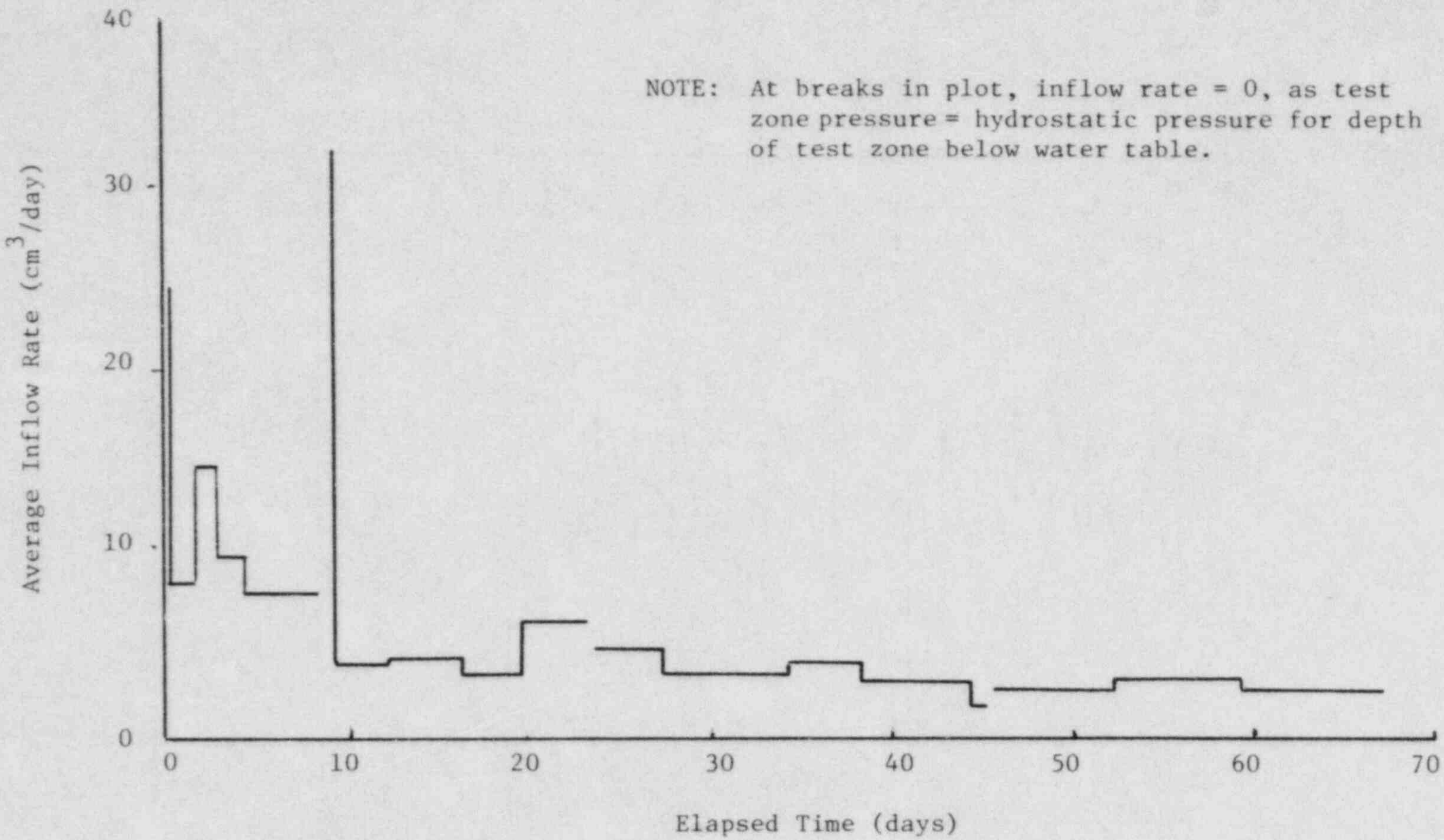

Figure 2.23 Average test zone inflow rate vs. elapsed time for fluid build-up testing in borehole UA-CB-1. Date at start of testing: 9-30-83.

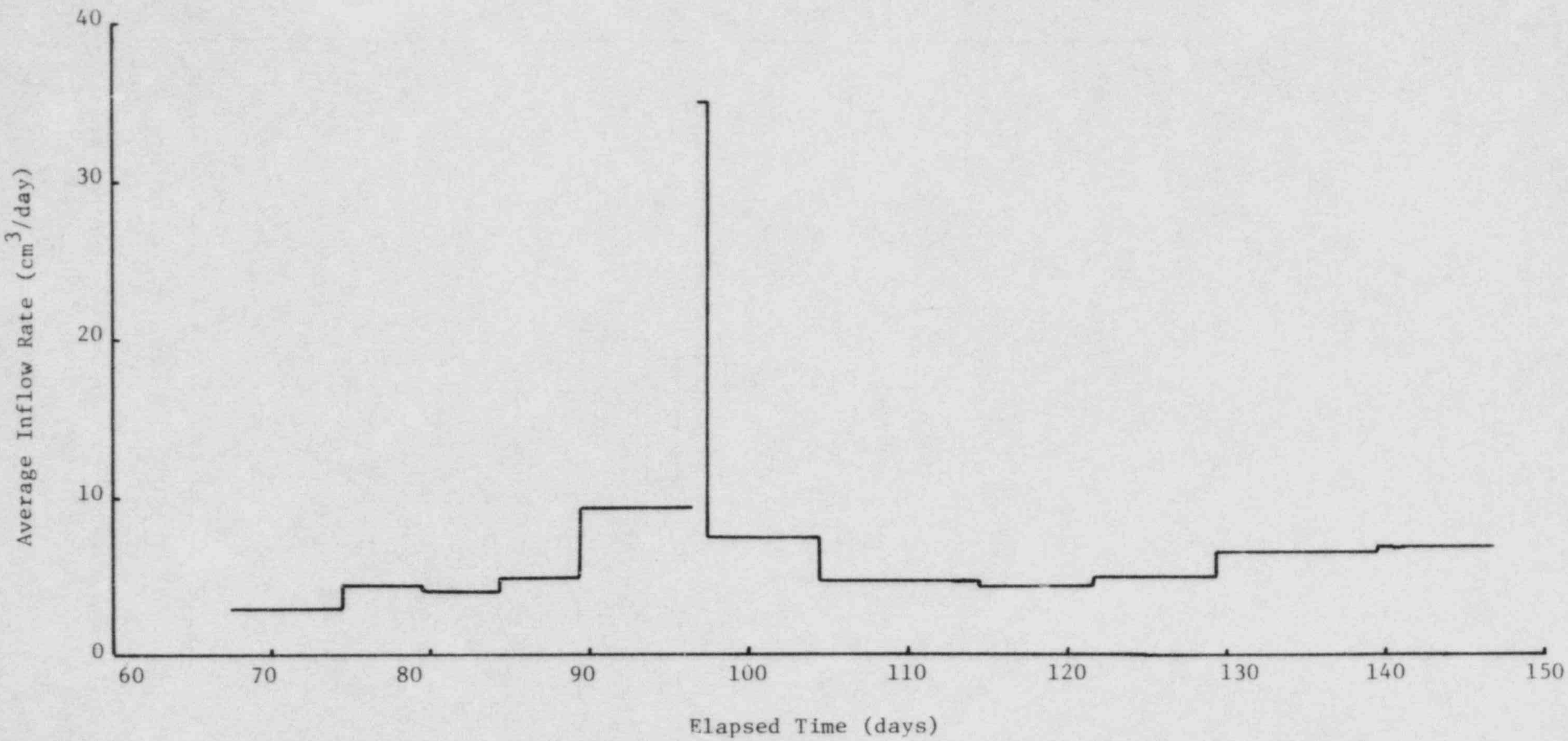

Figure 2.23 (cont.)

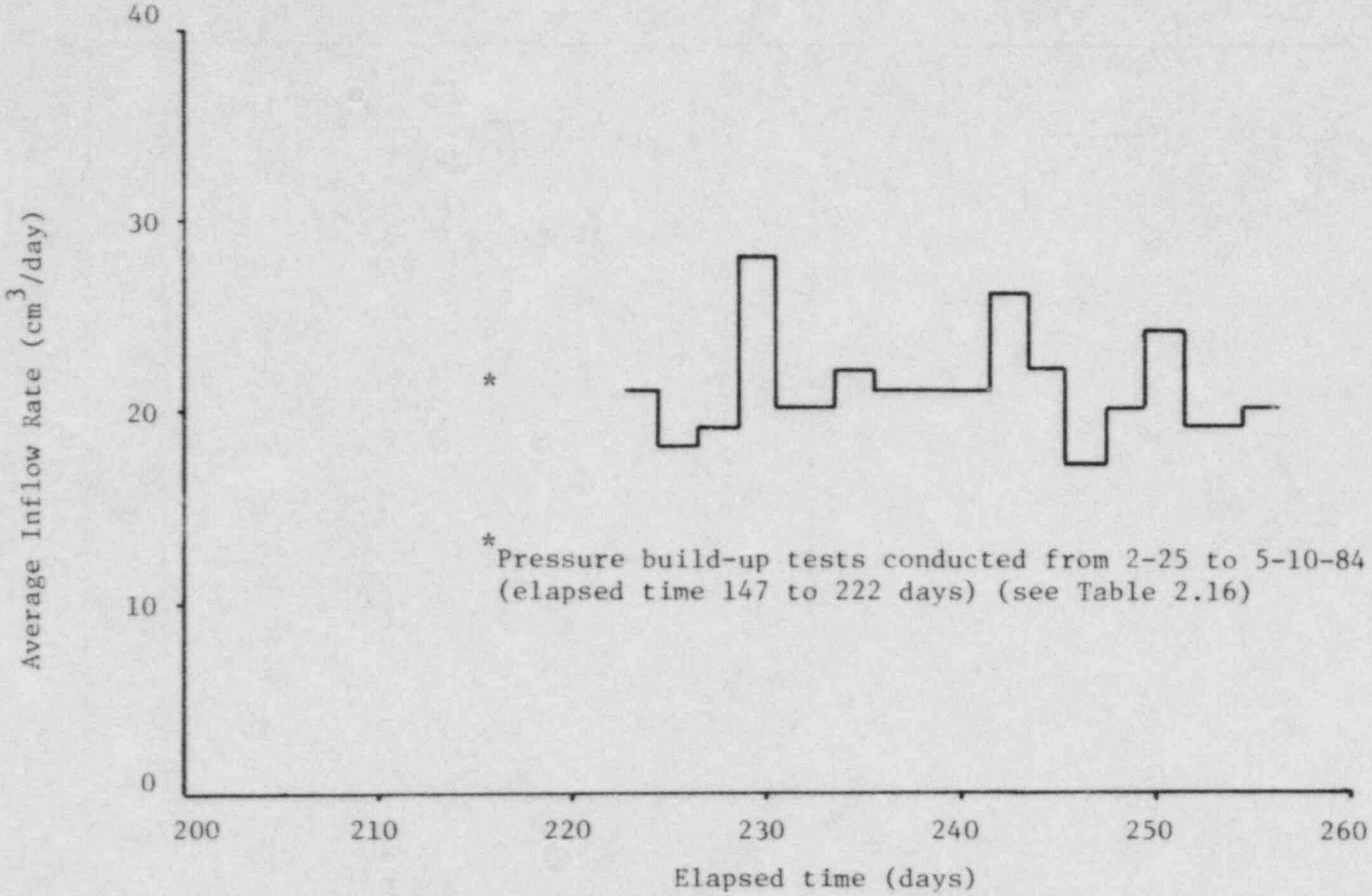

Figure 2.23 (cont.)

based on Table 2.16. Figure 2.22 is a plot of test zone pressure vs. time. ΔP_R, ΔP_D and Δt are shown for a typical fluid build-up test repetition. Figure 2.23 shows average test zone inflow rate vs. time. Inflow rates averaged 6 ml/day from September 30, 1983 to February 24, 1984. Higher inflow rates for May-June 1984 are believed to be due to leakage in the hoses or fittings of the plug tester. Repair of any leaks will be made promptly.

Boreholes UA-CB-4 and UA-CB-3. Initial test zone inflow rates for these two boreholes were significantly higher than for UA-CB-1. Because of the high flow rates a modified fluid build-up test was used. The procedure for the modified test is as follows:

(1) close gas-operated valve;

(2) flush lines thoroughly;

(3) open gas-operated valve for about 10 minutes; close valve;

(4) flush lines thoroughly, collecting the flushed sample.

For the modified test an average inflow rate is obtained by dividing the sample volume from the second flushing by the time period that the gas-operated valve was kept open (about 10 min). Results of the modified fluid build-up test are presented in Table 2.17. For UA-CB-3, the inflow rate remained relatively constant at an average of 85 ml/min from February 29 through April 30. This rate is about four orders of magnitude higher than the rate for UA-CB-1. For UA-CB-4, a marked decrease in inflow rate occurred on or about March 2. From March 2 through March 21, the inflow rate was relatively stable at about 6 ml/min. On or about March 22, the inflow rate in UA-CB-4 decreased again. The fluid build-up test was further modified to accommodate the lower flows in UA-CB-4. The procedure for the further modified fluid build-up test is as follows:

(1) Close gas-operated valve.

(2) Flush lines thoroughly.

(3) Open gas-operated valve for about 24 hours or longer.

(4) Close gas-operated valve.

(5) Flush lines thoroughly, collecting the flushed sample.

(6) Repeat steps 3 through 5 to make additional tests.

Results of the further modified fluid build-up test for UA-CB-4 are presented in Table 2.18. The inflow rate in UA-CB-4 from March 22 through May 1 averaged 58 ml/day, which is about 1 order of magnitude greater than the inflow rate in UA-CB-1.

2.2.7.3.3 Pressure Build-up Test for UA-CB-1. A pressure build-up test was conducted in borehole UA-CB-1 during the period February 25 - March 12. Test results are shown in Table 2.19 and Figure 2.24. If allowed to continue, test zone pressure would rise and finally level off at ambient pressure (approximately 363 kPa (52.6 psi) for the test zone

Table 2.17 Results of Modified Fluid Build-up Test

Borehole	(1) Date/Time of Test	(2) V_{mf} (ml)	(3) Δt_m (min)	(4) $Q = V_{mf}/\Delta t_m$ (ml/min)
UA-CB-4	2-28/1534	890	10	89
	3-1/1550	892	10	89
	3-2/0837	13	10	1.3
	3-3/0854	6	10	0.6
	3-10/0819	68	10	6.8
	3-12/0832	110	10	11
	3-13/0849	38	10	3.8
	3-14/0836	40	10	4.0
	3-15/0938	32	10	3.2
	3-16/0909	42	10	4.2
	3-19/0841	97	10	9.7
	3-20/1027	70	10	7.0
	3-21/1419	112	10	11.2
	3-22/1325	0	10	0
UA-CB-3	2-29/2012	836	15	56
	3-1/0833	840	12	70
	3-5/0849	826	10	83
	3-7/0848	842	10	84
	3-8/0848	838	10	84
	3-9/0913	844	10	84
	3-12/0831	848	10	85
	3-13/0844	860	10	86
	3-14/0835	844	10	84
	3-15/0934	842	10	84
	3-16/0900	854	10	85
	3-19/0840	856	10	86
	3-20/1030	856	10	86
	3-21/1424	866	10	87
	3-22/1321	?	10	
	3-23/1433	858	10	86
	3-24/0931	868	10	87
	3-26/0919	858	10	86
	3-27/0857	856	10	86
	3-28/0830	862	10	86
	3-29/0846	865	10	87
	3-30/0836	876	10	88
	3-31/0913	914	10	91
	4-2/0849	860	10	86
	4-3/0829	868	10	87
	4-4/0805	844	10	84
	4-5/0819	863	10	86
	4-6/0754	860	10	86
	4-9/0835	864	10	86
	4-10/0721	864	10	86
	4-11/0715	862	10	86

Table 2.17 Results of Modified FLuid Build-up Test--Continued

Borehole	(1) Date/Time of Test	(2) V_{mf} (ml)	(3) Δt_m (min)	(4) $Q = V_{mf}/\Delta t_m$ (ml/min)
	4-12/0916	870	10	87
	4-13/0940	866	10	87
	4-14/0918	862	10	86
	4-16/0915	860	10	86
	4-18/0827	857	10	86
	4-19/0857	860	10	86
	4-20/0909	840	10	84
	4-21/0829	872	10	87
	4-23/1400	856	10	86
	4-24/1324	860	10	86
	4-25/1339	862	10	86
	4-26/1432	860	10	86
	4-27/1431	865	10	87
	4-28/1016	860	10	86
	4-30/1338	866	10	87
	5-1/0950	710	5	140
	5-1/1014	packer deflated; plug tester raised		
	5-2	cap placed		
	5-10/1630	plug tester positioned above capped plug; packer inflated		
	5-30/0634	52	10	5.2
	6-4/0634	73	10	7.3
	6-9/0634	90	10	9.0
	6-14/0634	114	10	11.4

(1) Time that gas-operated valve was opened to allow inflow.
(2) Volume flushed after period Δt_m.
(3) Time period that gas-operated valve was kept open to allow inflow.
(4) Average test zone inflow rate during period Δt_m.

Table 2.18 Results of Further Modified Fluid Build-up Test for UA-CB-4

Date/Time	Action*	Δt# (min)	V_F† (ml)	$Q^{\S} = V_F/\Delta t$ (ml/min x 10^2)	(ml/day)
3-22/1338	O				
3-23/1425	C,F	1487	19	1.28	18.4
3-23/1429	O				
3-24/0933	C,F	1144	108	9.44	136
3-24/0937	O				
3-26/0909	C,F	2852	62	2.17	31.3
3-26/0913	O				
3-27/0857	C,F	1424	157	11.0	159
3-27/0901	O				
3-28/0831	C,F	1410	48	3.40	49.0
3-28/0835	O				
3-29/0847	C,F	1452	30	2.07	29.8
3-29/0851	O				
3-30/0832	C,F	1421	52	3.66	52.7
3-30/0836	O				
3-31/0913	C,F	1477	75	5.08	73.1
3-31/0917	O				
4-2/0850	C,F	2853	77	2.70	38.9
4-2/0854	O				
4-3/0830	C,F	1416	86	6.07	87.5
4-3/0834	O				
4-4/0806	C,F	1412	48	3.40	49.0
4-4/0810	O				
4-5/0820	C,F	1450	37	2.55	36.7

Table 2.18 Results of Further Modified Fluid Build-up Test for UA-CB-4--Continued

Date/Time	Action*	$\Delta t^{\#}$ (min)	$V_F^{\dagger}$ (ml)	$Q^{\S} = V_F/\Delta t$ (ml/min x 10^2)	(ml/day)
4-5/0824	0				
4-6/0813	C,F	1429	58	4.06	58.4
4-6/0817	0				
4-9/0837	C,F		-	-	-
4-9/0841	0				
4-10/0723	C,F	1362	110	8.08	116
4-10/0727	0				
4-11/0716	C,F	1429	46	3.22	46.4
4-11/0720	0				
4-12/0918	C,F	1558	46	2.95	42.5
4-12/0922	0				
4-13/0912	C,F	1430	62	4.34	62.4
4-13/0916	0				
4-14/0921	C,F	1445	46	3.18	45.8
4-14/0925	0				
4-16/0917	C,F	2872	92	3.20	46.1
4-16/0921	0				
4-17/0848	C,F	1407	65	4.62	66.5
4-17/0852	0				
4-18/0828	C,F	1416	45	3.18	45.8
4-18/0832	0				
4-19/0858	C,F	1466	50	3.41	49.1
4-19/0902	0				
4-20/0911	C,F	1449	74	5.11	73.5

Table 2.18 Results of Further Modified Fluid Build-up Test for UA-CB-4--Continued

Date/Time	Action*	$\Delta t^{\#}$ (min)	V_F† (ml)	$Q^{\S} = V_F/\Delta t$ (ml/min x 10^2)	(ml/day)
4-20/0915	0				
		1396		2.01	28.9
4-21/0831	C,F		28		
4-21/0835	0				
		3206		2.74	39.5
4-23/1401	C,F		88		
4-23/1405	0				
		1401		5.14	74.0
4-24/1326	C,F		72		
4-24/1330	0				
		1454		3.30	47.5
4-25/1344	C,F		48		
4-25/1348	0				
		1485		3.50	50.4
4-26/1433	C,F		52		
4-26/1437	0				
		1436		1.81	26.1
4-27/1433	C,F		26		
4-27/1437	0				
		1181		3.90	56.1
4-28/1018	C,F		46		
4-28/1022	0				
		3080		3.12	44.9
4-30/1342	C,F		96		
4-30/1346	0				
		1219		4.18	60.2
5-1/1005	C,F		51		
5-1/1010	0				
5-1/1014	Packer deflated; plug tescer raised;				
5-2	Cap placed				
5-10/1830	Plug tester positioned above capped plug; packer inflated.				
5-10/1944	C,F				
5-10/1948	0				
		9729		.576	8.29
5-17/1357	C,F		56		

Table 2.18 Results of Further Modified Fluid Build-up Test for UA-CB-4--Continued

Date/Time	Action*	$\Delta t^{\#}$ (min)	V_F† (ml)	$Q^{\S} = V_F/\Delta t$ (ml/min x 10^{-2})	(ml/day)
5-17/1401	O				
		5734		.872	12.6
5-21/1335	C,F		50		
5-21/1339	O				
5-21/1356	Packer deflated; plug tester raised.				
5-24/1440	Plug tester positioned above capped plug; packer inflated.				
5-25/0635	C,F				
5-25/0639	O				
		7196		.528	7.60
5-30/0635	C,F		38		
5-30/0639	O				
		7196		.667	9.61
6-4/0635	C,F		48		
6-4/0639	O				
		7196		.472	6.80
6-9/0635	C,F		34		
6-9/0639	O				
		7196		.417	6.00
6-14/0635	C,F		30		
6-14/0639	O				

*Action: O - open gas-operated valve; C - close gas-operated valve; F - flush water in lines above gas-operated valve.

#Δt = time interval over which water inflow to test zone occurred.

†V_F = volume flushed from lines above gas-operated valve. Flushing is always performed by injecting nitrogen gas into the flush line at 120 psi for 4 minutes.

§Q = average rate of water inflow to the test zone over the period Δt.

Table 2.19 Pressure Build-up Test, Borehole UA-CB-1, 2-25-84 to 3-12-84

Date/Time	Elapsed Time (min)	Elapsed Time (hr)	Test Zone Pressure (psig)	Test Zone Pressure (kPa)	Test Zone Pressure (cm of water)
2-25/2133	0	0	2.333	16.09	164.1
2-26/0733	600	10	4.367	30.11	307.1
2-26/1733	1200	20	5.767	39.76	405.6
2-27/0333	1800	30	6.567	45.28	461.9
2-27/1329	2396	40	7.433	51.25	522.8
2-27/2329	2996	50	8.267	57.00	581.5
2-28/0929	3596	60	9.067	62.51	637.7
2-28/2018	4245	71	9.900	68.26	696.4
2-29/0618	4845	81	10.67	73.54	750.3
2-29/1618	5445	91	11.43	78.83	804.2
3-1/0231	6058	101	12.17	83.89	855.8
3-1/1231	6658	111	12.80	88.25	900.3
3-1/2231	7258	121	13.60	93.77	956.6
3-2/0830	7857	131	14.40	99.29	1013
3-2/1831	8458	141	15.10	104.1	1062
3-3/0431	9058	151	15.87	109.4	1116
3-3/1433	9660	161	16.70	115.1	1175
3-4/0033	10260	171	17.43	120.2	1226
3-4/1033	10860	181	18.27	125.9	1285
3-4/2033	11460	191	19.00	131.0	1336
3-5/0633	12060	201	19.80	136.5	1393
3 5/1633	12660	211	20.67	142.5	1454
3-6/0233	13260	221	21.50	148.2	1512
3-6/1233	13860	231	22.40	154.4	1576
3-6/2233	14460	241	23.27	160.4	1637
3-7/0633	14940	249	23.97	165.2	1686
3-7/1833	15660	261	25.00	172.4	1758
3-8/0433	16260	271	26.03	179.5	1831
3-8/1433	16860	281	26.77	184.6	1883
3-9/0033	17460	291	27.67	190.8	1946
3-9/1033	18060	301	28.37	195.6	1995

Table 2.19 Pressure Build-up Test, Borehole UA-CB-1, 2-25-84 to 3-12-84--Continued

Date/Time	Elapsed Time (min)	(hr)	Test Zone Pressure (psig)	(kPa)	(cm of water)
3-9/2033	18660	311	29.07	200.4	2045
3-10/0633	19260	321	30.13	207.8	2120
3-10/1633	19860	331	31.07	214.2	2185
3-11/0233	20460	341	31.80	219.3	2237
3-11/1233	21060	351	32.70	225.5	2300
3-11/2233	21660	361	33.33	229.8	2345
3-12/0808	22235	371	34.07	234.9	2396

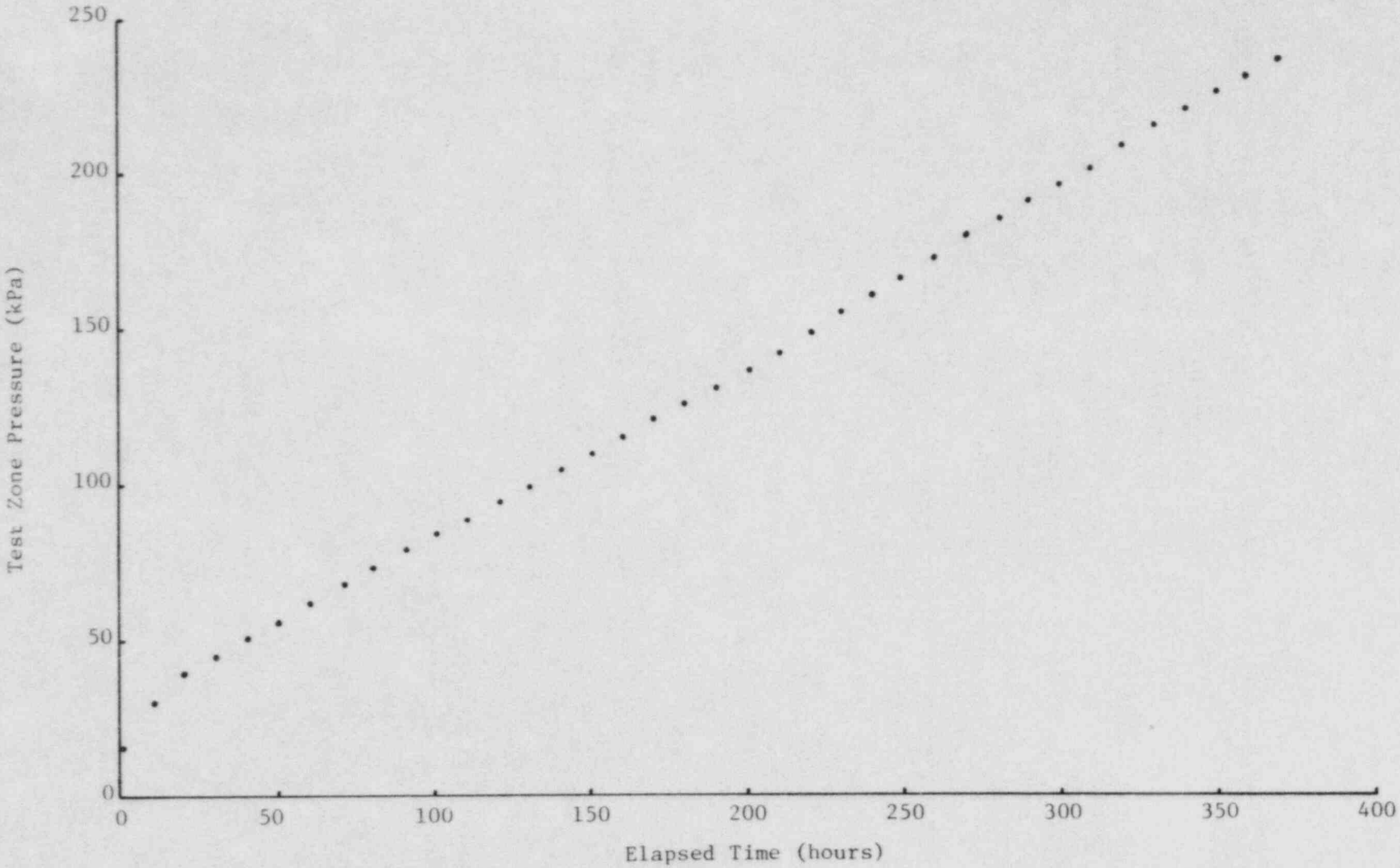

Figure 2.24 Pressure vs. elapsed time for pressure build-up test in borehole UA-CB-1. Date of start of test: 2-25-84.

depth. However, the test was terminated at 235 kPa (34.1 psi) so as not to exceed the limits of the test zone pressure transducer.

2.2.8 Capping of Plugs in UA-CB-3 and UA-CB-4

On May 2, 1984 the plugs in UA-CB-3 and UA-CB-4 were capped by placing additional cement directly on top of the plugs.

2.2.8.1 Procedure

Cement was prepared for each hole in exactly the same manner and volume as for the original plug (Section 2.2.6.1.3). The cement was placed using the dump bailer. After withdrawing the bailer, a plug tester unit was immediately lowered and positioned in each hole so that its lower end was 30 cm (12 in) above the top of the original plug. The plug tester packer was inflated very slowly with the gas-operated valve open. After the packer was inflated, the gas-operated valve was closed. The plug tester units were left in place for about seven days as the cement caps cured. On May 9 the plug tester units were removed.

At ground surface both plug tester packers were observed to have considerable cement residue deposited on horizontal surfaces at the upper end. Apparently, either in the process of removing the bailer, or in lowering the plug tester units, or in inflating the plug tester packers, significant turbulence was created, which caused some of the cement slurry to rise more than 2 m (7 ft) above the top of the original plug. The walls of boreholes UA-CB-3 and UA-CB-4 for 2.5 m (8 ft) above the caps were brushed with a stiff wire brush and the tops of the caps were scraped to remove soft cement material from the top of the cap. About 5 cm (2 in) of soft cement were scraped from the top of the cap in UA-CB-3 and 4 cm (1.5 in) from the cap top in UA-CB-4. After scraping, the boreholes were flushed vigorously for at least 25 min to remove loose cement material. After scraping and flushing, the thickness of the cap in UA-CB-3 was measured to be 17.8 cm (7.01 in) and the cap in UA-CB-4 was found to be 19.8 cm (7.79 in) thick.

2.2.8.2 Testing of Capped Plugs

The capped plug in borehole UA-CB-4 has been tested using the further modified fluid build-up test (Section 2.2.7.3.2). The results are presented in Table 2.18 (dates after May 10). With cap in place, the test zone inflow rate has been reduced to about 8 ml/day, which is comparable to inflow rates for the plug in borehole UA-CB-1.

The modified fluid build-up test has been used to test the capped plug in UA-CB-3. Results to data are presented in Table 2.17 (dates after May 10). Test zone inflow was reduced by the cap. However, the inflow rate is still three orders of magnitude higher than for the plug in UA-CB-1 and the capped plug in UA-CB-4.

2.3 Oracle Ridge Mine

2.3.1 Summary

Constant pressure injection tests have been underway on a cement plug, 12.7 cm (5.0 in) in length, in a 10 cm (3 15/16 in) diameter borehole at the Oracle Ridge Mine site since May 1983. Results of injection testing and some preliminary discussion of results are presented.

2.3.2 Borehole/plug site description

The Oracle Ridge Mine is located 4 kilometers (2.4 miles) northwest of Summerhaven, Mt. Lemmon, Arizona. The test borehole connects two mine drifts and thus is accessible from both ends. The 10 cm (3 15/16 in) diameter hole is 33.24 m (109.1 ft) in length and is inclined 9.3° from the horizontal. The borehole penetrates a dolomite formation that is normally unsaturated. The 12.7 cm (5.0 in) plug was placed approximately 3.4 m (11 ft) from the lower end of the hole in an interval with low fracture density. A full description of the borehole, the formation geology and the site selected for locating the plug is provided in Daemen et al. (1983).

2.3.3 Plug Testing

Constant pressure injection tests have been performed on the plug since May 1983. The testing consists of injecting water under constant pressure on one side of the plug and collecting outflow on the other side. The injection pressure, injection volume and outflow volume are monitored.

2.3.3.1 Instrumentation

2.3.3.1.1 Injection Pump and Injection-side Packer. Constant pressure water injection is achieved using the gas-over-water injection pump shown schematically in Figure 2.25. Injection may be accomplished using any one of the different diameter injection vessels, thus permitting injection over a wide range of flow rates. Flow rate is determined by timing the fall of the water level in the injection vessel being used. Pressure on the injection side of the plug is equal to the injection pump gas pressure plus the hydrostatic pressure due to the vertical height of the water-gas interface in the injection vessel above the plug [about 4.35 m (14.3 ft) of water, or 43 kPa (6.2 psi)]. A pneumatic packer (injection-side packer) is inflated in the borehole just above the plug. Water is delivered from the injection pump through the injection-side packer creating a pressurized injection zone at the upper end of the plug. The length of the injection zone has been maintained at about 62 cm (24.4 in) for most of the testing to date.

2.3.3.1.2 Outflow Collection. The instrumentation used to collect and measure outflow from below the plug has been changed several times since testing began. From June 2 to August 1, 1983, collection was made as depicted in Figure 2.26.* This system, while satisfactory for high outflow rates and/or long test periods, was inaccurate for short tests, especially those with low outflow rates. From August 1, 1983 to May 22,

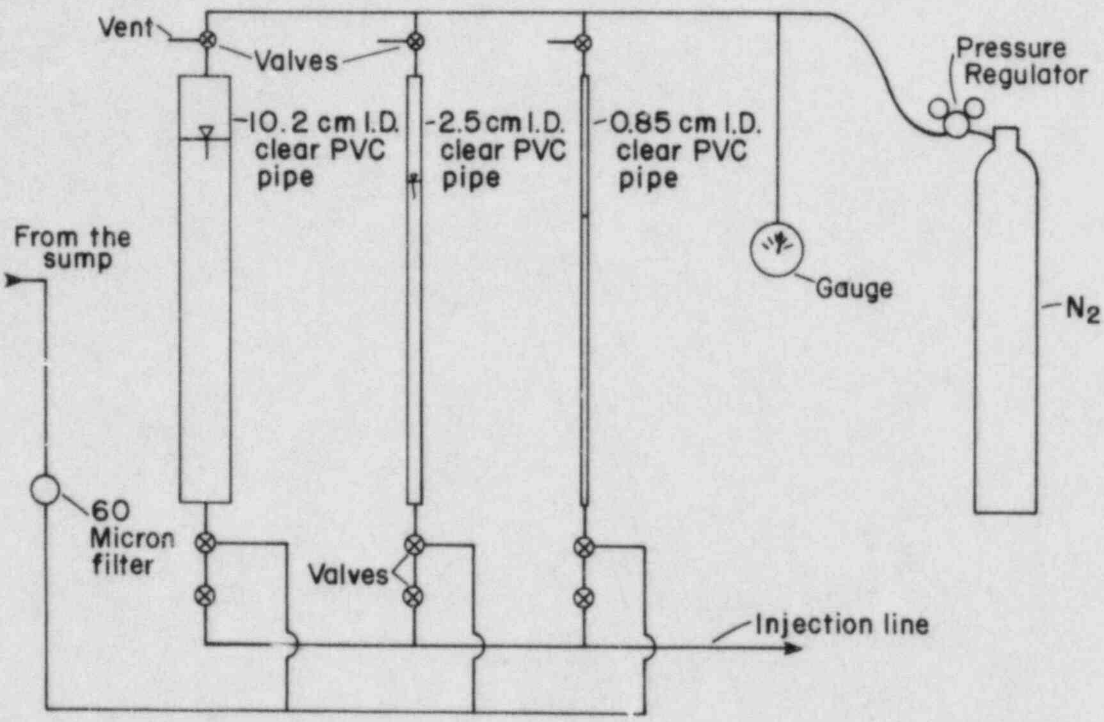

Figure 2.25 Oracle Ridge Mine Injection System

Clear PVC pipe injection vessels are filled with water pumped into them from the sump. The volume of water injected is monitored as a drop in water level within the selected vessel.

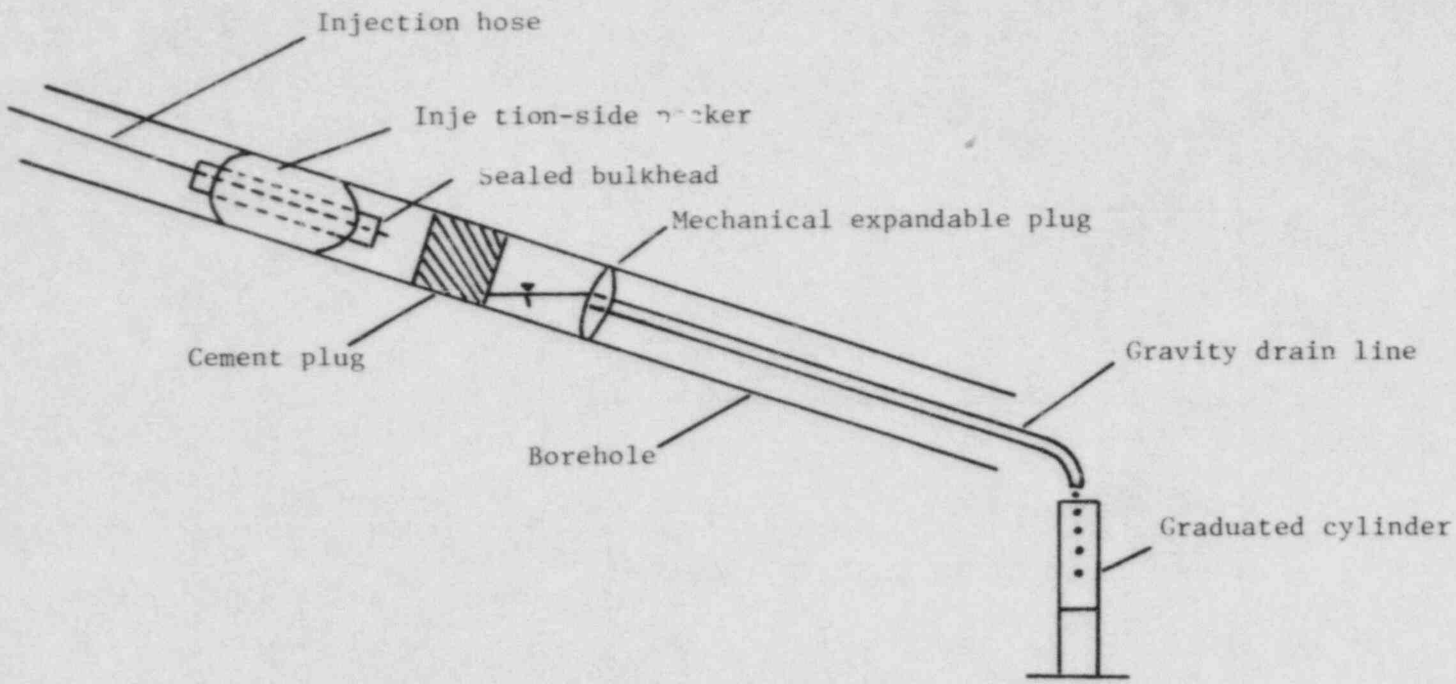

Figure 2.26 Oracle Ridge Mine outflow collection system 1; used from 6-2 to 8-1-83. Also shown are hose from injection pump and injection-side packer. (Drawing not to scale)

1984, the collection system shown in Figure 2.27 was used. For this second system, provided that the air pocket at the apex of the collection zone is insignificantly small, the outflow during a test from the plug and formation to the collection zone should equal (approximately) the volume displaced over the test in the graduated cylinder/pipet. However, should the air pocket be of significant size, the outflow-diplacement relationship may become complicated by the following factors:

(1) If the water level in the collection zone is above the intake of the line to the graduated cylinder/pipet, the volume displaced in the cylinder/pipet depends not only on the outflow volume but also on the pressure-volume relationship for air.

(2) If the water level in the collection zone is below the intake, the volume displaced no longer depends directly on the outflow volume, but rather it directly depends exclusively on the pressure-volume relationship for air.

(3) If the water level is below the intake and then rises above it, air bubbles may become trapped in the line to the cylinder/pipet, which may make flow in the line erratic.

The outflow rates as measured with the second system were somewhat erratic (Section 2.3.3.4.9). To eliminate the possibility of complications due to factors (2) and (3) a third collection system (Figure 2.28) was used from May 22 to June 5, 1984. With this system, if the apex air pocket is kept small, the outflow during a test to the collection zone is, again, equal (approximately) to the volume displaced in the cylinder/pipet over the test. If the air pocket is significant, the volume displaced depends on the pressure-volume relationship for air as well as on outflow volume [factor (1)]. By placing the graduated cylinder/pipet above the collection zone, the possibility of gravity drainage of the collection zone through line b to the cylinder/pipet is eliminated. The third system gave significantly higher outflow rates (Section 2.3.3.4.9) than were expected. These high rates may have been due to a minute leak in the pneumatic packer on the collection side causing a very gradual pressure build-up in the collection zone, which, of course, would cause the collection zone to empty to the graduated cylinder/pipet.**

---

*In each of the collection systems described it is assumed that the loss of water (if any) from the collection zone back into the formation is negligible compared to the outflow to the collection from the plug/formation.

**A packer leak would also cause the second system to give erroneous outflow volumes. The collection zone pressure build-up due to the leak would empty the zone above the intake and then empty the outflow tube into graduated cylinder/pipet.

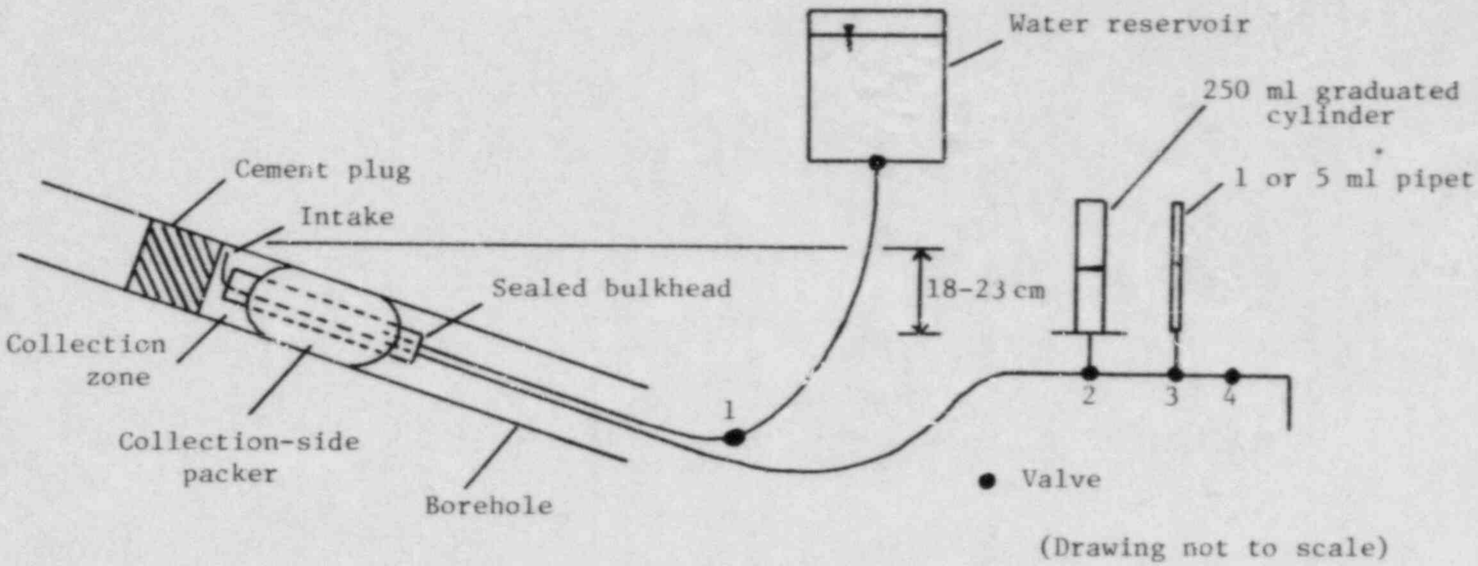

Figure 2.27 Oracle Ridge Mine outflow collection system 2; used from 8-1-83 to 5-22-84. Prior to testing, the collection zone is filled with water (except for perhaps a small air pocket) and the line to the graduated cylinder/pipet is bled of air by opening valve 1 and valve 2 (if the graduated cylinder is to be used) or valve 3 (if the pipet is to be used). Valve 1 is then closed. Using valve 4, the height in the cylinder or pipet is adjusted to an initial level. Outflow measurement may then begin. If the collection zone air pocket is small enough, outflow during the test to the collection zone from the plug/formation equals the volume displaced over the test in the cylinder or pipet.

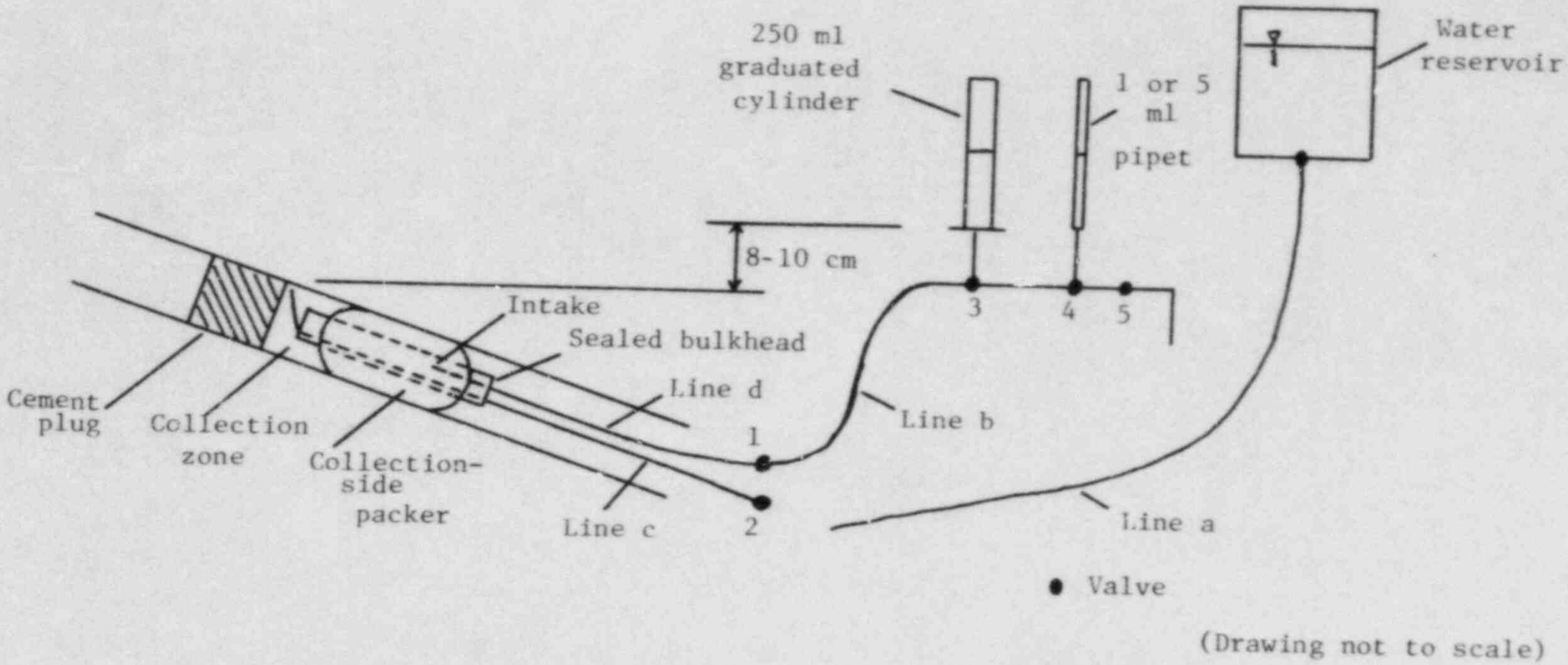

Figure 2.28 Oracle Ridge Mine outflow collection system 3; used from 5-22 to 6-5-84. Prior to testing the collection zone is filled with water (except for perhaps a small air pocket) and line c is bled of air bubbles by opening valve 2 and connecting line a to line d with valve 1 open (line b is disconnected from valve 1). Valves 2 and 1 are then closed and line a is disconnected from line d. Line b is then bled by draining water through the line from the graduated cylinder. Line b is then connected to line d and valve 1 is opened. To use the graduated cylinder (pipet) to measure outflow, valve 3 (4) and valve 5 are opened and an initial water level in the cylinder (pipet) is set. Valve 5 is then closed and testing may begin. If the collection zone air pocket is small enough, outflow during the test from the plug/formation to the test zone equals the volume displaced over the test in the cylinder/pipet.

From June 5 to June 15, 1984, a fourth system was used (system not illustrated). This system was identical to the second system except that the graduated cylinder/pipet was kept elevated above the collection zone (at the same height above the collection zone as for the third system).

A fifth collection (Figure 2.29) system was tried from June 15 to June 28, 1984. In this system the collection zone was much smaller than in the previous systems. The small collection zone was made possible by the use of a mechanical expandable plug which could almost butt up against the face of the cement plug. An advantage of the small collection zone is that the percentage of the total outflow coming to the collection zone through the cement plug and plug/formation interface (as opposed to coming from the formation) should be much higher. With this system, the outflow to the collection zone forms a pool. The vent tube keeps the pressure above the pool constantly at atmospheric pressure. The level of water in the pipet is the level of the pool in the collection zone. At the start of a test the water level in the pipet is noted. At the conclusion of the test, valve 1 (Figure 2.29) is opened and water is slowly drained into a graduated cylinder until the water level in the pipet is at the same position as at the start of the test. The outflow to the collection zone during the test is the volume drained into the graduated cylinder. The system should eliminate complications due to factors (1), (2) and (3). Also, since the expandable plug is not pneumatic, there can be no gas leak. In order to provide adequate resolution the collection zone must be kept quite small and tests should be of longer duration. The fifth system has not been successful. In tests using it the pool level has declined very slightly over the course of the test. This indicates that water loss (either past the expandable plug or back into the formation) exceeds the outflow rate to the collection zone. It should be noted, however, that since the system allows much less outflow from the formation to enter the collection zone, the total outflow rate to the collection zone may be much smaller for this than for the other systems.

A sixth system is planned. It will be similar to the third system, but it will have a smaller collection zone and an improvised pneumatic plug which will not leak gas and will eliminate any leakage of collected water past the pneumatic plug.

2.3.3.2 Test Procedure

Constant pressure injection testing has been underway since May, 1983. Initially, injection pressures were varied from 180 to 424 kPa (26.1 to 61.5 psi). From June 28 to July 7, 1983, pressure was held at about 318 kPa (461 psi). From July 7, 1983 o April 17, 1984, pressure was maintained at about 285 kPa (41.3 psi). Since April 17, pressure has been kept at about 183 kPa (26.5 psi).

Tests of about 1-hour duration using the 0.88 cm (.348 in) I.D. vessel (Figure 2.25) have been conducted every several days to several weeks. Between these 1-hour tests, injection testing has been continued using the 2.6 cm (1.02 in) I.D. tube. Average injection rates are computed based on both the 1-hour tests (short tests) and the longer tests (long

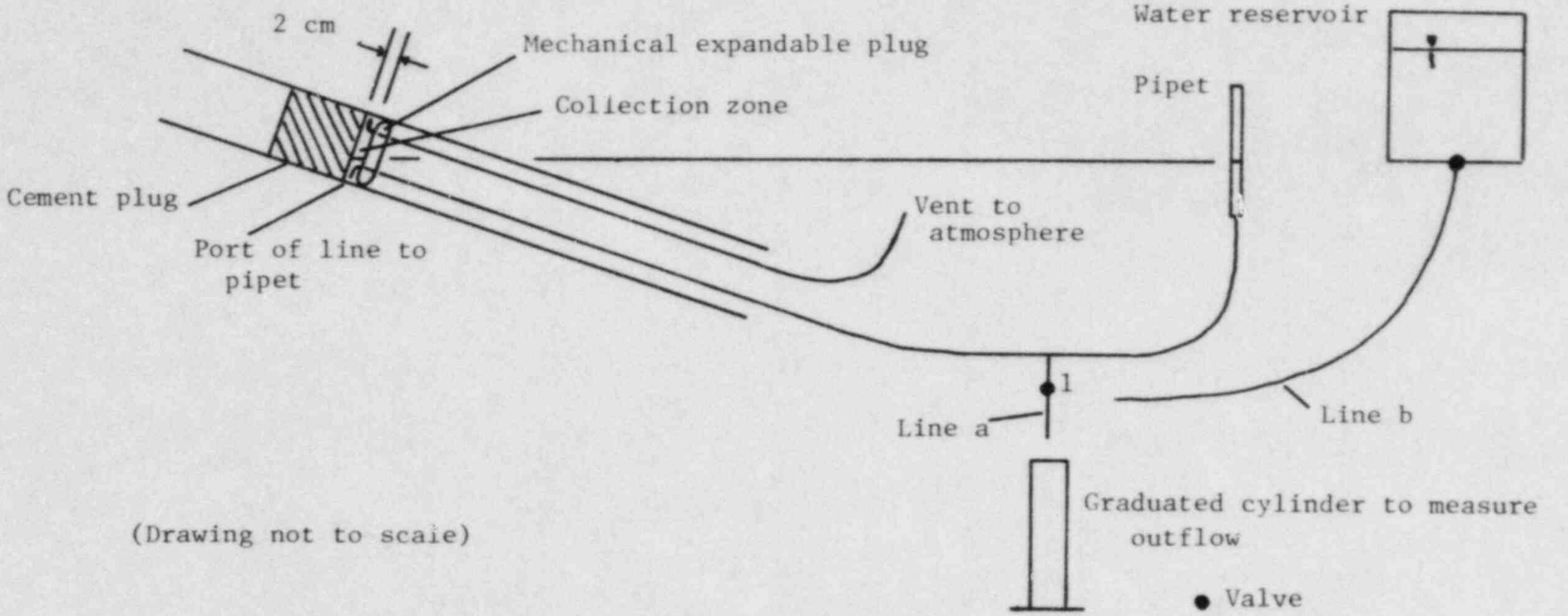

Figure 2.29 Oracle Ridge Mine outflow collection system 5; used from 6-15 to 6-28-84. Prior to testing, the collection zone is slowly filled to an initial level by connecting line b to line a with valve 1 cracked open. Valve 1 is then closed and line b is disconnected from line a. The level of water in the pipet (which is the same as the level in the collection zone) is recorded and testing is begun. At the conclusion of testing, valve 1 is cracked open and line a is very slowly drained into a graduated cylinder until the water level in the pipet returns to its initial level. The volume of water drained to the cylinder is the volume of outflow over the test.

tests) between the 1-hour tests. In the short tests, outflow is usually collected in a 1 ml or 5 ml pipet; in the long tests, a 250 ml graduated cylinder is generally used (see Section 2.3.3.1).

2.3.3.3 Test Results

Table 2.20 presents the results of all constant pressure injection testing on the plug to date. Figure 2.30 is a plot of injection flow rate vs. time from June 28, 1983 to June 19, 1984. Figure 2.31 is a plot of injection rate vs. injection pressure for four series of tests in May and June 1983. Figure 2.32 is a plot of average outflow collection rate vs. time for the period July 11, 1983 to April 17, 1984.

2.3.3.4 Discussion of Results

2.3.3.4.1 Components of Injection Flow. In the constant pressure injection tests conducted, the injection flow consists of three components:

(1) Flow to the formation through either the rock matrix which borders or fractures which intersect the injection zone.

(2) Flow through the plug or the plug/formation interface.

(3) Leakage through the injection-side packer mandrel or along the interface between the packer membrane and the borehole wall. Also included are leaks in the injection pump or injection hose.

Component (3) flow is considered negligible compared to components (1) and (2). "Injection flow" will be taken as the sum of components (1) and (2).

2.3.3.4.2 High Initial Injection Flow Rates. As Table 2.20 and Figure 2.30 indicate, at the start of testing,* injection flow rates were quite high. The flow rates were much higher than could have occurred due to flow from the injection zone into the rock matrix or intersecting fractures (component 1 flow) alone.** In the tests in May, 1983, water was visually observed flowing out of the plug at the crown on the lower (collection-side) end. Laboratory tests (Daemen et al., 1983) have shown that in near-horizontal plugs placed with a dump bailer or under low pressure a weak and highly permeable zone often forms along the crown. Initially, then, a significant gap*** or highly permeable zone existed at the plug/borehole interface along the crown of the plug permitting the observed high flow rates.

---

*Testing started on May 17, 1983, 18 days after placement of the plug (Daemen et al., 1983).

Table 2.20 Oracle Ridge Mine Constant Pressure Injection Test Results

Date	Injection Zone Pressure (kPa)	Injection Zone Length (cm)	Flow in Injection Vessel (in)	(cm^3/in) for Injection Vessel	Volume Injected (cm^3)	Time Span of Test (min)	Injection Flow Rate (cm^3/hr)	Volume Collected (cm^3)	Collection Zone Outflow Rate (cm^3/hr)
5/17/83	276	254	25	.804	20.1	1	1200		
	276	254	50	.804	40.2	1	2400		
5/27	181	189	59.0	.804	47.4	73.4	39		
	286	189	180.0	.804	145	69.6	130		
	424	189	201.0	.804	162	58.4	170		
6/1	180	189	20.00	.804	16.1	60.6	16		
	284	189	32.00	.804	25.7	60.3	26		
	422	189	46.00	.804	37.0	60.7	37		
6/2	284	77	23.00	.804	18.5	46.4	34		
6/21	186	62	8.50	1.55	13.2	61.6	13		
	285	62	14.00	1.55	21.7	63.2	21		
	423	62	21.00	1.55	32.6	61.6	32		
6/24	180	62	7.00	1.55	10.9	63.7	10		
	285	62	11.00	1.55	17.1	63.7	16		
	423	62	15.00	1.55	23.3	58.3	24		
6/28	318	62	8.00	1.55	12.4	65.1	11	21.9	20[a]
6/28-6/29	318	62	12.59	13.3	167	1191	8.4	118	5.9
6/29	318	62	16.00	1.55	24.8	230.2	6.5		
6/29-6/30	319	62	8.65	13.3	115	1151	6.0		
6/30	320	62	3.50	1.55	5.43	60.9	5.3		
6/30-7/1	318	62	10.06	13.3	134	1598	5.0		
7/1	316	62	2.75	1.55	4.26	55.5	4.6		
7/1-7/7	316	62	2.34	206	482	8390	3.4		
7/7	315	62	2.00	1.55	3.10	62.7	3.0		
7/7-7/11	299	62	19.83	13.3	264	5661	2.8		
7/11	283	62	1.75	1.55	2.71	64.6	2.5		
7/11-7/15	284	62	17.23	13.3	229	5510	2.5	89	.97
7/15	285	62	1.75	1.55	2.71	72.3	2.2		

Table 2.20 Oracle Ridge Mine Constant Pressure Injection Test Results--Continued

Date	Injection Zone Pressure (kPa)	Injection Zone Length (cm)	Flow in Injection Vessel (in)	(cm^3/in) for Injection Vessel	Volume Injected (cm^3)	Time Span of Test (min)	Injection Flow Rate (cm^3/hr)	Volume Collected (cm^3)	Collection Zone Outflow Rate (cm^3/hr)
7/15-7/18	285	62	12.68	13.3	169	4435	2.3	86	1.2
7/18	284	62	1.25	1.55	1.94	58.1	2.0		
7/18-7/22	284	62	15.07	13.3	200	5650	2.1	99	1.1
7/22	284	62	1.25	1.55	1.94	60.9	1.9	7	6.9
7/22-7/25	285	62	10.91	13.3	145	4299	2.0	69	.96
7/25	285	62	1.25	1.55	1.94	65.0	1.8		
7/25-7/29	285	62	13.15	13.3	175	5399	1.9	91(+)	1.0(+)
7/29	283	62	0.75	1.55	1.16	43.7	1.6		
7/29-8/1	283	62	9.36	13.3	124	4450	1.7	101	1.4
8/1	283	62	2.00	1.55	3.10	119.6	1.6		
8/1-8/4	283	62	9.11	13.3	121	4039	1.8	107	1.6[b]
8/4	282	62	0.75	1.55	1.16	47.3	1.5	1.10	1.4
8/4-8/8	280	62	12.53	13.3	167	5694	1.8	148	1.6
8/8	278	62	0.50	1.55	.775	32.6	1.4	.74	1.4
8/8-8/12	Injection pump not pressurized - no test.								
8/12	284	62	1.75	1.55	2.71	133.7	1.2	2.17	.97
8/12-8/15	274	62	5.25	13.3	69.8	4120	1.0	86	1.3
8/15	263	62	0.50	1.55	.775	52.4	.89	.69	.79
8/15-8/18	267	62	6.13	13.3	81.5	4260	1.1	84	1.2
8/18	251	62	1.25	1.55	1.94	111.7	1.0	1.38	.74
8/18-8/22	285	62	10.86	13.3	144	5725	1.5	88	.92
8/22	285	62	0.88	1.55	1.36	57.[illegible]	1.4	1.02	1.1
8/22-8/30	Injection packer tank dropped to 0 pressure about 8/25 - no test.								
8/30	284	62	1.00	1.55	1.55	51.2	1.8	1.86	2.2
8/30-9/2	284	62	7.03	13.3	93.5	4038	[illegible].4	125	1.9
9/2	284	62	0.75	1.55	1.16	49.3	1.[illegible]	.89	1.1
9/2-9/6	284	62	10.44	13.3	139	5958	1.4	83	.84
9/6	283	62	0.75	1.55	1.16	55.1	1.3	.88	.96

Table 2.20 Oracle Ridge Mine Constant Pressure Injection Test Results--Continued

Date	Injection Zone Pressure (kPa)	Injection Zone Length (cm)	Flow in Injection Vessel (in)	(cm^3/in) for Injection Vessel	Volume Injected (cm^3)	Time Span of Test (min)	Injection Flow Rate (cm^3/hr)	Volume Collected (cm^3)	Collection Zone Outflow Rate (cm^3/hr)
9/6-9/9	280	62	6.06	13.3	80.6	3994	1.2	47	.71
9/9	277	62	0.75	1.55	1.16	60.1	1.2	.96	.96
9/9-9/12	285	62	6.50	13.3	86.5	4373	1.2	45	.62
9/12	285	62	0.63	1.55	.977	51.7	1.1	.91	1.1
9/12-9/22	285	62	19.83	13.3	264	14407	1.1	133	.55
9/22	283	62	0.75	1.55	1.16	68.7	1.0	.96	.84
9/22-9/29	284	62	12.83	13.3	171	9957	1.0	93	.56
9/29	284	62	0.63	1.55	.977	59.8	.98	.75	.75
9/29-10/6	283	62	12.31	13.3	164	9976	.99	133	.80
10/6	283	62	0.50	1.55	.775	51.4	.90	.83	.97
10/6-10/14	283	62	13.45	13.3	179	11438	.94	96	.50
10/14	283	62	0.50	1.55	.775	59.4	.78	.84	.85
10/14-10/17	283	62	5.00	13.3	66.5	4410	.90	34	.46
10/17	286	62	0.50	1.55	.775	56.4	.82	.76	.81
10/17-10/28	286	62	17.19	13.3	229	15640	.88	125	.48
10/28	285	62	0.50	1.55	.775	58.8	.79	.79	.81
10/28-11/11	287	62	20.06	13.3	267	20166	.79	164	.49
11/11	289	62	0.38	1.55	.589	53.9	.66	.74	.82
11/11-11/30	289	62	23.34	13.3	310	27235	.68	125	.28
11/30	287	62	0.31	1.55	.481	51.6	.56	.58	.67
11/30-12/2	285	62	2.17	13.3	28.9	2758	.63	10	.22
12/2	283	62	0.19	1.55	.295	37.0	.48	-	-
12/2-12/14	280	62	13.84	13.3	184	17232	.64	97	.34
12/14	276	62	0.31	1.55	.481	52.4	.55	.84	.96
12/14-1/5/84	285	62	22.77	13.3	303	31572	.58	77	.15
1/5	285	62	0.31	1.55	.481	60.4	.48	.96	.95
1/5-1/19	285	62	13.89	13.3	185	19973	.56	-	-
1/19	285	62	0.25	1.55	.388	49.9	.47	1.08	1.3

Table 2.20 Oracle Ridge Mine Constant Pressure Injection Test Results--Continued

Date	Injection Zone Pressure (kPa)	Injection Zone Length (cm)	Flow in Injection Vessel (in)	(cm^3/in) for Injection Vessel	Volume Injected (cm^3)	Time Span of Test (min)	Injection Flow Rate (cm^3/hr)	Volume Collected (cm^3)	Collection Zone Outflow Rate (cm^3/hr)
1/19-2/10	284	62	20.75	13.3	276	31574	.52	70	.13
2/10	284	62	0.25	1.55	.388	59.6	.39	.68	.68
2/10-3/9	285	62	28.06	13.3	373	40266	.56	92	.14
3/9	285	62	0.31	1.55	.481	58.6	.49	1.01	1.0
3/9-4/3	284	62	25.97	13.3	345	35819	.58	82	.14
4/3	284	62	0.31	1.55	.481	45.9	.63	.90	1.2
4/3-4/17	286	62	14.66	13.3	195	19975	.59	46	.14
4/17	287	62	0.38	1.55	.589	64.3	.55	2.40	2.2[c]
4/17-4/26	180	62	1.63	13.3	21.7	12803	.10	97	.45
4/26	180	62	0.28	1.55	.434	84.3	.31	2.51	1.8
4/26-5/16	183[d]	62	4.81	13.3	64.0	28679	.13	39.5	0.83
5/16	184[d]	62	-			60.0		2.01	2.0[c]
5/16-5/22	185[d]	62	1.19	13.3	15.8	8346	.11	90	.65
5/22	185	62	0.44	-		89.8		2.71	1.8[e]
5/22-5/31	185	62	2.19	13.3	29.1	12739	.14	> 220	> 1.0
5/31	183	62	0.34	1.55	.527	65.6	.48	.86	.79
5/31	183	62	0.66	1.55	1.02	176.3	.35	-	-
5/31-6/5	182	62	1.50	13.3	20.0	7001	.17	224	1.9
6/5	181	62	0.13	1.55	.202	73.4	.17	2.42	2.0[c,f]
6/5-6/15	178	62	2.81	13.3	37.4	14205	.16	102	.43
6/15	177	62	0.19	1.55	.295	69.5	.25	-	-
6/15-6/19	180	62	1.25	13.3	16.6	5405	.18	-	-
6/19	181	62	0.19	1.5	.295	80.7	.22	-	-

[a]Collection system 1 used for tests from 6/28 to 8/1/83.

[b]Collection system 2 used for tests from 8/1 to 5/22/84 (Section 2.   ).

Table 2.20 Oracle Ridge Mine Constant Pressure Injection Test Results - Notes--Continued

[c]Air bled from line to pipet/graduated cylinder prior to this test.

[d]Pressure estimated by interpolation.

[e]Collection system 3 used for tests from 5/22 to 6/5/84 (Section 2.   ).

[f]Collection system 2 used for tests from 6/5 to 6/15/84 (Section 2.   ).

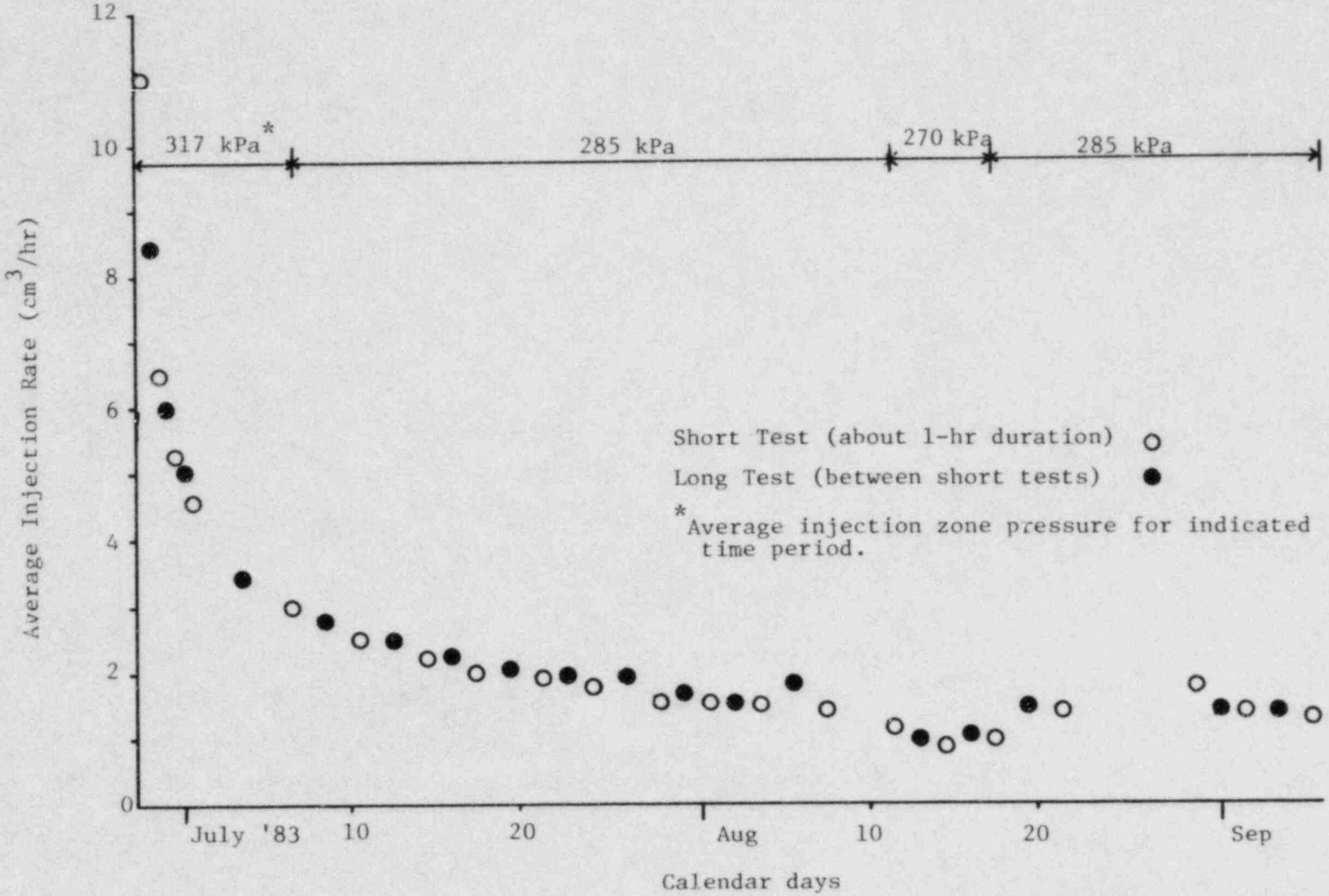

Figure 2.30 Oracle Ridge Mine average injection rate vs. time for constant pressure injection testing. Period: 6-28-83 to 6-19-84.

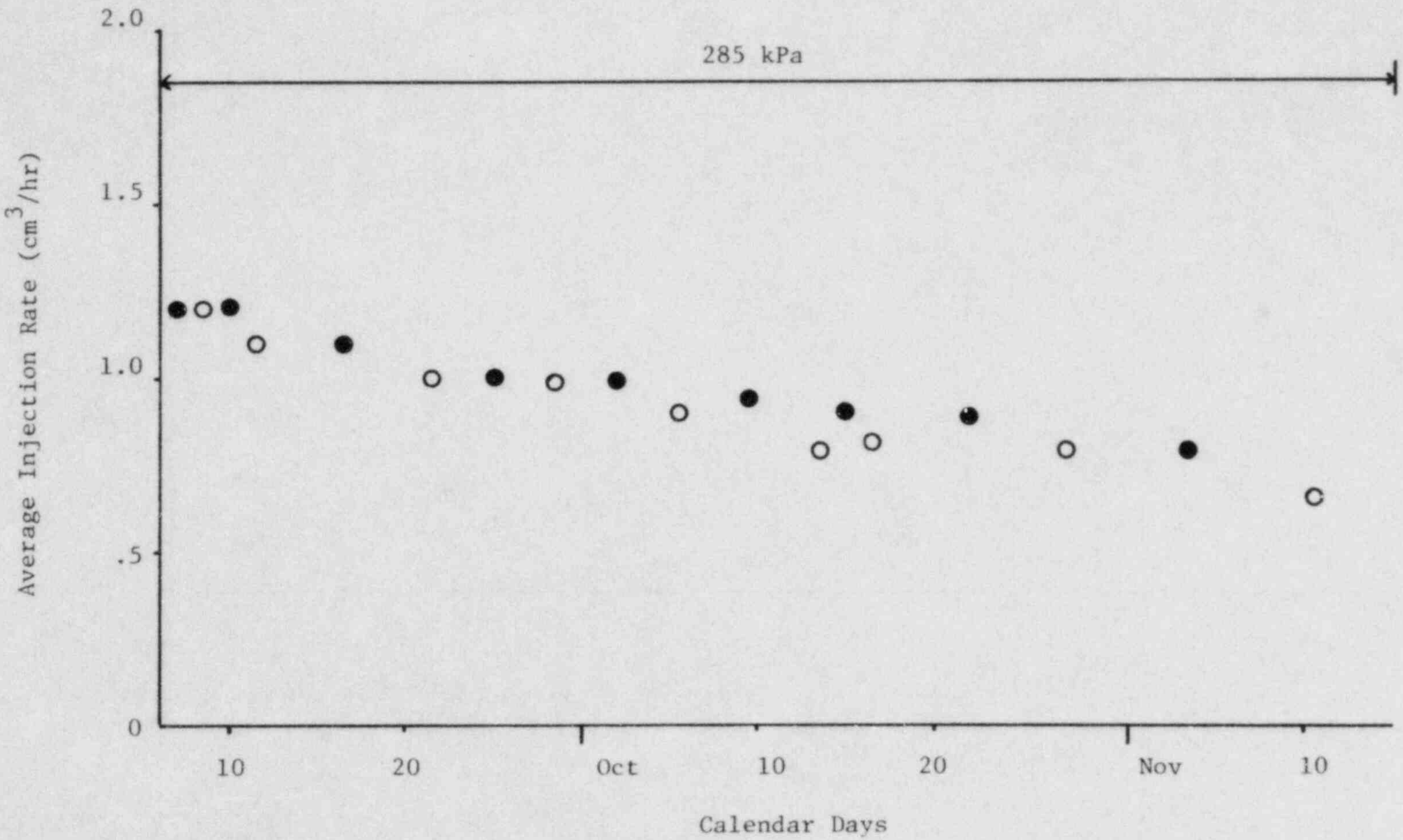

Figure 2.30 (cont.)

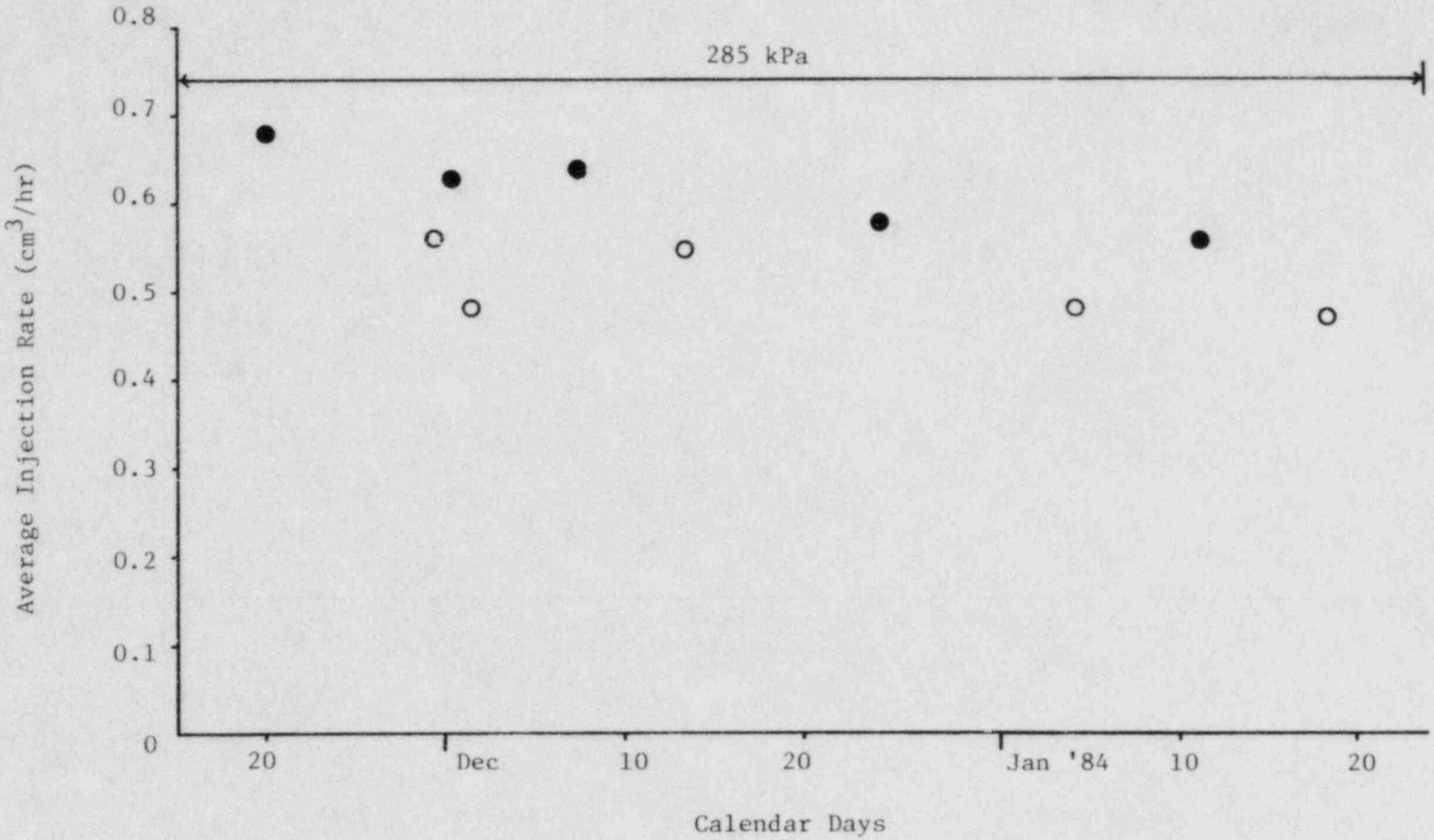

Figure 2.30 (cont.)

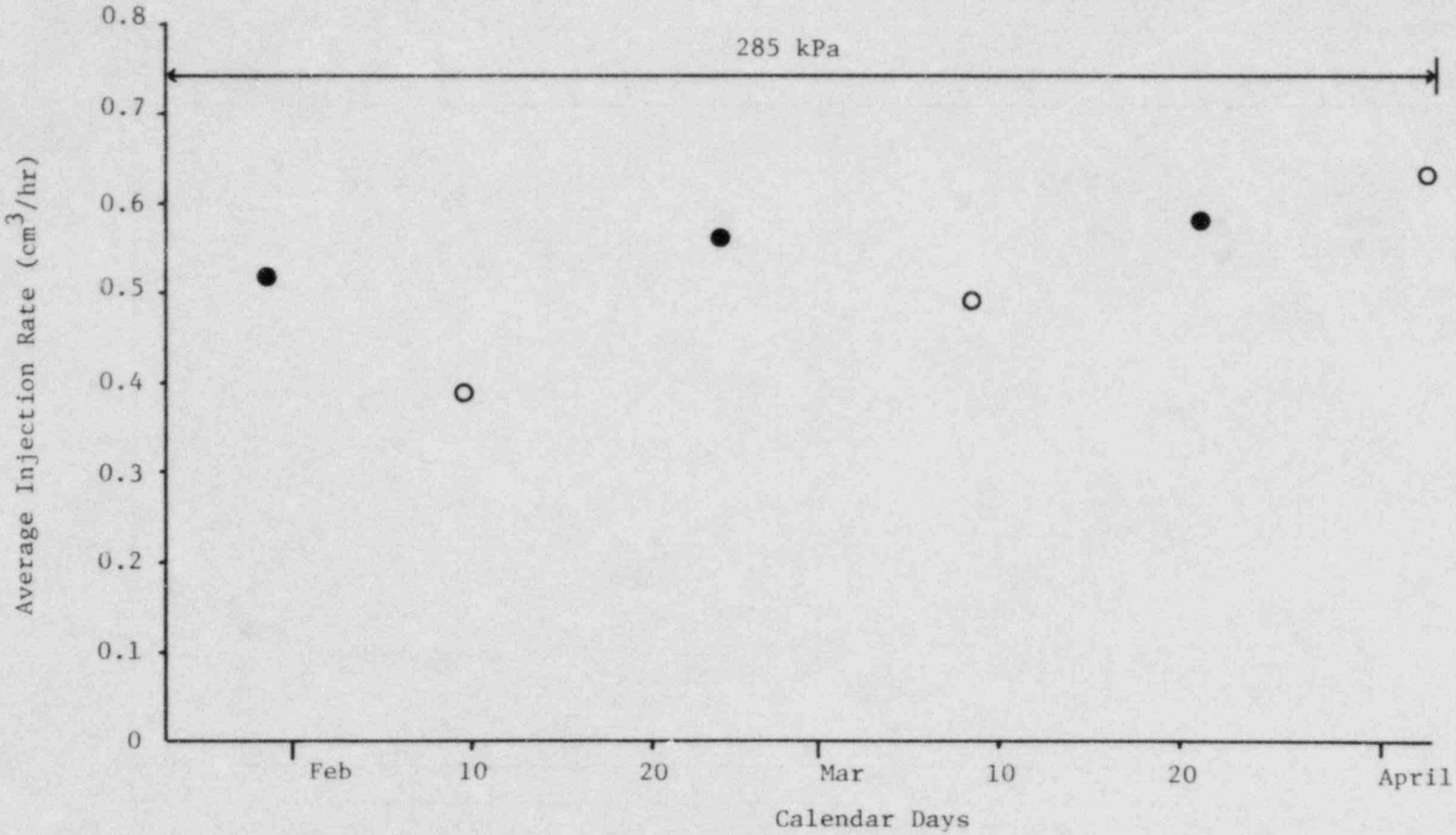

Figure 2.30 (cont.)

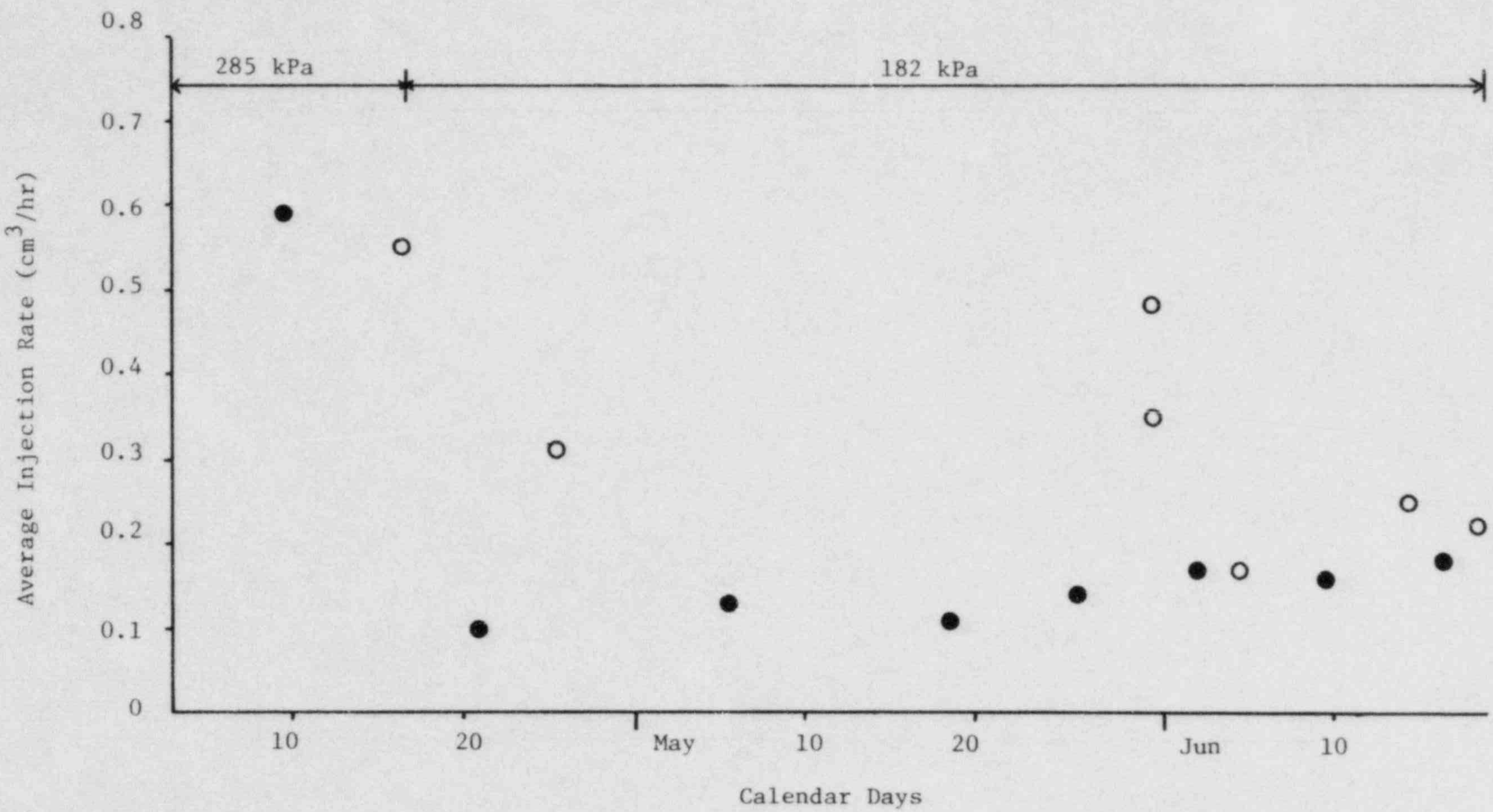

Figure 2.30 (cont.)

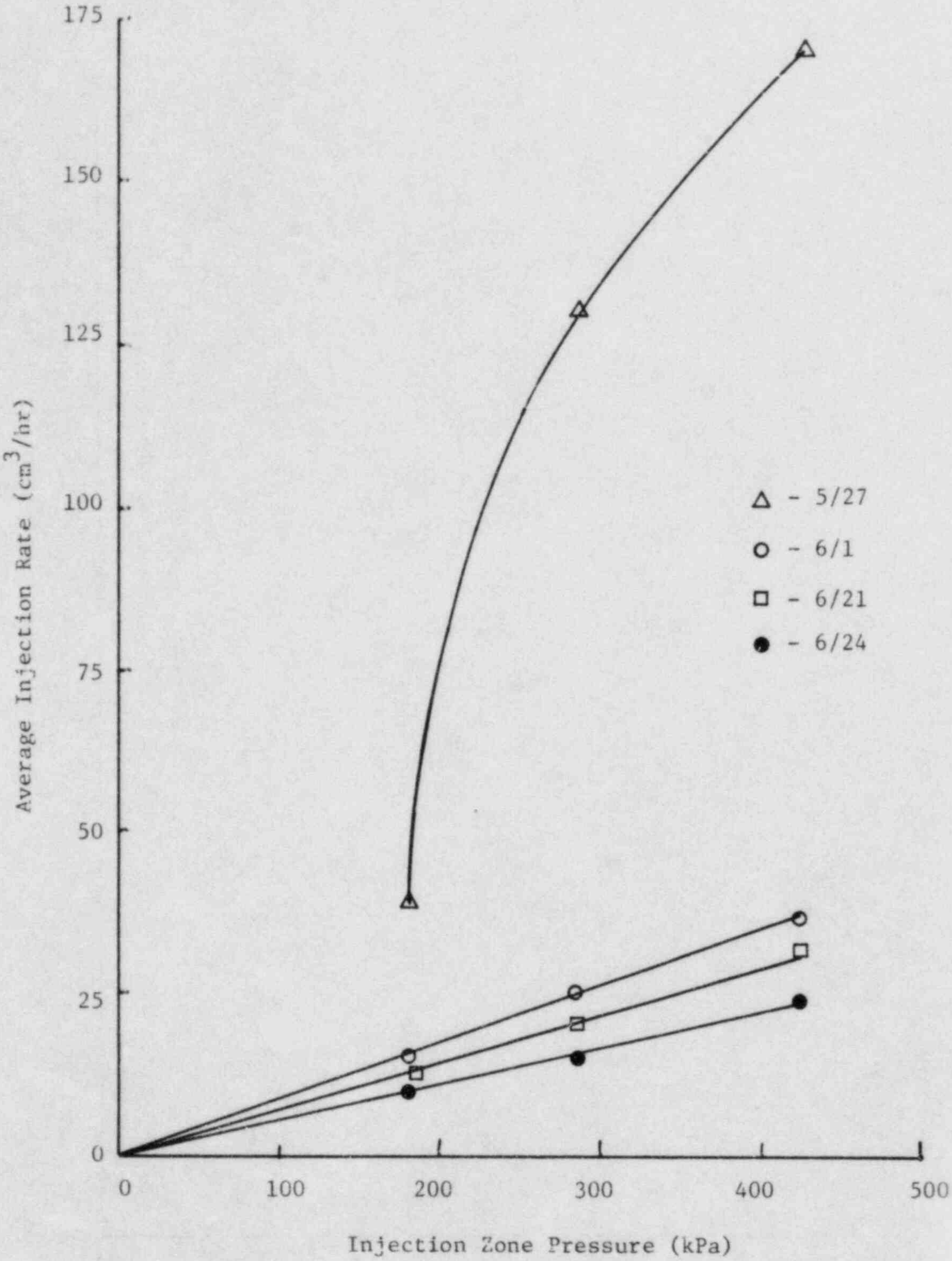

Figure 2.31 Oracle Ridge Mine average injection rate vs. injection zone pressure for constant pressure injection tests in May-June, 1983.

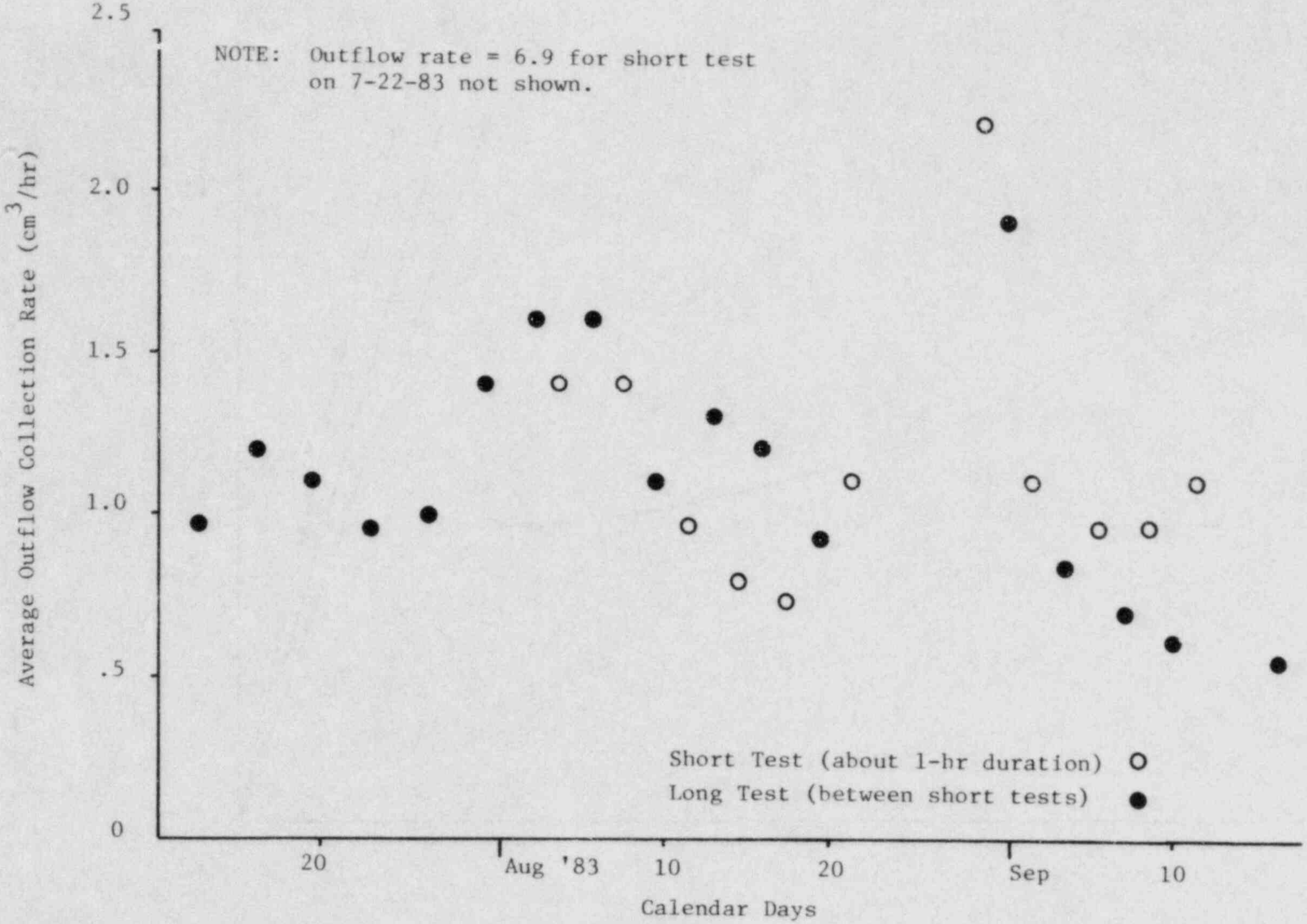

Figure 2.32 Oracle Ridge Mine average outflow collection rate vs. time for constant pressure injection testing. Period: 7-11-83 to 4-17-84.

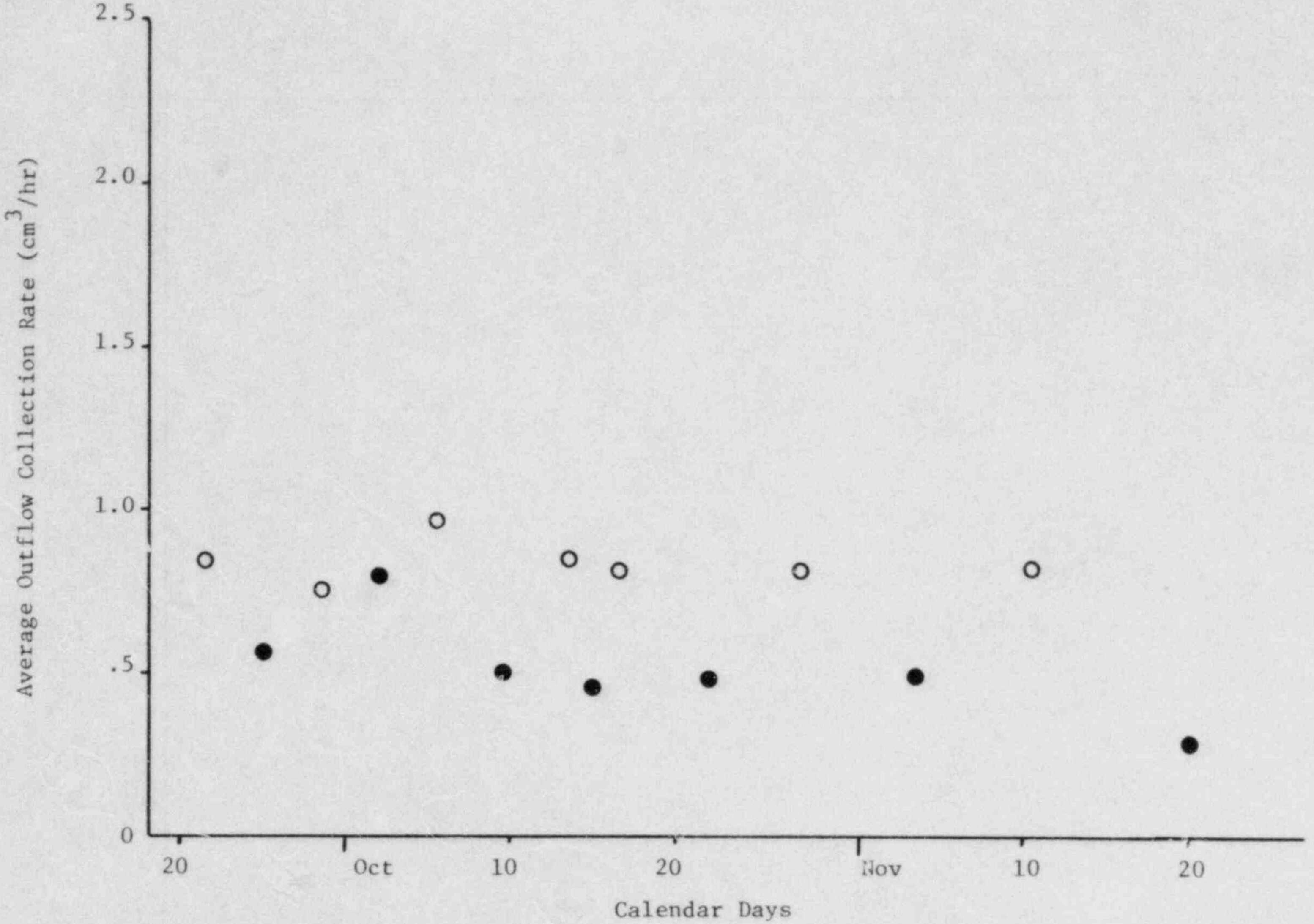

Figure 2.32 (cont.)

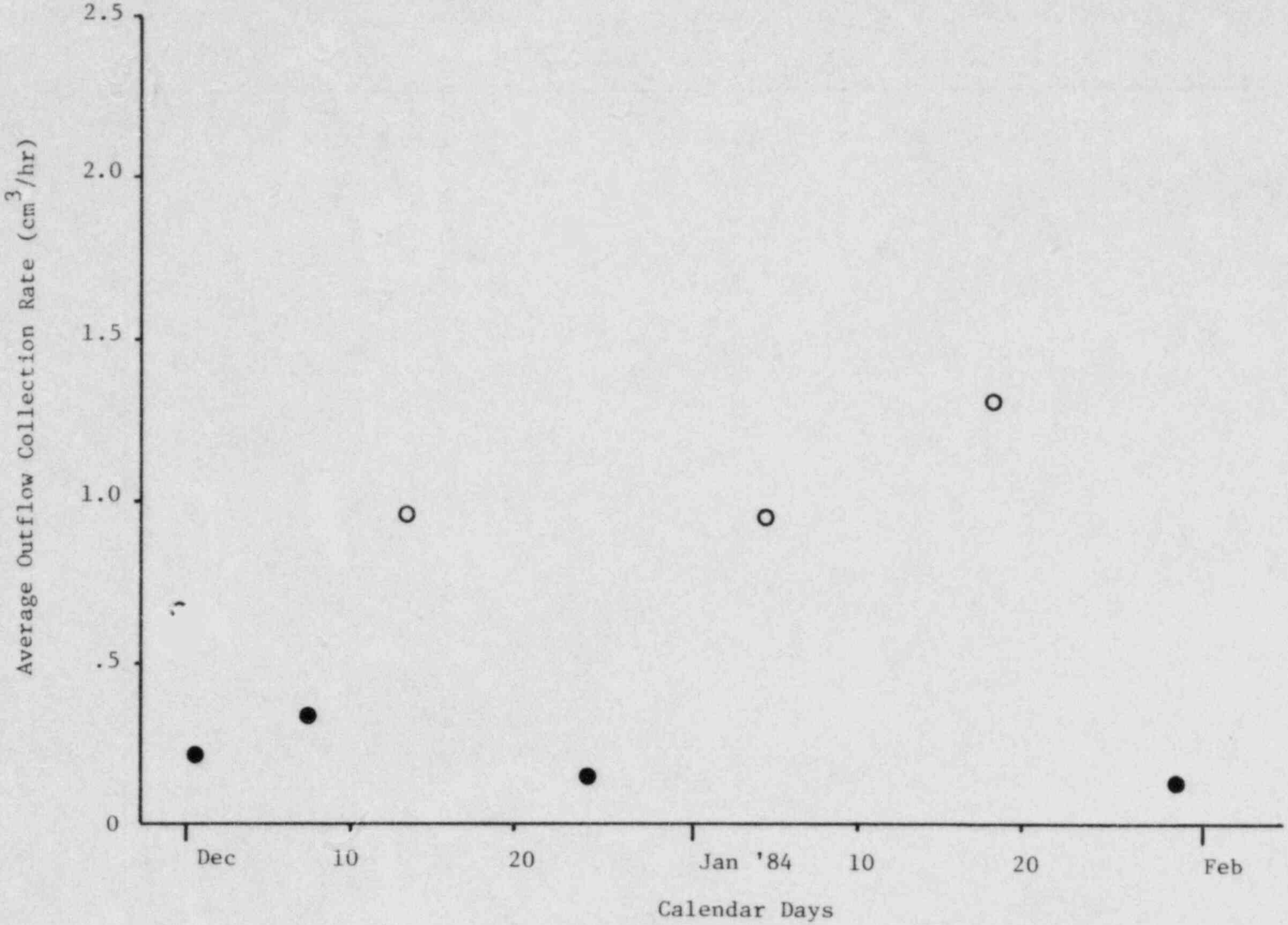

Figure 2.32 (cont.)

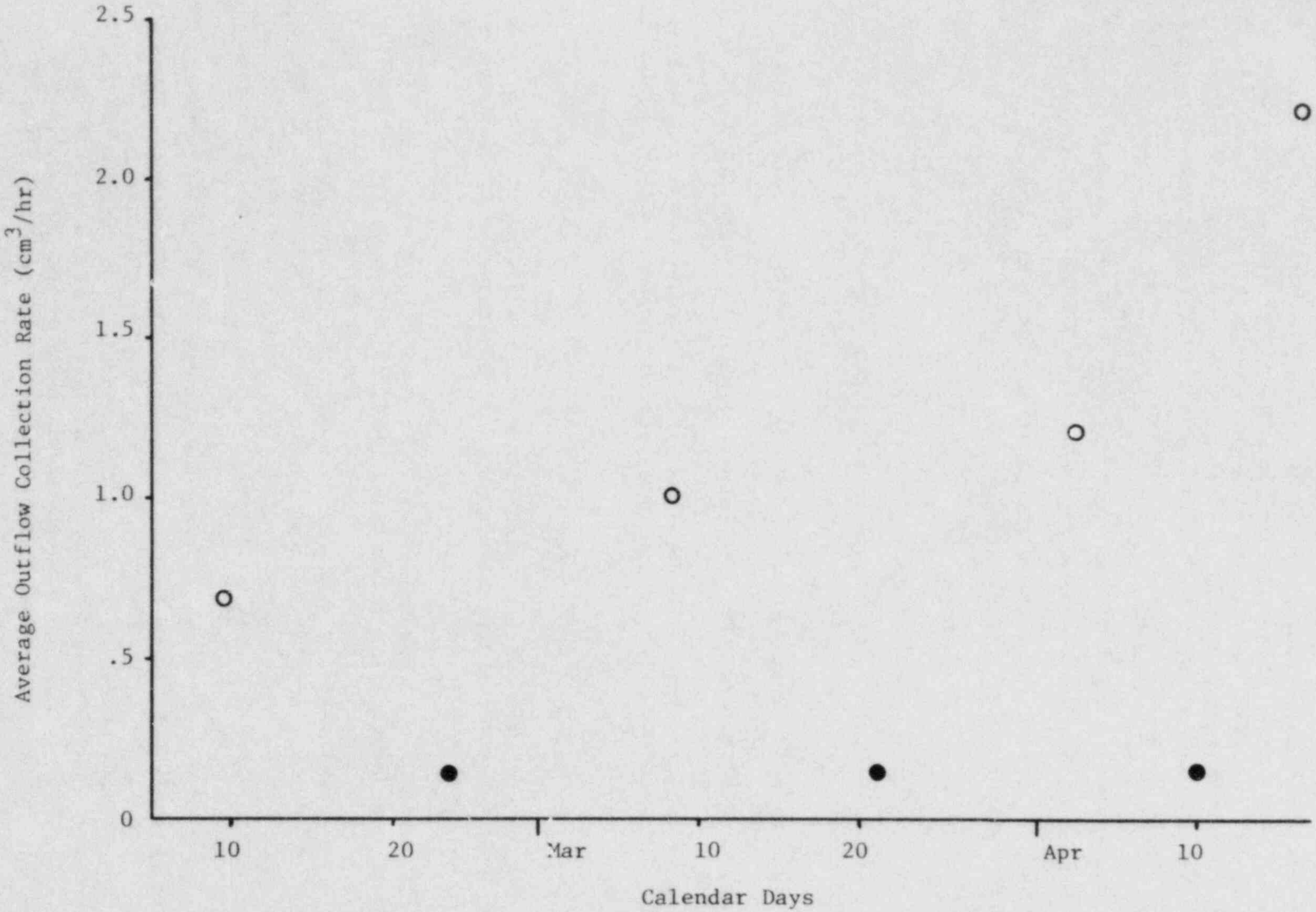

Figure 2.32 (<u>cont</u>.)

2.3.3.4.3 Injection Flow Rate Reduction Due to Interfacial Gap Closure. Though initial injection rates were quite high, as testing continued the injection rate dropped off dramatically (e.g. compare the flow rates of May 17 with those of June 1, 1983 for about the same pressure). This reduction, at least in part,† was due to the closure of the interfacial gap. It is certain that the gap closed at least to some degree. By June 1983 the rate of flow which could be visually observed coming through the plug during injection testing was greatly reduced. The mechanism causing the gap to close is not certain. At least four factors may have contributed to the closure:

(1) Radial expansion of the plug as the cement continued to cure.

(2) Chemical interaction between the cement and the dolomite host rock.

(3) Chemical interaction between the injection water and the cement/dolomite.

**For example, in packer tests prior to plug emplacement, the highest equivalent hydraulic conductivity (k_e) measured for any subinterval from 27.27 m to 29.81 m (or for 254 cm above the plug) was 5.1×10^{-9} cm/sec (Table 3.1 and Figure 3.3, Daemen et al., 1983). For $k_e = 5.1 \times 10^{-9}$ cm/sec, test zone length (ℓ) = 254 cm, test zone excess pressure (H_o) = 280 k[illegible] 2860 cm of water, borehole radius (r_o) = 5 cm and radius of influence (R) = ℓ = 254 cm, a steady-state injection rate (Q) for radial flow into a homogeneous, radially isotropic porous medium can be calculated using the follwing expression recommended by Ziegler (1976):

$$Q = (2\pi k_e \ell H_o)/(\ln(R/r_o))$$

Substituting the above values into this expression gives a flow rate Q = 21 cm^3/hr. May injection flow rates were 5 to perhaps 50 times this figure for comparable pressures.

***The term "gap", though imprecise, is used throughout this discussion to describe the interfacial crack or area of high permeability along the crown of the plug. The exact nature of the gap or highly permeable area is unknown. It is not unlikely, however, that the gap is due to a gravity induced settlement, the primary cause of gaps developing on top of plugs installed in tunnels and mine drifts, a major concern for all underground horizontal plug or dam installations.

†Some reduction in constant pressure injection with time would be expected even if the gap were not closing. This reduction would occur in that part of the injection flow passing into the rock matrix bordering and fractures intersecting the injection zone (component 1). This reduction has been demonstrated theoretically for some flow situations. For example, Jacob and Lohman (1952) have derived an expression showing that constant pressure radial injection "declines roughly as the inverse of the sum of a constant and the logarithm of the time." Their work applies to radial flow from a well in a saturated, homogeneous, radially isotropic and infinite porous medium.

(4) Deposition of particulates borne in the injection water.

Based on the expansive character of the Dowell System 1 cement (Daemen et al., 1983) used for the plug and based on the rapidity of the gap closure and injection rate reduction, it seems likely that the first factor was dominant. The fourth factor is not thought to be significant as the borehole was brushed and flushed prior to plug placement. Further, the sump water used for injection appears free of any significant suspended solids and, additionally, the sump water is filtered prior to use in the injection pump. Further analysis of the factors will be undertaken.

<u>2.3.3.4.4 Approximately Steady-State Injection Flow Rate</u>. With a relatively constant injection pressure of about 285 kPa (41.3 psi), the injection flow rate declined until an approximately steady* rate was achieved in January 1984. From January 1 to May 17, 1984, when testing at 285 kPa was terminated, the injection rate for the long duration tests averaged 0.56 cm^3/hr. The portion of this average "steady" flow rate which passed through the plug and/or plug/borehole interface (component 2 flow) is unknown.

<u>2.3.3.4.5 Significance of Gradual Attainment of Steady-State Injection</u>. The long time period required for the injection rate to attain approximate steady state indicates that, particularly in the later months of testing, component 1 flow (radial flow into rock matrix and fractures) constituted a significant portion of the overall injection flow. If flow through the plug/borehole interface (component 2) greatly exceeded component 1 flow (as may have been the case initially), then the flow rate should have equilibrated relatively rapidly since the hydraulic gradient driving component 2 flow is virtually constant. However, if a significant portion of the injection flow were component 1 flow, the flow rate would require a much longer period to approach approximate steady-state (see previous footnote).

<u>2.3.3.4.6 Darcian Flow Through Plug/Borehole Interface</u>. Figure 2.31 is a plot of injection rate vs. injection pressure for four series of tests conducted in May and June, 1983. The flow rates for the May series are

---

*In many constant pressure injection situations, the radial portion (component 1) of the flow from the injection zone theoretically never becomes steady, but, rather, continues to decrease (see previous footnote). But because the rate of decrease in the radial component is itself often decreasing with time, an approximately steady radial injection rate is often eventually achieved. On the other hand, the portion of the flow through the plug and/or plug/borehole interface (component 2) should become steady and should achieve steady state relatively quickly. The reason this portion of the flow should achieve steady-state and do so quickly is because the hydraulic gradient across the plug which drives this component of the flow is established relatively quickly and does not change with time.

quite high. The flow rates for the June series are much lower with each successive series having lower rates than the previous series for the same pressures. Presumably, the reduction in flow rate with time for a given injection pressure was due primarily to the closure of the plug/borehole interfacial gap (2.3.3.4.3).

The curve for the May 27 series is non-linear with decreasing slope. According to Louis and Maini (1970), and Ziegler (1976), such a curve indicates that injection flow is turbulent. The plots for the test series in June, however, are quite linear, indicating that the overall flow (i.e. sum of components 1 and 2) is in the linear-laminar range and therefore that Darcy's law* is applicable (Ziegler, 1976; Freeze and Cherry, 1979, pp. 72-74). Thus, with closure of the plug/borehole interfacial gap, it appears that the overall flow regime, for the range of pressures shown in Figure 2.31, changed from turbulent to linear-laminar.**

Assuming that in the June tests flow was linear-laminar and assuming that in these tests component 2 flow was dominant, then it seems clear that in later tests, where the injection rate was even lower, the flow through the plug and/or plug/borehole interface must also be linear-laminar. Justification for this conclusion is made based on the findings of Louis concerning the distinction of linear-laminar flow from transitional and turbulent flow for fracture flow between parallel

---

*Darcy's law is an empirical relationship which is foundational to most analyses of fluid flow in porous media and fractures. In its simplest form, applicable to flow in a homogeneous, isotropic porous medium, Darcy's law holds that $Q = -kiA$, where Q is the fluid discharge through cross-sectional area A, i is the hydraulic gradient in the direction of flow and k is a proportionality constant (hydraulic conductivity).

**The justification for plotting injection pressure in Figure 2.31 may be made as follows: If the injection flow were primarily radial (component 1 flow), then, strictly, the pressure to be plotted is excess pressure, that is, the injection pressure less the ambient pressure in the formation. However, since the formation is unsaturated, Ziegler recommends that the ambient pressure be taken as zero (Ziegler, 1976). Thus, for injection which is primarily radial in an unsaturated formation, the injection pressure is assumed to equal the excess pressure. If, on the other hand, injection flow is predominantly through the plug and/or plug/borehole interface (component 2 flow), then the pressure to be plotted is the injection pressure less the pressure on the collection side of the plug. The reason this difference in pressure is plotted is because the hydraulic gradient across the plug which drives component 2 flow is directly proportional to the pressure difference across the plug. However, the pressure on the collection side of the plug is zero (gage) or very nearly so. Thus, for predominantly component 2 flow, the injection pressure is equal to the pressure difference across the plug.

plates (Ziegler, 1976). To use Louis's findings it must be assumed that the flow through the plug and/or plug/borehole interface (component 2 flow) may be considered flow through a parallel plate fracture. This assumption seems reasonable since most of the flow appears to have passed through an interfacial gap along the crown of the plug, at least initially. Also, based on a laboratory estimate of the hydraulic conductivity of the plug cement, very little of the component 2 flow would be expected to pass through the plug itself.* Louis defined the Reynold's number for parallel plate fractures as $R_e = 2dv/V$, where v = flow velocity in the fracture, d = width of aperture between parallel plates, and V = kinematic viscosity of the fluid. Louis found that for model fissures where the surface roughness index** is less than or equal to 0.033, flow is linear-laminar for R_e less than about 2300.

Assuming that in the June 1983 tests the injection flow was linear-laminar (as Figure 2.31 indicates) and assuming that component 2 flow was dominant (i.e. greatly exceeded the component 1 flow), then the component 2 flow was probably linear-laminar in these tests. If the component 2 flow was linear-laminar and the parallel plate assumption for flow through the interfacial gap is valid, then the following Poiseuille expression for laminar flow of a fluid between two parallel plates should be valid (Ziegler, 1976):

$$v = gd^2i/12V$$

---

*A laboratory estimate of the hydraulic conductivity (k) of Dowell System 1 cement is 1.8×10^{-10} cm/sec (Section 2.4.3). Assuming 1-dimensional porous media flow across a homogeneous plug, the flow rate (Q) can be computed as follows:

$$Q = (k(H_1 - H_c)A)/L$$

where H_i = pressure load on injection side of plug
H_c = pressure head on collection side of plug
A = cross-sectional area of plug
L = plug length.

For $K = 1.8 \times 10^{-10}$ cm/sec, H_i = 285 kPa = 2910 cm H_2O, $H_c = 0$, $A = 78.5$ cm^2, and $L = 12.7$ cm,

$$Q = (1.8 \times 10^{-10})(2910 - 0)(78.5)/12.7 = 3.24 \times 10^{-6}\ cm^3/sec = 0.012\ cm^3/hr,$$

which is very small compared to the flow rates measured in the June tests.

**Surface roughness index (S) = Y/2a where Y = mean height of the asperities on the fissure walls and a = mean fissure aperture (Ziegler, 1976).

where v = fluid velocity
i = hydraulic gradient in the direction of flow
g = acceleration due to gravity
d and V are as previously defined.

But with the closure of the gap, d would diminish, thus decreasing v according to the above equation. (The decreasing of d and v is consistent with the observed decrease in component 2 flow with time.) But if d and v decrease and V remains unchanged, then the R_e for tests subsequent to the June tests should be less than it was for the June tests. Thus, the flow through the plug/borehole interface in tests subsequent to the June tests should be linear-laminar also.

2.3.3.4.7 Response to Reduction in Injection Pressure. On April 17, 1984 injection pressure was reduced from about 285 kPa (41.3 psi) to about 182 kPa (26.4 psi) (Table 2.20). The injection flow rate dropped immediately from about 0.56 cm^3/hr to about 0.10 cm^3/hr, but has been slowly rising since then (e.g. the injection rate had risen to 0.19 cm^3/hr for the test for June 15-19. The slow rise in flow rate after April 17 is perhaps due to the gradual depressurization of the formation immediately surrounding the injection zone. As the formation pressure drops to a new approximate equilibrium (corresponding to the lower injection pressure), the hydraulic gradient causing flow into the formation (component 1 flow) slowly rises until a new equilibrium is approximately attained.

2.3.3.4.8 Discrepancy Between Long and Short Injection Test Data. As shown in Table 2.20 and Figure 2.30, slightly lower injection rates were obtained from the short tests (approximately 1-hour duration) than from either the preceding or following long tests (several days to several weeks in duration). No explanation for this discrepancy is known. There is no significant interruption of or change in injection flow or pressure between tests. The calibration of the injection vessels of the injection pump has been checked. Based on their much longer duration and much greater injection volume, the long tests are probably the more accurate.

2.3.3.4.9 Collection Data. The following inconsistencies are noted in the outflow collection data presented in Table 2.20 and Figure 2.32.

(1) In general, the collection rates for short tests (approximately 1-hour duration) are considerably higher than collection rates for either the preceding or the following long tests (several days to several weeks in duration) for collection system 2 (used from August 1, 1983 to May 22, 1984). (2) In general, collection rates for long tests are higher when collection system 3 was used than when collection system 2 was used.

The observed inconsistencies and general variation in the data may be due to a number of causes, including (a) differences in the collection systems used, (b) differences in the degree of saturation and hydraulic head in the rock mass bordering and fractures intersecting the collection zone. Such differences may be due to variation in local rainfall or other factors affecting moisture availability as well as the effects of sustained injection, and (c) differences resulting from differences in procedure. For example, with collection system 3, in short tests where the line to the graduated cylinder/pipet was bled of air just before the test, collection rates were much higher than similar tests where the line was not bled.

Further analysis of collection data is being made. A more reliable collection system/procedure is being developed.

2.3.3.4.10 Future Work. An improved outflow collection system is in development. A tracer test to determine travel time for flow across the plug is in progress at the time of writing this report. Numerical modeling to aid in analysis of plug/formation flow is planned.

2.4 Laboratory Testing in Support of Field Tests

2.4.1 Bailer Placed Plugs

Cement plugs placed at the McNary Dam site were placed under submerged conditions using a dump bailer (Section 2.2.6.1.4). Prior to field emplacement a number of cement plugs were placed in the laboratory in transparent acrylic and translucent PVC tube sections under similar conditions to those anticipated in the field in order to evaluate the effectiveness of the method of installation. The initial laboratory testing was reported in the previous Annual Report (Daemen et al., 1983).

2.4.1.1 Minute Upward Channeling Water Streams in Curing Cement Plug

In placing a cement plug in the field, it was considered necessary to provide some type of highly permeable buffer material between the below-plug instrumentation and the cement plug. The buffer material would help protect the downhole instrumentation when the borehole plug is finally drilled out and recovered. The buffer would also provide a suitable surface on which to place the cement. A layer of clean sand and gravel was selected for use as the buffer. However, in laboratory tests, when plugs were placed underwater on a sand/gravel bed, a problem occurred in virtually every plug placed. Presumably due to its lighter density, water, in the form of minute streams, channeled upward through the heavier cement slurry within a few minutes after placement. As the water flowed upward, it separated the cement leaving a black and apparently more dense material in the channels. In some cases, when this action ceased, the channels appeared to partially or completely seal. In other cases, transparent crystals formed in the channels or the channels remained opened.

2.4.1.2 Reduction/Prevention of Channels

In order to prevent or reduce the extent of channeling, it was thought that a material several orders of magnitude higher in permeability than the cement, yet capable of reducing the rate of upward water flow, could be used either instead of the sand/gravel or placed on top of it. Materials considered included porous stone, sintered metal, sponge, foam rubber, a cement mix with high water content and plaster of paris. Of these materials, plaster of paris and polyurethane foam were tested.

2.4.1.2.1 Plaster of Paris Layer. In order to simulate the working conditions at the McNary Dam site, a 9.1 m (30 ft) well was constructed inside one of the campus buildings. The well consisted of 7.3 m (24 ft) of 10.2 cm (4-in) schedule 40 PVC pipe and 1.8 m (6 ft) of 11.4 cm (4.5 in) o.d. acrylic tubing with a 0.318 cm (0.125 in) wall thickness. The bottom of the PVC pipe was capped. The acrylic tube was spliced into the pipe 0.9 m (3 ft) from the bottom with Dressler couplings.

Four plaster plugs were placed underwater in the clear acrylic tubing section of the laboratory well. For each plug, 1600 g (3.53 lb) of plaster of paris were mixed for 5 minutes with 2000 g (4.41 lb) of 14°C (57°F) water. The plaster was lowered in the well with a bailer made from 6.4 cm (2.5 in) schedule 40 PVC pipe and released 1.3 cm (.5 in) above the sand. After initial set-up of the plaster, the acrylic section was removed and replaced with another section for the next plaster plug.

Water channeling occurred in each of the four plaster plugs placed. A falling head hydraulic conductivity test was performed on the first plug. The test was performed by filling the acrylic tube in which the plug was poured with water. The base of the plug was taken as the reference datum for the head measurement. The hydraulic conductivity is calculated from (Cedergren, 1977, pp. 49-51):

$$K = \frac{aL}{Adt} \ln\left(\frac{h_0}{h_1}\right) .$$

A and a are the same area and cancel. The plug length L is taken as 23 cm (9 in). The elapsed time between measurements is dt. The initial head is h_0 and the final head is h_1. The results are presented in Table 2.21.

Attempts to perform falling head tests on the second and third plugs failed. In both instances, the acrylic tube containing the plug was left in the laboratory well so that the full head of water of the well was available for the test. However, with the second plug, the tube shattered as a hole was being drilled in the acrylic to reduce the pressure below the plug to atmospheric. With the third plug, the water channels gradually eroded until the entire 8.5 m (28 ft) of water in the well gushed past the plug. Figure 2.33 shows the plug after being washed out. The erosion took place along the most heavily channeled portion of the plug.

The fourth plaster plug was also left in the laboratory well and was allowed to cure for three days. Then the top of the plug was ground down until 11.4 cm (4.5 in) of solid plaster remained. The loose plaster was flushed out of the well with water.

A cement plug was then placed over the plaster. The cement plug was made out of five standard batches (South et al., 1982) of System 1 cement which were individually prepared and then mixed together. The cement was lowered into the well in the bailer and released. This formed a 15 cm (6 in) section of the plug that was fairly uniform except

Table 2.21 Hydraulic Conductivity of Plaster Plug #1

Date	Time of day (hr:min)	Time (min)	Head (in)	K x 10^3 (cm/sec)
8/3/83	12:30		16.50	
	2:05	95	12.50	1.120
	2:15		23.50	
	2:34	19	22.31	1.048
	2:46	12	21.50	1.174
	3:22	36	19.25	1.170
	4:32	70	15.88	1.047
	5:31	69	13.44	0.921
8/5/83	3:40		21.50	
	4:40	60	17.87	1.174
	6:37	117	12.62	1.133
8/11/83	12:40		26.75	
	1:10	30	24.75	0.987
	1:50	40	22.75	0.803
	3:30	100	17.62	0.974
	4:35	65	15.12	0.897
	5:20	45	13.62	0.885
	6:05	45	12.12	0.988
8/19/83	11:45		25.88	
	12:25	40	23.50	0.919
	2:20	115	17.37	1.001
	2:45	25	16.50	0.783

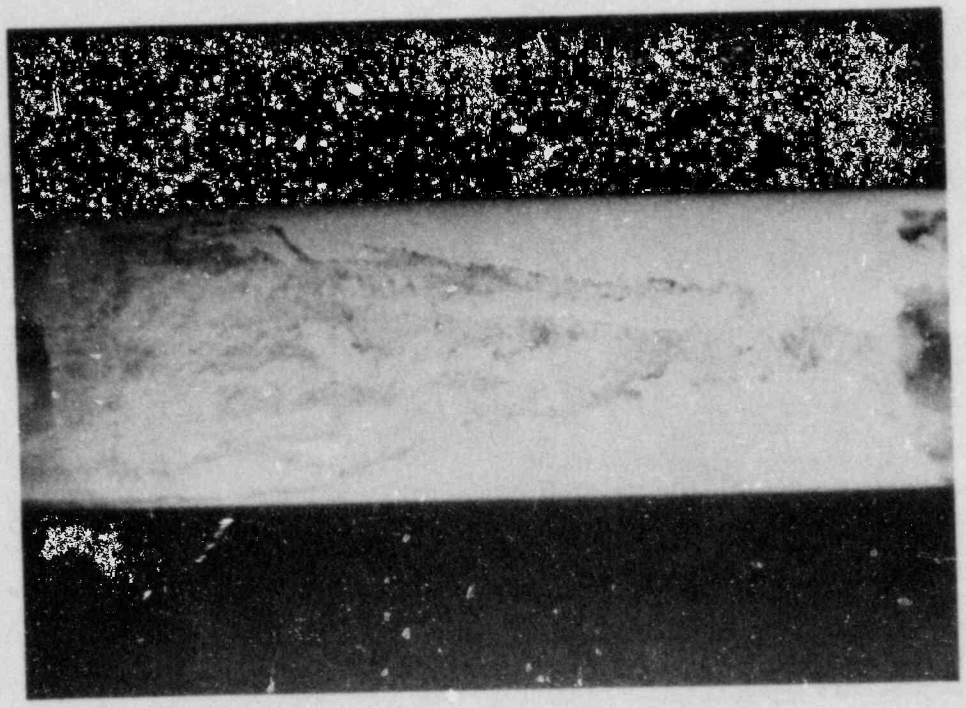

Figure 2.33 Plaster plug #3 after falling head test.

Small channels formed by water that flowed upward through the plug immediately after it was poured gradually eroded into a large gap during a falling head test.

that four channels developed. Each channel was a continuation of a channel already existing in the plaster plug. However, channels did not form in the cement above every channel that existed in the plaster. The ratio was about one channel in the cement per five channels in the plaster. The flow of water through the channels in the cement was considerably less than observed in cement plugs poured directly over sand (Daemen et al., 1983). Some cement mixed with water when the cement was released, which created a light colored swirl of cement for the upper 6.4 cm (2.5 in). Below the swirl was a 5 cm (2 in) layer of light cement that probably washed off the bailer as it was removed from the well. Figure 2.34 is a picture of the plug intact.

Three days after the cement plug was poured on top of the plaster, a rubber stopper in the bottom section of the PVC pipe was removed, thus equalizing the pressure below the plug with that of the atmosphere. With the well full of water, the top of the pipe was plugged with an expandable stopper (like those shown in Figure 3.9 of the previous annual report (Daemen, et al., 1983)). A 25 ml (0.85 fl oz) pipet was placed inverted in the center hole of the stopper. The well above the plug and pipet were filled with water. A constant head permeability test of the plug and plaster was performed by observing the fall of the water level in the pipet over time. After the first week of testing, the stopper began to leak and was eventually replaced with a PVC end cap. This too developed a leak which was repaired.

The water loss over the final 49 days of the test averaged 1.0 cc/day (0.061 cu in/day). The recorded flow rates varied considerably, due in part to temperature variations. A day-by-day log of water loss is recorded in Table 2.22.

From the average flow rate, an approximate hydraulic conductivity can be calculated. For a constant head test, Lambe and Whitman (1969) provide the equation

$$k_v = \frac{4qL}{H_c \pi C^2}$$

where q is the flow rate, L is the sample length, H_c is the head, C is the plug diameter, and k_v is the vertical hydraulic conductivity.

Based on this equation, an average hydraulic conductivity of 4×10^{-9} cm/sec was calculated. During the last one to two weeks of observation, some seepage occurred out of two stress cracks. The cracks started to appear in the acrylic tube, primarily around the solid section of cement, shortly after the plug was installed. The cracks gradually increased in number until the tube finally ruptured. The cracks reduce the reliability of the calculated hydraulic conductivity.

2.4.1.2.2 Polyurethane Foam Layer. Another material tested in the laboratory for its effectiveness in reducing the upward channeling of water was polyurethane foam. In the laboratory experiment a thick cushion of foam disks was used in place of the sand/gravel layers. The success of the foam in reducing the upward channeling of water streams

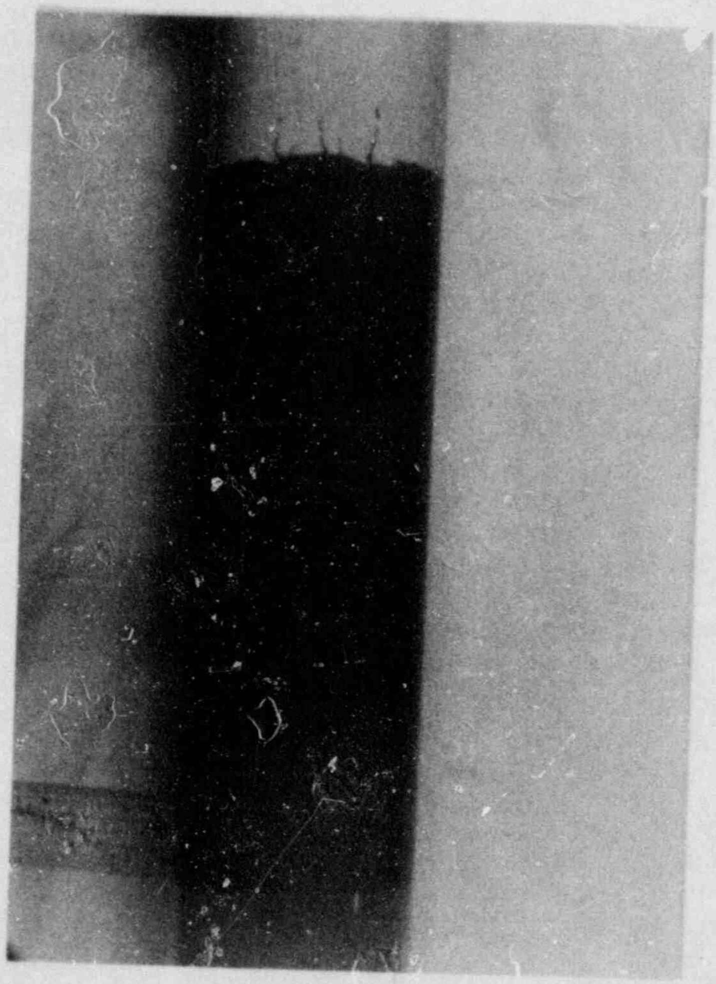

Figure 2.34 Cement plug placed over plaster.

A plaster plug was placed by a bailer over a sand base, the top ground off, and a cement plug placed on top of it. This resulted in fewer channels being formed in the cement plug.

Table 2.22 Cement Bailed Over Plaster Plug

Date	Time of Day	in Pipet (ml)	Water Loss (ml)	Comments
Aug 22	11:25 am	12.0		
	12:15 pm	6.4	+5.6	added water to pipet
	12:15 pm	20.8	-	
	2:22 pm	21.2	-0.4	
	4:00 pm	21.4	-0.2	
23	6:00 pm	18.8	+2.6	
24	5:50 pm	19.9	-1.1	
26	9:45 am	13.8	+6.1	
29	9:30 am	3.8	+10.0	
	9:40 am	13.8	-	added water
	5:30 pm	15.2	-1.4	
30			+15-50	water disappeared below pipet
	10:40 am	16.6	-	added water
31	9:40 am	15.8	+0.8	
Sept 1	9:20 am	14.4	+1.4	
2	9:30 am	10.8		
6	10:05 am	14.7	+18.6	added 22.5 ml to get reading
7	9:25 am	14.3	+20.4	added 20 ml to get reading
7	5:40 pm	15.0		changed expandable packers - previous one leaked
8	9:30 am	15.1	+18.5	added 18.6 ml to get reading
	10:50 am	7.7	+7.4	water on top of expandable plug indicated leak
				replaced expandable plug with a 4-in pvc cap
20	5:20 pm	13.9	-	added 25.0 ml to get reading
22	4:50 pm	13.2	+0.7	
23	10:40 am	-	-	found water on top of pvc cap
24	10:40 am	-	-	found and sealed leak
27	12:15 pm	21.2	-	added water to pipet

Table 2.22 Cement Bailed Over Plaster Plug--<u>Continued</u>

Date	Time of Day	in Pipet (ml)	Water Loss (ml)	Comments
Sept 28	11:00 am	18.7	+2.5	
29	10:00 am	15.0	+3.7	
30	12:15 pm	12.5	+2.5	
Oct 3	10:05 am	6.8	+5.7	+1.9 ml/day ave
3	10:06 am	15.8	-	added water
4	10:00 am	14.6	+2.2	
5	10:00 am	13.6	+1.0	
6	10:50 am	13.5	+0.1	
7	11:45 am	11.2	+2.3	
10	11:25 am	9.3	+1.9	+0.62 ml/day ave
12	11:25 am	8.4	0.9	+0.45 ml/day ave
13	12:25 pm	6.9	+1.5	
14	10:00 am	6.4	+0.5	
17	10:30 am	4.3	+2.1	+0.7 ml/day ave
17	10:30 am	21.0	-	added water
18	10:45 am	19.0	+2.0	
19	9:20 am	19.1	-0.1	
20	10:00 am	17.9	+1.2	
21	9:25 am	15.2	+2.7	
24	9:05 am	14.1	+1.1	+0.37 ml/day ave
25	9:25 am	14.2	+0.1	room was cold
26	9:25 am	13.1	+1.1	room was cold
27	9:45 am	11.5	+1.6	room was cold
28	9:20 am	8.7	+2.8	room was warmer
31	9:30 am	6.5	+2.2	+0.73 ml/day ave
Nov 1	9:25 am	5.4	+1.1	
2	8:45 am	4.5	0.9	Noticed that water had been seeping out of a stress crack in the acrylic for days.
3	9:45 am	4.5	0.0	

Table 2.22 Cement Bailed Over Plaster Plug--Continued

Date	Time of Day	in Pipet (ml)	Water Loss (ml)	Comments
Nov 4	8:35 am	2.4	+2.1	
4	8:35 am	22.4	-	added water
7	8:40 am	19.8	+2.6	+0.87 ml/day ave
8	10:00 am	18.1	+1.7	
9	8:45 am	19.3	-1.2	
10	8:45 am	19.1	+0.2	
11	9:35 am	-	-	Found acrylic split open and all of the water drained out.

led to its use in the plug emplacements at McNary Dam. However, in the field emplacements it was decided to retain the sand/gravel layers and to place a thinner layer of foam disks on top.

The foam disk experiment was conducted in a 10.2 cm (4 in) i.d. translucent PVC pipe. First, the tracer injection canister (the upper part of the below-plug instrumentation package; see Section 2.2.6.1.1) was lowered in the laboratory well and covered with three 12.7 cm (5 in) diameter, 5 cm (2 in) thick foam disks. The polyurethane foam has a 1 mm (0.04 in) pore diameter and a 0.02 gm/cc (7.2×10^{-4} lb/cu in) density. The disks were saturated and compressed into a 7.6 cm (3 in) o.d. pipe and released by pushing them out of the pipe with a 2.5 cm (2 in) pipe. Seven more disks were placed on top of the previous three by the same method.

The plug consisted of five standard batches of cement mixed together. The mix was poured into a bailer made out of 7.6 cm (3 in) schedule 40 stainless steel pipe. One end of the pipe had a plug in it with a 2.5 cm (1 in) diameter hole drilled through the center of it. A rubber stopper fit in the hole and had a rope attached to it. The other end of the pipe had a handle. The weight of the bailer alone was about 27 kg (60 lbs).

The bailer, loaded with cement, was lowered into the well via a hoist. The foam was compressed by the weight of the bailer. When the stopper was released, the foam held back the cement. The bailer was gradually raised with the hoist about 5 cm (2 in) and the cement was released. The resulting plug was far better than any of the previous plugs poured underwater. Figures 2.35 and 2.36 show a picture and a diagram of the plug. The plug was homogeneous for 16.3 cm (6.4 in) except for the top 2.3 cm (0.9 in), which had some segregation. The top 13.2 cm (5.2 in) were not solid and were easily ground off with a drill fashioned out of PVC.

It must be recognized that all these approaches are poor substitutions for and alternatives to conventional plugging procedures (e.g. South, 1979), necessitated by the requirement to place instrumentation below the plug, as well as by cost limitations. To some extent the channeling, and more generally the mixing of water (and some sand) in the plug might be comparable to frequently observed field cementing contamination problems by drill cuttings or especially drilling muds. However, the effects observed here are not or only poorly controlled. The tests, even if somewhat simulating some field problems, are a more or less random simulation, and certainly not a simulation of "optimum" plug performance. The severity of the problem was not anticipated, and time constraints do not allow a major revision of installation procedures for the present measurement campaign at the McNary damsite.

That channeling is not merely an academic problem or an artificial problem created by our installation procedures only, is indicated by Figure 2.37. The channels in this figure (from Sitz, 1981), mapped along the interface of a concrete plug installed in a 5 m diameter shaft show considerable similarity to the channeling observed in the laboratory installations described in more detail in the last annual

Figure 2.35 Cement plug placed underwater over foam.

The cement was lowered with a bailer into a 10 cm (4 in) i.d. clear pvc well and gradually released over the foam. As the bailer was raised, the foam drew in excess water and cement. This action and the low permeability of the foam prevented any channeling (piping) from occurring. This plug is by far the most ideal one yet formed underwater.

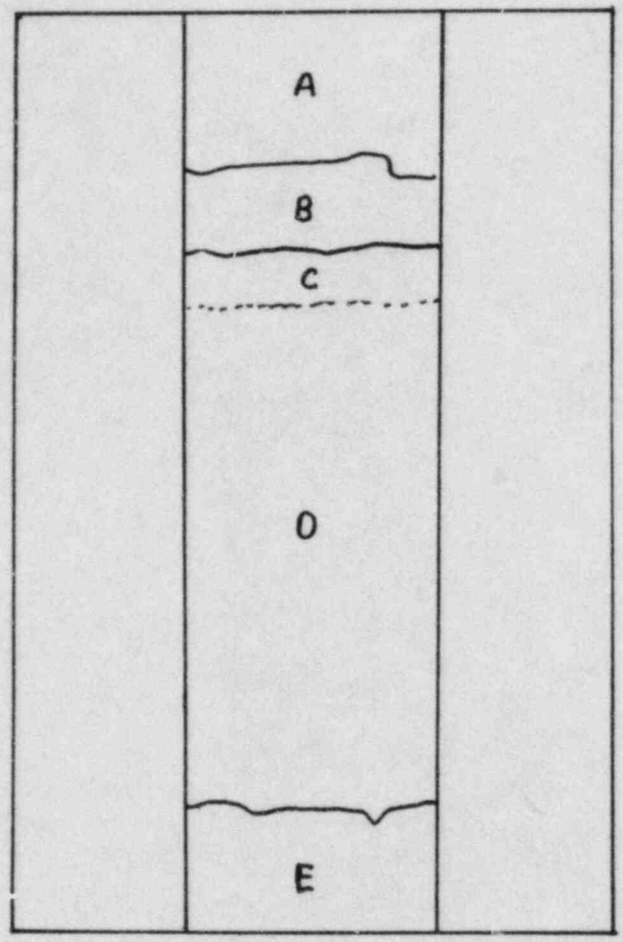

Figure 2.36 Diagram of Figure 2.35.

A) a 10 cm (4 in) thick layer of cement that washed out of the bailer as it was raised.

B) a 3 cm (12.2 in) thick spongy layer of cement that had excess water and probably includes the D47 additive.

C) a 2.3 cm (0.9 in) thick portion of solid cement that exhibited some slight segregation.

D) a 14 cm (5.5 in) long solid cement section that was homogeneous and included no channelling.

E) compressed polyurethane disks.

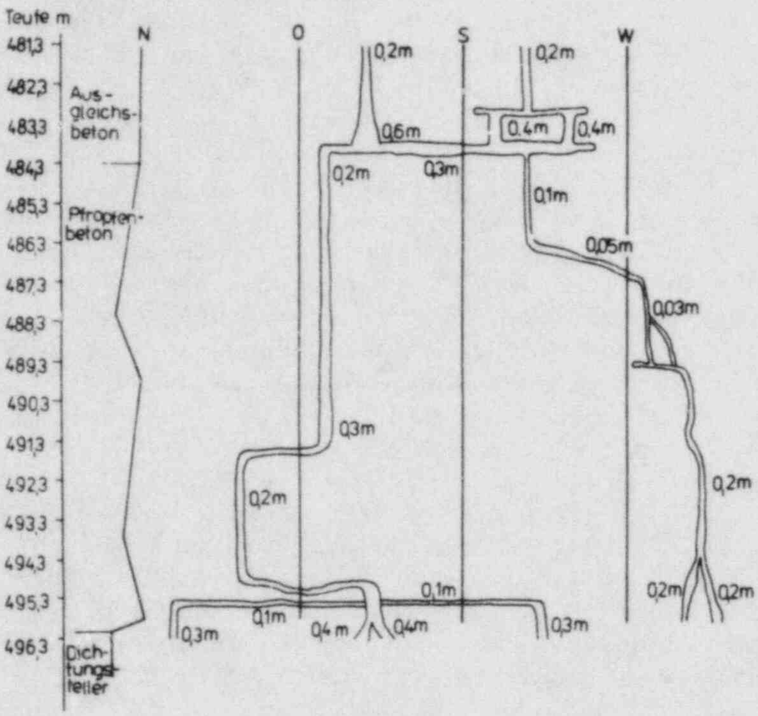

Figure 2.37 Piping (channeling) mapped along the interface between a concrete plug and the surrounding rock in the plugged rock salt section of the 5 m diameter Bernsdorf shaft. Numbers on the channels give channel width. Scale on th left shows depth below the surface, in meters.

Reproduced with permission from Sitz, 1981 (Freiberger Research Report A643, P. 11).

report (Daemen et al., 1983). It appears from the text that some of these channels also have been enlarged by water wash-out erosion.

2.4.2 Radial Permeameter Test

Two dolomite samples representative of the rock in the vicinity o the Oracle Ridge Mine borehole have been tested in one of the radial permeameters developed by South; a complete description of the permeameter and the test procedure is given by South et al. (1982). The first sample, ORM2, is 15.1 cm (5.94 in) in diameter and 30.0 cm (11.8 in) long. A 9.63 cm (3.79 in) rock bridge was left between two 2.59 cm (1.02 in) diameter holes drilled 10.3 cm (4.06 in) and 10.1 cm (3.98 in) deep in the center of the top and bottom ends, respectively. The second sample, ORM1, is 30.6 cm (12.0 in) long and 15.0 cm (5.91 in) in diameter. A 2.54 cm (1.00 in) diameter hole was drilled 9.70 cm (3.82 in) deep in the top of the sample and a 2.70 cm (1.06 in) diameter hole was drilled 10.2 cm (4.02) deep in the bottom, leaving a 10.7 (4.21 in) long rock bridge in place in the middle of the sample. The samples were stressed axially and radially. Water under pressure was then injected into the hole in the top of the samples and outflow was collected at the bottom hole at atmospheric pressure. Tables 2.23 and 2.26 summarize the results for tests with the rock bridge in place. Following tests with the rock bridges in place, the bridges were drilled out and replaced by cement plugs. The cement plugs were made using Dowell System 1 cement (Daemen et al., 1983). In ORM2, the cement plug was 10.3 cm (4.06 in) long and 9.5 cm (3.74 i) from the top and 10.2 cm (4.02 in) from the bottom of the 30.0 cm (11.8 in) long sample. In ORM1, the plug was 10.2 cm (4.0 in) long and 10.8 cm (4.3 in) from the top and 9.6 cm (3.8 in) from the bottom of the 30.6 cm (12.0 in) long sample. Tables 2.24, 2.25 and 2.27 summarize the results for tests with the cement plug replacing the rock bridge.

2.4.3 Cement Plug in Inclined Pipe

In January, 1983, an 18 cm (7 in) cement plug was placed in a 10 cm (4 in) i.d. galvanized steel pipe. The plug was cured so that the longitudinal axis of the pipe section inclined at 10° from the horizontal in order to duplicate the orientation of a curing plug at the Oracle Ridge Mine site. Since February 1983, the plug in the inclined pipe has been tested by injecting water at constant pressure into one end of the plug. The plug, the emplacement procedure and the testing procedure are described in Daemen et al., 1983, pp. 55-57. Test results through June 18, 1983 are presented in Table 2.28. From Table 2.28, the weighted (by time) average injection rate for the period March 15, 1984 through June 18, 1984 is 2.9×10^{-2} cm^3/hr. Assuming one-dimensional porous media flow through a homogeneous plug (neglecting any plug/pipe interface effects), the hydraulic conductivity (k) of the cement plug (for water flow) can be estimated using the following expression (Lambe and Whitman, 1969):

$$K = \frac{4qL}{\pi H_c D^2}$$

Table 2.23 Radial Permeameter Test Results for Sample ORM-2 with Rock Bridge

Date	Elapsed Time (min)	Axial Stress (MPa)	Confining Stress (MPa)	Top Pressure (MPa)	Flow Rate In $\times 10^3$ (cc/min)	Flow Rate Out $\times 10^3$ (gm/min)	V_A (cc)	V_I (cc)	V_O (gm)
6/17-6/18	1596	7.6	6.8	0.4	2.68	2.89	0.39	4.27	4.62
6/18-6/19	1411	7.6	6.9	0.4	2.66	2.72	0.27	3.76	3.84
6/19-6/20	1282	7.6	6.9	0.4	2.57	2.57	0.21	3.30	3.30
6/20	217	7.6	6.9	0.5	3.59	3.23	0	0.78	0.70
6/20	257	7.6	6.9	0.5	2.88	3.27	0.09	0.74	0.84
6/20-6/21	716	7.6	6.9	0.45	3.16	2.97	0.46	2.26	2.13
6/21	151	7.6	6.9	0.4	2.85	3.77	0.16	0.43	0.57
6/21	226	7.6	6.9	0.4	3.01	3.01	0.05	0.68	0.68
6/21	121	7.6	6.9	0.4	3.06	2.98	0.12	0.37	0.36
6/21-6/22	1049	7.6	6.8	0.4	3.13	3.11	0.35	3.28	3.26
6/22	117	7.6	6.9	0.4	2.74	2.99	0.06	0.32	0.35
6/22-6/23	1155	7.6	6.7	0.4	3.06	3.04	0.47	3.53	3.51
6/23	147	7.5	6.9	0.4	2.99	2.79	0.10	0.44	0.41
6/23	120	7.5	6.9	0.4	3.00	3.00	0.04	0.36	0.36
6/23	182	7.6	6.9	0.4	3.13	2.86	0.02	0.57	0.52
6/23-6/24	1002	7.6	6.8	0.4	3.01	3.00	0.38	3.02	3.01
6/24	103	7.5	6.9	0.4	2.91	2.81	0.10	0.30	0.29
6/24	145	7.5	6.9	0.4	2.97	2.90	0.03	0.43	0.42
6/24-6/25	1418	7.5	6.7	0.4	3.09	3.00	0.67	4.38	4.25
6/25-6/26	1457	7.5	6.6	0.4	2.96	3.02	0.76	4.31	4.40
6/26-6/27	150	7.5	6.8	0.4	2.20	2.20	0.28	3.29	3.34
6/27	408	7.5	6.9	0.4	2.75	0.245	0.10	1.12	0.10
6/27-6/28	1159	7.5	6.8	0.4	6.44	2.60	0.38	7.47	3.02
6/28	239	7.5	6.9	0.4	7.45	2.97	0.09	1.78	0.71
6/28-6/30	2660	7.5	6.6	0.4	3.03	3.19	0.93	8.07	8.49
6/30	176	7.6	6.9	0.4	2.95	2.90	0.11	0.52	0.51
6/30-7/1	1147	7.5	6.8	0.4	3.12	3.16	0.27	3.58	3.62

Table 2.23 Radial Permeameter Test Results for Sample ORM-2 with Rock Bridge--Continued

Date	Elapsed Time (min)	Axial Stress (MPa)	Confining Stress (MPa)	Top Pressure (MPa)	Flow Rate In $\times 10^3$ (cc/min)	Flow Rate Out $\times 10^3$ (gm/min)	V_A (cc)	V_I (cc)	V_O (gm)
7/1-7/2	1490	7.5	6.8	0.4	7.00	3.50	0.18	10.37	5.24
7/2-7/3	1391	7.5	6.9	0.4	3.01	3.30	0.12	4.19	4.59
7/3-7/4	1679	7.5	5.4	0.4	2.94	3.09	4.09	4.93	5.19
7/4	227	7.5	6.9	0.4	2.91	2.95	0.05	0.66	0.67
7/4-7/5	1291	7.5	6.8	0.4	2.82	1.58	0.17	3.64	-2.04
7/5-7/7	2493	7.5	6.8	0.4	2.86	5.36	0.16	7.15	13.36
7/7	361	7.6	6.9	0.45	3.83	3.30	0.00	1.38	1.19
7/7-7/8	1015	7.6	6.9	0.45	3.02	2.80	0.20	3.07	2.87
7/8	352	7.6	6.9	0.4	2.78	21.02	0.00	0.98	7.40
7/8-7/9	1314	7.5	6.8	0.4	3.03	3.11	0.26	3.98	4.09
7/9-7/10	1533	7.5	6.8	0.4	2.93	3.09	0.00	4.49	4.74
7/10-7/11	962	7.5	6.9	0.4	2.90	2.93	0.09	2.79	2.82
7/11-7/12	1548	7.4	6.8	0.4	2.80	3.00	0.84	4.34	4.65
7/12-7/13	1372	7.4	6.9	0.4	2.85	2.94	0.11	3.91	4.03
7/13-7/14	1484	7.5	6.8	0.4	2.77	5.63	0.16	4.11	8.38
7/14-7/15	1347	7.5	6.8	0.4	2.61	2.90	0.22	3.52	3.91
7/15-7/17	2922	7.4	6.7	0.4	2.72	2.86	0.43	7.96	8.37
7/17-7/18	1468	7.4	6.8	0.4	2.63	2.77	0.23	3.86	4.06
7/18-7/19	1388	7.4	6.8	0.4	2.59	2.77	0.16	3.60	3.85
7/19-7/20	1421	7.4	6.9	0.4	2.56	2.73	0.09	3.64	3.88
7/20-7/21	1583	7.4	6.8	0.4	2.51	2.59	0.19	3.97	4.10
7/21-7/22	1321	7.4	6.8	0.4	2.58	2.73	–	3.41	3.60
7/22-7/23	1485	7.4	6.8	0.4	2.57	2.71	0.17	3.81	4.03
7/23-7/24	1646	7.4	6.8	0.5	4.54	3.71	0.17	7.47	6.11
7/24-7/25	1245	7.4	6.8	0.45	3.86	3.70	0.16	4.80	4.61
7/25-7/26	1308	7.4	6.8	0.5	4.09	4.01	0.23	5.35	5.25
7/26-7/27	1416	7.4	6.9	0.5	33.69	3.53	0.13	47.71	5.00

Table 2.23 Radial Permeameter Test Results for Sample ORM-2 with Rock Bridge--Continued

Date	Elapsed Time (min)	Axial Stress (MPa)	Confining Stress (MPa)	Top Pressure (MPa)	Flow Rate In $\times 10^3$ (cc/min)	Flow Rate Out $\times 10^3$ (gm/min)	V_A (cc)	V_I (cc)	V_O (gm)
7/27-7/28	1515	7.4	6.8	0.5	3.06	3.25	0.23	4.63	4.92
7/28-7/29	1385	7.4	6.8	0.5	2.92	3.18	0.19	4.05	4.40
7/29-7/30	1596	7.4	6.8	0.5	2.90	3.07	0.22	4.63	3.07
7/30-7/31	1313	7.4	6.8	0.5	1.67	2.66	0.21	2.19	2.66
8/1-8/2	1573	7.4	6.7	0.4	5.87	3.92	0.26	9.23	6.16
8/2-8/3	1355	7.4	6.8	0.5	10.69	10.48	0.30	14.49	14.20
8/3-8/4	1413	7.4	6.8	0.5	3.74	3.80	0.02	5.28	5.37
8/4-8/6	3111	7.4	6.8	0.4	2.90	3.53	0.28	9.03	10.99
8/6-8/7	1648	7.4	6.8	0.4	3.04	3.28	0.28	5.01	5.41
8/7-8/8	995	7.4	6.8	0.4	3.05	3.05	0.30	3.03	3.03
8/8-8/9	1492	7.4	6.9	0.4	3.00	3.20	0.01	4.47	4.78
8/9-8/10	1328	7.4	6.8	0.6	4.85	5.06	0.53	6.44	6.72
8/10-8/11	1101	7.4	6.8	0.6	6.30	6.45	0.28	6.94	7.10
8/11-8/12	1718	7.4	6.8	0.6	4.71	4.97	0.16	8.10	8.54
8/12-8/13	1306	7.4	6.8	0.6	4.56	4.72	0.31	5.95	6.16

NOTES: Bottom pressure is always zero. V_A is the volume of water added to annulus; V_I is the volume of water pumped into top hole; V_O is the weight of water flowing from bottom hole.

Table 2.24 Radial Permeameter Test Results for Sample OKM-2 with Cement Plug

Date	Elapsed Time (min)	Axial Stress (MPa)	Confining Stress (MPa)	Top Pressure (MPa)	Flow Rate In x 10^3 (cc/min)	Flow Rate Out x 10^3 (gm/min)	V_A (cc)	V_I (cc)	V_O (gm)
9/8-9/9	1065	7.5	6.3	0.4	3.15	2.57	1.72	3.35	2.74
9/9-9/13	5738	7.5	6.3	0.4	2.51	2.73	1.77	14.39	15.64
9/13-9/14	1453	7.6	6.7	0.4	-	2.57	0.48	*-	3.74
9/14	396	7.6	6.9	0.4	2.22	2.93	0.11	0.88	1.16
9/14-9/15	1059	7.6	6.8	0.4	2.59	2.90	0.40	2.74	3.07
9/15	427	7.6	6.8	0.4	2.51	2.72	0.10	1.07	1.16
9/15-9/17	2842	7.6	6.6	0.4	2.48	2.16	0.74	7.04	6.14
9/17-9/19	2542	7.6	6.7	0.4	2.31	3.33	0.67	5.86	8.47
9/19-9/20	1306	7.6	6.7	0.4	2.24	2.53	0.43	2.92	3.30
9/20	145	7.6	6.9	0.4	2.07	2.34	-	0.30	0.34
9/20-9/22	2723	7.6	6.8	0.4	1.93	2.32	0.41	5.25	6.32
9/22-9/23	1347	7.6	7.5	0.4	2.71	2.96	1.16	3.65	3.99
9/23-9/26	4714	7.5	6.4	0.4	2.41	2.76	1.40	11.34	13.0
9/26-9/27	828	7.6	7.7	0.4	2.22	2.54	0.47	1.84	2.10

NOTES: Bottom pressure is always zero. V_A is the volume of water added to annulus; V_I is the volume of water pumped into top hole; V_O is the weight of water flowing from bottom hole.

Table 2.25 Radial Permeameter Test Results for Sample ORM-2 with Cement Plug and Nearly In-situ Confining Conditions

Date	Elapsed Time (min)	Axial Stress (MPa)	Confining Stress (MPa)	Top Pressure (MPa)	Flow Rate In $\times 10^3$ (cc/min)	Flow Rate Out $\times 10^3$ (gm/min)	V_A (cc)	V_I (cc)	V_O (gm)
9/27-9/28	1603	1.83	1.50	0.30	2.79	2.49	0.10	4.47	3.99
9/28-9/29	1246	1.72	1.52	0.28	2.59	2.64	0.06	3.23	3.29
9/29-9/30	1509	1.74	1.48	0.27	2.37	2.55	0.14	3.57	3.85
9/30-10/3	4343	1.76	1.44	0.26	-	2.38	0.20	-	10.35
10/3-10/4	1725	1.78	1.48	0.26	1.40	2.32	0.10	2.42	4.01
10/4-10/5	1455	1.78	1.48	0.32	3.04	3.13	0.14	4.43	4.55
10/5-10/6	1220	1.79	1.48	0.32	2.92	2.90	0.14	3.56	3.54
10/6-10/7	1678	1.80	1.48	0.30	2.68	2.77	0.09	4.50	4.64
10/7-10/10	4205	1.72	1.42	0.27	2.09	2.17	0.37	8.79	9.13
10/10-10/11	1312	1.72	1.48	0.30	3.32	2.82	0.17	4.35	3.70
10/11-10/12	1286	1.72	1.48	0.30	2.60	1.46	0.09	3.34	1.88
10/12-10/13	1677	1.73	1.48	0.30	2.45	5.63	0.13	4.11	9.44
10/13-10/14	1581	1.74	1.46	0.28	2.41	2.24	0.17	3.81	3.54
10/14-10/17	4249	1.74	1.40	0.28	2.65	2.46	0.38	11.28	10.46

NOTES: Bottom pressure is always zero. V_A is the volume of water added to annulus; V_I is the volume of water pumped into top hole; V_O is the weight of water flowing from bottom hole.

Table 2.26 Radial Permeameter Test Results for Sample ORM-1 with Rock Bridge

Date	Elapsed Time (min)	Axial Stress (MPa)	Confining Stress (MPa)	Top Pressure (MPa)	Flow Rate In x 10^3 (cc/min)	Flow Rate Out x 10^3 (gm/min)	V_A (cc)	V_I (cc)	V_O (gm)
10/26-10/28	2851	7.5	6.5	0.4	3.42	2.90	1.11	9.74	8.28
10/28-10/31	4645	7.4	5.9	0.4	4.21	3.62	3.19	19.54	16.82
10/31-11/1	1235	7.6	6.8	0.5	5.43	4.23	0.30	6.71	5.22
11/1-11/2	1314	7.6	6.8	0.5	5.10	3.77	0.18	6.70	4.95
11/2-11/4	2832	7.6	6.8	0.4	5.00	2.95	0.34	14.15	8.36
11/4-11/7	4344	7.6	6.8	0.4	4.31	2.01	0.40	18.74	8.72
11/7-11/8	1432	7.6	6.8	0.4	4.63	2.12	0.25	6.63	3.03
11/8-11/9	1539	7.6	6.9	0.4	4.38	2.12	0.12	6.74	3.26
11/9-11/15	8743	7.6	6.7	0.4	4.67	2.59	0.54	40.86	22.68
11/15-11/16	1381	7.6	6.9	0.4	5.27	3.23	-	7.28	4.46
11/16-11/17	1470	7.6	6.8	3.5	47.16*	45.92*	0.14	69.32	67.50
11/17-11/18	1268	7.6	6.9	3.4	45.86*	45.71*	0.18	58.15	57.96
11/18-11/21	4380	7.5	6.8	0.4	4.99	3.33	-	21.84	14.58
11/21-11/22	1685	7.4	6.7	0.4	4.23	2.73	0.50	7.12	4.60
11/22-11/23	1147	7.4	6.9	0.4	5.68	4.10	0.08	6.52	4.70
11/23-11/28	7081	7.6	6.7	0.4	5.24	3.98	0.56	37.08	28.18
11/28-11/28	1380	7.6	-	0.4	5.25	3.79	-	7.24	5.23
11/29-11/30	1592	7.6	6.8	0.4	5.52	4.13	0.16	8.79	6.57

NOTES: Bottom pressure is always zero. V_A is the volume of water added to annulus; V_I is the volume of water pumped into top hole; V_O is the weight of water flowing from bottom hole.

* Top pressure increased for two days in an attempt to improve the mass balance by saturating the sample.

Table 2.27 Radial Permeameter Test Results for Sample ORM-1 with Cement Plug

Date	Elapsed Time (min)	Axial Stress (MPa)	Confining Stress (MPa)	Top Pressure (MPa)	Flow Rate In x 10^3 (cc/min)	Flow Rate Out x 10^3 (gm/min)	V_A (cc)	V_I (cc)	V_O (gm)
12/11-12/12	1629	7.5	6.8	.3	4.24	3.94	.18	6.91	6.42
12/12-12/13	1122	7.5	6.8	.4	5.36	4.92	.20	6.01	5.52
12/13-12/14	1666	7.5	6.9	.4	5.08	4.64	.16	8.46	7.73
12/14-12/16	2917	7.5	6.8	.4	4.92	4.36	.24	14.34	12.71
12/16-12/19	4199	7.5	6.8	.4	5.54	5.50	.32	23.28	23.08
12/19-12/20	1392	7.5	6.9	.4	4.93	4.39	.14	6.86	6.11
12/20-12/21	1449	7.5	6.9	.4	4.60	3.49	.12	6.67	5.05
12/21-12/22	1653	1.9	1.5	.3	4.31	1.67	0	7.13	2.76
12/22-1/5/84	no readings								
1/5-1/6	1464	1.7	1.3	.3	4.58	2.47	1.05	6.71	3.61
1/6-1/9	4174	1.7	1.2	.3	4.02	1.66	1.46	16.80	6.93
1/9-1/10	1461	1.8	1.5	.3	4.83	2.70	.14	7.06	3.95
1/10-1/11	1186	1.9	1.5	.3	4.04	2.16	.05	4.79	2.56
1/11-1/12	1407	1.9	-	.3	3.82	1.75	-	5.83	2.46
1/12-1/13	1431	1.9	1.5	.3	3.99	1.07	.10	5.71	1.53
1/13-1/16	4315	1.9	1.5	.3	3.65	-	.09	15.73	-
1/16-1/17	1442	1.9	1.5	.3	4.20	3.88	.05	6.06	5.60
1/17-1/18	1537	1.9	1.5	.3	4.05	3.85	.05	6.22	5.91
1/18-1/19	1305	1.9	1.5	.3	3.59	3.52	.09	4.68	4.59
1/19-1/20	1568	1.9	1.5	.3	4.20	4.25	.03	6.58	6.67
1/20-1/23	4272	1.9	1.5	.3	3.97	4.05	.23	16.98	17.29
1/23-1/24	1537	2.0	1.5	.3	2.47	2.54	.15	3.80	3.90
1/24-1/25	1249	2.0	1.5	.3	2.00	1.91	.05	2.50	2.39
1/25-1/26	1441	2.0	1.5	.3	4.27	4.02	.10	6.15	5.79
1/26-1/27	1460	2.0	1.5	.3	3.86	3.78	.03	5.63	5.52
1/27-1/30	4258	2.0	1.5	.3	3.47	3.34	.18	14.76	14.22
1/30-1/31	1430	2.0	1.5	.3	3.69	3.41	.09	5.28	4.87

Table 2.27 Radial Permeameter Test Results for Sample ORM-1 with Cement Plug--<u>Continued</u>

Date	Elapsed Time (min)	Axial Stress (MPa)	Confining Stress (MPa)	Top Pressure (MPa)	Flow Rate In $\times 10^3$ (cc/min)	Flow Rate Out $\times 10^3$ (gm/min)	V_A (cc)	V_I (cc)	V_O (gm)
1/31-2/1	1450	2.0	1.5	.3	3.45	3.31	.06	5.00	4.80
2/1-2/2	1444	2.0	1.5	.3	3.23	3.14	.02	4.66	4.53
2/2-2/3	1390	2.0	-	.3	3.47	3.36	-	4.83	4.67
2/3-2/6	4343	2.0	1.5	.3	3.45	3.38	.16	14.99	14.69
2/6-2/7	1440	2.0	1.5	.3	3.44	3.07	.08	4.95	4.42
2/7-2/8	1465	2.1	1.5	.3	3.33	3.21	.03	4.88	4.70
2/8-2/9	1374	2.1	1.5	.3	3.24	3.15	.07	4.45	4.33
2/9-2/10	1413	2.1	1.5	.3	3.16	3.01	.06	4.46	4.26
2/10-2/13	4460	2.1	1.5	.3	3.38	3.07	.19	15.06	13.68
2/13-2/14	1282	2.1	1.5	.3	3.07	2.84	.05	3.93	3.64
2/14-2/15	1502	2.1	1.5	.3	2.96	2.77	.05	4.44	4.16
2/15-2/16	1416	2.1	1.6	.3	2.71	2.80	-.11	3.84	3.97
2/16-2/17	1418	2.1	1.5	.3	3.42	3.35	.05	4.85	4.75
2/17-2/20	4249	2.1	1.4	.3	3.28	3.20	.43	13.93	13.60
2/20-2/21	1697	2.1	1.5	.3	3.30	3.38	.11	5.60	5.74
2/21-2/22	1182	2.1	1.5	.3	3.29	3.39	.07	3.89	4.01
2/22-2/23	1426	2.1	1.5	.3	3.21	3.11	.12	4.58	4.44
2/23-2/24	1494	2.1	1.5	.3	3.14	3.15	.10	4.69	4.70
2/24-2/27	4338	2.1	1.5	.3	2.94	2.81	.20	12.76	12.21
2/27-2/28	no data								
2/28-2/29	1498	2.2	1.5	.7	10.9	10.1	.05	16.27	15.14
2/29-3/1	1539	2.2	1.5	.7	10.5	9.75	.09	16.21	15.00
3/1-3/2	1345	2.2	1.5	.7	9.30	7.06	.06	12.51	9.50
3/2-3/5	4316	2.2	1.5	.7	9.96	9.73	.12	42.99	41.98
3/5-3/6	1371	2.2	1.5	.5	9.99	10.1	.10	13.69	13.81
3/6-3/8	2874	2.2	1.5	.7	10.4	10.4	.12	29.82	29.78
3/8-3/9	1381	2.2	1.5	.7	10.2	10.3	.09	14.05	14.24

Table 2.27 Radial Permeameter Test Results for Sample ORM-1 with Cement Plug--<u>Continued</u>

Date	Elapsed Time (min)	Axial Stress (MPa)	Confining Stress (MPa)	Top Pressure (MPa)	Flow Rate In $\times 10^3$ (cc/min)	Flow Rate Out $\times 10^3$ (gm/min)	V_A (cc)	V_I (cc)	V_O (gm)
3/9-3/12	4265	2.2	1.5	.7	10.9	11.0	.18	46.34	47.05
3/12-3/13	1425	2.3	1.5	.7	10.4	10.7	.08	14.88	15.20
3/13-3/15	2912	2.3	1.5	.7	10.5	10.7	.12	30.71	31.28
3/15-3/16	1767	2.3	1.5	.7	9.12		.07	16.11	0.01
3/16-4/24	no data								
4/24-4/25	1523	2.2	1.3	.5	4.83	5.15	.31	7.36	7.85
4/25-4/27	2885	2.2	1.4	.7	.506	6.99	0	1.46	20.16
4/27-4/30	4321	2.3	1.2	.6	5.91	6.21	0	25.55	26.84
4/30-5/2	2881	2.4	1.0	.7	3.13	5.70	2.43	9.01	16.42
5/2-5/4	2764	2.5	1.1	.7	0.3	3.38	2.23	.09	9.35

NOTES: Bottom pressure is always zero. V_A is the volume of water added to annulus; V_I is the volume of water pumped into top hole; V_O is the weight of water flowing from bottom hole

Table 2.28 Inclined Pipe Constant Pressure Injection Test Results

Date/Time	Time Interval (min)	Average Injection Pressure (MPa)	Displacement in View Tube (cm)	Volume Injected (cc)	Average Injection Rate x 10^2 (cc/hr)
2-3-83/0915					
	5750	1.14	74.0	23.4	24
2-7/0905					
	10150	1.10	30.2	9.56	5.7
2-14/1015					
	10005	1.10	43.2	13.7	8.2
2-21/0900					
	10080	1.10	21.0	6.65	4.0
2-28/0900					
	10080	1.10	27.3	8.64	5.1
3-7/0900					
	10090	1.10	35.7	11.3	6.7
3-14/0910					
	10270	1.10	20.3	6.42	3.8
3-21/1220					
	9835	1.07	18.4	5.82	3.6
3-28/0815					
	10075	1.00	16.5	5.22	3.1
4-4/0810					
	10085	1.02	16.8	5.32	3.2
4-11/0815					
	10125	1.03	15.9	5.03	3.0
4-18/0900					
	10100	1.03	9.5	3.01	1.8
4-25/0920					
	10180	1.03	16.5*	5.22	3.1
5-2/1100					
	9980	1.03	24.9	11.0	6.6
5-9/0920					
	10145	1.01	24.5	7.75	4.6
5-16/1025					
	10005	1.00	44.2	14.0	8.4
5-23/0910					
	10155	1.00	11.4	3.61	2.1
5-30/1025					
	10035	1.00	18.4	5.82	3.5
6-6/0940					
	10060	1.00	16.2	5.13	3.1
6-13/0920					
	10100	1.00	13.3	4.21	2.5
6-20/0940					
	10085	1.00	15.6	4.94	2.9
6-27/0945					
	12995	1.00	6.1	1.93	.89
7-6-1020					

Table 2.28 Inclined Pipe Constant Pressure Injection Test Results--Continued

Date/Time	Time Interval (min)	Average Injection Pressure (MPa)	Displacement in View Tube (cm)	Volume Injected (cc)	Average Injection Rate x 10^2 (cc/hr)
	10040	1.00	3.2	1.01	.60
7-13/0940					
	10100	1.00	6.4	2.03	1.2
7-20/1000					
	10152	1.00	24.8	7.85	4.6
7-27/1112					
	11468	1.00	21.4	6.77	3.5
8-4/1020					
	10065	1.00	21.9	6.93	4.1
8-11/1005					
	10060	1.00	16.2	5.13	3.1
8-18/0945					
	10085	1.00	15.2	4.81	2.9
8-25/0950					
	10045	1.00	11.9	3.77	2.3
9-1/0915					
	10085	1.00	11.9	3.77	2.2
9-8/0920					
	10100	1.00	12.2	3.86	2.3
9-15/0940					
	10120	1.00	18.2	5.76	3.4
9-22/1020					
	10060	1.00	20.5	6.49	3.9
9-29/1000					
	10050	1.00	15.1	4.78	2.9
10-6/0930					
	10255	1.00	26.2	8.29	4.9
10-13/1225					
	9915	1.00	24.4	7.72	4.7
10-20/0940					
	10065	1.00	19.8	6.27	3.7
10-27/0925					
	10115	1.00	16.0	5.06	3.0
11-3/1000					
	10025	1.00	18.2	5.76	3.4
11-10/0905					
	10005	1.00	27.3	8.64	5.2
11-17/0835					
	8665	1.00	22.6	7.15	5.0
11-23/0900					
	10105	1.00	13.0	4.11	2.4
11-30/0925					
	10075	1.00	10.5	3.32	2.0
12-7/0920					

Table 2.28 Inclined Pipe Constant Pressure Injection Test Results--Continued

Date/Time	Time Interval (min)	Average Injection Pressure (MPa)	Displacement in View Tube (cm)	Volume Injected (cc)	Average Injection Rate x 10^2 (cc/hr)
	9985	1.00	7.2	2.28	1.4
12-14/0745					
	10173	1.00	15.7	4.97	2.9
12-21/0918					
	10091	1.00	3.5	1.11	.66
12-28/0929					
	10076	1.00	16.5	5.22	3.1
1-4-84/0925					
	10080	1.00	7.1	2.25	1.3
1-11/0925					
	10195	1.00	10.7	3.39	2.0
1-18/1120					
	9960	1.00	13.8	4.37	2.6
1-25/0920					
	10080	1.00	3.9	1.23	.73
2-1/0920					
	10140	1.00	7.3	2.31	1.4
2-8/1020					
	8570	1.00	10.0	3.17	2.2
2-14/0910					
	11495	1.00	5.2	1.65	.86
2-22/0845					
	10114	1.00	15.9	5.03	3.0
2-29/0919					
	8701	1.00	4.2	1.33	.92
3-6/1020					
	12920	1.00	9.5	3.01	1.4
3-15/0940					
	8665	1.00	12.6	3.99	2.8
3-21/1005					
	13211	1.00	12.5	3.96	1.8
3-30/1416					
	10101	1.00	13.5	4.27	2.5
4-6/1437					
	8289	1.00	13.8	4.37	3.2
4-12/0846					
	8726	1.00	20.9	6.61	4.5
4-18/1012					
	9993	1.00	26.1	8.26	5.0
4-25/0845					
	7373	1.00	14.6	4.62	3.8
4-30/1138					
	9082	1.00	19.3	6.11	3.7
5-7/1000					

Table 2.28 Inclined Pipe Constant Pressure Injection Test Results--Continued

Date/Time	Time Interval (min)	Average Injection Pressure (MPa)	Displacement in View Tube (cm)	Volume Injected (cc)	Average Injection Rate x 10^2 (cc/hr)
	9993	1.00	19.7	6.24	3.7
5-14/0833					
	10108	1.00	16.7	5.29	3.1
5-21/0901					
	11544	1.00	12.9	4.08	2.1
5-29/0925					
	8669	1.00	10.1	3.20	2.2
6-4/0954					
	10157	1.00	8.5	2.69	1.6
6-11/1111					
	10024	1.00	6.8	2.15	1.3
6-18/1015					

*Experiment interrupted; displacement estimated.

Weighted average flow rate for 3-15-84 to 6-18-84: 2.9×10^{-2} cc/hr where q = flow rate = 2.9×10^{-2} cm^3/hr = 8.1×10^{-6} cm^3/sec; L = plug length = 18 cm; H_c = hydraulic head difference across the plug = 1 MPa = 1.02×10^4 cm of water; D = hole diameter = 10 cm. Substituting into the above expression yields K = 1.8×10^{-10} cm/sec.

Through June 18, 1984, no visible outflow from the plug could be detected. However, the flow rate is so small that if well distributed across the cross-section of the plug it could easily evaporate even before reaching the outflow end of the plug. This appears to indeed be the case. At the time of this writing the outflow end of the pipe has been capped and filled with water. A pipet is tapped into the cap. Outflow from the plug causes a displacement of water in the pipet equal to outflow volume. Only preliminary tests with the outflow pipet have been made to date. Results have not been analyzed, but they do indicate that there is a reasonable outflow from the plug. Test results will be included in the next quarterly report.

2.5 References

Cedergren, H.R., 1967, Seepage, Drainage and Flow Nets, Second Edition, John Wiley and Sons, Inc., New York, 534 pp.

Christensen, C.L. and E.W. Peterson, 1981, "The Bell Canyon Test Summary Report," SAND80-1375, Sandia National Laboraties, Albuquerque, New Mexico.

Cobb, S.L., W.B. Greer, R.G. Jeffrey, S.P. Mathis, D.L. South, and J.J.K. Daemen, 1981, "Rock Mass Sealing - Annual Report, September 1, 1980 - May 31, 1981," prepared for the Nuclear Regulatory Commission, SAFER Division, by the Department of Mining and Geological Engineering, University of Arizona, Tucson.

Daemen, J.J.K., D.L. South, W.B. Greer, J.C. Stormont, S.A. Dischler, G.S. Adisoma, N.I. Colburn, K. Fuenkajorn, D.E. Miles, B. Kousari, and J. Bertuca, 1983, "Annual Report, Rock Mass Sealing, June 1, 1982 - May 31, 1983," NUREG/CR-3473, prepared for U.S. Nuclear Regulatory Commission, Division of Health, Siting and Waste Management, by the Department of Mining and Geological Engineering, University of Arizona, Tucson.

Freeze, R.A. and J.A. Cherry, 1979, Groundwater, Prentice-Hall, Inc., Englewood Cliffs, New Jersey, 604 pp.

Jacob, C.E. and S.W. Lohman, 1952, "Nonsteady Flow to a Well of Constant Drawdown in an Extensive Aquifer," Transactions, American Geophysical Union, Vol. 33, no. 4, pp. 559-569.

Lambe, T.W. and R.V. Whitman, 1969, Soil Mechanics, John Wiley and Sons, Inc., New York, 553 pp.

Louis, C. and Y.N. Maini, 1970, "Determination of In-situ Hydraulic Parameters in Jointed Rock," Proceedings, Second Congress on Rock Mechanics, Belgrade, Vol. 1, pp. 235-245.

IMAGE EVALUATION
TEST TARGET (MT-3)

150mm

6"

IMAGE EVALUATION
TEST TARGET (MT-3)

150mm

6"

Sitz, P., 1981, "Querschnittsabdichtungen untertägiger Hohlräume durch Dämme und Pfropfen" (Sealing the cross section of underground excavations with dams or plugs), Freiberger Forschungshefte A643, 151 pp., VEB Deutscher Verlag für Grundstoffindustrie, Leipzig.

South, D.L., W.B. Greer, N.I. Colburn, S.L. Cobb, B. Kousari, S.P. Mathis, R.G. Jeffrey, C.A. Wakely, and J.J.K. Damen, 1982, "Annual Report, Rock Mass Sealing, June 1, 1981 - May 31, 1982," prepared for U.S. Nuclear Regulatory Commission, SAFER Division, by the Department of Mining and Geological Engineering, University of Arizona, Tucson.

Ziegler, T.W., 1976, "Determination of Rock Mass Permeability," Technical Report S-76-2, U.S. Army Engineer Waterways Experiment Station, Vicksburg, Mississippi.

CHAPTER THREE

EXPERIMENTAL ASSESSMENT OF THE EFFECT OF DYNAMIC LOADING ON BOREHOLE SEAL PERFORMANCE

3.1 Introduction

This chapter summarizes an upcoming topical report (Adisoma and Daemen, 1984).

Flow testing has been conducted to measure the hydraulic conductivity of cement borehole seals in granite. The effect of dynamic loading on the performance of these seals has been assessed experimentally, using a shaking table. Dynamic loads have been applied to the samples in between the flow tests to determine the change in hydraulic conductivity of the plug-rock system that might be induced by dynamic loads.

In determining the effect of dynamic loading, this study deals with two types of cement seals. The first ones are saturated cement seals, i.e. those always kept saturated under water. The second type are cement seals that have been allowed to dry after the normal curing period.

3.2 Steady-State Flow Testing and Dynamic Testing on Saturated and on Dried Cement Plugs in Granite

3.2.1 Introduction

Effective long-term isolation of high-level nuclear wastes in deep underground repositories relies on the natural barrier (i.e. the rock itself) and engineered barriers (waste canister, packing, backfill, sealing materials). Hydrogeologic transport is the most important mechanism for potential transfer of radionuclides to the biosphere (Boulton, 1978; ONWI, 1980; Moody, 1982; etc.). The presence of manmade penetrations, such as an open borehole, intersecting a repository rock mass compromises the integrity of the surrounding rock in slowing down the radionuclide-contaminated water migration (Kocher et al., 1983; Bredehoeft et al., 1978; Barbreau et al., 1980; Heineman et al., 1978; and many others). Therefore, all penetrations in the vicinity of deep underground repositories must be sealed reliably.

Of interest in the study of these seals is the effect dynamic loading might have on their performance, such as in the event of earthquake or large-scale, especially subsurface, blasting nearby. The Nuclear Regulatory Commission has not yet established a design response criteria for nuclear waste storage facilities (Vortman, 1982).

A review of the past performance of underground openings during earthquakes indicates that underground structures in general are less severely affected than surface structures at the same location (Owen and Scholl, 1981). Another approach is to use numerical modeling techniques to predict damage due to ground motion (Yanev and Owen, 1978; Wahi et al., 1980). In general, these numerical techniques are used to evaluate the stability of underground openings during an earthquake. Although this will be of interest during the operational phase of an underground nuclear waste repository, greater interest in the long term will be in seismic damage that causes cracks which may increase the permeability of the plug-rock system.

The objective of this study is to assess the performance of cement borehole seals under simulated laboratory dynamic loading conditions.

3.2.2 Experimental Procedures

The basic approach used in this study is to establish a steady-state flow through the cement borehole seal in a rock specimen, then subject the plugged specimen to dynamic loads using a shaking table, and finally assess the influence on seal performance by comparing flow rates before and after the dynamic loading.

Cylindrical Charcoal granite specimens, approximately 150 mm (6 in) in diameter and 300 mm (12 in) long, had a 25 mm (1 in) diameter coaxial hole drilled from both ends. In the center of the hole either a rock bridge is left or a cement plug is installed. Details of rock type and origin, cement composition, and mixing procedures, are given in the previous annual report (Daemen et al., 1983). Water injected at a constant pressure into the top hole, using high pressure nitrogen-driven pressure intensifiers or hydraulic accumulators, flows through the specimen to the bottom hole (Figure 3.1). Steady-state flow rates are measured.

During the flow testing of three rock specimens, liquid concentrate dye marker has been injected with the water in the top hole. The dye injection testing has been performed to allow observation of the flow paths in saturated and in dried-out cement seals.

For the dynamic loading tests, the rock specimen is securely placed on top of a shaking table using a set of clamps and tensioned cables. To measure the acceleration along the horizontal axis generated by the shaking table motion, a sinusoid-g-meter is used. Details of the equipment used and testing procedures are described in the last annual report (Daemen et al., 1983) and in the upcoming topical report (Adisoma and Daemen, 1984). Figure 3.2 shows the laboratory arrangement for the steady-state flow testing and dynamic testing of borehole plugs.

The dynamic testing is performed while the specimen is under a steady-state flow condition. Therefore, the flow rate prior to and after a dynamic load is applied can be compared directly. The test is repeated at various injection pressures and with increasingly severe dynamic loads, i.e. longer durations and higher accelerations.

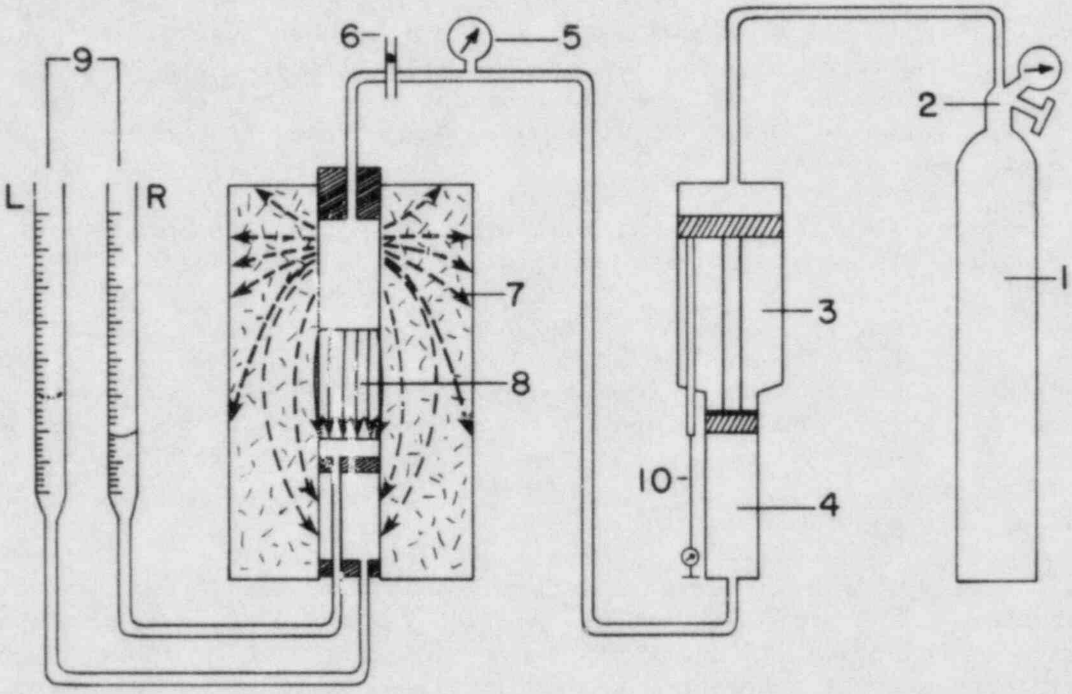

1. Nitrogen gas tank.
2. Pressure regulator.
3. Low pressure(gas) cylinder of pressure intensifier.
4. High pressure(water) cylinder of pressure intensifier
5. Water injection pressure gauge.
6. Rotameter (flowmeter).
7. Rock sample.
8. Borehole plug.
9. Measuring pipettes for outflow collection.
10. Dial gauge for piston displacement measurement.

Figure 3.1 Steady-state flow testing layout. The outflow collection system collects separately the one-dimensional flow through the plug and the plug-rock interface in the right (R) pipette, and peripheral flow through the rock around the plug in the left (L) pipette. Broken arrows in rock sample are qualitative indications of possible flow paths.

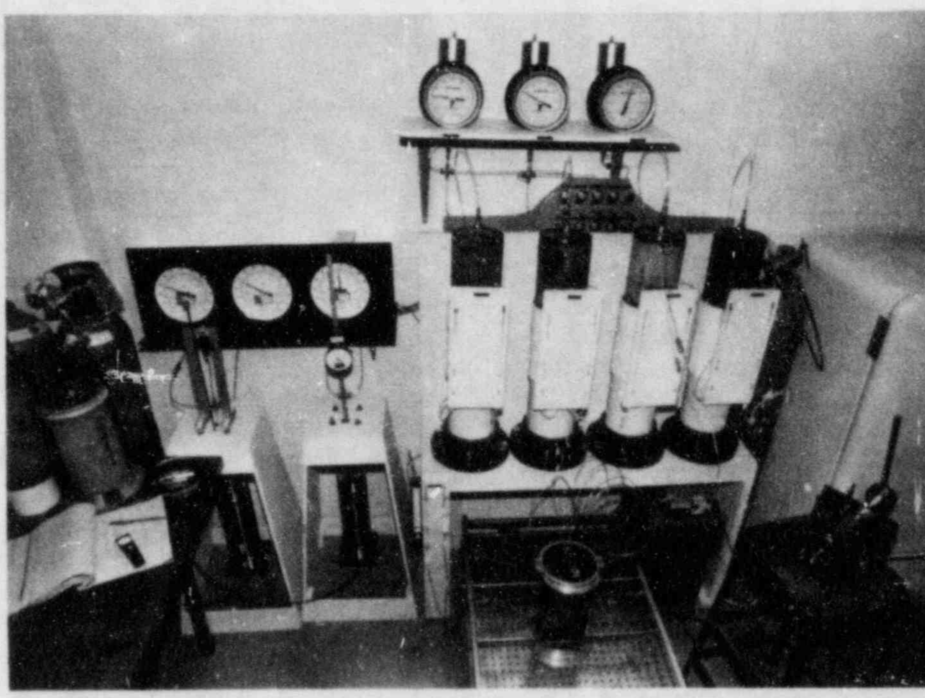

Figure 3.2 Laboratory arrangement for steady-state flow testing and dynamic loading of borehole plugs. Two pressure intensifiers, bottom left, and three hydraulic accumulators, top, provide the constant injection pressures for five specimens simultaneously. One of the specimens is mounted on the shaking table, bottom left. A positive-displacement hand pump, bottom right, is shown during refilling of one of the testing stations with water.

3.2.3 Experimental Results

Five granite samples with saturated and with dried-out cement seals and with rock bridges have been flow-tested previously and have been reported on in the last annual report. Flow testing and dynamic loading has been continued on four of these samples during the period reported on here. Four additional samples have been tested, including one with a saturated cement seal which, after flow-and-dynamic testing were completed, was allowed to dry out in the heating oven and was flow-tested again. In three of these samples dye has been injected after the dynamic testing has been completed, and two have been sawed in half lengthwise to allow inspection of flow paths, interface, plug and rock.

Visual inspection of the sawed half of the specimens shows that the dye uniformly penetrates the body of the saturated cement seal. On the other hand, for the dried-out cement seal the interface clearly acts as the preferential flow path, as evident from the dye traces in the interfacial area and from their absence in the plug body.

The results of the steady-state flow testing are plotted by giving the outflow as a function of time, to obtain the flow rate for each injection pressure. Linear regression gives the best fit for the data with the coefficient of determination, r^2, equal to or close to unity. Figures 3.3 and 3.4 give the flow vs. time plot of the outflow through the saturated cement plug and through the plug-rock interface of a dried-out cement plug, respectively.

The flow rate has been plotted as a function of elapsed time since the beginning of the flow testing. The permeability, k, has been calculated using Darcy's law and assuming one-dimensional flow through the saturated cement plug or through the rock bridge. For the dried-out plugs, where a preferential flow path exists along the plug-rock interface, a flow through a fissure law is used, analyzed by the equivalent parallel plate flow concept. The fissure permeability, k_j, is then computed after the equivalent parallel plate aperture, e, has been found.

The flow through Charcoal granite is shown in Figure 3.5, the permeability in Figure 3.6, in which are plotted the 1-D flow through the rock bridge and its permeability, respectively, as a function of elapsed time. The permeability, calculated using Darcy's Law for one-dimensional flow, is in the order of 10^{-8} darcy for Charcoal granite. The permeability seems to be fairly constant with time for the specimen used (sample CG5309-04).

Figure 3.7 is a typical example of the flow rate through a saturated cement plug as a function of time (this plot is for sample CG5309-06). Distinct flow rates can be recognized for different injection pressures, the higher the injection pressure the higher the flow rate. These values have been converted to permeability and plotted as a function of elapsed time (Figure 3.8). The permeability is in the order of 10^{-9} darcy from the beginning of the flow testing to day 220, the last 40 days of which correspond to the dye injection test. This is an order of

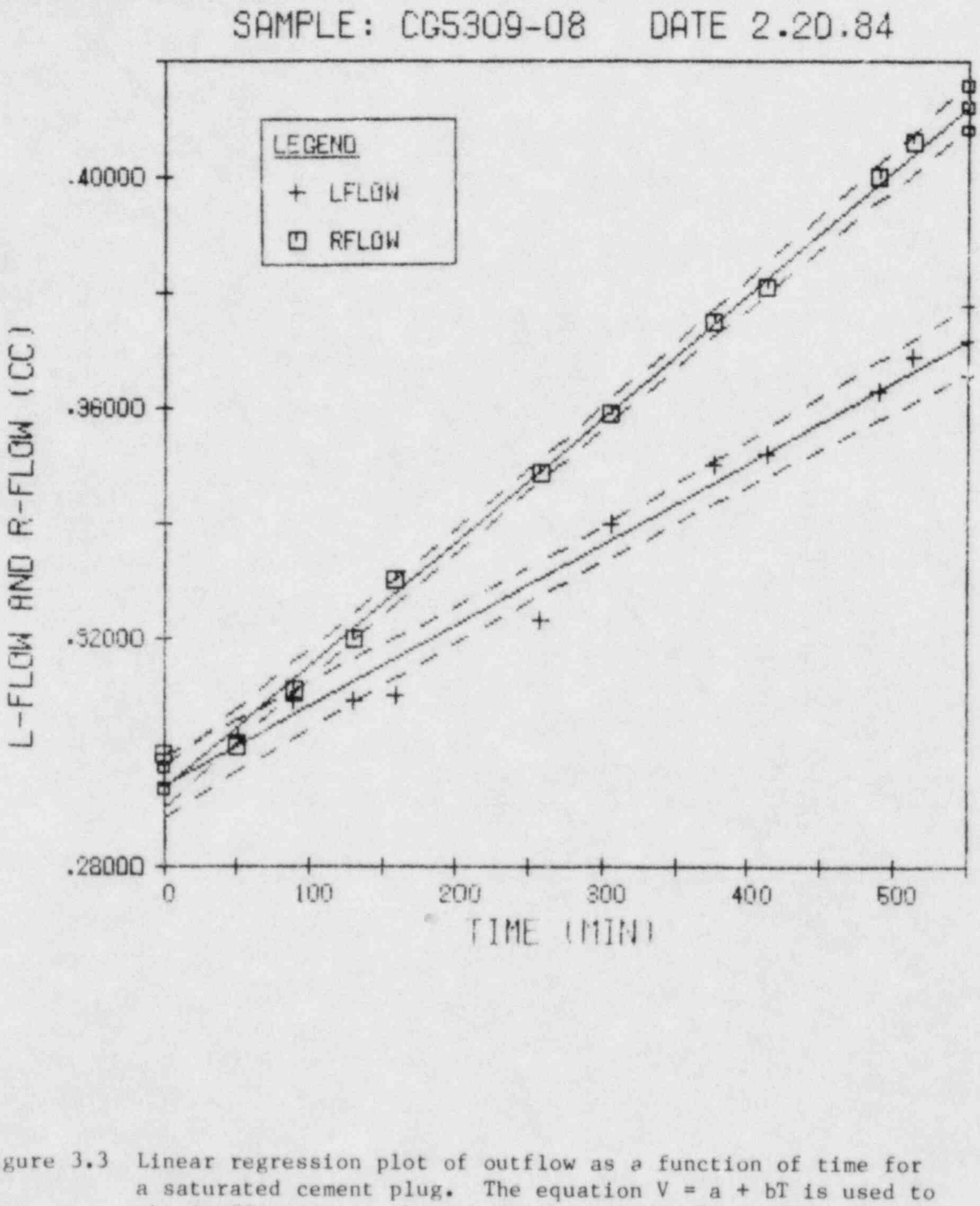

Figure 3.3 Linear regression plot of outflow as a function of time for a saturated cement plug. The equation V = a + bT is used to obtain flow rate, where V is the volume of the flow, T is the time, and a and b are the regression coefficients. For the injection pressure used here (4 MPa), the 1-D flow rate was 1.99×10^{-4} cm^3/min, with $r^2 = 0.99$. R-flow is the 1-D flow through cement and L-flow is the peripheral flow through the rock around the cement plug. A 95% confidence band is shown around each regression line.

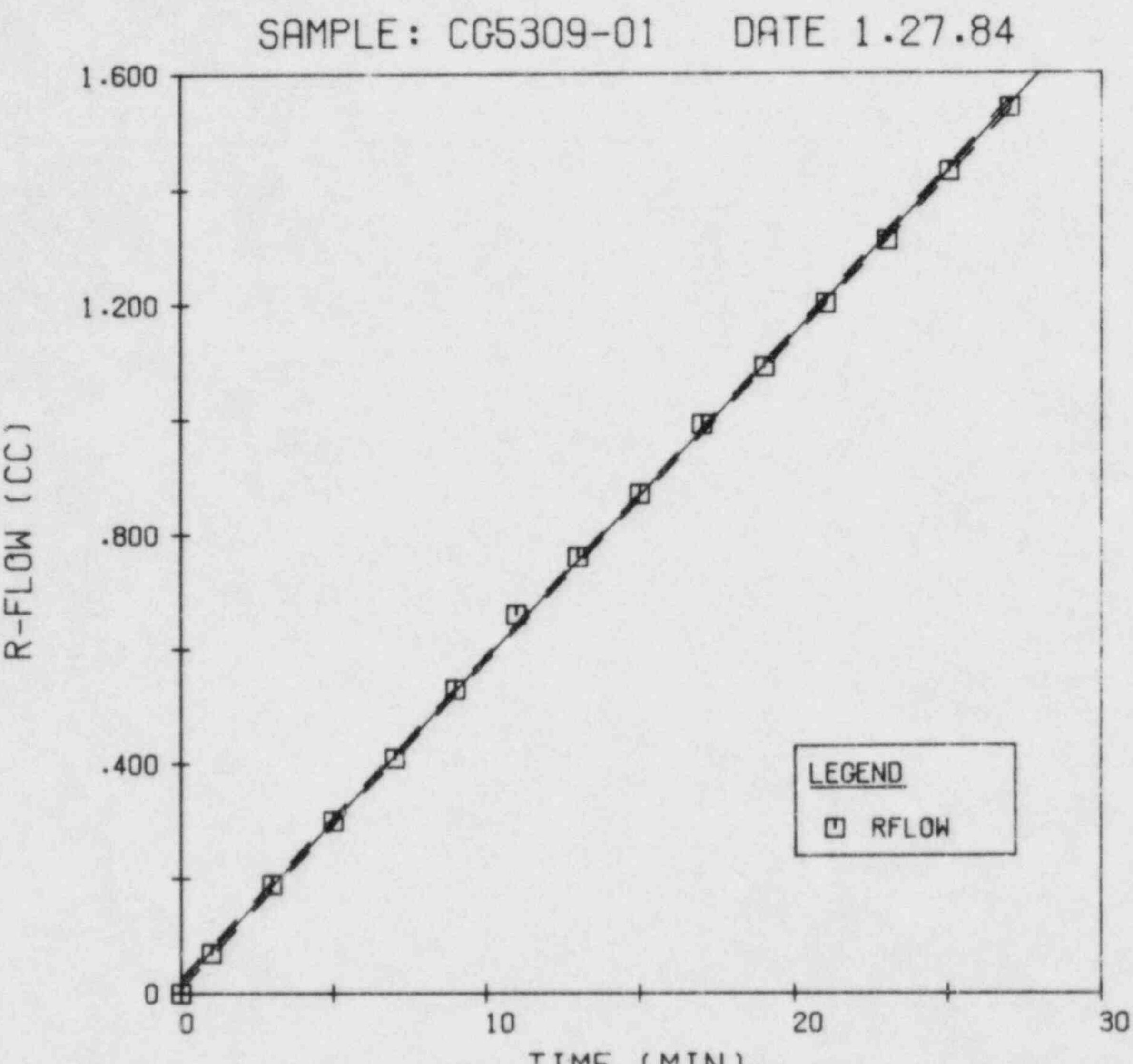

Figure 3.4 Linear regression plot of outflow as a function of time for a dried-out cement plug. The 1-D flow rate through the plug-rock interface is obtained using the same equation, $V = a + bT$, as in the saturated case, which was found to be 5.75×10^{-2} cm^3/min for the injection pressure of 1.5 MPa, with $r^2 = 1.00$.

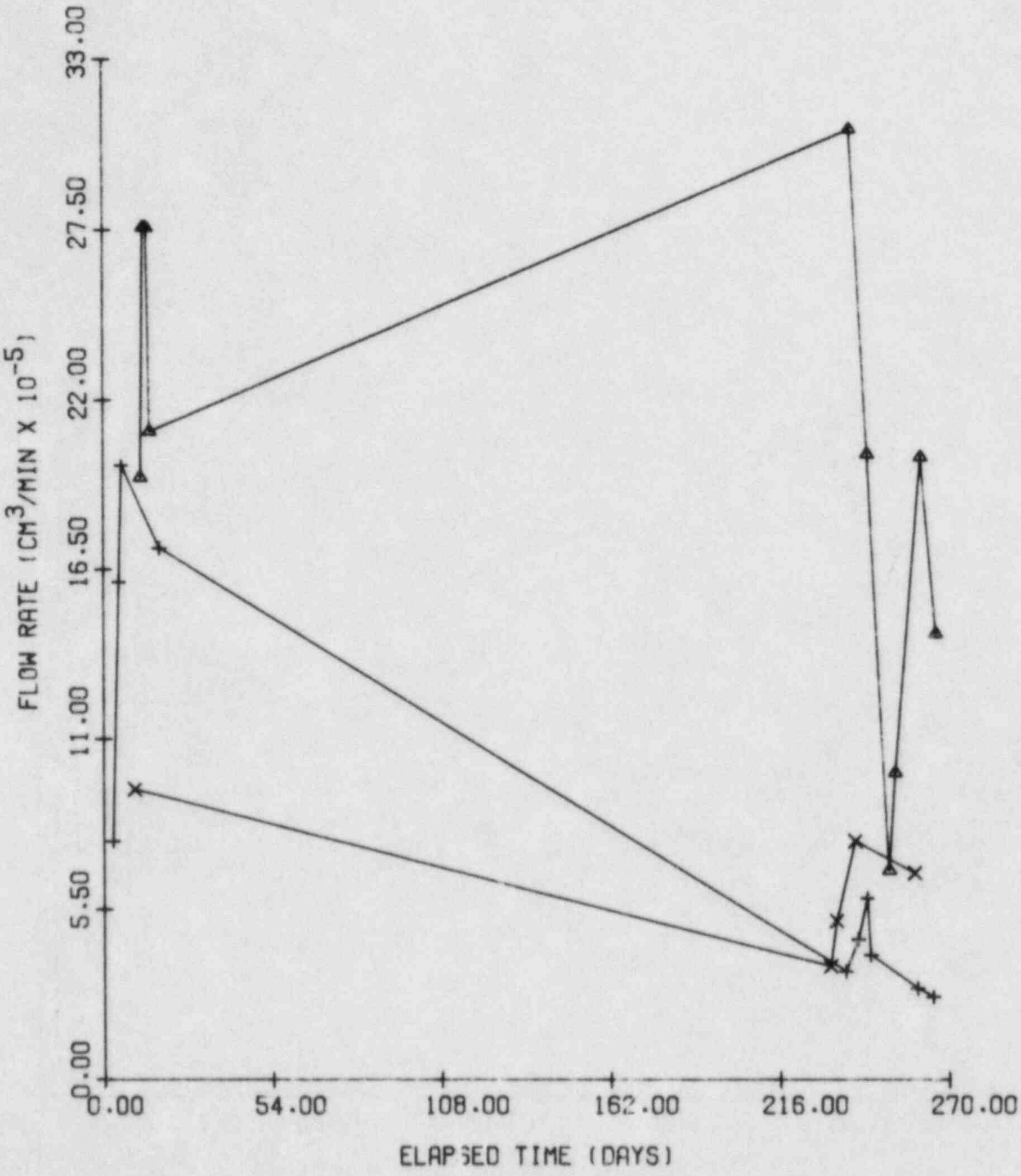

Figure 3.5 One-dimensional flow rate through Charcoal granite as a function of elapsed time since the beginning of flow testing.

Δ - Δ : flow rate at injection pressure of 4 MPa

\+ - + : flow rate at injection pressure of 2 MPa

x - x : flow rate at injection pressure of 1 MPa

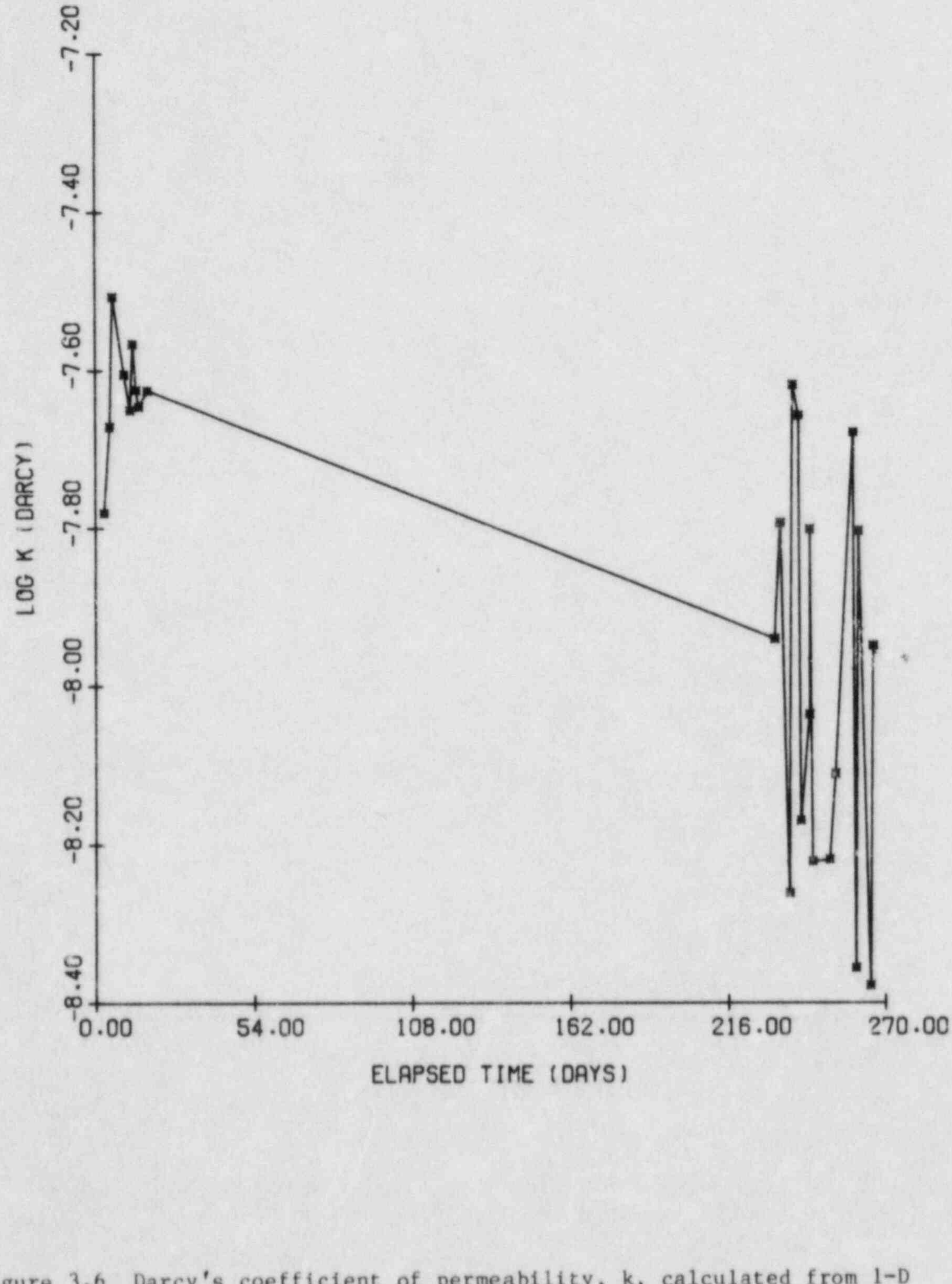

Figure 3.6 Darcy's coefficient of permeability, k, calculated from 1-D flow through Charcoal granite, as a function of elapsed time. It is more or less constant with time at 10^{-8} darcy.

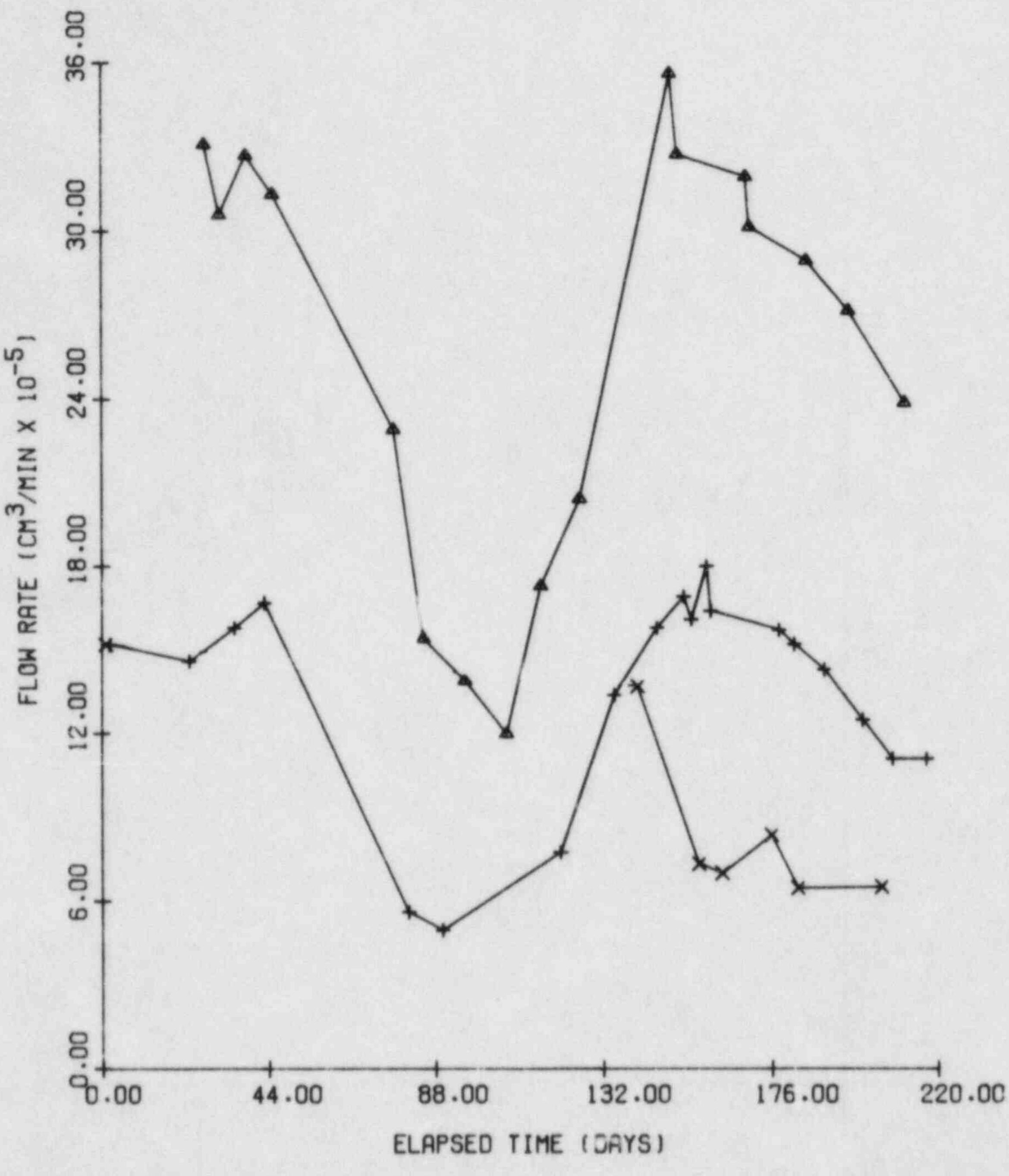

Figure 3.7 One-dimensional flow rate through a saturated cement seal as a function of elapsed time.

Δ - Δ : flow rate at injection pressure of 4 MPa

+ - + : flow rate at injection pressure of 2 MPa

x - x : flow rate at injection pressure of 1 MPa

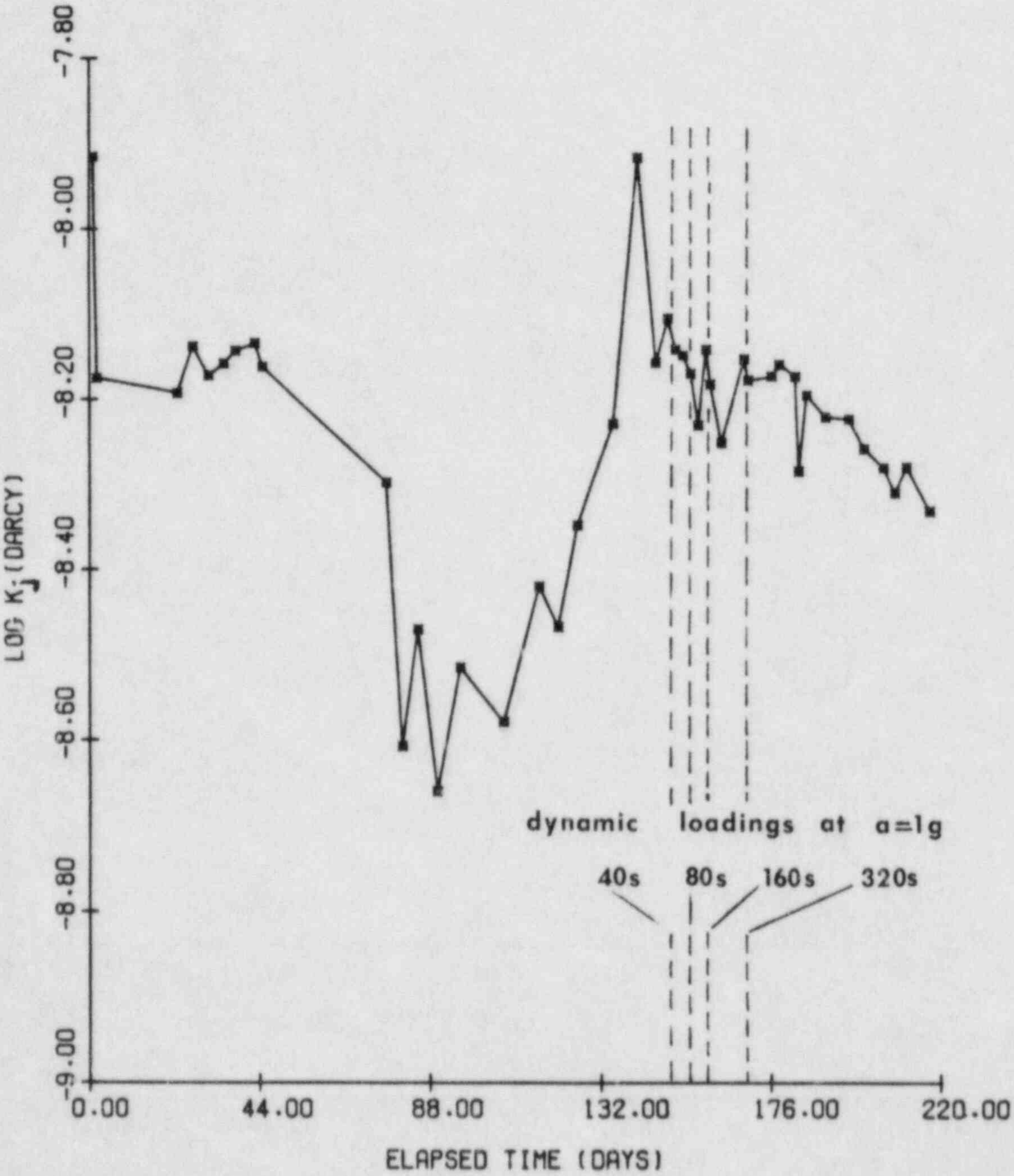

Figure 3.8 Permeability, k, calculated from 1-D flow through a saturated cement seal, as a function of elapsed time. The value is constant with time at 10^{-9} darcy. Dynamic loading at an acceleration of 1 g and increasing duration of up to five minutes did not affect the permeability.

magnitude lower than the permeability of granite. Dynamic loading at an acceleration of 1 g (and 2 g for sample CG5309-08) and for a duration of up to five minutes does not significantly affect the permeability.

Figure 3.9 shows the 1-D flow rate through a cement plug dried out for seven months prior to testing, as a function of elapsed time since the beginning of the flow test. This sample (CG5309-01) had been undergoing continuous flow testing for more than eight months, including 39 days of dye injection during the last stage of the test. The sharp decline of flow rate during the first 60 days of resaturation indicates a re-expansion of the cement plug that tightens the plug-rock interface (a preferential flow path, as confirmed by the dye injection test). The flow rate continued to drop afterwards but at a lower rate.

The fissure permeability has been calculated from the flow rate and plotted as a function of elapsed time (Figure 3.10). It has decreased from 10^{+1} darcy to 10^{-1} darcy in eight months; however, it is very unlikely that it will regain the permeability which existed prior to drying, which is eight orders of magnitude lower. This degradation in performance seems to be related to the length of drying-out period. A sample with a cement plug which was allowed to dry for three months prior to resaturation (sample CG5309-28) has a similar permeability-time curve. It has a lower initial fissure permeability of 10^{-1} darcy that rapidly decreased during the first 60 days of resaturation and thereafter becomes more or less constant at 10^{-2} darcy.

Dynamic loading tests performed on these samples still did not cause an adverse effect on plug performance. At an acceleration of 2 g for sample CG5309-01, and duration up to five minutes, the dynamic loads did not increase the permeability in a significant way (see Figure 3.10). The same held true for sample CG5309-28, which was dynamically loaded at an acceleration of 1 g and for increasing durations up to five minutes. The applied dynamic loads are much more severe, though in a more simplistic way, than what might be experienced during an actual earthquake or other likely types of in-situ dynamic loading.

3.2.4 Conclusions

Cement plugged granite specimens have been tested to assess the borehole seal performance when subjected to dynamic loads. Steady-state flow testing to collect reference flow data prior to the dynamic testing showed that the permeability of saturated cement seals is an order of magnitude lower than that of granite. This indicates that saturated cement seals could perform as good or better than intact low-permeability granite in preventing flow.

Seal performance degrades severely when the cement is dried out. This might be the case for a seal located above the groundwater table, in locations near the waste emplacement where the heat generated drives water away during the initial period of storage, or in locations where repository drainage (during construction) results in temporary desaturation. When cement plugs are allowed to dry, they shrink and the subsequent separation along the plug-rock interface is a preferential

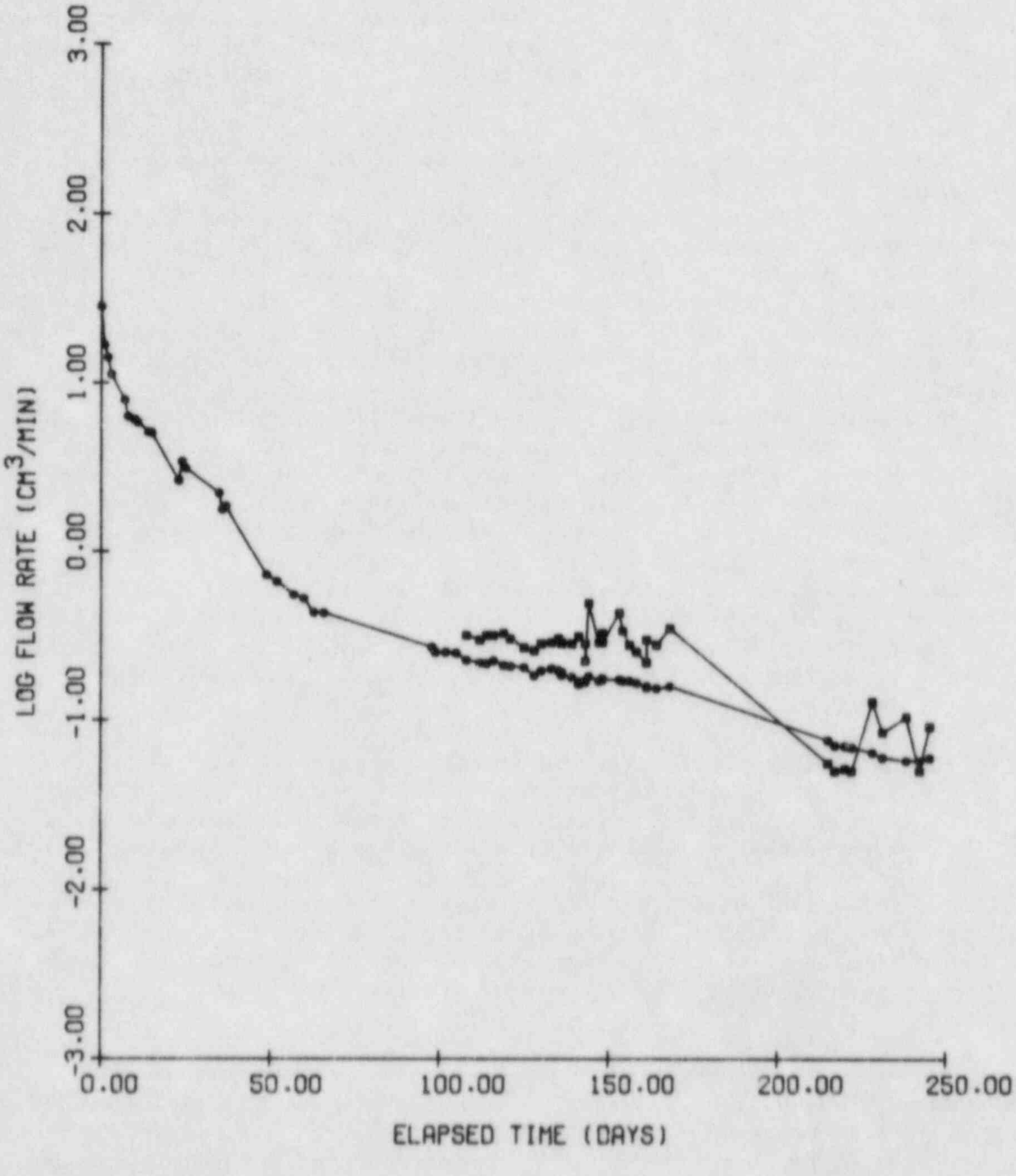

Figure 3.9 One-dimensional flow rate through the plug-rock interface of a dried-out cement seal as a function of time of resaturation. The flow rate decreases rapidly as resaturation started and levels off with time thereafter, indicating cement re-expansion. These flow rates are for an injection pressure of 1.5 MPa.

□ - □ : inflow rate

o - o : outflow rate

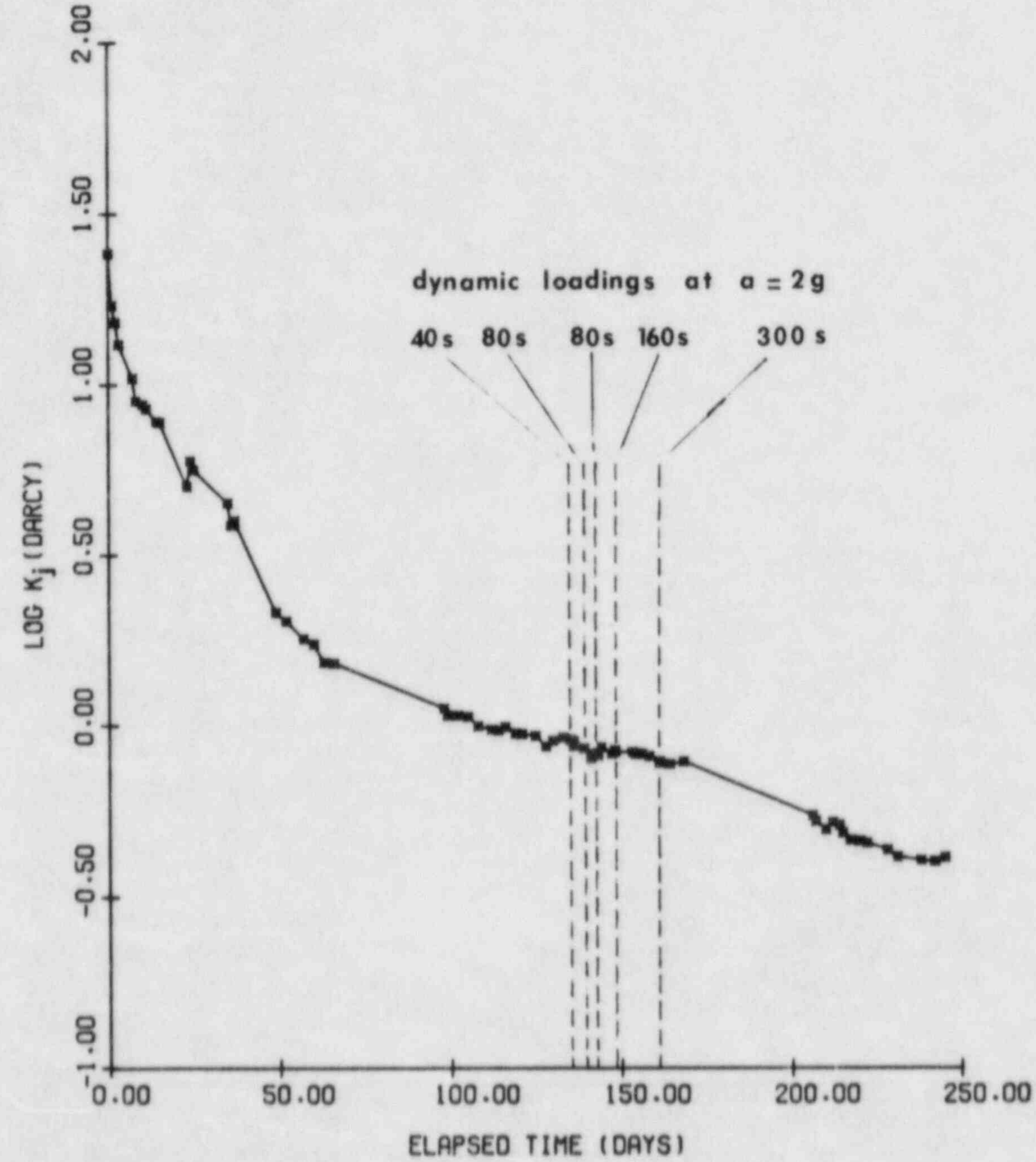

Figure 3.10 Fissure permeability of a dried-out cement plug as a function of time of resaturation. The seal performance was degraded severely by drying, as compared to the saturated case. Dynamic loading at an acceleration of 2 g and increasing duration up to 5 minutes did not affect seal performance.

flow path. The fissure permeability decreases rapidly during the first two months of resaturation and levels off thereafter, indicating an improvement in seal performance. However, it still is several orders of magnitude higher than the permeability of saturated cement prior to drying; hence, the seal performance could not be fully recovered.

The extent of seal performance degradation seems related to the length of drying time prior to resaturation; the longer the cement is allowed to dry, the more severe is the extent of performance degradation. This is due in part to cracking in the cement body itself, which acts as an additional preferential flow path. The presence of a preferential flow path in a dried-out cement seal, as well as the absence thereof in a saturated cement seal, are confirmed by the dye injection testing.

Dynamic loading performed on specimens with saturated and dried cement seals does not cause any adverse effect on seal performance. Performed at accelerations up to 2 g and durations up to five minutes, the tests resulted in no noticeable change in the permeability of the plug-rock system.

3.2.5 Recommendations

In terms of duration and peak acceleration, the dynamic loading test performed on the cement-plugged granite specimens were much more severe than what may be realistically experienced. However, size may have an effect on seal performance of a nuclear waste repository during an actual earthquake. In a centrifuge test using models with linear scaling $1/n$, an acceleration scaling factor of n times that in the field is commonly used (Schofield, 1981; Craig, 1982). For example, an acceleration of 2g in a model seal 1 inch in diameter (as used in these tests) results in identical stresses with an acceleration of 0.02 g in a prototype seal in the field 100 times in diameter (about 8.3 ft). Another factor to be considered in dynamic loading simulations is the duration of the applied load. For models having a linear scaling of $1/n$, time scaling for dynamic displacement which eventually results in increased flow is also $1/n$. On the other hand, for diffusion processes or fluid flow the scale factor is $1/n^2$. Difficulties may arise from the possible conflicts in determining these scaling factors, and more detailed study along these lines is required.

At the very extreme case, dynamic loading can be considred to be impact or transient loading, such as when blasting is carried out adjacent to the plug-rock system. The tensile stresses that might be induced in the seal-rock interface can be simulated by a hammer blow to the sides of a rock specimen containing a borehole seal. This type of experiment is inexpensive and relatively easy to perform, and might be worth pursuing.

Every effort should be made to keep cement seals saturated at all times. Allowing cement seals to dry out will cause cement shrinkage that creates preferential flow paths due to the separation of the plug-rock interface and the subsequent cracking in the cement body. Minimizing seal shrinkage by mixing the cement with sand, aggregates or other materials, or by using techniques such as carbonization, is another area in need of further investigation.

To better understand the time-dependent behavior of cement seals in terms of their permeability, long-term flow testing would be necessary. It is important not only for saturated cement seals, but also for dried-out cement seals to see to what extent the improvement in seal performance will continue with continuous resaturation.

Lastly, the cement and interface behavior under different moisture conditions are still not fully understood. A more comprehensive test could be devised to measure the expansive stress and stress relief of cement seals at different stages from pouring, during curing and hardening, at saturated condition, during drying out and finally resaturation. It would be desirable to perform such tests at several temperatures, covering the temperature ranges likely to be encountered in the repository environment.

3.3 References

Adisoma, G.S. and J.J.K. Daemen, 1984, "Experimental Assessment of the Effect of Dynamic Loading on Borehole Seal Performance," Topical Report to U.S. Nuclear Regulatory Commission, Division of Health, Siting and Waste Management, Contract No. NRC-04-78-271, by Department of Mining and Geological Engineering, University of Arizona, Tucson, AZ.

Adisoma, G.S. and J.J.K. Daemen, 1984, "Laboratory Assessment of the Effect of Drying on the Performance of Cement Borehole Plugs,' Proc. Waste Management '84 Symposium, Tucson, AZ, March 11-15.

Barbreau, A., R. Heremans, and B. Skytte Jensen, 1980, "Radionuclide Migration in Geological Formations: Radioactive Waste Management in Geological Formations," Proceedings of the First European Community Conference, Luxemburg, May 20-23, p. 528.

Boulton, J. (ed), 1978, "Management of Radioactive Fuel Wastes: The Canadian Disposal Program," AECL-6314, Atomic Energy of Canada, Limited, Atomic Energy of Canada Research Co., Whiteshell Nuclear Research Establishment, Pinawa, Manitoba, p. 45.

Bredehoeft, J.D., A.W. England, D.B. Stewart, N.J. Trask, and I.J. Winograd, 1978, "Geologic Disposal of High-Level Radioactive Wastes - Earth Science Perspectives," Geological Survey Circular 779, p. 8.

Craig, W.H., 1982, "Conflicts in Dynamic Modeling in Geomechanics," in Design for Dynamic Loading, the Use of Model Analysis, ed. by G.S.T. Armer and F.K. Garas, Construction Press, London and New York, pp. 1-6.

---

*Personal communications with Erik Nelson (Dowell) and Herbert Brunner (Nukem GmbH), 1984.

Daemen, J.J.K., J.C. Stormont, N.I. Colburn, D.L. South, S.A. Dischler, K. Fuenkajorn, W.B. Greer, G.S. Adisoma, D.E. Miles, B. Kousari, and J. Bertucca, 1983, "Rock Mass Sealing - Experimental Assessment of Borehole Plug Performance," NUREG/CR-3473, Annual Report, June 1982 - May 1983, prepared for U.S. Nuclear Regulatory Commission, by Department of Mining and Geological Engineering, University of Arizona, Tucson, AZ.

Heineman, R.E., W.A. Carbiener, and S.J. Basham, 1978, "The Technical Program for Establishing the Scientific Basis for Geological Disposal," DOE Environmental Control Symposium, Washington, DC, November 28-30, p. 4.

Kocher, D.C., A.L. Sjoreen, and C.S. Bard, 1983, "Uncertainties in Geologic Disposal of High-level Wastes - Groundwater Transport of Radionuclides and Radiological Consequences," NUREG/CR-2506, ORNL-5838, prepared for U.S. Nuclear Regulatory Commission by Oak Ridge National Laboratory, Oak Ridge, TN, p. 54.

Moody, J.B., 1982, "Radionuclide Migration/Retardation: Research and Development Technology Status Report," Technical Report, ONWI, Battelle Memorial Institute, Columbus, OH, p. 5.

ONWI -33(2), 1980, "NWTS Criteria for the Geologic Disposal of Nuclear Wastes: Site Qualification Criteria," Office of Nuclear Waste Isolation, Battelle Memorial Institute, Columbus, OH, p. 6.

Owen, G.N. and R.E. Scholl, 1981, "Earthquake Engineering of Large Underground Structures," FHWA/RD-80/195, Final Report, prepared for Federal Highway Administration and National Science Foundation, Washington, DC.

Schofield, A.N., 1981, "Dynamic and Earthquake Geotechnical Centrifuge Modeling," Proc. Int. Conf. on Recent Advances in Geotechnical Earthquake Engineering and Soil Dynamics, Vol. 3, ed. by S. Prakash, Rolla, MO, pp. 1081-1100.

Vortman, L.J., 1982, "Ground Motion from Earthquakes and Underground Nuclear Weapon Tests: A Comparison as it Relates to Siting a Nuclear Waste Storage at NTS," SAND81-2214, Sandia National Laboratories, Alburquerque, NM, April.

Wahi, K.K., B.C. Trent, D.E. Maxwell, R.M. Pyke, C. Young, and D.M. Ross-Brown, 1980, "Numerical Simulation of Earthquake Effects on Tunnels for Generic Nuclear Waste Repositories," DP-1579, E.I. du Pont de Nemours & Co., Savannah River Laboratory, Aiken, SC.

Yanev, P.I. and G.N. Owen, 1979, "Facility Hardening Studies: Design Cost Scoping Studies," JAB-99-123, prepared for U.S. Department of Energy, Nevada Operations Office, Nevada Nuclear Waste Storage Investigations, Las Vegas, NV, by URS/John A. Blume & Associates, Engineers, San Francisco, CA, April, 109 pp.

CHAPTER FOUR

EXPERIMENTAL ASSESSMENT OF BOREHOLE DRILLING DAMAGE

4.1 Introduction

The objective of this work is to assess experimentally the risk that waterflow might bypass a plug through a damaged zone induced by drilling in basaltic rocks. This chapter contains two sections. The first one summarizes a topical report to be issued shortly on the experimental assessment of borehole drilling damage. The second section describes ongoing work not covered in the topical report.

4.2 Experimental Assessment of Borehole Drilling Damage

4.2.1 Introduction

This section is the executive summary of a topical report to be issued shortly (Fuenkajorn and Daemen, 1984b).

Disposal in geological media has the potential for isolating radioactive waste from the biosphere. To provide maximum containment, it is necessary to identify and seal all penetrations within and near the repository site. When a hole is drilled in rock, some fracturing may occur in the sidewall as a result of the bit action, stress relief, and circulation of fluid under high pressure-velocity in the hole. If significant cracking is induced in the borehole wall, leakage patterns may develop around a plug (Lingle et al., 1982).

To evaluate the potential for leakage, the physical characteristics of cracks around the walls of boreholes drilled in basaltic rocks are being investigated. This effort includes ring tension tests, permeability tests, and microscopic fracture studies (Mathis and Daemen, 1982, describe similar work on granitic rocks). The investigation is aimed at: (1) determining the density and orientation of the cracks induced in the borehole wall by drilling (diamond coring, rotary, and percussion); (2) determining the influence of the hole size; and (3) determining the influence of the damaged zone on the flow path around the plug. The rock samples tested are Grande basaltic andesite, Pomona basalt, and Wanapum basalt (South et al., 1982, and Daemen et al., 1983, give a description of the rocks, their mechanical properties, the drilling specifications, and the locations from which they were obtained).

4.2.2 Ring Tension Tests

The ring tension test study (e.g. Daemen et al., 1983, p. 181) includes an extensive laboratory investigation and an analytical examination of the tensile strength and tensile stiffnes of the rock within the damaged zone around the hole. This includes determination of the damaged zone tensile strength, determination of size and shape effects of the ring test specimen, measurement of the damaged zone tensile strains, and investigation of the stress-strain distribution in the specimen using finite element analysis.

4.2.2.1 Results of Ring Tension Tests

The complete ring test and Brazilian test results are shown in Figure 4.1. The sample preparation, testing procedures, and tensile strength calculations are described in detail by Daemen et al., 1983. The results imply some significant conclusions: (a) For each size, different drilling techniques induce different degrees of damage, as indicated by the difference in the tensile strengths. (b) The tensile strength decreases as the specimen size increases for each drilling method. This probably is caused by size effects (Davidenkov et al., 1947; Bieniawski, 1968; Hodgson and Cook, 1970), shape effects [Addinall and Hackett (1964), Hobbs (1964), and Jaeger and Hoskins (1966) conclude that ring tensile strengths decrease as the relative hole radius, $\bar{r}$, increases], and characteristics of the damage zone (a larger drill bit might induce more damage than a smaller one). (c) Laboratory drilled diamond holes show less damage (higher strength) than diamond holes drilled in the field. This might be due to the fact that field drills are more powerful, apply more force and input more energy into the rock. (d) The difference in ring tensile strengths between the two rock types is larger than the difference in Brazilian tensile strengths for the same disk diameters. This suggests that more damage is induced around the hole in the weaker rock than in the stronger one, as can also be observed in the petrographic studies discussed later. (e) Damage induced by diamond drilling tends to decrease as the hole size increases while the damage intensity induced by percussion and rotary drilling tends to increase as the hole size increases. (f) Extrapolation of the results to larger holes is questionable due to the complexity of the drilling mechanism and the variation of drilling parameters.

4.2.2.2 Size and Shape Effects

In order to compare the damage induced by different sizes of drill bits in terms of tensile strength, eliminating both shape and size effects from the ring test results is attempted as follows:

(a) Shape Effect Elimination: Ring tests are performed on 229 mm rock disks with 25, 57, 108, 133, and 159 mm laboratory drilled diamond holes in Pomona basalt and Grande basaltic andesite. The results obtained indicate that the tensile strength decreases as the relative hole radius, $\bar{r}$, increases (Table 4.1).

A power equation is introduced to represent a mathematical relationship between the strength and relative hole radius:

$$\sigma_R = C(\bar{r})^{-\beta} \tag{4.1}$$

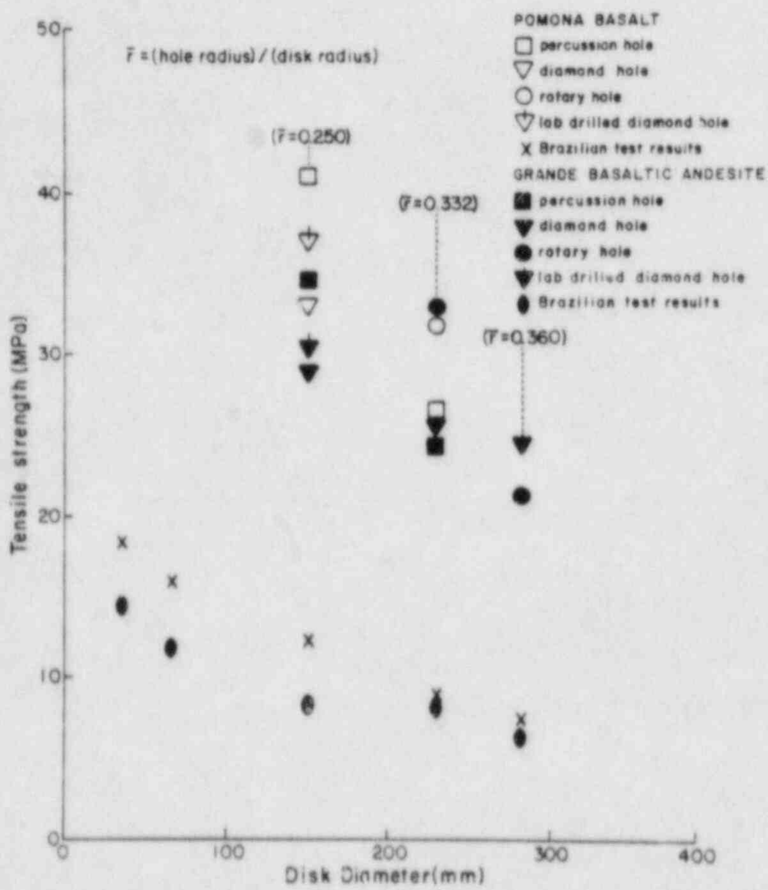

Figure 4.1 Results of Brazilian and ring tensile strength tests. Each "point" represents results from a minimum of 12 and a maximum of 22 tests.

Table 4.1 Results of Ring Tension Tests on 229 mm Diameter Disks

Hole Diameter mm;(inches)	Relative Hole Radius; $\bar{r}$	Ring Test Tensile Strength, σ_R MPa;(psi) Grande Basaltic Andesite	Pomona Basalt
25;(1.00)	0.111	32.9 ± 5.6 (4,770 ± 840)	35.1 ± 1.4 (5,090 ± 200)
57;(2.25)	0.250	28.6 ± 3.1 (4,160 ± 460)	28.3 ± 3.9 (4,100 ± 570)
108;(4.25)	0.472	24.3 ± 5.6 (3,530 ± 810)	25.2 ± 3.5 (3,660 ± 520)
127;(5.00)	0.555	22.9 ± 1.3 (3,330 ± 180)	22.9 ± 2.0 (3,330 ± 300)
159;(6.25)	0.694	21.2 ± 2.1 (3,080 ± 300)	22.0 ± 0.6 (3,190 ± 90)

where σ_R is the ring test tensile strength, $\bar{r}$ is the relative hole radius ($0 < \bar{r} < 1$), and C and β represent the coefficients of strength and size, respectively. These coefficients are assumed to be constants for a given rock type. By using least square fitting, the tensile strength can be presented as a function of relative hole radius, as shown in Table 4.2 and Figures 4.2 and 4.3. The mathematical relationship obtained provides a method for isolating ring test results from the effect of specimen shape. The approach is to adjust mathematically each tensile strength to a new value which corresponds to a new value of $\bar{r}$. Equation (4.1) can be rewritten as:

$$\frac{\sigma_{R_1}}{\sigma_{R_2}} = \left[\frac{\bar{r}_1}{\bar{r}_2}\right]^{-\beta} \tag{4.2a}$$

or

$$\sigma_{R_{(adjusted)}} = \sigma_{R_{(initial)}} \left[\frac{\bar{r}_{(reference)}}{\bar{r}_{(initial)}}\right]^{-\beta} \tag{4.2b}$$

The reference relative hole radius, $\bar{r}_{(reference)}$, is assigned to equal the critical relative hole radius, $\bar{r}_c$ (e.g. the minimum hole size that has an effect on the ring test tensile strength). This is done because at the critical relative hole radius the ring test tensile strengths can be correlated with Brazilian test tensile strengths. The calculated results are shown in Tables 4.3 and 4.4.

<u>(b) Size Effect Elimination:</u> This includes determination of a mathematical relationship between the ring tensile strength and disk diameter and isolation of the strength results from the effect of specimen size. Evans (1961) proposes a power equation to represent the relationship between Brazilian tensile strength and specimen diameter. Since at the critical relative hole radius the ring test tensile strength equals six times the Brazilian test tensile strength, Evans' power equation can be modified as:

$$\sigma_R = N(D)^{-\lambda} \tag{4.3}$$

where σ_R is the ring tensile strength, D is the disk diameter, and N and λ are coefficients of strength and size, respectively. By using least square fitting, the tensile strength of both rock types can be presented as a function of disk diameter as shown in Table 4.5 and Figure 4.4.

The size effect of the ring test specimen can be eliminated from the strength results obtained from Section 4.2.2.2(a) by rewriting the above equation (Eq. 4.3) as:

Table 4.2 Results of Shape Effect Calculation

Proposed equation:	$\sigma_R = C(\bar{r})^{-\beta}$
Grande basaltic andesite	$\sigma_R = 19.97(\bar{r})^{-0.236}$
Pomona basalt	$\sigma_R = 20.15(\bar{r})^{-0.252}$

where σ_R = ring test tensile strength in MPa,

$\bar{r}$ = relative hole radius ($0 < \bar{r} > 1$),

C = strength coefficient, and

β = shape coefficient.

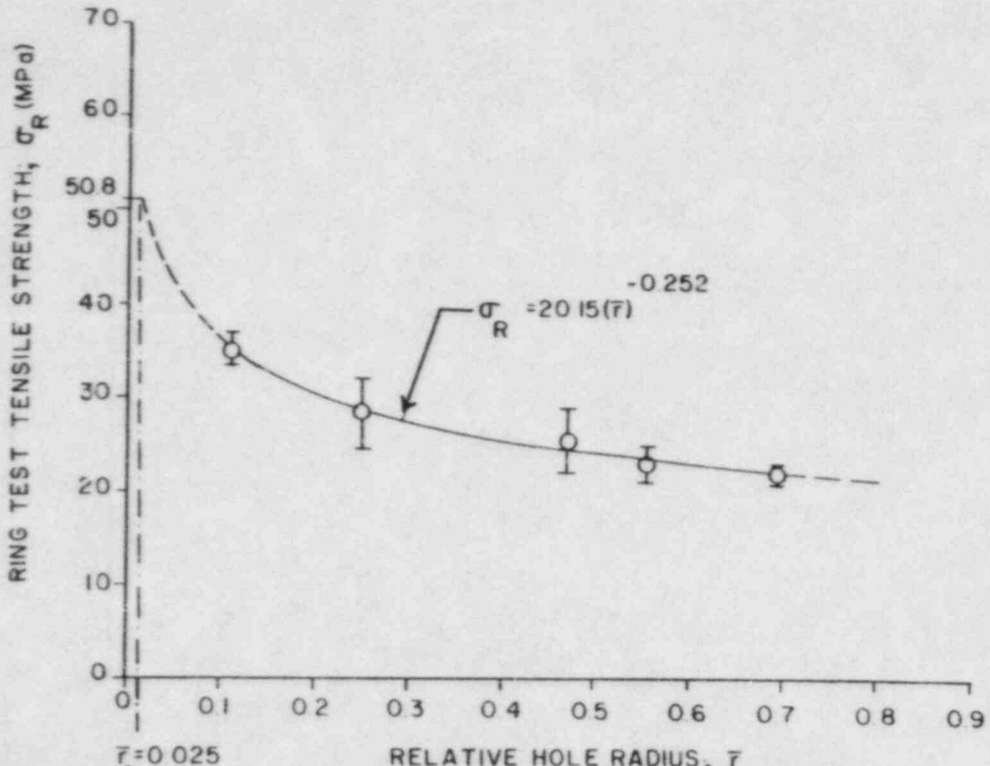

Figure 4.2 Shape effect on ring test tensile strengths of Pomona basalt. Experimental results and curve fitted, $\sigma_R = C(\bar{r})^{-\beta}$.

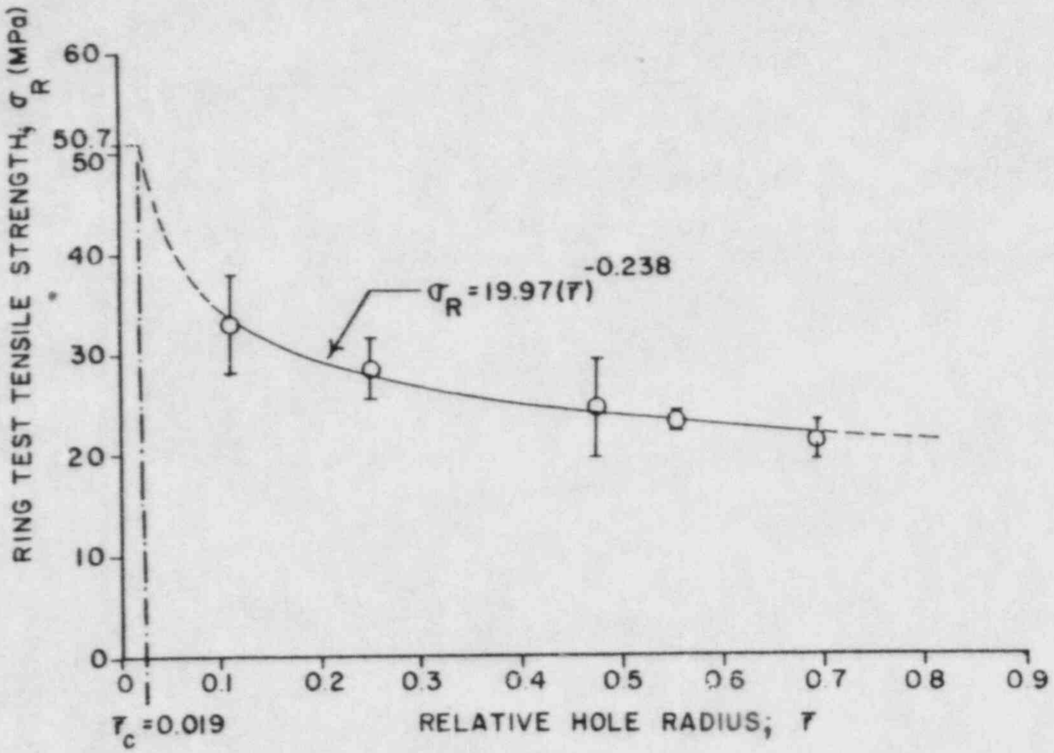

Figure 4.3 Shape effect on ring test tensile strengths of Grande basaltic andesite. Experimental results and curve fitted, $\sigma_R = C(\bar{r})^{-\beta}$.

Table 4.3 Shape Effect for Grande Basaltic Andesite

Hole Diameter (mm)	Hole Type	Initial Relative Hole Radius $\bar{r}_{(initial)}$	Initial Ring Tensile Strength $\sigma_{R(initial)}$ (MPa)	Reference Relative Hole Radius $\bar{r}_{(reference)}$	Shape Coefficient β	Adjusted Ring Tensile Strength* (MPa)
38	Diamond	0.250	29.2	0.019	0.236	53.6
38	Diamond (lab. drilled)	0.250	30.6	0.019	0.236	55.1
38	Percussion	0.250	34.7	0.019	0.236	63.7
102	Diamond	0.360	24.6	0.019	0.236	49.3
102	Rotary	0.360	21.3	0.019	0.236	42.6
76	Diamond	0.332	25.3	0.019	0.236	49.7
76	Percussion	0.332	24.8	0.019	0.236	48.7
76	Rotary	0.332	33.1	0.019	0.236	65.0

* $\sigma_{R(adjusted)} = \sigma_{R(initial)} \left(\frac{\bar{r}_{(reference)}}{\bar{r}_{(initial)}}\right)^{-\beta}$

Table 4.4 Shape Effect for Pomona Basalt

Hole Diameter (mm)	Hole Type	Initial Relative Hole Radius $\bar{r}_{(initial)}$	Initial Ring Tensile Strength $\sigma_{R(initial)}$ (MPa)	Reference Relative Hole Radius $\bar{r}_{(reference)}$	Shape Coefficient β	Adjusted Ring Tensile Strength* (MPa)
38	Diamond	0.250	33.2	0.025	0.252	59.3
38	Diamond (lab. drilled)	0.250	37.0	0.025	0.252	66.1
38	Percussion	0.250	41.0	0.025	0.252	73.2
76	Percussion	0.332	26.9	0.025	0.252	51.6
76	Rotary	0.332	32.0	0.025	0.252	61.4

$$* \quad \sigma_{R(adjusted)} = \sigma_{R(initial)} \left(\frac{\bar{r}_{(reference)}}{\bar{r}_{(initial)}}\right)^{-\beta}$$

Table 4.5 Results of Size Effect Calculations*

Proposed equation: $\sigma_R = N(D)^{-\lambda}$

Grande basaltic andesite: $\sigma_R = 285.5(D)^{-0.340}$

Pomona basalt: $\sigma_R = 488.5(D)^{-0.408}$

where σ_R = ring test tensile strength in MPa,

D = disk diameter in mm

N = strength coefficient

λ = size coefficient.

*Tensile strength of solid disk determined by using $\sigma_R = \frac{2PK}{\pi Dt}$

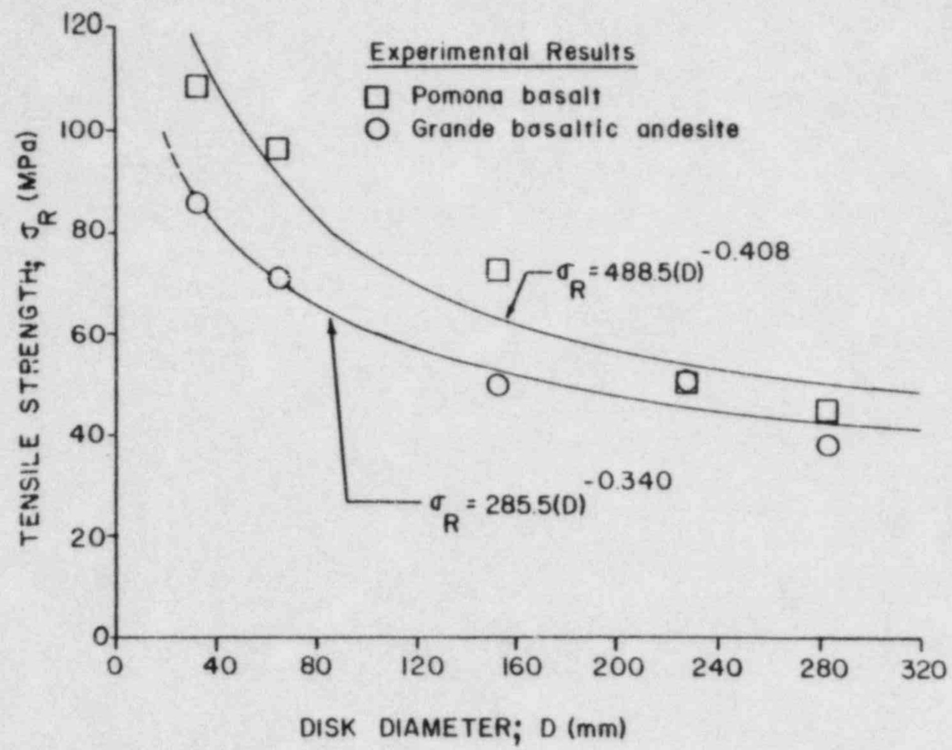

Figure 4.4 Size effect on ring test tensile strength. Experimental results and curve fitted, $\sigma_R = N(D)^{-\lambda}$.

$$\frac{\sigma_{R_1}}{\sigma_{R_2}} = \left[\frac{D_1}{D_2}\right]^{-\beta} \tag{4.4a}$$

or

$$\sigma_{R(\text{adjusted})} = \sigma_{R(\text{initial})} \left[\frac{D_{(\text{reference})}}{D_{(\text{initial})}}\right]^{-\lambda} \tag{4.4b}$$

The reference diameter, $D_{(\text{reference})}$, is assigned to be 229 mm. The results are shown in Tables 4.6 and 4.7.

(c) Calculated Results: The strength results, adjusted for size and shape effects are plotted as a function of hole diameter in Figure 4.5. Analytically, these are the ring test tensile strengths of 229 mm (9 in) diameter disks with 4.35 mm and 5.73 mm center holes (at $\bar{r}_c$ = 0.019 and 0.025) for Grande basaltic andesite and Pomona basalt, respectively. The relative differences of the tensile strengths indicate that larger percussion and rotary drill bits tend to induce more damage than do smaller ones. On the other hand, a larger diamond core bit induces slightly less damage than does the smaller one. Generally, the results agree with the microscopic observations discussed later in this chapter.

4.2.2.3 Strain-Gaged Ring Tests

The purpose of this investigation is to monitor the tangential tensile strain along the loaded diameter as the load increases until failure. Electrical strain gages are installed along the loaded rock disk diameter. Each gage is oriented normal to the loading line in order to obtain the tangential strain. The strains are read at each 2,200 newtons load increment, until failure. The last strains measured prior to failure are plotted as a function of distance from the hole in Figure 4.6. The maximum tangential tensile strains always occur at the hole boundary. At the boundary of 38 mm center holes, percussion specimens show higher strain (lower tensile stiffness) than do diamond specimens. For 76 mm center holes, the strains obtained from each hole type tend to be similar. This supports the previous conclusion that as the hole size increases, the effects on rock damage of the three drilling techniques are not significantly different.

4.2.2.4 Finite Element Analysis

The purpose of this investigation is to determine the stress-strain distribution along the loading diameter of the ring test specimen. The program DESABEL (Desai and Abel, 1972) is used in this investigation. The analysis is performed in plane stress. The mesh consists of 196 elements covering an area of 42 cm^2 (1.9 cm inner radius, 7.6 cm outer radius). The Young's modulus and Poisson's ratio of the intact rock are assigned to be 86.0 x 10^3 MPa and 0.24, respectively (determined experimentally by Daemen et al., 1983). The Young's modulus of the 1 mm-thick damaged zone around the hole is assumed to be 22.5 x 10^3 MPa (one fourth of the value for intact rock).

Table 4.6 Size Effect for Grande Basaltic Andesite

Hole Diameter (mm)	Drilling Method	Initial Disk Diameter $D_{(initial)}$ (mm)	Initial Ring Tensile Strength $\sigma_{R(initial)}$ (MPa)	Reference Disk Diameter $D_{(reference)}$ (mm)	Size Coefficient β	Adjusted Ring Tensile Strength* (MPa)
38	Diamond	152	53.6	229	0.340	46.6
38	Diamond (lab. drilled)	152	55.1	229	0.340	48.0
38	Percussion	152	63.7	229	0.340	55.4
102	Diamond	283	49.3	229	0.340	53.0
102	Rotary	283	42.6	229	0.340	45.8
76	Diamond	229	49.7	229	0.340	49.7
76	Percussion	229	48.7	229	0.340	48.7
76	Rotary	229	65.0	229	0.340	65.0

* $\sigma_{R(adjusted)} = \sigma_{R(initial)} \left(\frac{D_{(reference)}}{D_{(initial)}}\right)^{-\lambda}$

Table 4.7 Size Effect for Pomona Basalt

Hole Diameter (mm)	Drilling Method	Initial Disk Diameter $D_{(initial)}$ (mm)	Initial Ring Tensile Strength $\sigma_{R_{(initial)}}$ (MPa)	Reference Disk Diameter $D_{(reference)}$ (mm)	Size Coefficient β	Adjusted Ring Tensile Strength* (MPa)
38	Diamond	152	59.3	229	0.408	50.2
38	Diamond (lab. drilled)	152	66.1	229	0.408	55.9
38	Percussion	152	73.2	229	0.408	61.9
76	Percussion	229	51.6	229	0.408	51.6
76	Rotary	229	61.4	229	0.408	61.4

* $\sigma_{R_{(adjusted)}} = \sigma_{R_{(initial)}} \left(\frac{D_{(reference)}}{D_{(initial)}}\right)^{-\lambda}$

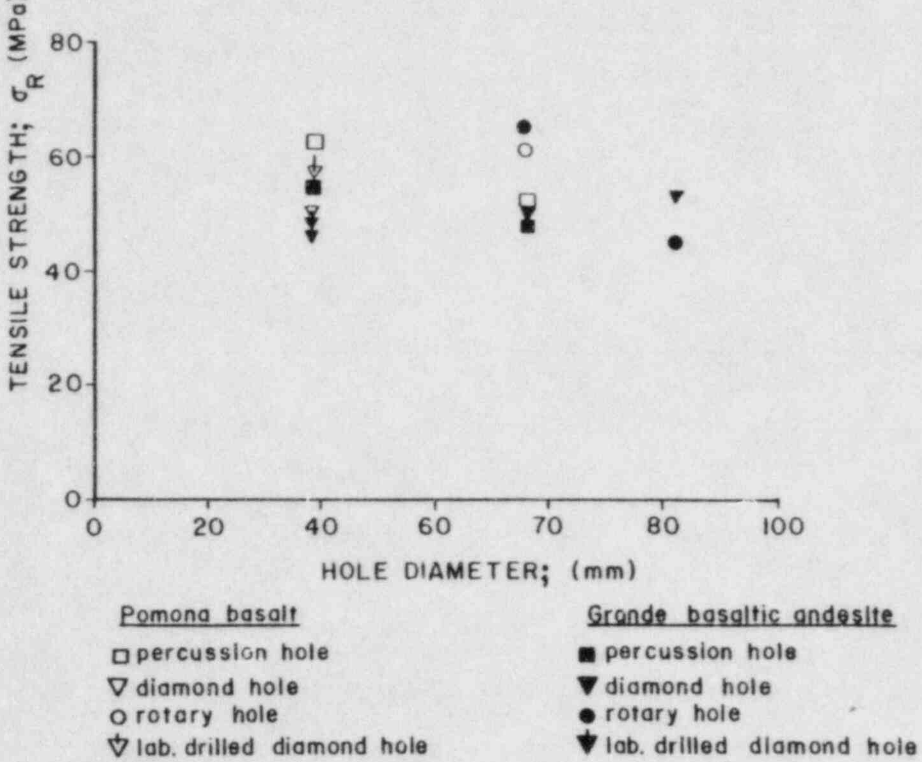

Figure 4.5 Ring test tensile strengths, adjusted for size and shape effects, are plotted as a function of hole diameter. Analytically, these results represent the ring tensile strengths of 229 mm diameter disks with 4.35 mm and 5.73 mm center holes for Grande basaltic andesite and Pomona basalt, respectively.

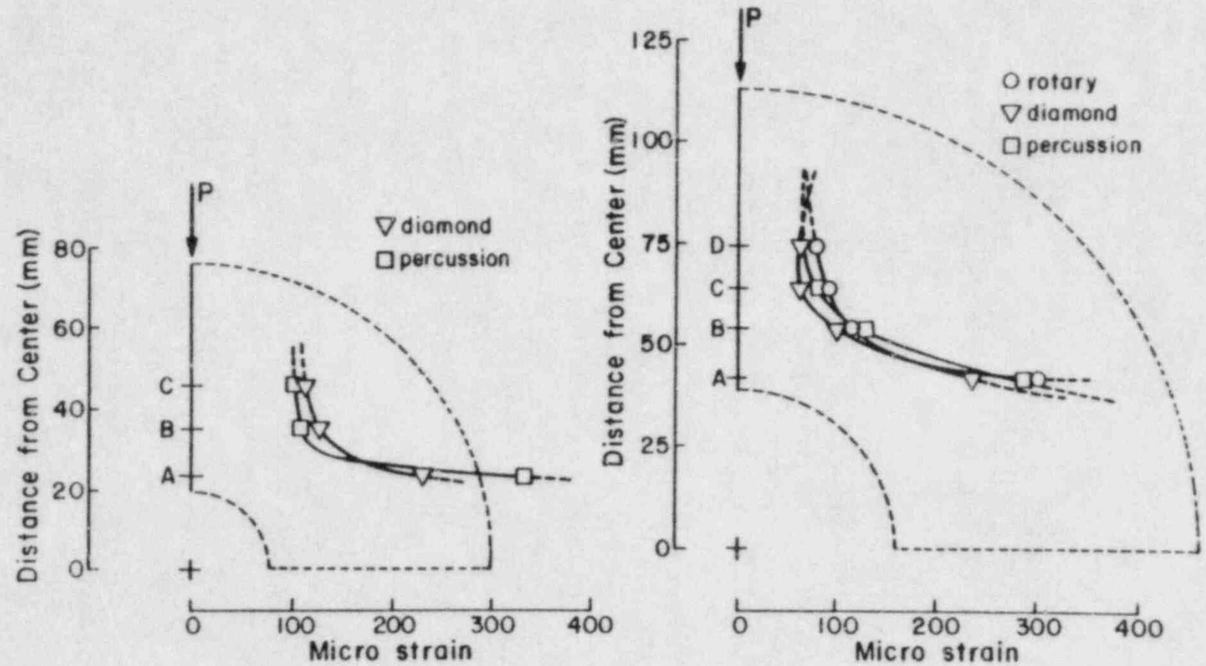

Figure 4.6 Strain distribution measured during ring tests. Tangential strains on 152 mm disk with 38 mm centered hole (left) and 229 mm disk with 76 mm centered hole (right) in Grande basaltic andesite. The strains immediately prior to failure, at a load of 34×10^3 N and of 57×10^3N, respectively, are plotted as a function of distance from the hole. A, B, C and D are strain gage locations. Arrows (P) indicate the direction of loading.

The stress-strain distribution along the loaded diameter, obtained from finite element analysis, is plotted as a function of distance from the hole in Figures 4.7 and 4.8. By comparing the stress-strain distribution between undamaged specimens and damaged specimens (1 mm thick damaged zone around the center hole) it is found that:

(a) If a damaged zone exists around the hole the maximum tangential tensile stress will not occur at the hole boundary.

(b) The location of the maximum tensile stress is governed by the thickness of the damaged zone.

(c) The maximum tangential tensile strain always occurs at the hole boundary. Higher maximum strain is an indicator of lower damaged zone stiffness (Young's modulus, E), or of a wider damaged zone.

4.2.3 Permeability Tests

The purpose of this work is to determine the influence of the damaged zone on the flow path around a borehole plug in Pomona basalt. Laboratory set-up, sample preparation, and testing procedures are described in the last annual report (Daemen et al., 1983).

Nine specimens with different sizes (e.g. 152, 229 and 283 mm cylinders with 38, 76 and 102 mm centered holes, respectively) have been tested. Their dimensions and flow test parameters are shown in Tables 4.8 and 4.9. The inflow has been measured by monitoring the movement of a piston in a constant diameter water pump and with a Matheson flowmeter. The longitudinal outflow (flow through cement plug, cement-rock interface, and damaged zone) is collected and read in a high-precision pipette. The radial outflow through the rock cylinder has not been recorded.

For 152 mm cylinders with 38 mm center hole, a large variation of inflow rates has been observed among the specimens. No inflow has been seen until the injection pressure reaches 3.15 MPa and 3.50 MPa for the field drilled diamond hole and for the percussion hole, respectively (Tables 4.10 and 4.11). For both samples, no outflow has been obtained throughout the experiment even though the water pressure has been increased up to 3.78 MPa (550 psi), the limit of the pressure intensifier. Inflow and outflow for the laboratory drilled diamond hole specimen were obtained immediately after the pressure reached 0.74 MPa. The flow rates increase as the injection pressure increases (Table 4.12).

For 229 mm cylinders with 76 mm center hole and 283 mm cylinders with 102 mm center hole, high inflow rates have been measured at injection pressures ranging from 0.014 to 0.16 MPa (Tables 4.13 through 4.17). However, no longitudinal outflow is obtained from any sample. This is because the water leaks from the center hole through pre-existing cracks in the rock cylinders instead of flowing through the borehole plug, interface, and/or damaged zone. The crack orientations appear to be random. The crack frequency is approximately 1-2 per 30 cm.

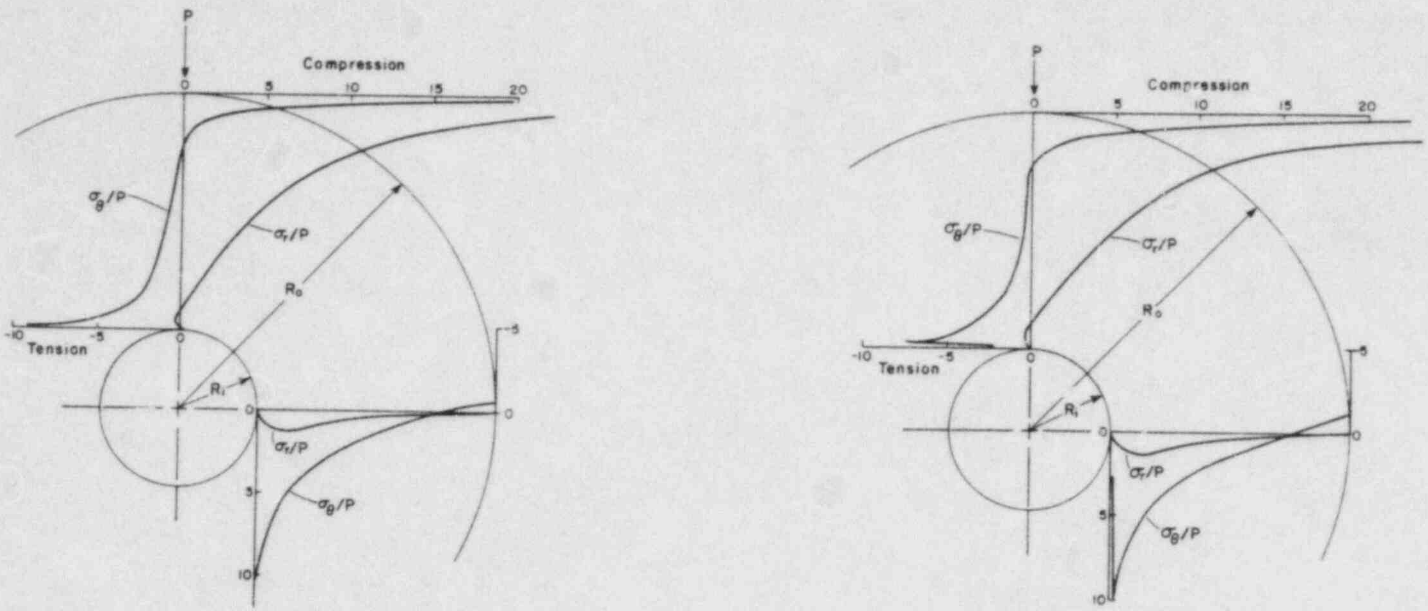

Figure 4.7 Distribution of tangential stress (σ_θ/P) and radial stress (σ_r/P) along loading diameter of ring test specimen, obtained from finite element analysis. Arrows indicate the direction of loading. For undamaged specimen (left), the maximum tensile stress occurs at the hole boundary. For damaged specimen (right) (1 mm thick around the hole), the maximum tensile stress shifts and redistributes further away from the hole. (R_i = 19 mm, R_o = 76mm, $\bar{r}$ = 0.250, P = 2 x 10^4 N)

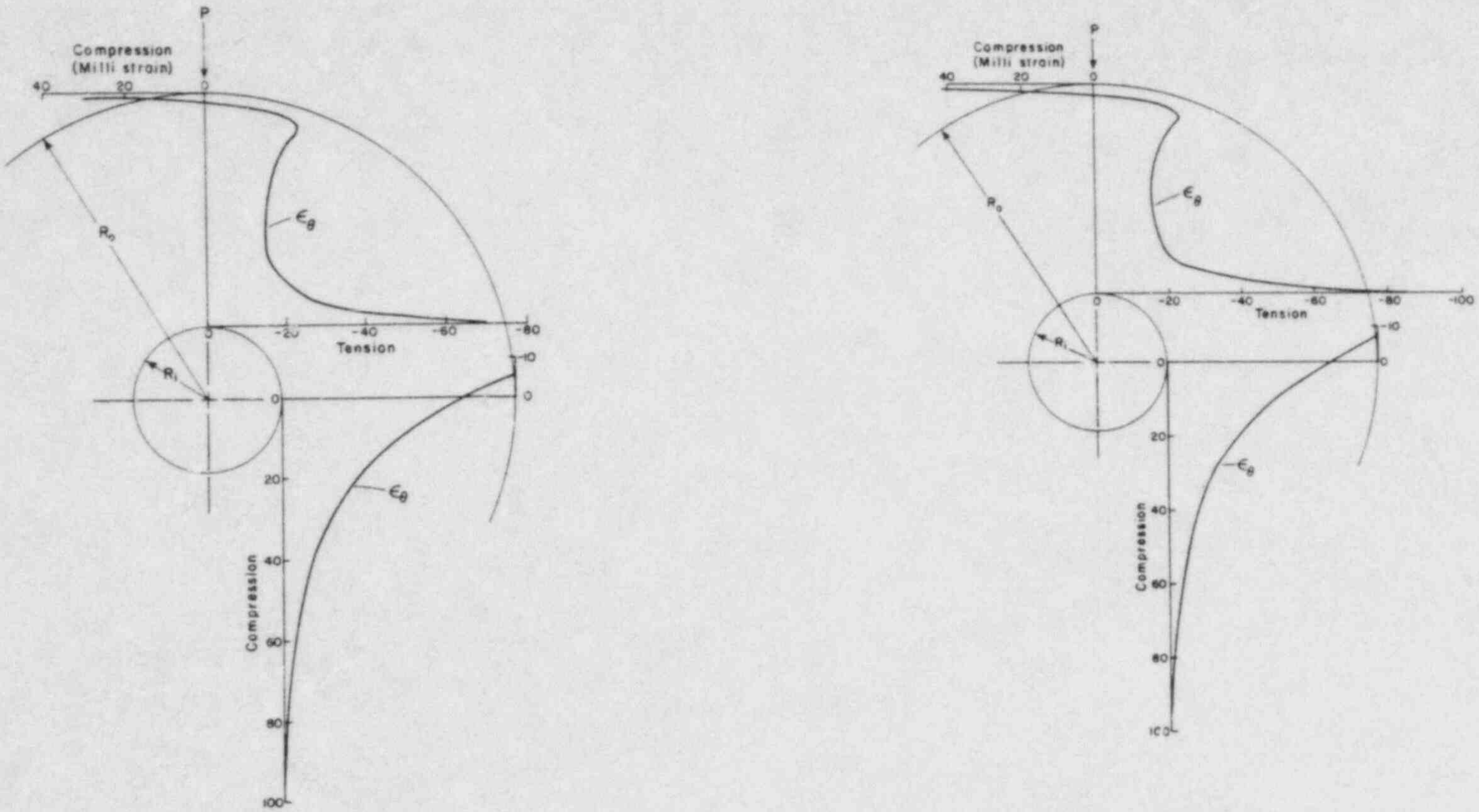

Figure 4.8 Distribution of tangential strain (ε_θ) along loading diameter of ring test specimen, obtained from finite element analysis. Arrows (P) indicate the direction of loading. At the hole boundary, damaged specimen (right) shows higher tensile strain than does undamaged specimen (left).

Table 4.8 Dimensions of Specimens Used in Permeability Test

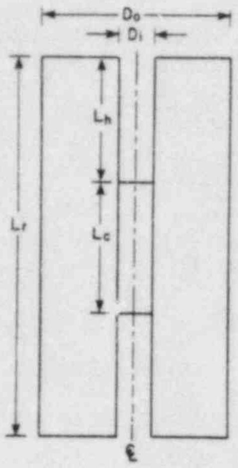

D_o = cylinder diameter
D_i = hole diameter
L_r = cylinder length
L_h = top hole length
L_c = cement plug length

Sample No.	Dimensions (cm)				
	D_o	D_i	L_r	L_h	L_c
BDLPm 6-4	15.2	3.8	30.8	10.2	10.2
BDLPm 6-15	15.2	3.8	30.3	9.8	9.9
BDFPm 6-11	15.2	3.8	30.4	9.9	9.9
BDFPm 6-12	15.2	3.8	30.3	10.3	10.1
BDFPm 6-13	15.2	3.8	30.2	10.0	9.9
BDFPm 9-1	22.9	7.6	42.5	12.0	13.9
BRFPm 9-1	22.9	7.6	45.6	14.6	15.0
BRFPm 9-2	22.9	7.6	47.4	13.2	17.3
BDFPm 12-1	28.3	10.2	52.2	19.3	21.5
BRFPm 12-1	28.3	10.2	50.0	18.5	20.0

Table 4.9 Flow Test Parameters

	152 mm Cylinders	229 mm and 283 mm Cylinders
Cement Type	S stem 1*	System 1*
Cement Curing Period	[illegible] days	90 days
Saturating Period of Specimen	14 days	2 days
Room Temperature	21 ± 2°C	21 ± 2°C
Room Humidity	42 ± 1%	42± 2%
Room Pressure	101 ± 3 kPa	99 ± 4 kPa

*A description of Cement System #1 is given in the last annual report (Daemen et al., 1983).

Table 4.10 Flow Testing Results for 38 mm Diamond Hole (Sample no. BDFPm 6-12)

Injection Pressure (MPa)	Rate of Inflow ($\times 10^{-6}$ cc/min)	Longitudinal Outflow ($\times 10^{-6}$ cc/min)	Testing Period (hrs)	Number of Readings
0.64	0	0	72	25
1.50	0	0	76	30
2.28	0	0	72	16
2.80	0	0	72	12
3.15	0 - 200	0	72	32
3.50	225	0	96	21
3.78	250	0	72	17

Table 4.11 Flow Testing Results for 38 mm Percussion Hole (Sample no. BPFPm 6-13)

Injection Pressure (MPa)	Rate of Inflow ($\times 10^{-6}$ cc/min)	Longitudinal Outflow ($\times 10^{-6}$ cc/min)	Testing Period (hrs)	Number of Readings
0.64	0	0	72	25
1.50	0	0	76	30
2.28	0	0	72	16
2.80	0	0	72	12
3.15	0	0	72	32
3.50	0 - 200	0	96	21
3.78	0 - 200	0	4	2

Table 4.12 Flow Testing Results for 38 mm Laboratory Drilled Diamond Hole (Sample no. BDLPm 6-4)

Injection Pressure (MPa)	Rate of Inflow ($\times 10^{-6}$ cc/min)	Longitudinal Outflow ($\times 10^{-6}$ cc/min)	Testing Period (hrs)	Number of Readings
0.74	200	72	70	11
1.50	225	150	96	10
2.20	400	260	72	14
2.28	415	360	72	16
2.30	455	392	72	10
2.80	675	495	72	16

Table 4.13 Flow Testing Results for 76 mm Diameter Rotary Hole (Sample no. BRFPm 9-1)

Injection Pressure (MPa)	Rate of Inflow (x 10^{-6} cc/min)	Longitudinal Outflow (x 10^{-6} cc/min)	Testing Period (min)	Number of Readings
14	0.12	0	15	4
31	0.36	0	10	4
35	0.46	0	20	5
39	0.55	0	15	4
43	0.76	0	15	4
47	0.78	0	20	5
53	0.90	0	10	4
96	1.65	0	22	3

Table 4.14 Flow Testing Results for 76 mm Diameter Percussion Hole (Sample no. BPFPm 9-1)

Injection Pressure (MPa)	Rate of Inflow (x 10^{-6} cc/min)	Longitudinal Outflow (x 10^{-6} cc/min)	Testing Period (min)	Number of Readings
20	0	0	30	6
29	0	0	10	4
35	0	0	10	4
45	0 - 0.002	0	10	4
55	0 - 0.002	0	30	6
90	0.005	0	20	4
96	0.002	0	30	6
117	0.007	0	120	7
138	0.010	0	30	4
158	0.02	0	30	4

Table 4.15 Flow Testing Results for 76 mm Diameter Rotary Hole (Sample no. BRFPm 9-2)

Injection Pressure (MPa)	Rate of Inflow ($\times 10^{-6}$ cc/min)	Longitudinal Outflow ($\times 10^{-6}$ cc/min)	Testing Period (min)	Number of Readings
21	1.0	0	15	7
31	3.5	0	15	6
62	20.0	0	5	4
75	~ 50.0	0	5	5

Table 4.16 Flow Testing Results for 102 mm Diameter Rotary Hole (Sample no. BRFPm 12-1)

Injection Pressure (MPa)	Rate of Inflow ($\times 10^{-6}$ cc/min)	Longitudinal Outflow ($\times 10^{-6}$ cc/min)	Testing Period (min)	Number of Readings
29	1.0	0	15	8
35	1.0	0	15	6
39	2.0	0	10	4
43	7.5	0	10	4
55	7.5	0	10	4
90	30.2	0	10	4
117	~ 70.0	0	5	4

Table 4.17 Flow Testing Results for 102 mm Diameter Diamond Hole (Sample no. BDFPm 12-1)

Injection Pressure (MPa)	Rate of Inflow (x 10^{-6} cc/min)	Longitudinal Outflow (x 10^{-6} cc/min)	Testing Period (min)	Number of Readings
21	1.0	0	15	8
34	30.0	0	15	6
55	35.5	0	15	8
90	150	0	5	2
100	> 200	0	2	2

The results imply that the effect of the damaged zone on the flow path around the borehole plug might not be a significant factor compared with the high variation of the rock permeability. This high variation might be caused by the presence of cracks and flow layers, and by nonuniform distribution of the vesicles in basalt samples. Generally, the conclusions from these results agree reasonably well with the experimental results performed by Lingle et al. (1982) on anhydrite, granite, basalt and tuff and by Mathis and Daemen (1982) on granitic rocks.

4.2.4 Microscopic Fracture Studies

4.2.4.1 Petrographic Microscopy

Sample preparation and method of investigation are described in detail by Fuenkajorn and Daemen (1984b). Damage induced by drilling can be described by using the following criteria: roughness of the borehole wall (average difference in "elevation" of the borehole wall), cracks within grains - cleavage fractures, intergranular cracks, missing particles (presented as [(area of missing grain/total area around the hole) x 100], and damaged zone thickness. Results of the investigation of Pomona basalt are shown in Table 4.18.

Damage characteristics are controlled by the drilling mechanism, drilling parameters, grain size of particles around the hole, and orientation of the particles. The thickness of the damaged zone is usually not larger than 1.5 mm. The largest damaged zone (1.7 mm thick) is seen around 76 mm percussion holes while the smallest damaged zone (0-0.3 mm thick) appears around 38 mm laboratory drilled diamond holes. These results agree with the experimental results obtained by Burns et al. (1982), and by Lingle et al. (1982).

Cracks within grains or cleavage fractures are more likely to appear in coarse grained rock (e.g. Pomona basalt; larger than 0.5 mm grain size), while intergranular cracks are predominant in fine grained rock (e.g. Grande basaltic andesite; smaller than 0.01 mm grain size).

No partial cleavage fractures appear in a grain; if a grain is damaged, the damage appears throughout the grain. This phenomenon has also been observed by Mathis and Daemen (1982) in granitic rocks.

Generally, for all drilling methods, as the hole size increases, the damage intensity tends to increase.

Based on the information obtained from petrographical investigation, typical damaged zone characteristics induced by each drilling technique in coarse grained rocks are proposed. Figure 4.9, left, shows typical damage induced by diamond drilling. The borehole wall is relatively smooth. The damaged zone is uniform. Every damaged grain shows the same degree of damage. Only a few particles are missing. A high degree of roughness is typical for percussion drilled holes (Figure 4.9, middle); sharp edges, missing particles, and loose edge grains always appear along the entire hole wall. The damage intensity within a grain is uniform. Grains near the hole show more damage than grains away from

Table 4.18 Summary of Petrographic Microscope Observations on Pomona Basalt

Drilling Technique	Hole Diameter (mm)	Damage Zone Thickness (mm)	Missing Particles (%)	Roughness of the Wall (mm)	Number of Samples Studied
Diamond	38	0 - 0.6	10 - 20	0.1 - 0.3	12
Lab Drilled Diamond	38	0 - 0.3	0 - 5	0 - 0.1	12
Percussion	38	0 - 1.7	60 - 90	0.5 - 1.5	12
Percussion	76	1.0 - 1.5	70 - 90	0.5 - 1.5	8
Rotary	76	0 - 0.3	10 - 20	0.1 - 1.3	8
Rotary	102	0 - 0.8	25 - 30	0.1 - 0.4	8
Diamond	102	0 - 0.6	25 - 30	0.1 - 0.4	8

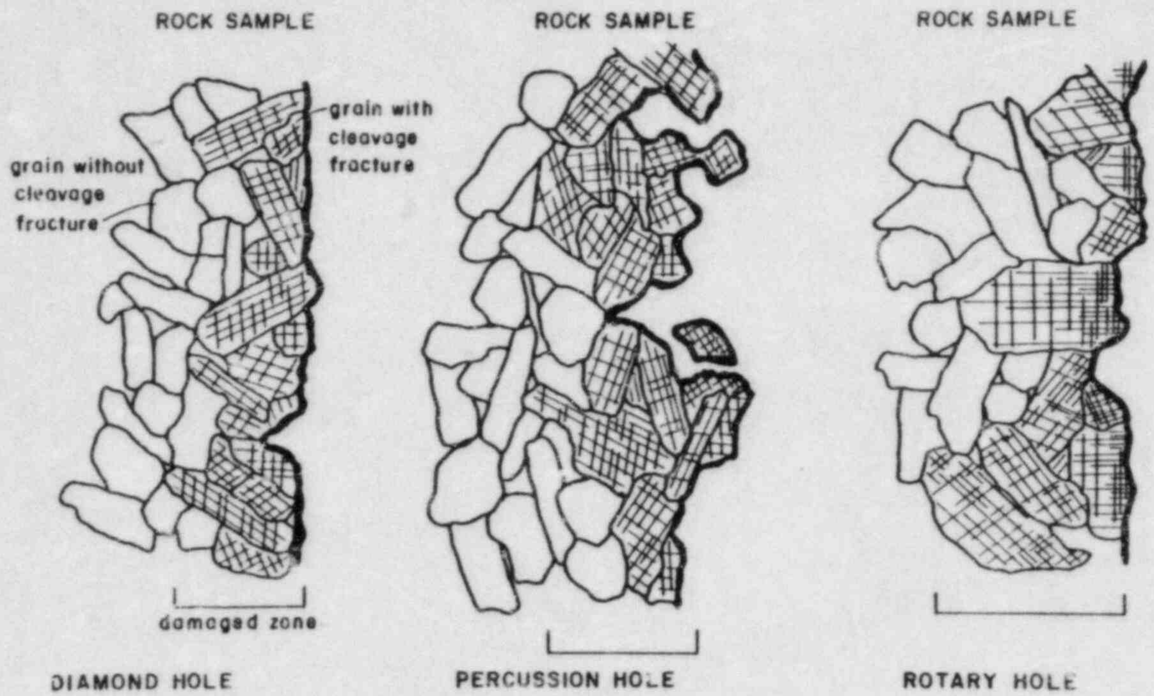

Figure 4.9 Typical drilling damage characteristics:

Diamond hole: smooth wall, uniform damaged zone, few missing particles, uniform fracture density within damaged grains.

Percussion hole: rough wall, irregular damaged zone, numerous missing particles, uniform fracture density within damaged grains.

Rotary hole: relatively smooth wall, irregular damaged zone, higher fracture intensity closer to the hole within damaged grains.

the hole. The borehole wall produced by rotary drilling is smooth (Figure 4.9, right). A few traces of missing particles occur. No sharp edge surfaces have been observed. The intensity of cracking in a damaged grain is not uniform; higher fracture density always occurs at the side closer to the hole. The shape of the damaged zone is irregular.

The typical characteristics proposed here might be applicable to other rocks wih similar petrographical properties (mineral composition, grain size, and hardness).

4.2.4.2 Scanning Electron Microscopy (SEM)

Scanning electron microscopy (e.g. Black, 1974) is performed to obtain three-dimensional images of microscopic fractures induced around the borehole wall. This investigation concentrates on determination of the characteristics of an individual crack (orientation, length, width, and relative displacement). Sample preparation and investigating procedures are described by Fuenkajorn and Daemen (1984b). Diamond and percussion specimens of Grande basaltic andesite are investigated by using as criteria: roughness of the borehole wall, intergranular cracks, cleavage fractures, depth of the damaged zone, and intensity of the cracks. The results are summarized in Table 4.19.

4.2.5 Factors Controlling Damage Zone

Based on the results obtained from the ring tension tests and microscopic fracture studies, two categories of factors controlling the damaged zone around the borehole can be proposed: petrographical factors and drilling factors. The petrographical factors include some of the physical properties of the rock drilled. The significant properties are grain size, grain orientation, breakage mechanism of the grain, and interaction between the grains. The drilling factors include drilling method, bit size, rotational speed, and weight on the drill bit.

Extrapolation of this concept to larger holes (beyond the studied range, 38-102 mm diameter) is uncertain due to the complexity of the drilling mechanism and the variation of the drilling parameters.

4.2.6 Conclusions

A damaged zone induced by drilling around the borehole does exist. The thickness of the zone ranges from 0.0 to 1.7 mm (or on the scale of grain size dimensions). A larger drill bit induces more wall damage than a smaller one. Different drilling techniques show different damage characteristics (intensity and distribution). The damage characteristics are governed not only by drilling parameters (bit size, weight on bit, rotational speed, and energy), but also by physical properties of the rock (grain size, grain orientation, breakage mechanism, and interaction between the grains). The weaker rock tends to show more intense damage than does the stronger one. Cleavage fractures are more likely to appear in coarse grained rock, e.g. Pomona basalt, while intergranular cracks are more likely to appear in fine

Table 4.19 Characteristics of Cracking Near Borehole Walls Observed by Scanning Electron Microscopy

	Width (μ)	Length (μ)	Frequency	Orientation
Cleavage fractures	0.5 - 2	1 - 50	1 per μ (for percussion) 2 - 10 per 100μ (for diamond)	Controlled by orientation of the grain
Inter-granular cracks	10 - 100	10 - 600	1 per 2 mm	Random

grained rock, e.g. Grande basaltic andesite. The damaged zones play no significant role in the flow path around the borehole plug. The preferred migration path of water near a borehole appears to be through pre-existing fractures.

4.3 Ongoing Work

Permeability tests are being performed on two 152 mm cylinders with 38 mm diamond and percussion center holes to monitor the flowrates over a long term period. The tests were started on May 20, 1984. The injection water pressure has been maintained at 1 MPa (145 psi). For both samples, the inflow rates observed have been less than 0.002 cc/min. No longitudinal outflow (flow through cement plug, interface, and damaged zone) has been observed. The samples are not submerged in the water-tight chamber. No attempt has been made to measure the radial outflows.

Finite element analysis is being performed to determine the stress-strain distribution in the permeability tests specimen. The result may lead to an understanding of flow behavior within the specimen. The finite element mesh and boundary conditions are shown in Figure 4.10. The program SAP IV (Bathe et al., 1974) used in this investigation provides an axisymmetric analysis. The mesh consists of 582 elements covering an area of 193 cm^3 (inner radius = 19 mm, outer radius = 76 mm, and the cylinder length = 3.0 cm). The smallest elements located in the damaged zone region have an area of 0.50 mm x 0.50 mm. The results are expected to be presented in the next quarterly report.

4.4 References

Addinall, E. and P. Hackett, 1964, "Tensile Failure in Rock-Like Material," Proceedings of the Sixth Rock Mechanics Symposium, Rolla, Missouri, pp. 527-534.

Bathe, K.J., E.L. Wilson, and F.E. Peterson, 1974, "A Structural Analysis Program (SAPIV) for Static and Dynamic Response of Linear Systems," Earthquake Engineering Research Center, Report no. EERC 73-11, College of Engineering, University of California, Berkeley.

Bieniawski, Z.T., 1968, "The Effect of Specimen Size on Compressive Strength of Coal," International Journal of Rock Mechanics and Mining Sciences, Vol. 5, pp. 325-335.

Black, J.T., 1974, Principles and Techniques of Scanning Electron Microscopy, Van Nostrand, Reinhold Co., New York.

Burns, F.L., R. Lingle, and A. Andrews, 1982, "Cement-Plug Leakage and Drilling Damage Evaluated," Oil and Gas Journal, Nov. 22.

Daemen, J.J.K., D.L. South, W.B. Greer, J.C. Stormont, S.A. Dischler, G.S. Adisoma, N.I. Colburn, K. Fuenkajorn, D.E. Miles, B. Kousari, and J. Bertucca, 1983, "Annual Report, Rock Mass

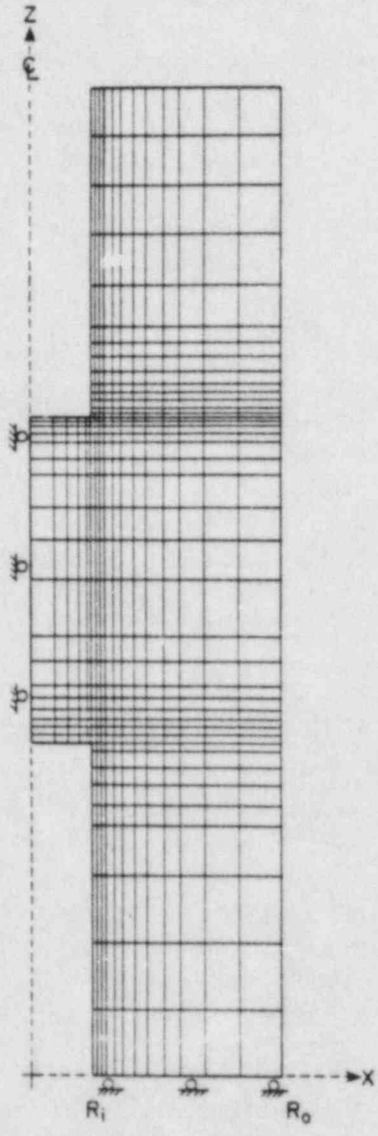

Figure 4.10 Schematic diagram of mesh used for finite element analysis of permeability test specimen. The hole radius (R_i) is 19 mm, and the cylinder radius (R_0) is 76 mm. Cylinder length is 305 mm.

Sealing, June 1, 1982 - May 31, 1983," prepared for the U.S. Nuclear Regulatory Commission, Division of Health, Siting and Waste Management, by the Department of Mining and Geological Engineering, University of Arizona, Tucson.

Davidenkov, N., E. Shevandin, and F. Whittmann, 1947, "The Influence of Size on the Brittle Strength of Steel," Journal of Applied Mechanics, pp. A63-A67.

Desai, C.S. and J.F. Abel, 1972, Introduction to the Finite Element Method, Van Nostrand, Reinhold Co.

Evans, I., 1961, "The Tensile Strength of Coal," Colliery Engineering, Vol. 38, pp. 428-434.

Fuenkajorn, K. and J.J.K. Daemen, 1984a, "Experimental Assessment of Borehole Drilling Damage in Basaltic Rocks," Proceedings of the Twenty-Fifth Rock Mechanics Symposium, Northwestern University, Evanston, Illinois, pp. 774-783.

Fuenkajorn, K. and J.J.K. Daemen, 1984b, "Drilling Damage in Basalt," Topical Report to U.S. Nuclear Regulatory Commission, Division of Health, Siting and Waste Management, by the Department of Mining and Geological Engineering, University of Arizona, Tucson.

Hobbs, D.W., 1964, "The Tensile Strength of Rocks," International Journal of Rock Mechanics and Mining Sciences, Vol. 1, pp. 385-394.

Hodgson, K. and N.G.W. Cook, 1970, "The Effect of Size and Stress Gradient on the Strength of Rock," The Second Congress International Society of Rock Mechanics, Belgrade, pp. 31-34.

Jaeger, J.C. and E.R. Hoskins, 1966, "Stresses and Failure in Rings of Rock Loaded in Diametral Tension or Compression," British Journal of Applied Physics, Vol. 17, pp. 685-692.

Lingle, R., K.L. Stanford, P.E. Peterson, and S.F. Woodhead, 1982, "Technical Report, Wellbore Damage Zone Experimental Determination," Report No. ONWI-349, prepared for Office of Nuclear Waste Isolation by Terra Tek, Inc., University Research Park, Salt Lake City, Utah.

Mathis, S.P. and J.J.K. Daemen, 1982, "Rock Mass Sealing - Borehole Wall Damage Induced by Drilling: An Assessment of Diamond and Percussion Drilling Effects," Topical Report, prepared for the U.S. Nuclear Regulatory Commission, SAFER Division, by Nuclear Fuel Cycle Research Program, Department of Mining and Geological Engineering, University of Arizona, Tucson, AZ.

South, D.L., W.B. Greer, N.I. Colburn, S.L. Cobb, B. Kousari, S.P. Mathis, R.G. Jeffrey, C.A. Wakely, and J.J.K. Daemen, 1982, "Annual Report, Rock Mass Sealing, June 1, 1981 - May 31, 1982,"

prepared for the U.S. Nuclear Regulatory Commission, SAFER Division, by Nuclear Fuel Cycle Research Program, Department of Mining and Geological Engineering, University of Arizona, Tucson, AZ.

CHAPTER FIVE

EXPERIMENTAL ASSESSMENT OF BENTONITE BOREHOLE SEALING PERFORMANCE

5.1 Introduction

This chapter is the executive summary of a topical report (Sawyer and Daemen, 1985, to be issued shortly), in which sealing aspects of seven commercially available bentonites have been studied.

Bentonite, and more broadly earthen materials, have been proposed frequently as one of the prime candidate sealing materials for HLW repositories, as well as for various backfill and engineered barrier structures (e.g. Giuffre et al., 1979; Koplik et al., 1979; Smith et al., 1980; Ellison et al., 1981), although severe reservations about their use have been expressed also (e.g. Claiborne, 1982, Abstract). Bentonite and earthen materials have been investigated for sealing and backfill purposes (e.g. Martin, 1975; Fernandez et al., 1976; Pusch et al., 1982, pp. 2-24; Singh, 1982; Pusch, 1983; Meyer, 1983), but there remains considerable uncertainty about their performance (e.g. Fyfe et al., 1984; Koplik et al., 1979, p. 2-24).

5.2 Bentonites Used in Laboratory Experiments

Bentonites being considered as a possible sealing material for boreholes or shafts are composed of montmorillonite, a clay mineral of the smectite group that is composed of an aluminum octahedral sheet sandwiched between two silica tetrahedral sheets. Isomorphous substitution within the octahedral sheet structure results in a net negative electric charge on the montmorillonite clay particle. Cations are absorbed at sites between successive montmorillonite unit cells and are held in electrostatic attraction. These cations are exchangeable with other cations of similar or different valence. The cation exchange reaction is generally reversible and obeys stoichiometric and mass action laws. A diffuse double layer develops between the negatively charged clay particles and hydrated adsorbed cations. The diffuse double layer thickness or extent is directly proportional to the fluid's dielectric constant and temperature and inversely proportional to the electrolyte concentration and valence. Both the cation exchange reaction and diffuse double layer development will affect the engineering behavior of a bentonite plug or seal (Mitchell, 1976).

The suppliers and bentonite products tested here are listed alphabetically in Table 5.1. According to the suppliers, all seven bentonites are the Na-rich, Wyoming variety and are "pure bentonites" that have no chemical additives.

Copper State Analytical Labs, Inc., of Tucson, Arizona, performed "whole-rock" chemical analyses of the bentonites. The results are

Table 5.1 Bentonite Products Tested and Their Suppliers

Supplier	Product
American Colloid Corp.	C/S Granular
Dresser Minerals	Arrow Head^{TM} *
Federal Bentonite	Akwa Seal^{TM} *
Georgia Kaolin	Hi-Jell #1^{TM} *
International Minerals & Chemical Corp.	Rainbow Seal^{TM} *
Slope Indicator	1/2 Inch Tablets**
Whitaker, Clark & Daniels	149 Bentonite 325 Mesh***

*Arrow Head^{TM} is a registered trademark of Dresser Minerals; Akwa Seal^{TM} is a trademark of Federal Bentontie; Hi-Jell #1^{TM} is a trademark of Georgia Kaolin; Rainbow Seal^{TM} is a trademark of International Minerals and Chemical Corp.

**Obtained by Slope Indicator from a bentonite supplier in Seattle, Washington.

***Obtained from an unnamed producer.

reported in Table 5.2 and have been compared to published analyses of various bentonites. The chemical composition of "bentonites" varies significantly from source to source. Some of the variation may be attributed to gangue minerals and analysis errors; however, it is clear that the term bentonite (and even montmorillonite) encompasses a number of minerals and compositions.

Because of the wide range in reported chemical analyses, it was decided to test the chemical variation within a particular product. American Colloid Corp. had supplied three 50 lb. samples from June to November, 1983. Samples were cut from the second and third batches and sent to Copper State Labs. The results are reported in Table 5.3. The SiO_2 values range from 60 to 62%; Al_2O_3 values were approximately 20%.

From the results reported in Tables 5.2 through 5.3, it appears that gangue minerals (including "unreacted-parent" rock and impurities) are present in all commercial bentonites. These impurities may affect the engineering behavior and should be identified prior to seal construction and installation. X-ray diffraction could prove useful in identifying the mineral constituents of bentonites. It is recognized that x-ray diffraction has limited value in quantitative determination of the mineral constituents (Mitchell, 1976), nevertheless, this technique is able to qualitatively identify mineral components that are present in small percentages.

5.3 Reference Testing

Reference testing is performed to determine fundamental conventional engineering properties of the seven bentonite products. The engineering properties of repository sealing materials are important not only for their in-situ sealing performance, but also for the seal installation. For instance, sealing materials could be emplaced pneumatically or in a slurry form, in which case the water content necessary to form bentonite slurry must be determined as well as the expected sealing efficiency. This "slurry water content" would be the liquid limit as a minimum.

The following engineering properties have been determined:

1) Shrinkage Limit

2) Plastic Limit

3) Liquid Limit

4) Specific Gravity of Solids

5) Moisture-Density

These tests revealed serious difficulties in testing bentonite. Results varied within a test, between technicians and between independent laboratories. Comparison of experimental results to published results proved inconsistent due (in part) to the variability of bentonite and montmorillonite composition.

Table 5.2 Whole-rock Chemical Analysis of Bentonites Used in This Research

Sample	% SiO_2	% Al_2O_3	% CaO	% MgO	% K_2O	% Na_2O	% Fe_2O_3	% H_2O	% TiO_2	% P_2O_5
Federal Bentonite	67.8	19.17	.24	4.05	0.53	4.02	3.17	0.2	0.13	0.27
Slope Indicator	68.9	16.40	.20	4.61	0.56	3.61	2.86	0.3	0.15	0.555
American Colloid Co.	69.2	16.63	.25	1.99	0.94	3.52	3.20	0.4	0.22	0.078
Int. Minerals & Chemical	65.9	19.17	.28	6.64	0.51	2.48	2.66	0.2	0.15	0.033
Dresser Minerals	73.9	14.78	.28	2.49	0.52	3.56	3.32	0.2	0.17	0.040
Whitaker, Clark & Daniels	70.4	19.40	.24	2.16	0.54	3.61	3.02	0.5	0.15	0.033
Georgia Kaolin	72.4	16.47	.31	1.99	0.58	3.11	2.63	0.4	0.11	0.035

Table 5.3 Whole-Rock Chemical Analysis of American Colloid C/S Granular

	% SiO_2	% Al_2O_3	% CaO	% MgO	% K_2O	% Na_2O	% Fe_2O_3	% H_2O	% TiO_2	% P_2O_5
Batch #2	61.6	20.4	3.4	3.56	1.42	3.40	5.00	0.3	0.16	0.10
Batch #3	59.8	20.1	4.9	3.78	1.72	3.32	5.43	0.4	0.17	0.09

5.4 Permeability Testing

5.4.1 Introduction

The primary purposes of the seals are to exclude or delay ground-water contact with the waste form, to retard the release of radionuclides and of ground water if contact is made, and to prevent communication between aquifers (Gureghian, et al., 1983, and U.S. Department of Energy, 1982). It is evident, therefore, that the relative ease with which fluids (including gases as well as groundwaters) can be transmitted through a seal is of extreme importance.

Two types of flow testing have been performed. Falling head permeability testing has been used to determine the permeabilities of the seven bentonites. Radial permeameter testing allows a direct comparison of the permeability of a specific bentonite to that of intact rock, and provides actual borehole sealing performance data on bentonite installed in rock.

The hydraulic conductivities determined from falling head tests, in the 10^{-9} cm/sec order of magnitude, are in the higher range of values reported in the literature, which vary from 10^{-8} to 10^{-13} cm/sec, depending on the testing procedures and conditions.

Compacted bentonite plugs tested in the radial permeameters under constant head water injection exhibit hydraulic conductivities in the 10^{-10} - 10^{-11} cm/sec order of magnitude. The plug compacted in the hole shows lower flow rates than the plug that has been compacted, extruded and trimmed to fit the rock cylinder. Analysis of flow rates vs. injection pressure reveals apparent deviations from Darcy's Law. The deviations have been attributed to particle migration and unequal pore size.

Flow rates through C/S Granular compacted bentonite plugs are two orders of magnitude higher than flow rates through Sentinel Gap basalts (at similar stress and water injection pressures).

The following are recommendations for future permeability tests:

(1) A "synthetic" or site-specific water should be used for the permeant. Physio-chemical interactions (particularly the double layer phenomenon) are important in testing bentonites. Distilled or de-ionized water will yield hydraulic conductivities that are conservative when compared to results obtained using permeants containing mono- and di-valent cations.

(2) The pressure gradient expected in the repository environment should be used for constant head permeability tests. The water injection pressure tends to consolidate clay plugs, thus decreasing the hydraulic conductivity. If the water injection pressure produces a hydraulic gradient that is higher or lower than "field" conditions, the flow rates and hydraulic conductivities determined from laboratory measurements will be anomalous.

(3) Different methods of compacting bentonite plugs should be attempted. Mitchell (1976, p. 247) indicates that the hydraulic conductivity is a function of compactive effort and method. Therefore, future tests might compare impact, static and kneading compactive efforts in an attempt to optimize the hydraulic conductivity.

(4) The volume of compacted bentonite plugs should be held constant during permeability tests. If plugs are allowed to expand during testing, the void closure induced by swelling pressures is minimized and the hydraulic conductivity will be greater than plugs that have a constant volume. If possible, measurements should be made of the pore pressure in the plug; then these measurements can be related to the total stress and swelling pressure generated by the volumetrically confined plug.

5.5 Strength Testing

5.5.1 Introduction

Strength testing is intended to assess the probability that bentonite seals might fail, either by slip along the seal-rock interface, or by failure of the bentonite seal itself. Any testing of plugs or seals must take into consideration the probable field conditions that the plug will experience. The predicted field conditions should be reproduced by the testing procedure. Two limiting field conditions are envisioned. The first is immediately after construction of the shaft or borehole seal before groundwaters have infiltrated and saturated the sealing materials. In this condition the sealing material has pore volumes that contain a gas as well as a liquid phase and is in an unsaturated condition (this assumes that installation will not be at saturation). The second limiting condition is at some time after construction where groundwaters have completely infiltrated the sealing materials. In this condition the pore volumes contain a liquid phase only, the saturated condition. A situation corresponding to the first condition results if the heat generated by the emplaced waste drives water away from the repository area, and causes drying, resulting again in unsaturated conditions.

For engineering purposes "soil strength" is adequately described by the Mohr-Coulomb Failure Theory (e.g. Mitchell, 1976):

$$\tau = c + \sigma \tan\phi \qquad (5.1)$$

where the shear stress at failure (τ) is a function of both a cohesion intercept (c), the normal stress (σ) on the failure plane and an internal friction angle (ϕ). Theoretical and experimental arguments show that the strength of a soil (c and ϕ) is generally not an inherent soil characteristic, but depends on a number of factors (Lambe, 1969), e.g. composition, drainage conditions, stress loading path, stress history of the soil, and strain rate (Mitchell, 1976), orientation of the planes of maximum shear stress, loading rate, specimen size, test type and apparatus (Parry and Wroth, 1981).

For strength testing purposes the bentonite has been considered to be a "soil". The testing provides data on the strength of both the bentonite plug and the plug-rock interface. Strength testing includes direct shear testing and swelling pressure testing.

5.5.2 Direct Shear Testing

The University of Arizona's Large-Scale Direct Shear machine (Wykeham-Farrance) is used to shear samples and the HP 7035B records horizontal load and displacements. The vertical loads (load normal to the shear failure surface) are applied using both the hydraulic loading frame, which supplies a minimum vertical load of approximately 1000 lbs, and "free weights" wich supply approximately 127 lbs, 211 lbs, and 338 lbs. A rate of 0.048 in/min is used in all testing.

American Colloid C/S Granular bentonite and distilled water has been used in all Direct Shear testing. Shear molds (to hold the samples while shearing) are made of quick-setting rock bolt cement (F-181 Bolt Anchor Sulfaset® produced by Randustrial® Corporation).

Direct shear testing includes four phases: 1) clay/clay unsaturated, 2) clay/basalt unsaturated, 3) clay/clay saturated, and 4) clay/basalt saturated. The clay/clay tests determine the shear strength of the bentonite clay, while the clay/basalt tests determine the shear strength of the bentonite clay in contact with a piece of Columbia Plateau basalt. The unsaturated tests refer to samples with pore volumes that contain both liquid and gas phases while the saturated tests refer to tests in which the pore volumes contain only a liquid phase.

Tables 5.4 and 5.5 contain summaries of peak and residual shear strength results.

The coefficient of variation, R^2, is an indicator of how well the data is approximated by the equation. An R^2 value near unity indicates a very good fit between the data and the equation. Tables 5.4 and 5.5 report R^2 values of 0.78 for clay/clay saturated to 0.99 for clay/basalt saturated. Overall, the coefficients of variation indicate a good linear approximation of the experimental data.

Table 5.4, Summary of Peak Shear Strengths, reveals that the clay/clay strength is greater than the clay/basalt strength for both saturated and unsaturated conditions. This implies that the clay/basalt interface would fail in shear before the clay plug itself. The unsaturated conditions produce greater friction angles than saturated conditions for both clay/clay and clay/basalt tests. This means that as water content and saturation level increase in a plug, the stress normal to a failure surface is less critical to the overall plug strength than in "drier" conditions. As saturation increases, the clay/basalt interface develops more adhesion while the clay/clay cohesion remains essentially unchanged.

Table 5.4 Peak Shear Strengths

Test	Unsaturated			Saturated		
	R^2	c (psi)	ϕ (degrees)	R^2	c (psi)	ϕ (degrees)
Clay/clay	0.89	13.7	24	0.78	13.5	24
Clay/basalt	0.94	0.4	18	0.92	7.9	6

Table 5.5 Residual Shear Strengths

Test	Unsaturated			Saturated		
	R^2	c (psi)	ϕ (degrees)	R^2	c (psi)	ϕ (degrees)
Clay/clay	0.97	1.8	30	0.82	4.4	15
Clay/basalt	0.93	0.6	19	0.99	3.3	10

NOTE: In Tables 5.5 and 5.6, the clay is American Colloid C/S Granular bentonite, and the basalt is from either the Grande Basalts or Frechman Springs of the Wanapom Basalts, Hanford, Washington.

A comparison between peak (Table 5.4) and residual (Table 5.5) results yields several general trends. First, upon shear failure, the cohesion (or adhesion) decreases in all cases except for the clay/basalt unsaturated where the adhesion remains essentially unchanged. The decrease would be expected as particle bonds (cementation, electrostatic, and primary valence) are stretched and ruptured (Mitchell, 1976, p. 319). This is important in plug strength considerations because plug "displacement" due to driving mechanisms will decrease the cohesion within the clay and the adhesion between the wall rock and plug. Second, the residual angles of friction increase 1^{o} to 6^{o} over the peak values. This may be due to experimental error introduced by lack of instrument sensitivity. However, if the clay saturations were less than 100%, the increase in friction angle may be explained by dissipation of pore air pressure and the effective stress concept.

Two interesting observations made during the direct shear testing:

(1) For unsaturated clay/clay testing, the shearing force compacts the plug until the peak shear strength is exceeded, at which point a planar failure surface develops. This failure mode resembles a "progressive" failure with portions of the plug shearing until a critical shear stress is reached and then the entire plug fails in shear.

(2) For saturated clay/clay testing, the plug does not produce a failure surface normal to the applied vertical load. The relative movement within the failed plug is approximately parallel to the applied vertical load. One slip plane corresponds closely to a layer produced by the compaction method. This failure mode is observed on all six saturated clay/clay plugs and indicates a complex shearing mechanism.

Five limits are recognized to the Direct Shear Testing:

(1) The direct shear machine does not put a "pure shear" force on the test samples. This conclusion is based on the observation that the top shear box tends to rotate or dip in the direction of shearing. The rotation or dipping indicates a vertical component to the shearing force, or a "shearing" component to the normal force.

(2) The clay/basalt tests use basalt surfaces cut with a diamond saw blade, producing a very smooth surface. Field borehole and shaft conditions may be different depending upon how the penetrations are produced. Therefore, the actual clay/basalt interface friction angle for a field installation may be higher than the one observed in laboratory testing.

(3) The "saturated" tests (both clay/clay and clay/basalt) produce saturations ranging from 88 to 124%. Saturations greater than 100% are theoretically impossible so the errors must be in laboratory measurements - possibly misreading a scale weight or variabililty in product properties (i.e. specific gravity). Saturations less than 100% tend to generate pore air pressures and negative pore water

pressures. The effect is that the "normal stress" may be increased greatly - particularly with negative pore water pressures. It is quite possible that "true" or actual saturations of 100% are impossible to attain, because as the saturating pressure (often 300 psi or more) is released, pore air which is dissolved in the pore fluid comes out of solution and lowers the saturation. To overcome the pore air dissolution phenomenom would require shearing the sample under the saturating pressure, which is not possible with the testing machine used here.

(4) The shear strength is a function of strain rate (Mitchell, 1976, p. 292). The faster the test, the higher the soil strength. A strain rate of 0.048 in/min is used. A slower rate would allow the dissipation of excess pore water pressures, but calculations reveal that a 4-inch diameter bentonite plug with a hydraulic conductivity, k, equal to 1×10^{-9} cm/sec would require roughly 50 days to reach 50% consolidation under a given stress increment. This indicates that a very slow strain rate would be required to insure that all excess pore pressures are dissipated.

(5) The direct shear tests give only "relative" strengths between the clay and basalt and <u>not</u> design quality parameters. Because the clay/basalt interface appears to have the lowest strength, additional strength tests should focus on "push-out" tests (Stormont and Daemen, 1983). Bentonite plugs could be compacted in drilled holes and pushed out while measuring displacements and forces. Additional study should also focus on the stress distribution in a vertically-loaded, laterally-confined plug; of particular interest is the stress normal to the plug wall interface.

5.5.3 Swelling Pressure Testing

Swelling pressure testing determines the swelling pressures generated by hydrating compacted bentonite clay plugs.

The swelling pressures generated by bentonites may prove a useful characteristic as air voids, rock fractures, and waste canister cracks could be filled in by the expanding bentonites (Pusch et al., 1982). Conversely, if the swelling pressure is too high, fractures and joints may propagate (e.g. Chapter 7, Chapter 9, Figure 9.3), which may have a deleterious effect on waste isolation and even on the stability of the waste repository. Montmorillonite (the predominant mineral in bentonites) has an unbalanced electronic charge in its crystal structure (Mitchell, 1976). The unbalanced charge can be satisfied by cations, hydrated cations and polar fluids (e.g. water). As water is adsorbed between successive "sheets" of montmorillonite crystals, the crystal lattices are separated from one another with a resulting expansion or swelling. This swelling (or dispersion) can be best explained by the diffuse double layer theory. The thickness of the double layer is directly proportional to the square root of both increasing dielectric constant and temperature, but inversely proportional to the square root of increasing cation concentration and cation valence. If water is the electrolyte, an increase in temperature results in a decrease in dielectric constant such that the double layer thickness is not greatly influenced. Other factors held constant, the cation concentration and valence control the double layer thickness. It is possible to reverse the swelling process and cause flocculation of clay particles by increasing cation valence and/or the pore water cation concentration.

The swelling pressure tests have been performed using the Soil Test FHA Volume Change meter. This device is essentially a frame with a displacement-reading dial gage attached to a proving ring. A bentonite sample is compacted in a circular, aluminum ring and loaded into the swell meter. Porous stones are placed on the top and bottom of the compacted bentonite. The proving ring (1000 lbs capacity) is placed in contact with the bentonite (through an aluminum seat) and adjusted. Distilled water is poured into a plastic container surrounding the bentonite/aluminum ring. Water is absorbed into the bentonite through holes in the aluminum ring and the porous stones.

Giuffre et al. (1981) indicate that the swelling pressure is a function of dry unit density, while Meyer and Howard (1983, p. 58) state that the swelling pressure of compacted shale materials shows little relation to initial density. Dry density is a function of "soil" type, compactive energy, and initial water content. American Colloid C/S Granular Bentonite has been used in all swelling pressure tests. An impact energy effort is used to compact the bentonite in the swell meter and to vary the dry density. The initial water content varies between 19 and 41%, which is 8-30% wetter than Harvard Miniature Mold results at Standard Proctor energy effort. The mix and pore water is either distilled water or 5000 ppm NaCl solution.

For fourteen tests, distilled water has been used to both mix the bentonite prior to compaction and to saturate the compacted bentonite during the test. For four tests the 5000 ppm NaCl solution has been used to both mix and to saturate the bentonite samples. For three tests distilled water has been used to mix the bentonite and the 5000 ppm NaCl solution to saturate the compacted bentonite during testing.

The bentonites mixed and saturated with the salt solution exhibit the highest swelling pressures. The bentonites mixed with distilled water and saturated with the salt solution exhibit the lowest swelling pressures, while the bentonites mixed and saturated with only distilled water exhibited slightly higher swelling pressures. This indicates that mixing the bentonite with an electrolyte solution will generate a higher swelling pressure.

The following recommendations are suggested for future swelling pressure testing:

1) Swelling pressure is a function of volumetric strain. The swelling meter used in the testing summarized here allows a 4% volumetric strain at a swelling pressure of 250 psi. According to the investigations by Kassif et al. (1969) on disturbed clays, at zero percent volumetric strain (i.e. no swelling) and 20% initial moisture content, swelling pressures could be 100% greater than swelling pressures generated at 4% volumetric strains. Meyer and Howard (1983,

p. 58) state that "as little as 1% axial strain in compacted pulverized shale model plugs (optimum water content) reduces the swelling pressure by about 50%." This suggests that bentonite plugs or seals that are completely constrained laterally and vertically may generate significantly higher swelling pressures than reported here.

2) Mitchell (1976, p. 240) indicates that swelling pressure is related to soil structure or fabric. Soils compacted dry of optimum generate more swelling potential than those compacted wet of optimum at the same dry density. This difference is attributed to differences in soil structure. Future tests should consider compacting dry of optimum to determine if any additional swelling pressure may be generated. Also, the effect of compactive effort (i.e. static, impact and dynamic) on swelling pressure should be investigated.

3) An interesting phenomenon was noticed when compaction was done near the swelling meter. A Standard Proctor Compaction sample was being prepared on a counter top near the swelling meter; as compaction proceeded, the lab technician noticed that the swelling pressure decreased. Subsequent investigation showed that the swelling pressure had decreased almost 7% from its peak value. The swelling test was allowed to continue, but the sample never re-swelled to its former peak pressure. The compactive effort probably produced vibrations that caused realignment of the clay particles such that settlement took place. This observed decrease in swelling pressure indicates that swelling pressures might prove sensitive to dynamic loading such as induced by earthquakes, blasting or heavy construction equipment. Future tests should investigate this phenomenon because a loss of swelling could jeopardize repository sealing integrity.

5.6 Summary Conclusions

The following points summarize the results of both experimental research on seven bentonite samples and a literature search:

1) Commercial bentonites exhibit a wide range of chemical compositions.

2) The following reference data have been determined:

a) Shrinkage Limit

b) Plastic Limit

c) Liquid Limit

d) Specific Gravity of Solids

e) Moisture Density Relations

Experimental results vary widely between the seven bentonites tested (Table 5.6). Experimental and published results vary significantly depending upon the adsorbed cation, mix water, curing time, temperature of testing, and test technician.

3) Falling head permeability tests have been performed on seven bentonites. The bentonites were compacted to a point slighly wet of

Table 5.6 Summary of Results of Reference Tests on Bentonite Samples

Company Product	Shrinking Limit Average (Stan. Dev.)	Plastic Limit Average (Stan. Dev.)	Liquid Limit Average	Specific Gravity Average (Stan. Dev.)	Standard Proctor Compaction lbs/ft^3 (Opt. Moist.)	Harvard Compaction lbs/ft^3 (Opt. Moist.)
American Colloid C/S Granular	26.04 (3.01)	33 (7.18)	392	2.72 (0.04)	95.20 (4.62%)	86.75 (11.21%)
Dresser Minerals Arrowhead	31.74 (3.66)	55 (5.71)	596	2.66 (0.06)	73.34 (13.32%)	66.77 (7.87%)
Federal Bentonite Akwa-Seal	19.14 (11.03)	41 (0.49)	693	2.82 (0.11)	73.55 (29.30%)	72.73 (8.42%)
Georgia Kaolin Hi Jell #1	15.68 (0.69)	37 (2.02)	340	2.66 (0.03)	79.27 (24.14%)	75.62 (25.68%)
Intl. Minerals & Chem. Rainbow Seal	20.65 (2.76)	54 (3.95)	263	2.73 (0.12)	74.42 (29.03%)	72.95 (10.08%)
Slope Indicator 1/2" Tablets	38.46 (3.92)	50 (3.16)	454	2.64 (0.02)	93.24 (11.0%)	91.73 (9.34%)
Whitaker, Clark & Daniels 149 Bentonite 325 Mesh	25.45 (17.25)	48 (2.54)	541	2.75 (0.04)	71.31 (32.95%)	68.94 (8.94%)

NOTE: Stan. Dev. = Standard Deviation; Opt. Moist. = Optimum Moisture optimum moisture content for the Standard Proctor Compaction test. Difficulty in saturating the bentonite was encountered. Hydraulic conductivities, K, were in the order of magnitude of 10^{-9} cm/sec.

4) Radial permeameter testing was performed on a volcanic tuff and basalt.

5) Radial permeameter tests proved that bentonite plugs compacted in the basalt cores are more permeable to water flow than the intact basalt. The hydraulic conductivity of the plugs varied from 10^{-9} to 10^{-11} cm/sec, depending upon the water injection pressure.

7) Direct shear testing was performed on compacted bentonite plugs and compacted bentonite juxtaposed with basalt. The compacted bentonite plugs yielded the highest peak and residual shear strength values (cohesion and angle of internal friction) under both saturated and unsaturated conditions.

8) Swelling pressures in excess of 250 psi were measured with a displacement reading swell meter; if the bentonite is confined to zero-volumetric strain, much higher swelling pressures are expected.

Bentonite is a material that deserves further examination as a possible construction material in a multi-component engineered barrier. The permeability of compacted bentonite approaches that of a very low permeability intact rock. In the actual repository environment where the in-situ rock contains naturally occurring joints, fissures, faults, bedding planes, etc., compacted bentonite seals may prove more efficient in limiting groundwater ingress and egress than the host rock. The shear strength of compacted bentonite is low compared to that of the majority of rocks. Therefore, bentonite seals should be used in conjunction with a stronger, stiffer bulkhead such as concrete or with sufficient "overburden" in the form of backfills, waste rock, etc., to prevent seal displacement initiated by high hydraulic heads. The swelling pressure generated by confined, compacted bentonite is sufficient to close cracks and air voids in a seal and if allowed to "free-swell" (i.e. no load on the free surface), bentonite could expand and fill cracks in waste canisters and also fractures and joints in the host rock. Careful study is necessary to insure that the swelling pressure generated by a volumetrically confined bentonite seal will not have a deleterious effect on waste isolation and the repository stability.

Suggestions for further research are:

1) Further laboratory tests need to be performed on bentonites using a water that is site-specific or at least representative of groundwater expected in a repository environment. Reference, permeability and strength testing that uses a water containing representative cations and anions will yield more realistic predictions of how a bentonite seal will function in the repository groundwater environment.

2) The temperature effects on bentonite properties need to be identified. Reference, permeability and strength testing should be

performed at the temperature extremes expected in the repository environment.

3) The permeability should be measured as a function of both dry density and compactive effort. Static, impact and dynamic compaction methods should be considered.

4) Flow rate tests should be performed on dry bentonite plugs to determine the time period necessary for bentonite to swell and seal the plug/wall rock interface and any cracks in the plug.

5) Swelling pressure measurements should be peformed for volumetrically confined, compacted plugs.

6) Swelling pressure may be an anistropic property and experiments should be made to determine the swelling pressure normal and perpendicular to compaction layers.

7) The relationship between swelling pressure and pore pressure is complex. A permeability test that measures swelling pressure and pore water pressure could provide insight into this problem.

8) Finally, quality control of bentonite is necessary due to the wide variance in chemical and engineering properties. Chemical analysis and x-ray diffraction of bentonite samples should be investigated as a possible tool for quality control.

5.7 References

American Geological Institute, 1976, Dictionary of Geological Terms, Anchor Books, Garden City, New York.

Brown, E.T., ed., 1981, Rock Characterization, Testing and Monitoring: ISRM Suggested Methods, Pergamon Press, London, 212 pp.

Claiborne, H.C., 1982, "The Efficacy of Backfilling and Other Engineered Barriers in a Radioactive Waste Repository in Salt," ORNL/TM-8372, 32 + iii pp., Oak Ridge National Laboratory, Oak Ridge, Tennessee, September.

Ellison, R.D., D.E. Stephenson, and D.K. Shukla, 1981, "Sealing of Shafts, Tunnels, and Boreholes for Waste Repositories," Ch. 77, pp. 1251-68, Vol. 2, Proceedings Rapid Excavation and Tunneling Conference, San Francisco, California, May 1981. Published by Society of Mining Engineers of AIME, New York, 1981.

Fernandez, R., C. McGowen, E. Nolan, R. Moray, and A. Palty, 1976, "Borehole Plugging by Compaction Process," Y/OWI/Sub-7087/1, Charles Stark Draper Laboratory, Inc., Cambridge, Massachusetts, 195 pp. Prepared for Office of Nuclear Waste Isolation, Union Carbide Corporation, Nuclear Division, Oak Ridge, Tennessee.

Fyfe, W.F., V. Babuska, N.J. Price, E. Schmid, C.F. Tsang, S. Uyeda, and B. Velde, 1984, "The Geology of Nuclear Waste Disposal," Nature, Vol. 310, pp. 537-540, August 16.

Giuffre, M.S., C.M. Koplik, R.L. Plum, and R. Talbot, 1979, "Information Base for Waste Repository Design," Volume 5 "Decommissioning of Underground Facilities," prepared by Analytic Sciences Corporation, 6 Jacob Way, Reading, Mass., 01867, for U.S. Nuclear Regulatory Commission, Division of Waste Management, NUREG/CR-0495.

Gureghian, A.B., L.A. Scott, and G.E. Raines, 1983, "Performance Assessment of a Shaft Seals System in a HLW Repository in the Gibson Dome Area," Technical Report ONWI-494, Office of Nuclear Waste Isolation, Battelle Memorial Institute, Columbus, Ohio.

Kassiff, G., et al., 1969, "Pavements on Expansive Clays," Jerusalem Academic Press, Jerusalem. Results reported in Blight, G.E., 1980, "The Mechanics of Unsaturated Soils," notes used a series of lectures delivered as part of course 270 C at the University of California, Berkeley, May 1980.

Kelsall, P.C., W.E. Coons, and D. Meyers, 1983, "Repository Sealing Program Plan: Repository in Salt," Technical Report ONWI-414, prepared by D'Appolonia Consulting Engineers, Inc., for the Office of Nuclear Waste Isolation, Battelle Memorial Institute, Columbus, Ohio.

Koplik, C., David L. Pentz, and R. Talbot, 1979, "Information Base for Waste Repository Design, Vol. 1: Borehole and Shaft Sealing," NUREG/CR-0495 Vol. I, prepared for U.S. Nuclear Regulatory Commission, Division of Waste Management, Office of Nuclear Material Safety and Safeguards, by The Analytical Sciences Corporation, Reading, Massachusetts, February.

Lambe, W.T. and R.V. Whitman, 1969, Soil Mechanics, John Wiley and Sons, New York, 453 pp.

Martin, R.T., 1975, "Feasibility of Sealing Boreholes with Compacted Natural Earthen Material," ORNL/Sub-3960/2, Oak Ridge National Laboratory, Oak Ridge, Tennessee.

Meyer, D. and J.J. Howard, eds., 1983, "Evaluation of Clays and Clay Minerals for Application to Repository Sealing," ONWI-486, prepared by D'Appolonia Consulting Engineers, Inc., and Material Research Laboratory, The Pennsylvania State University, for Office of Nuclear Waste Isolation, Battelle Memorial Institute, Columbus, Ohio.

Mitchell, James K., 1976, Fundamentals of Soil Behavior, John Wiley and Sons, Inc., New York.

Parry, R.H.G. and C.P. Wroth, 1981, "Shear Stress-Strain Properties of Soft Clay," Ch. 4, pp. 311-364 of Soft Clay Engineering, E.W.

Brand and R.P. Brenner, eds., Elsevier Scientific Publishing Co., Amsterdam.

Pusch, R., 1983, "Borehole Sealing for Underground Waste Storage," Journal of Geotechnical Engineering, Vol. 109, No. 1, pp. 113-119, ASCE, January.

Pusch, R., T. Eriksen, and A. Jacobsen, 1982, "Ion/Water Migration Phenomena in Dense Bentonites," in Scientific Basis for Nuclear Waste Management V, Materials Research Society Symposia Proceedings, Vol. 11, pp. 649-659.

Sawyer, W.D. and J.J.K. Daemen, 1985, "Experimental Assessment of Bentonite Borehole Sealing Performance," Topical Report to the U.S. Nuclear Regulatory Commission, Division of Health, Siting and Waste Management, Contract No. NRC-04-78-271, by the Department. of Mining and Geological Engineering, University of Arizona, Tucson.

Singh, S.K., 1982, "Chemical, Physical, and Engineering Characterization of Candidate Backfill Clays and Clay Admixtures for a Nuclear Waste Repository - Part I," in Scientific Basis for Nuclear Waste Management V, Materials Research Society Symposia Proceedings, Vol. 6, pp. 413-433.

Smith, M.J., G.J. Anttonen, G.S. Barney, W.E. Coons, F.N. Hodges, R.G. Johnston, J.D. Kaser, R.M. Manabe, S.C. McCarel, E.L. Moore, A.F. Noonan, J.E. O'Rourke, W.W. Schulz, C.L. Taylor, B.H. Wood, and M.I. Wood, 1980, "Engineered Barrier Development for a Nuclear Waste Repository in Basalt: An Integration of Current Knowledge," RHO-BWI-ST-7, Rockwell International, Richland, Washington, May.

South, D.L., 1980, "Borehole Sealing with Clay, Part A," Topical Report to the U.S. Nuclear Regulatory Commission, on Contract NRC-04-78-271, by Department of Mining and Geological Engineering, University of Arizona, Tucson, March.

Stormont, J.C. and J.J.K. Daemen, 1983, "Axial Strength of Cement Borehole Plugs in Granite and Basalt," NUREG/CR-3594, Topical Report on Rock Mass Sealing, prepared for the Division of Health, Siting and Waste Management, U.S. Nuclear Regulatory Commission, by the Department of Mining and Geological Engineering, University of Arizona, Tucson.

U.S. Department of Energy, 1982, "NWTS Program Criteria for Mined Geologic Disposal of Nuclear Waste Repository Performance and Development Criteria," DOE/NWTS-33(3), Office of NWTS Integration, Battelle Memorial Institute, Columbus, Ohio, July, Public Draft.

Vennard, J.K. and R.L. Street, 1975, Elementary Fluid Mechanics, John Wiley and Sons, Inc., New York, 740 pp.

CHAPTER SIX

EFFECT OF TEMPERATURE ON CEMENT PLUG SEALING PERFORMANCE

6.1 Introduction

Testing the influence of temperatures above room temperature (up to 95°C) has been initiated. For the present series of experiments the temperature range has been selected to simulate temperatures up to a distance from the actual waste (distance determined by waste age, configuration, etc.) where steam generation is unlikely, as steam is likely to induce significant additional effects. Results are presented from scouting experiments on one dried-out cement sample and on two saturated plugs.

6.2 Apparatus

The laboratory set-up for the flow rate testing of cement plugs consists of 1) a nitrogen tank, 2) a gas-over-water pressure intensifier, 3) a flowmeter, 4) a cement permeameter, 5) the water collecting unit, 6) the heating unit, 7) temperature sensors, 8) a pressure gage, and 9) valves and connecting tubing (stainless steel 304, 1/8" O.D.). This arrangement is illustrated in Figure 6.1.

This set-up has been expanded into two independent systems by replacing the pressure intensifier with two accumulators and the addition of another cement permeameter. This has facilitated the study of two cement plugs at ambient temperature (22 ± 2°C) and at elevated temperatures (above room temperature and less than 100°C (212°F)). Figures 6.2 and 6.3, respectively, show these set-ups. Different components of these systems are as follows:

6.2.1 Water Pressure Intensifier

Figure 6.4 illustrates the gas-over-water pressure intensifier. This apparatus provides a constant water line pressure to the system. It has a capacity of about 500 cc, and a pressure ratio of 4 to 1. Maximum output pressure is approximately 6900 kPa (1,000 psi).

6.2.2 Flowmeter

The Gilmont flowmeter is marketed by Cole-Parmer Co., Oak Park, Illinois. The principle of the flowmeter is based on Stokes' Law. The device can withstand a maximum pressure of 4.14 MPa (600 psi), and its flowrate is between 0.001 - 1.0 cc/min for water. (It can also be used to measure air flow.) This flowmeter has been used successfully for the inflow measurements of dried plugs. Fresh plugs, i.e. plugs that are maintained wet throughout the pouring, curing and testing period, exhibit such low permeabilities that the flowmeter has not been able to measure flows. A cutaway section of this apparatus is shown in Figure 6.5.

Schematic of System for Cement Permeameter

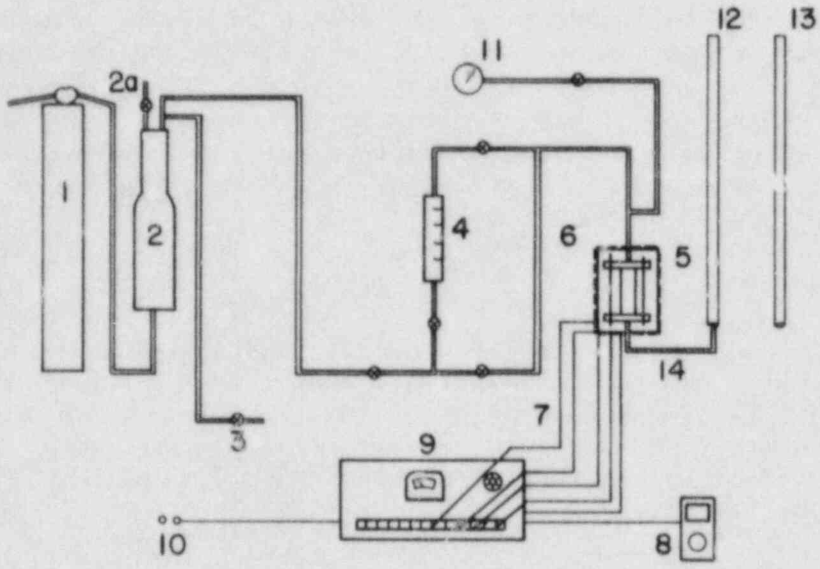

1. Nitrogen tank
2. Intensifier(gas/water)
2a. Dial gauge
3. Inlet valve
4. Flowmeter
5. Cement permeameter
6. Heating mantle
7. Wires
8. Hand-held thermometer
9. Temperature controller
10. Outlet
11. Pressure gauge
12. Read-out burette
13. Evaporation/reference burette (closed)
14. Tygon hose

Figure 6.1 Laboratory set up for flow testing of cement plugs using a pressure intesifier.

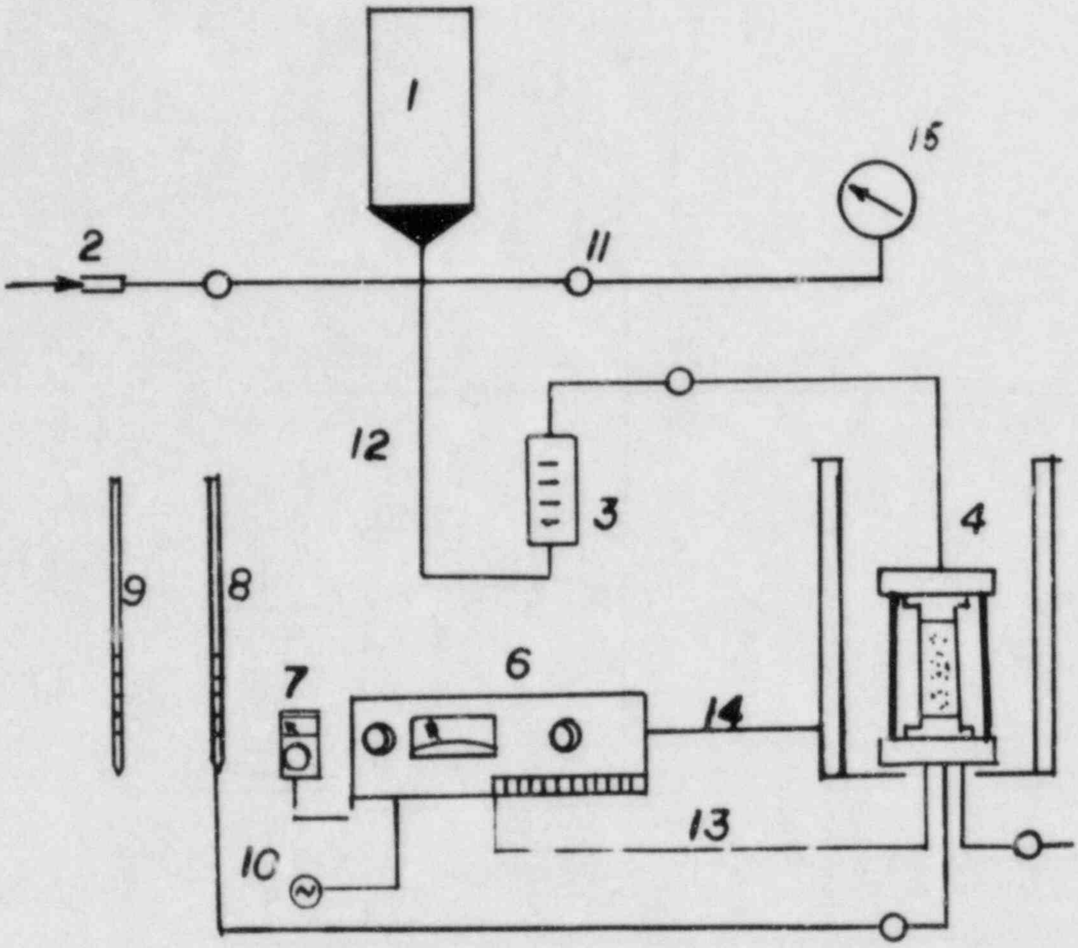

1. Bladder accumulator
2. Intake port (quick connect fitting)
3. Gilmont flowmeter
4. Cement permeameter
5. Heating mantle
6. Temperature controller
7. Digital thermometer
8. Water collecting pipet
9. Reference pipet
10. Electrical outlet
11. Valves
12. Stainless steel tubing
13. Thermocouple wires
14. Wire
15. Gage

Figure 6.2 Laboratory set-up for flowrate testing of cement at elevated temperatures.

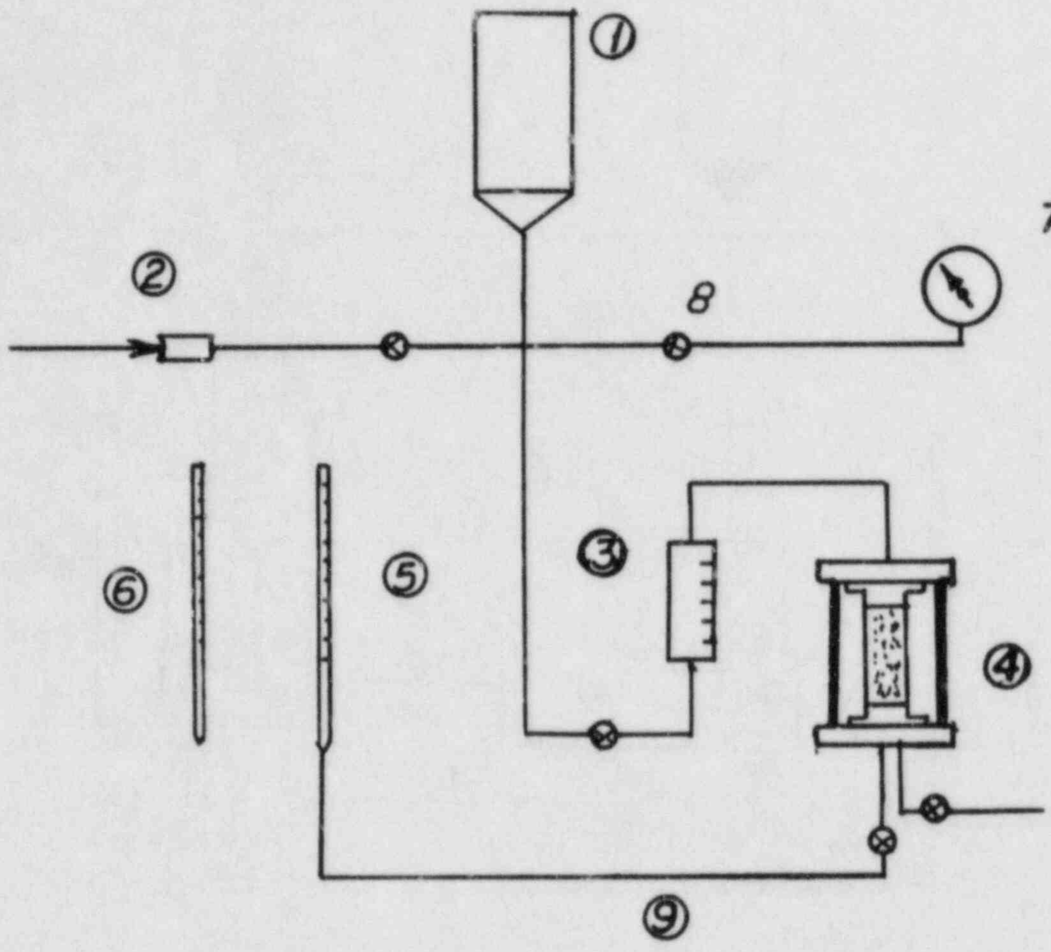

1. Bladder accumulator
2. Intake port
3. Gilmont flowmeter
4. Cement permeameter
5. Water collecting pipet
6. Reference pipet
7. Pressure gage
8. Valves
9. Stainless steel tubing

Figure 6.3 Laboratory set-up for flowrate testing of cement at ambient temperatures.

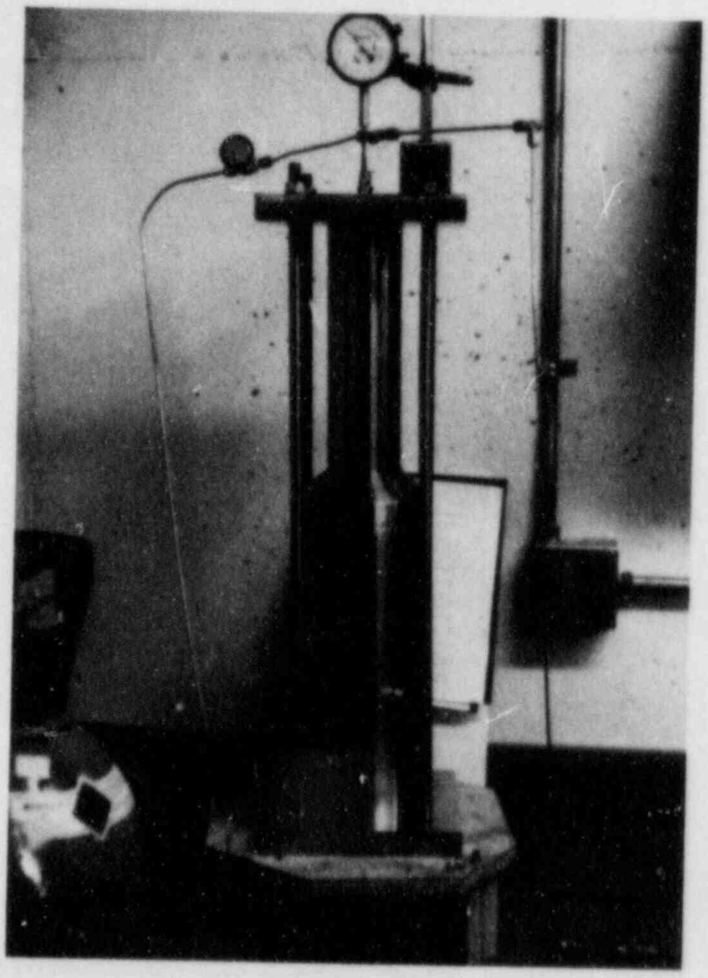

Figure 6.4 Gas-over-water pressure intensifier.

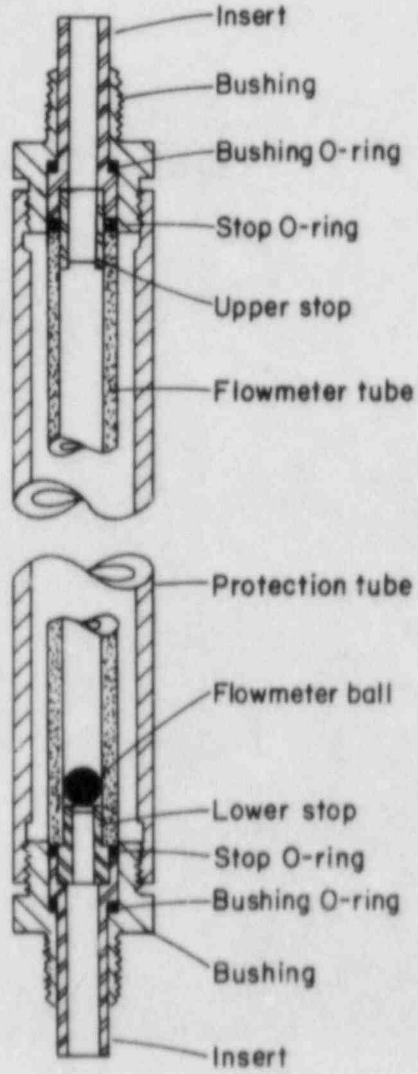

Figure 6.5 Cutaway section of a typical Gilmont flowmeter (Cole-Parmer).

6.2.3 Cement Permeameter

A cement permeameter is shown in Figures 6.6, 6.7 and 6.8. It has been built at the Instrument Shop at the University of Arizona. The permeameter is built from stainless steel (ss. 304), except for the cement pipe, which is either a mild steel or a stainless steel (interchangeable).

This cement permeameter consists of 1) the upper and lower plates, 2) three tightening rods, 3) six nuts, 4) the upper and lower O-rings, 5) four thermocouple fittings, 6) a stainless steel or mild steel cement pipe (chamber), 7) the water injecting port, 8) the water collecting port, and 9) main and auxiliary shut-off valves.

Tightening the rods (Figures 6.6 and 6.8) seals the top and bottom by means of the O-ring. Water is injected at the top and collected at the bottom (Figure 6.9). One can study the effect of gravity forces on flow by turning the permeameter upside down and injecting the water from the bottom.

The main and auxiliary valves facilitate filling and deaerating of the water in the collecting port. Thermocouple fittings are used for 1/16" thermocouple probes.

6.2.4 Heating Unit

The heating unit consists of a heating mantle, a temperature controller, and a digital thermometer. The heating mantle (Figure 6.10) is a hollow double-walled cylinder designed to hold a sample up to about 16 cm (6 in) in diameter and 30 cm (12 in) long. Heating elements and insulation are placed between the inner and outer walls of the unit. After the cement permeameter is loaded, the water injecting tube and outflow hoses are connected through the holes in the top cap and in the base, respectively. The heating mantle is monitored directly by the temperature controller.

The temperature controller consists of a solid state relay, a temperature setting knob, a channel knob to switch channels, a dial-type thermometer, and twenty channels for thermocouple connections (Figure 6.11). The digital thermometer (Figure 6.12) is connected to the temperature controller and can read the temperature of various thermocouples in tenths of a degree (°C or °F).

6.2.5 Water Collecting Units

A pipet is used to measure the outflow through the plug. The bottom reservoir (collecting port) of the cement permeameter is initially filled with water and connected to the measuring pipet by a tygon tube. In order to eliminate any water head that might result from the water rise, the collecting pipets have been installed horizontally. Figure 6.13 illustrates the original set-up (with vertical pipet) for the outflow end of the cement permeameter. An identical pipet is used to evaluate the rate of evaporation in the laboratory.

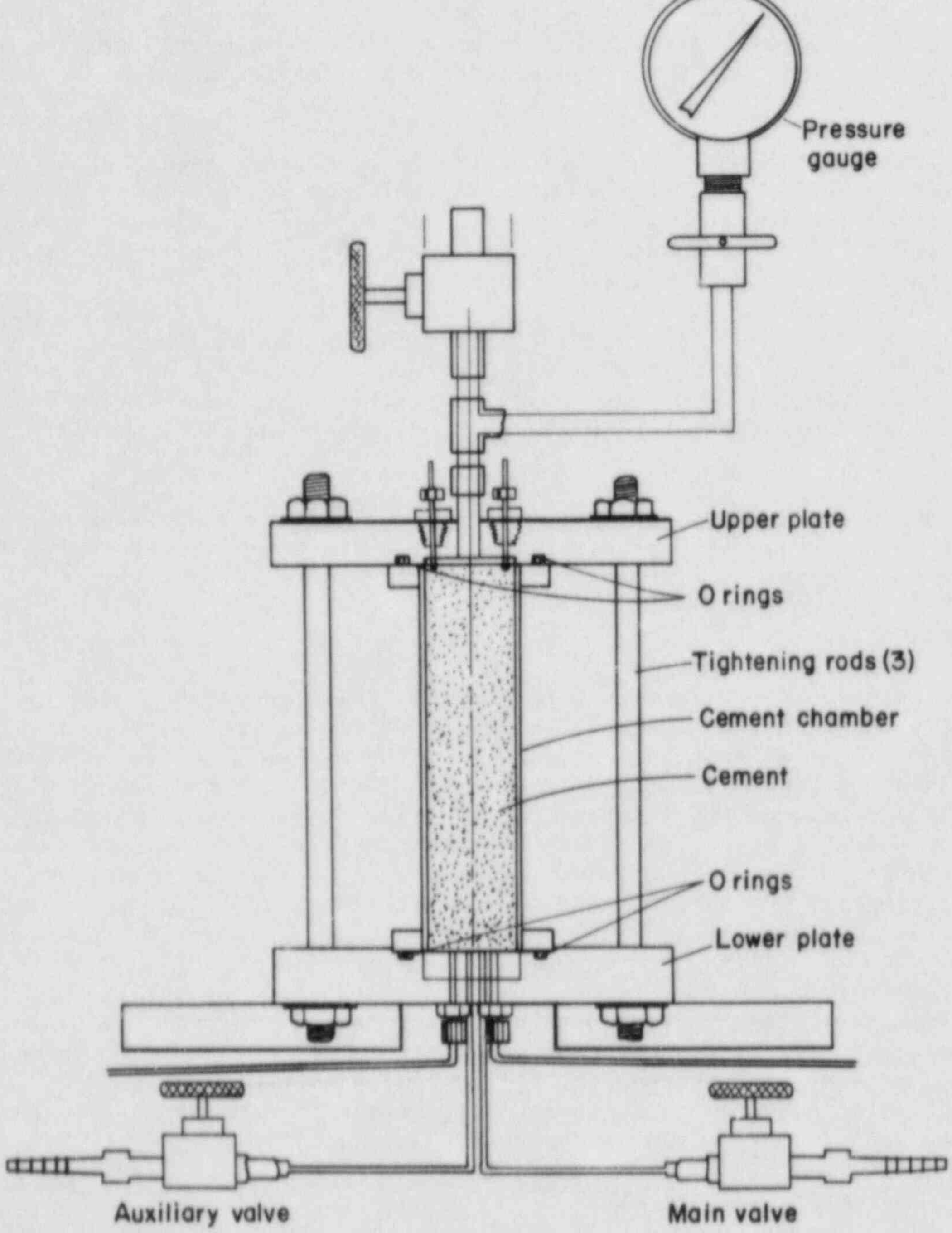

Figure 6.6 Cross-sectional view of a typical cement permeameter.

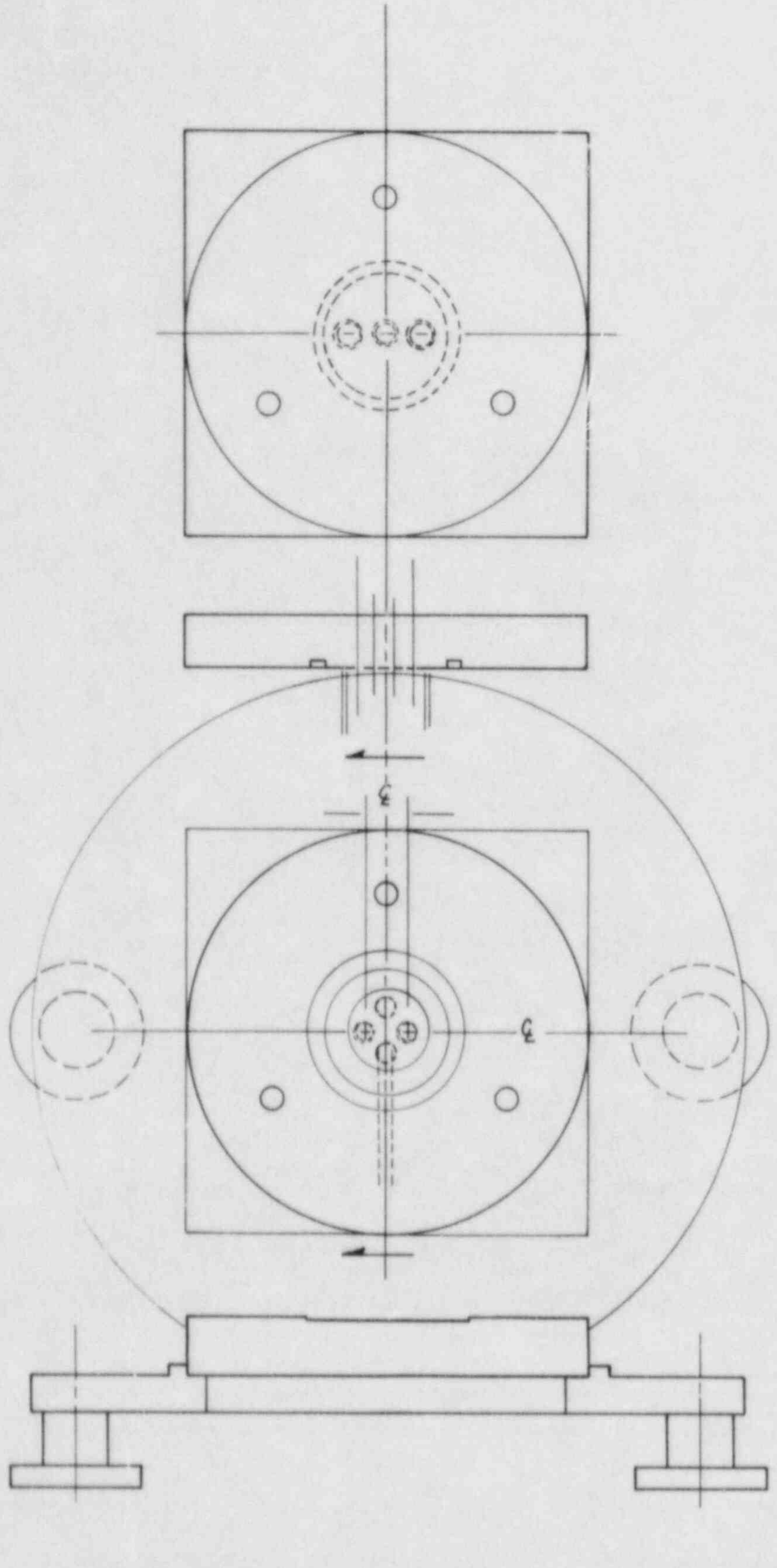

Figure 6.7 Top and bottom views of cement permeameter.

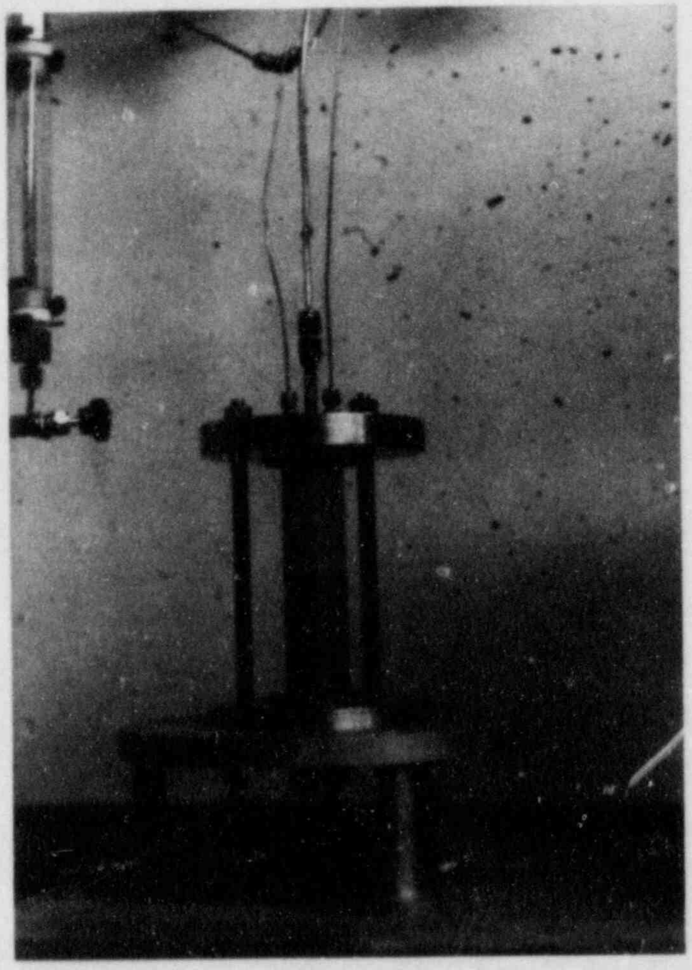

Figure 6.8. Cement permeameter.

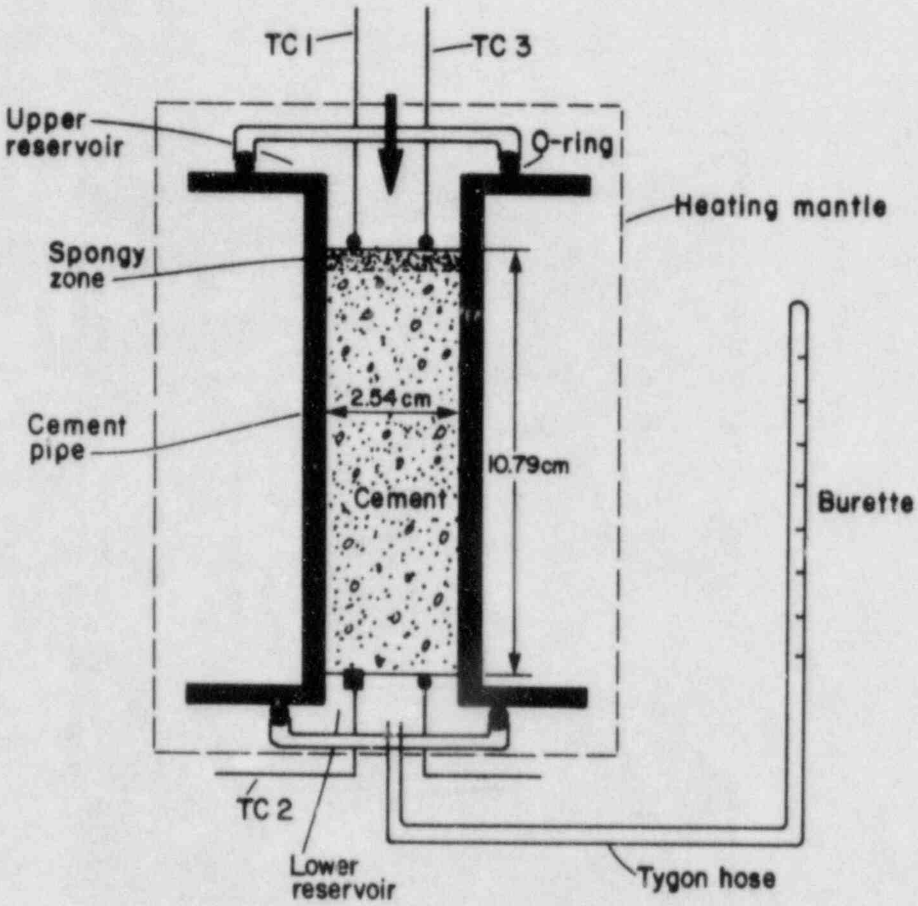

Figure 6.9 Water flow through the cement plug in the cement permeameter pipe.

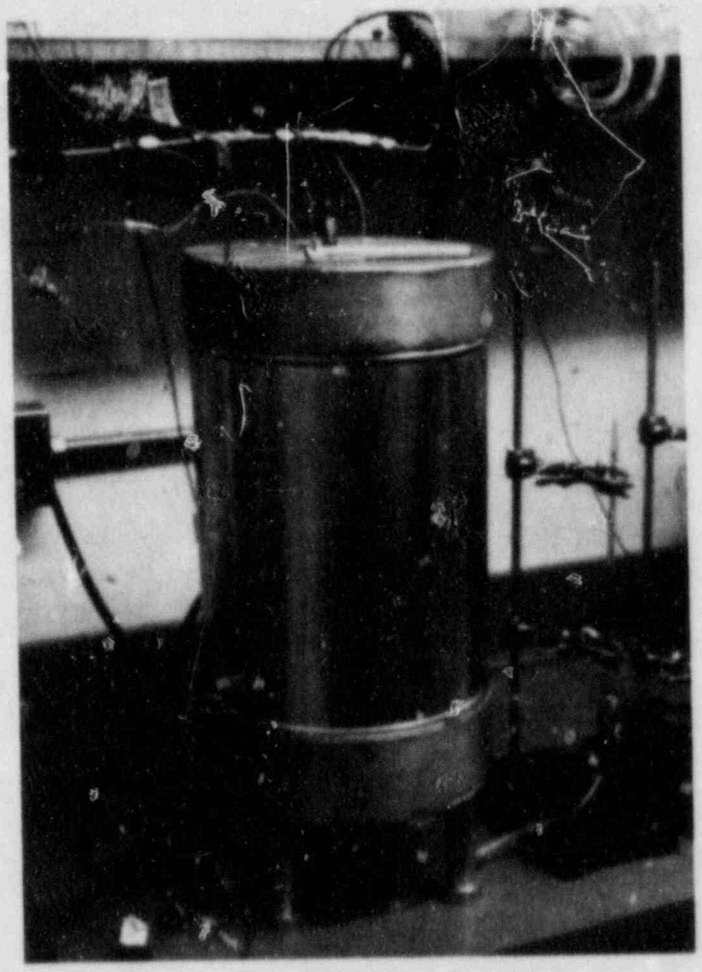

Figure 6.10 Heating mantle for cement permeameter.

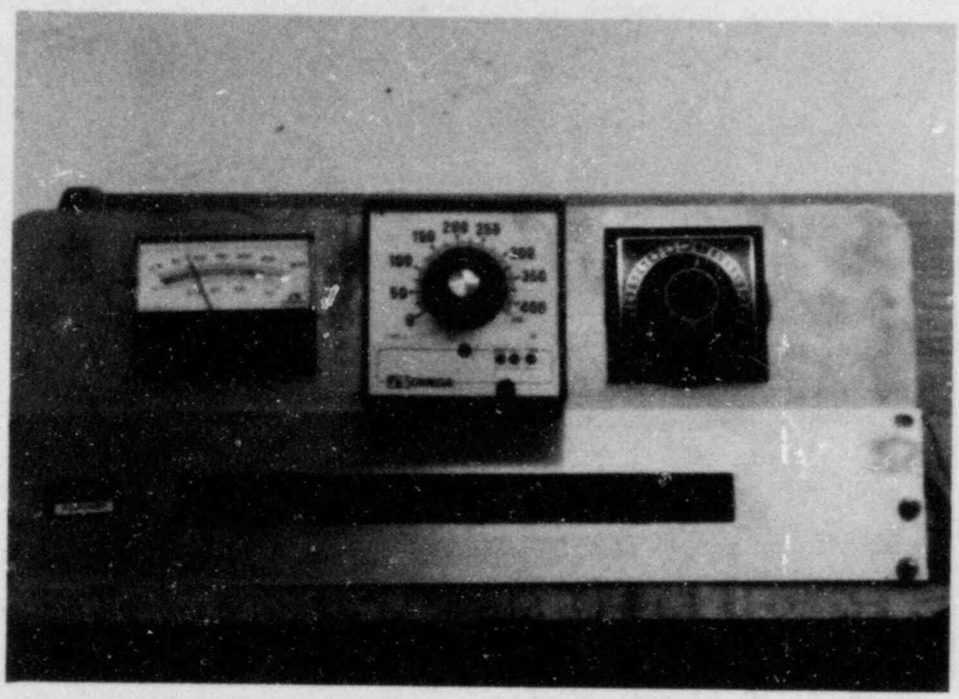

Figure 6.11 Temperature controller (Omega).

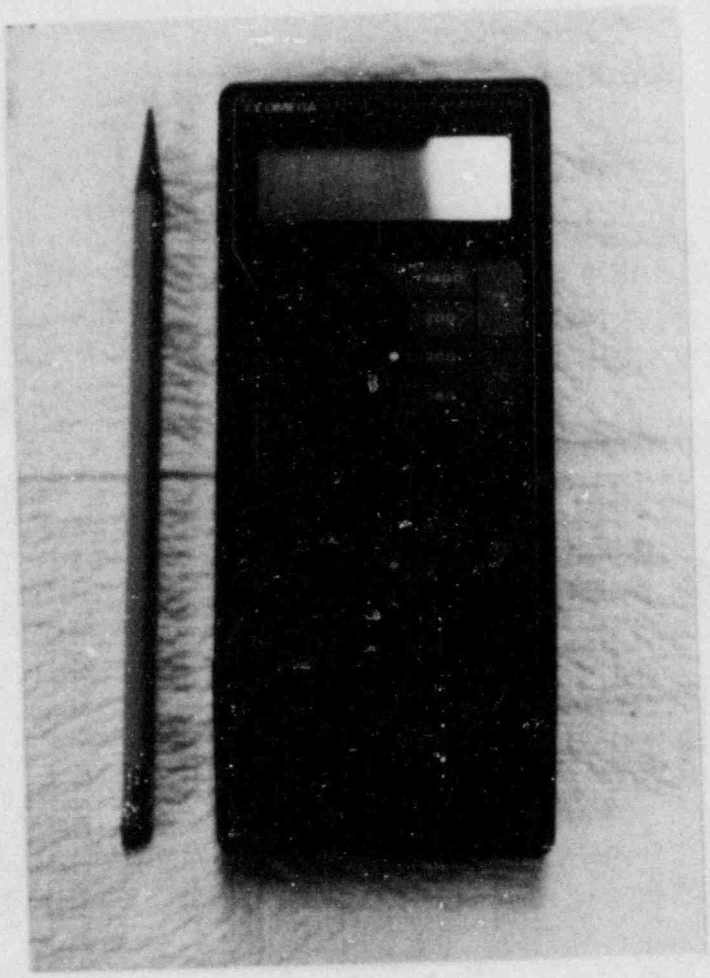

Figure 6.12 Digital thermometer (Omega Type JTC, Omega Engineering Co., Samford Connecticut).

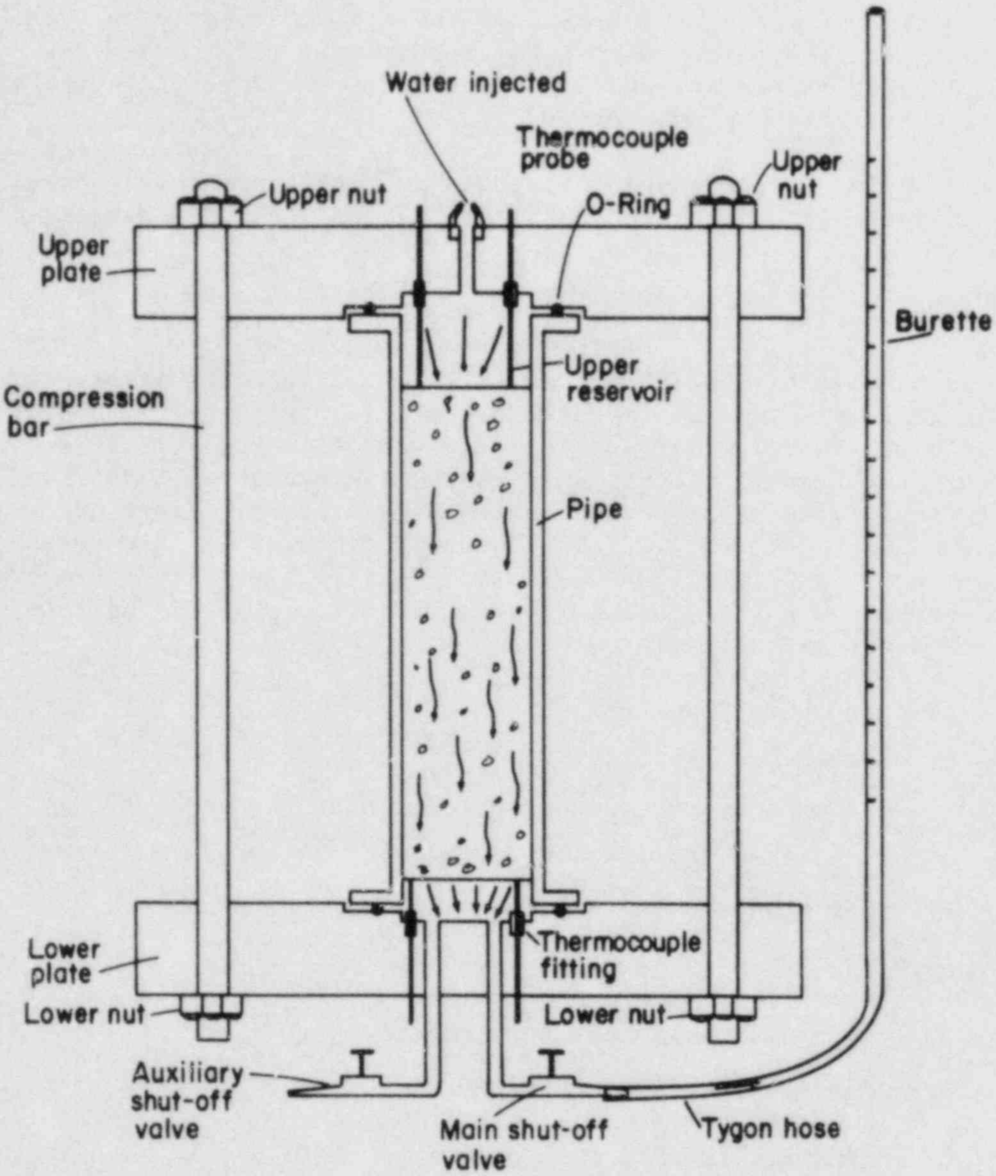

Figure 6.13 Water collecting mechanism of the flow testing with a cement permeameter.

6.2.6 Temperature Sensors

Iron/constantan (type J) thermocouple probes, manufactured by Omega Engineering Co., are used. They are protected by a stainless steel sheath against wear and corrosion. The tips of the probes must be in contact with the points whose temperatures are to be measured. Four thermocouple probes are usually installed to measure the temperature at the top and bottom of the plugs.

Thermocouple wires connect the probes to the temperature controller. The compatibility of thermocouple probes and wires is essential (both are type J).

6.2.7 Accumulator

Figure 6.14 is a cutaway diagram of the bladder accumulator. A bladder, which is located inside the accumulator, is precharged with nitrogen gas through the charging valve. The accumulator is then filled with water through the hydraulic port. The bladder accumulators being used are "Kwik-Kap" type, manufactured by EMG Accumulators. These accumulators can hold up to 473 cc (1 pint) of water. The maximum pressure recommended is 20 MPa (3000 psi) at 93°C (200°F). Bladder accumulators have performed satisfactorily. They have the following advantages over the pressure intensifier:

a) highly mobile

b) better availability

c) no need for continuous usage of nitrogen tank

d) no stick-slip, frequently observed in pressure intensifiers

e) very economical.

The drawbacks of these devices are:

a) rapid discharge when experiencing high flowrates

b) no direct measurement of water volume discharged.

6.3 Experimental Procedure

The procedure to load the cement permeamter is as follows:

(1) open all nuts at the upper plate of the permeameter.

(2) Remove the upper plate (watch for upper O-ring).

(3) Remove the cement pipe (stainless steel jacket).

(4) Cure the cement in the chamber.

(5) Place the pipe back in its place.

(6) Pass the tightening bars through the holes.

(7) Fasten the nuts on top.

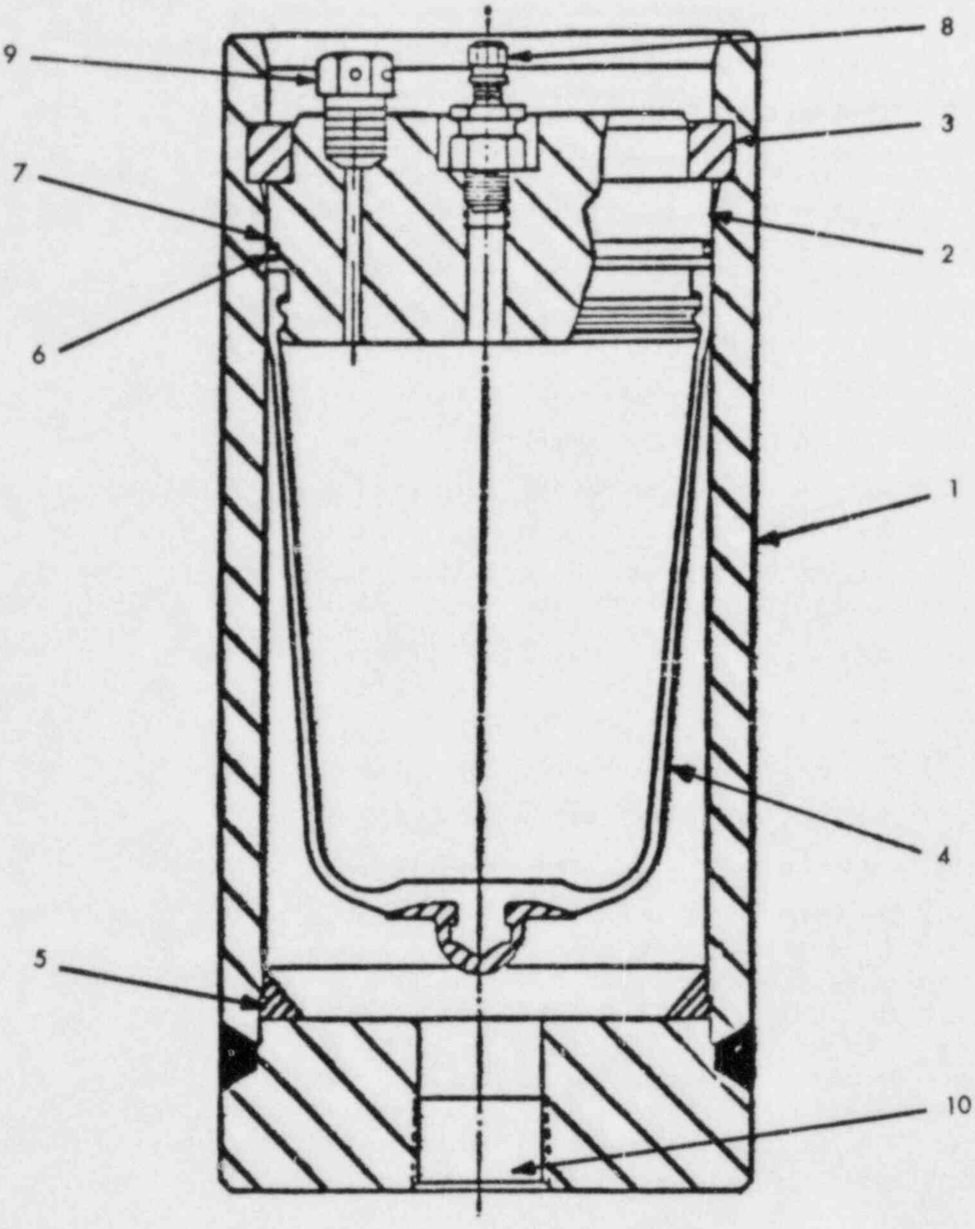

Figure 6.14 Cutaway view of the hydraulic accumulator.

1 - Housing assembly
2 - Cap
3 - Lockring set
4 - Bladder assembly
5 - Grommet
6 - O-ring
7 - Back-up
8 - Charging valve
9 - Burst disc
10 - Hydraulic port

(from EMG Accumulators, Inc., 1982)

(8) Pass the thermocouple probes through their fittings.

(9) Tighten the fittings.

The procedure to fill the lower reservoir of the cement permeameter with water is (either valve at the lower part of the permeameter can be used as the main valve):

(1) connect the main valve to a measuring pipet by a hose (transparent, e.g. Tygon).

(2) connect the vacuum line to the other side of the pipet.

(3) Open both main and auxiliary valves.

(4) Connect the Ruska manual injection pump to the auxiliary valve and open it.

(5) Pump water through the auxiliary valve into the lower reservoir.

(6) When pipet is half-way full and there are no air bubbles throughout the Tygon hose or burrette, disconnect the vacuum hose from the top of the burette.

(7) Pump more water into the lower reservoir with the Ruska pump.

(8) Shut off the auxiliary valve.

(9) Remove enough water from the pipet to calibrate.

(10) Connect the permeameter to the rest of the system (Figure 6.2).

After the cement permeameter is assembled into the system, the intensifier is filled with water.

Once the cement permeameter is loaded and assembled into the system, the test can be started. Figure 6.15 is a general schematic of the system. The heating unit is used only in studies involving temperature applications.

6.4 Permeameter Tests

Cement System 1, provided by Dowell, is used for the plug material. This system is composed of Ideal Type A Portland Cement (from Tijeras Canyon, New Mexico), 50% distilled water, 10% D53 (an expansive agent), and 1% D65 (a dispersant). All percentages are weight percent with respect to cement. Mixing is performed according to American Petroleum Institute Specifications, API Standard No. RP-10B (American Petroleum Institute, 1977).

Two types of plug curing have been followed: 1) dry (SC-1), and 2) underwater (saturated or fresh). Fresh plugs have been kept underwater and are thought to be saturated. Both types of plugs are cured in steel pipes (chamber) of the cement permeameters for at least 8 days at ambient temperatures (22 ± 2°C or 72 ± 6°F) (Figure 6.16).

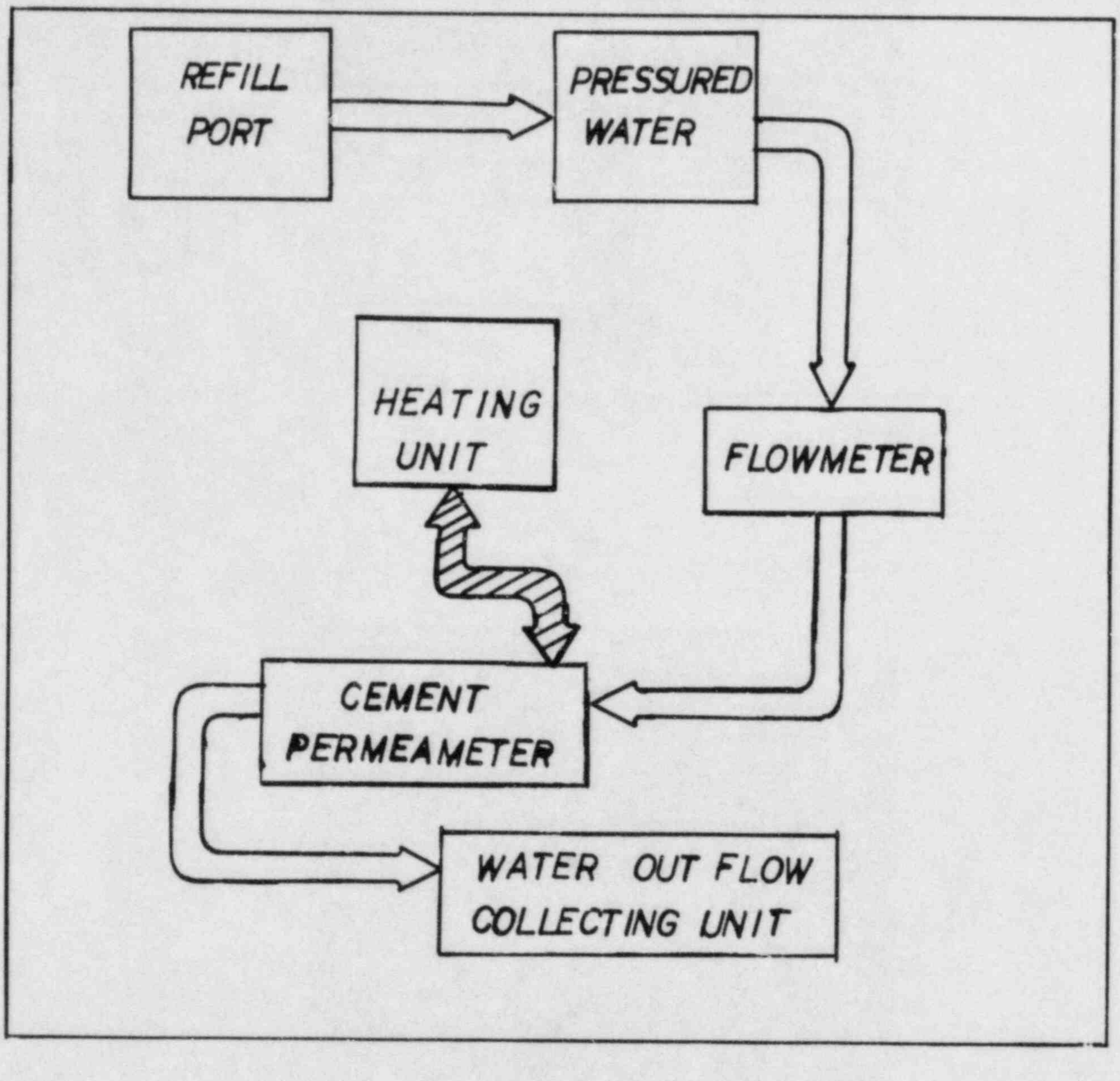

Figure 6.15 Schematic of flowmeter testing of cement plugs.

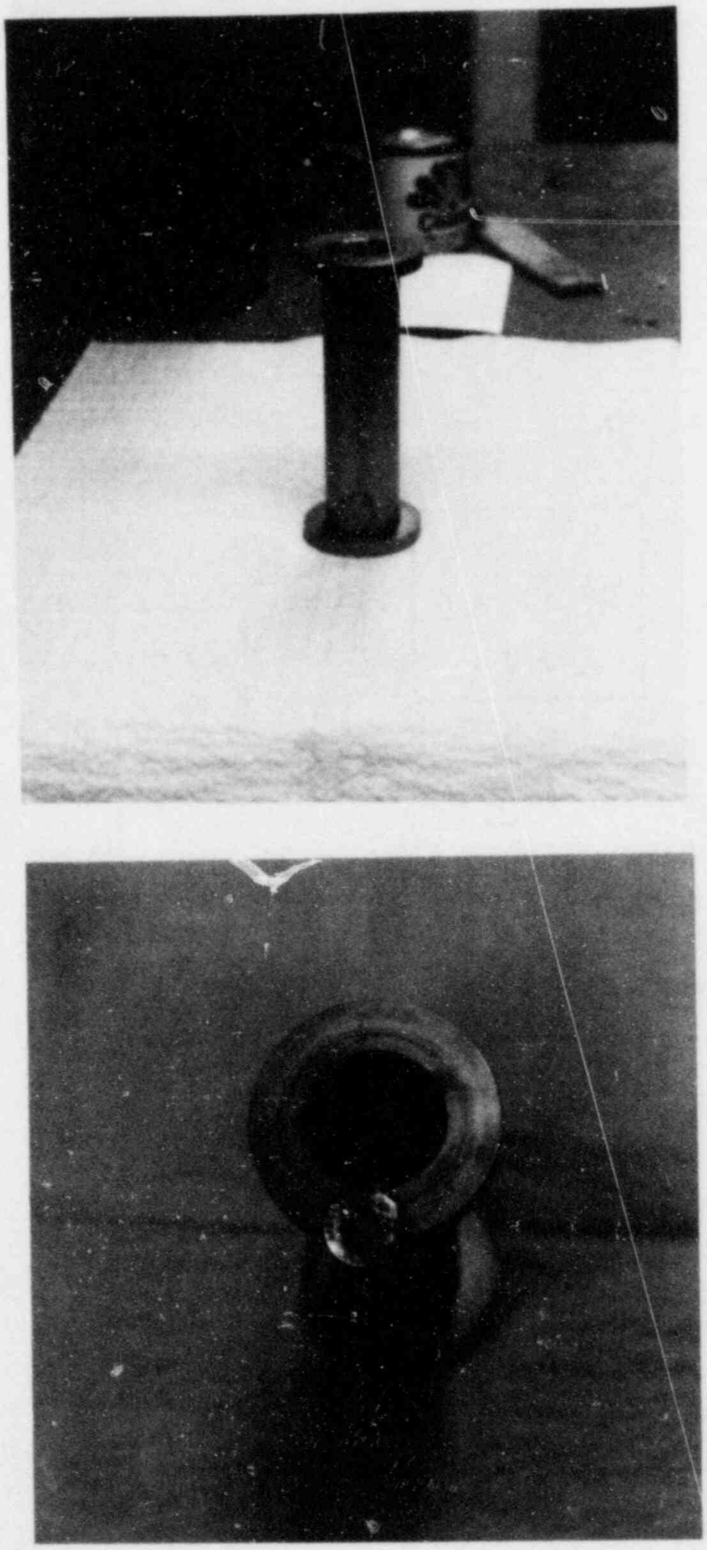

Figure 6.16 Permeameter pipe with cement curing inside.

6.4.1 Sample SC-1

Cement was cured dry for 8 days at ambient temperatures. The plug was 2.54 cm (1 in) in diameter and 10.97 cm (4.3 in) long. The spongy zone on the top was about 2 mm thick and was not ground away. The experiment was performed in two phases: 1) at ambient temperatures and 2) at temperatures of 40-55°C (104-131°F). The first phase took 9 days. The second phase had to be stopped after a day because of complications, such as excessive temperature gradients at the top and bottom of the plug (over 10°C or 18°F) and leakage in the water collecting unit.

6.4.2 Sample SC-2

This sample had been cured underwater for 8 days at ambient temperatures before testing started. The plug is 2.54 cm (1 in) in diameter and 10.67 cm (4.2 in) long. Laitance has not been ground off. This plug has been studied since November 15, 1983. It has first undergone flowrate testing at ambient temperatures and then at elevated temperatures (less than 100°C or 212°F). Table 6.1 illustrates the tests this plug has undergone to date.

6.4.3 Sample SC-3

Sample SC-3 was set on February 16, 1984. The curing period took 9 days underwater. The plug is 2.54 cm (1 in) in diameter and 9.94 cm (3.9 in) long. So far, all the tests have been conducted at room temperature. Table 6.2 illustrates the tests conducted. The laitance has not been removed. This plug is the first one on which injected water flows against the gravitational forces (water is being injected from the bottom and collected at the top).

6.5 Results

Two types of curve fitting have been conducted: 1) linear regression for the best fit-line, and 2) linear regression forcing the fit-line to pass through the origin. All figures with plots of outflow volume vs. time are of the first kind. This type of modeling may not work near the origin. The meaning of such a line is that at the time zero, there is an outflow volume equal to B cc ($V = Qt + B$, where V = outflow volume, Q = flowrate, t = time, and B = constant $\neq 0$). Theoretically and physically this is not possible.

The hydraulic conductivity is calculated as follows (Davis and Dewiest, 1966, Ch. 6):

$$K = \frac{QL}{A\Delta H} = \frac{VL}{A(\Delta H)t}$$

where K = cement hydraulic conductivity (cm/min)

Q = flowrate through the plug (cc/min)

Table 6.1 Summary of Flowrate Testing on Plug SC-2

Test No.	Temperature °C (°F)	Injecting Pressure MPa (psi)	Test Duration (hrs)
1	22 ± 2 (72 ± 3.6)	0.41 - 0.55 (60 - 80)	265
2	22 ± 2 (72 ± 3.6)	0.66 - 0.69 (95 - 100)	320
3	49 - 55 (120 - 131)	0.75 (108)	388
4	40 - 43 (104 - 109)	1.15 (167)	171
5	40 - 43 (104 - 109)	3.35 (486)	293
6	49 - 50 (120 - 122)	2.0 (290)	716
7	57 - 58.5 (134 - 137)	2.0 (290)	842
8	71.4 ± 0.5 (160 - 0.9)	2.0 (290)	136
9	83 - 84.5 (181 - 184)	2.0 (290)	130

Table 6.2 Summary of Flowrate Testing on Plug SC-3

Test No.	Temperature °C (°F)	Injecting Pressure MPa (psi)	Test Duration (hrs)
1	22 ± 2 (72 ± 3.6)	2.0 (290)	716
2*	22 ± 2 (72 ± 3.6)	2.0 (290)	288

*Test with water flow against the force of gravity.

ΔH = head difference between the top and bottom of the plug (cm water)

A = cross-sectional area of the plug (cm^2)

V = volume of water in the collecting pipet at time t (cc)

t = time elapsed for V to be collected (min).

Once the hydraulic conductivity is calculated, one can calculate the intrinsic permeability which is representative of the hydraulic behavior of the medium itself, excluding fluid properties. The following equation has been used to obtain the instrinsic permeability of the cement plug:

$$k = K \frac{\gamma}{\mu}$$

where k = intrinsic permeability (cm^2)

γ = specific weight of the fluid (N/cm^3)

μ = viscosity of the fluid ($N \cdot sec/cm^2$).

6.5.1 Hydraulic Behavior of Plug SC-1

Sample SC-1, cured dry, exhibited larger hydraulic conductivities (compared to fresh plugs at ambient temperatures). A healing process started as soon as water flowed through the plug. The flow rate decreases with time. Water is thought to bypass the plug through a steel/plug interface channel. Water injection helps the plug regain some of the water it had lost during drying. Resaturation and reswelling closes the interface gap (at least partially).

Figures 6.17 through 6.19 illustrate the outflow volume vs. time for SC-1 at ambient temperatures (Tables 6.3 through 6.5). The flow continued to decrease despite the increase in injecting pressure. The high flowrate made this test more accurate than similar measurements for plugs never dried out. Figure 6.20 is the plot of outflow volume vs. time for the same plug at 40-55°C (104-131°F) and .55 MPa (80 psi) injecting pressure. Higher temperature increases the flowrate through the plug. The differential expansion of the sample and steel wall probably is the major reason for this increase. Moreover, the viscosity of water decreases with the increase in temperature which, in turn, can induce a higher flow. A problem encountered is the excessive temperature difference between top and bottom of the sample (as high as 10°C or 18°F). The effect of differential heating is not known. Lack of good insulation in the heating mantle was the major reason for the difference. This problem has been substantially resolved by placing additional insulating materials on the top and bottom of the cement permeameter (inside the heating mantle).

The linear regression model (through the origin) seems to be sufficient for the experiments performed on this plug. The coefficients of

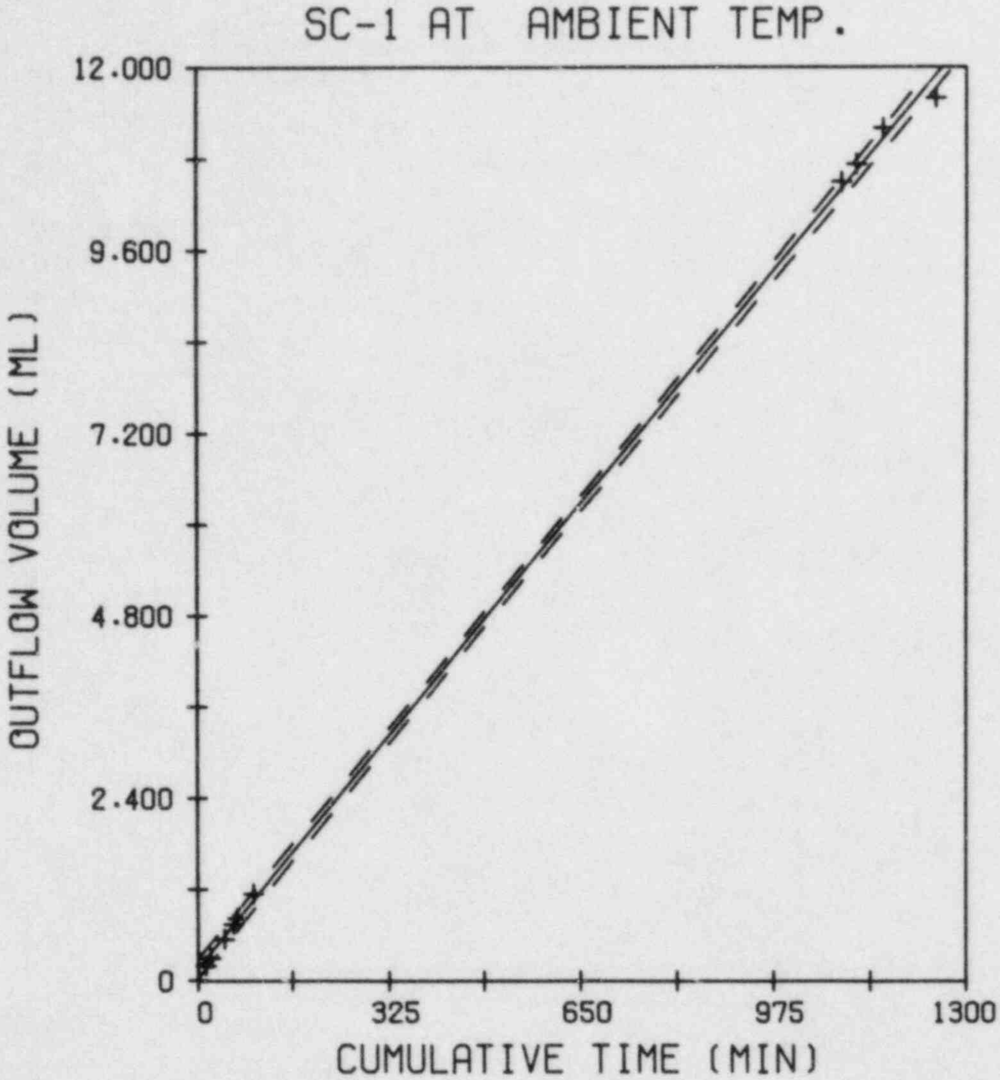

Figure 6.17 Water outflow vs. time for sample SC-1 at ambient temperature and .52 MPa (75 psi) injecting pressure.

+ : volume of water at given time (measurements)

———————— : best-fit straight line

- - - - - - - : 95% confidence interval

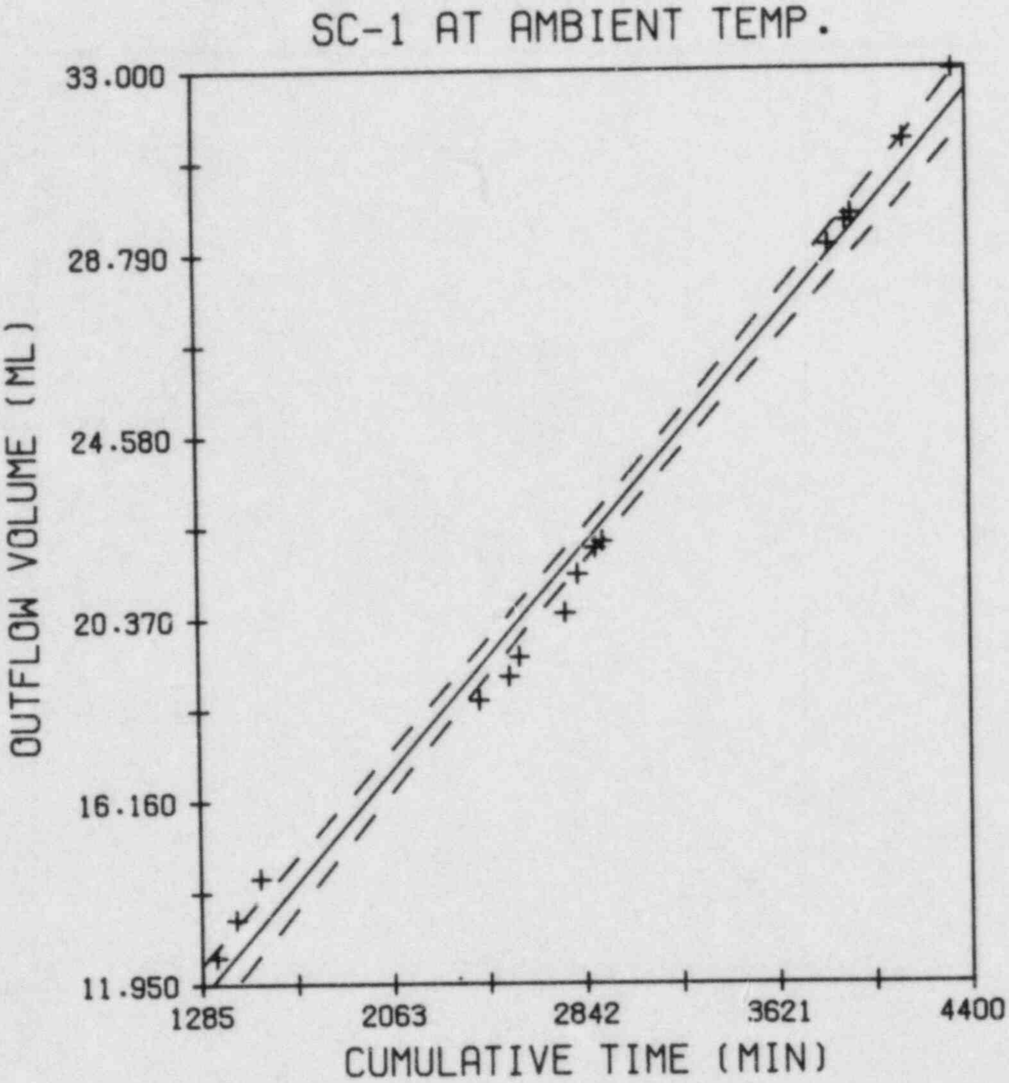

Figure 6.18 Water outflow vs. time for sample SC-1 at ambient temperature and .55 MPa (80 psi) injecting pressure.

+ : volume of water at given time (measurements)

———————— : best-fit straight line

- - - - - - - - : 95% confidence interval

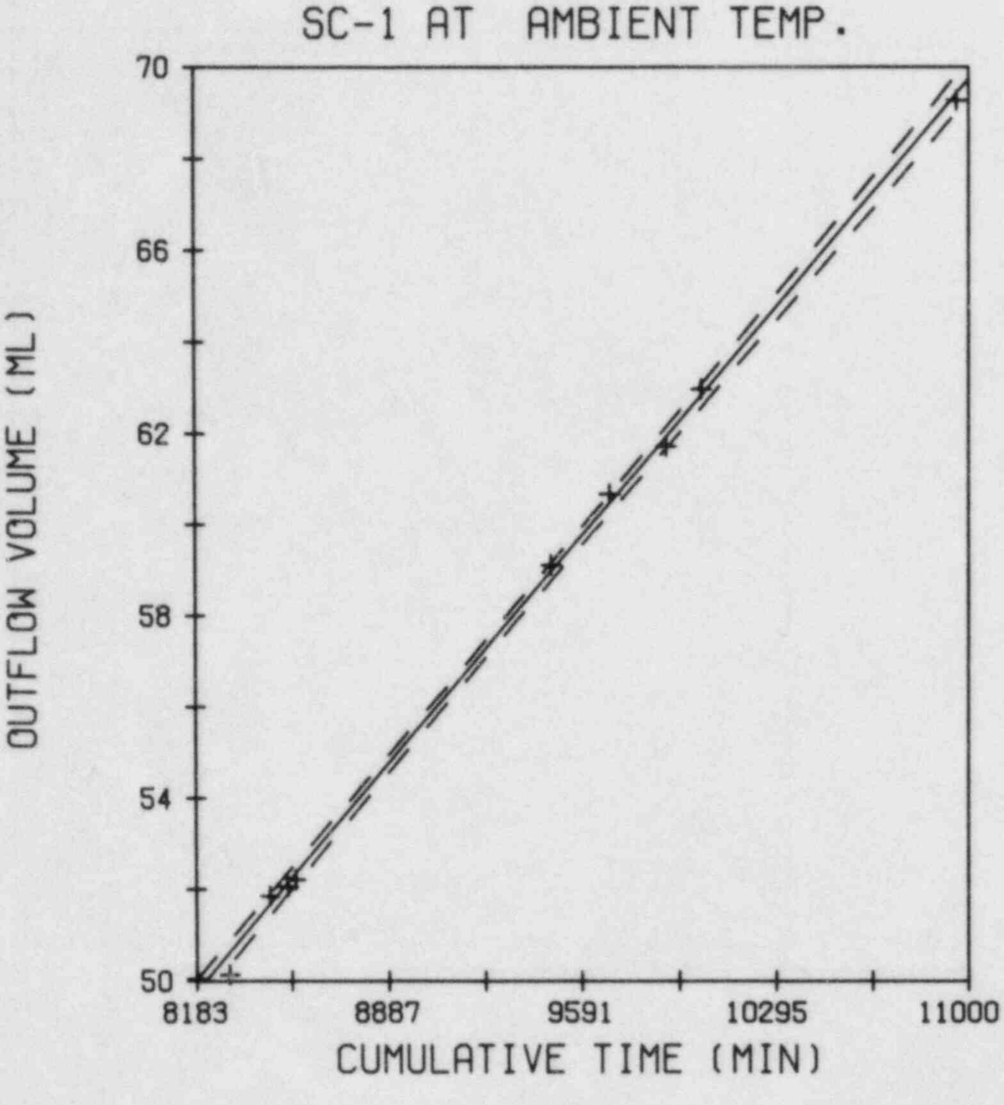

Figure 6.19 Water outflow vs. time for sample SC-1 at ambient temperature and .57 MPa (82 psi) injecting pressure.

+ : volume of water at given time (measurements)

———————— : best-fit straight line

- - - - - - - - : 95% confidence interval

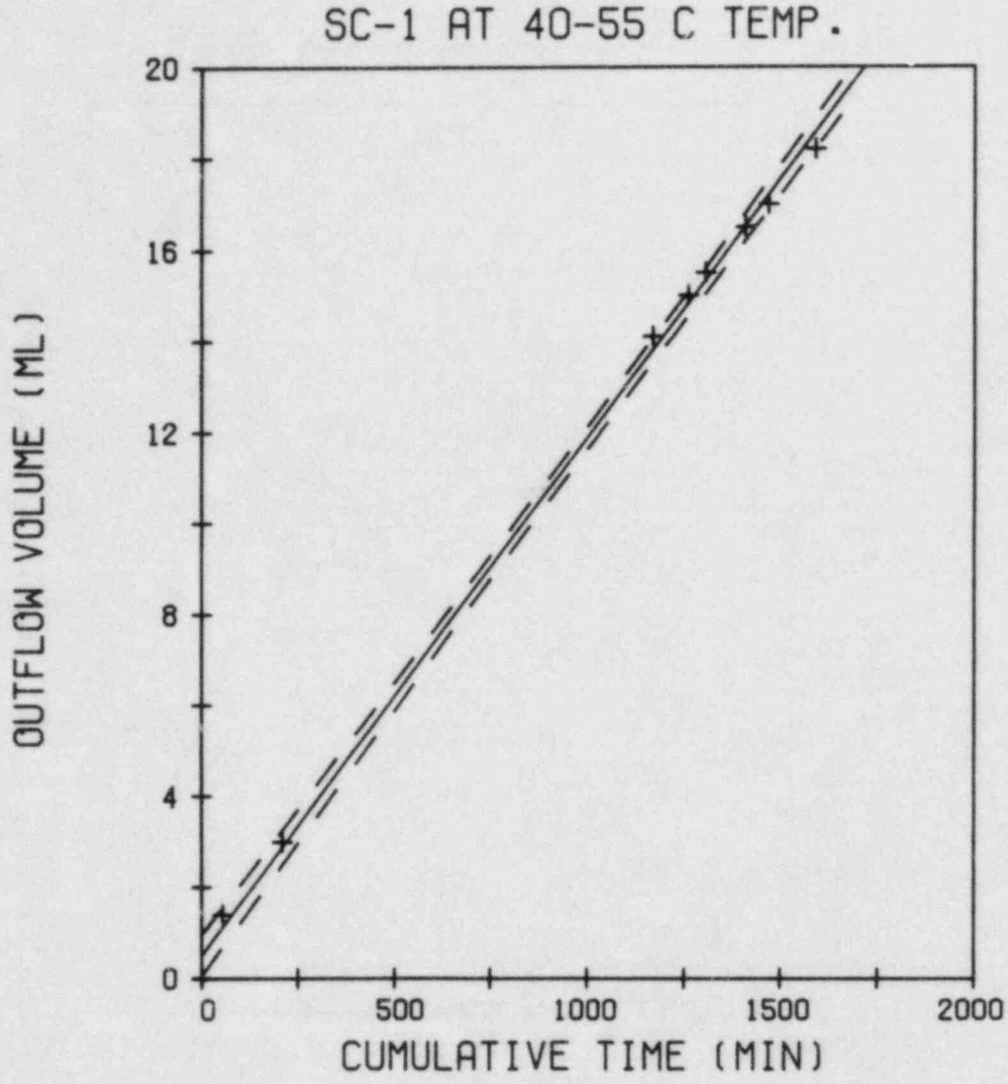

Figure 6.20 Water outflow vs. time for sample SC-1 at ambient temperature and .55 MPa (80 psi) injecting pressure.

+ : volume of water at given time (measurements)

———————— : best-fit straight line

- - - - - - - - : 95% confidence interval

Table 6.3 Data obtained from SC-1 at ambient temperature (22 ± 2°C or 71 ± 4°F) and .52 MPa (75 psi) injecting pressure. (γ = 9.7842 KN/m^3, $\mu = 0.9578 \times 10^{-3}$ $N \cdot sec/m^2$, L = 10.97 cm)

Volume Outflow (cm^3)	Cumulative time (min)	Injecting Pressure MPa (psi)
0.20	13	.52 (75)
0.30	21	"
0.55	45	"
0.75	60	"
0.825	67	"
1.15	95	"
10.50	1090	"
10.73	1115	"
11.20	1160	"
11.60	1248	"

Table 6.4 Data obtained from SC-1 at ambient temperature (22 ± 2°C or 71 ± 4°F) and .55 MPa (80 psi) injecting pressure. (γ = 9.7842 KN/m^3, $\mu = 0.9578 \times 10^{-3}$ $N \cdot sec/m^2$, L = 10.97 cm)

Volume Outflow (cm^3)	Cumulative time (min)	Injecting Pressure MPa (psi)
11.95	1285	.552 (80)
12.58	1345	"
13.45	1425	"
14.40	1525	"
18.50	2420	"
19.05	2545	"
19.50	2585	"
20.50	2770	"
21.40	2820	"
22.00	2890	"
22.15	2920	"
28.95	3840	"
29.50	3910	"
29.65	3933	"
31.35	4145	"
32.95	4348	"

Table 6.5 Data obtained from SC-1 at ambient temperature (22 ± 2°C or 71 ± 4°F) and .57 MPa (82 psi) injecting pressure. (γ = 9.7842 KN/m^3, $\mu = 0.9578 \times 10^{-3}$ $N \cdot sec/m^2$, L = 10.97 cm)

Volume Outflow (cm^3)	Cumulative time (min)	Injecting Pressure MPa (psi)
50.75	8183	.565 (82)
50.83	8303	"
52.50	8453	"
52.70	8520	"
52.85	8548	"
59.50	9483	"
61.00	9693	"
62.00	9896	"
63.20	10,025	"
69.30	10,957	"

Table 6.6 Data Obtained from Sample SC-1 at 40-55°C (104-131°F) and Injecting Pressure of .55 MPa (80 psi). (γ = 9.689 KN/m^3, μ = 0.547 x 10^{-3} $N \cdot sec/m^2$, L = 10.97 cm)

Cumulative Volume (cc)	Cumulative Time (min)	Temperature (°C) TC1	TC2	Pressure MPa (psi)
1.4	55	44.8	56.8	.55 (80)
3.0	210	41.2	50.3	"
14.1	1170	39.1	53.4	"
15.0	1260	45.9	54.6	"
15.5	1305	45.5	55.0	"
16.5	1410	46.1	55.9	"
17.0	1470	46.6	55.8	"
18.2	1590	45.6	55.2	"

determination (R^2) for various tests conducted on SC-1 are all above 99%. Tables 6.7 and 6.8 contain the computed values for linear regression lines forced through the origin and linear regression with best fit lines. There is no major difference in the two tables. Flow through the plug decreases from 9.548×10^{-3} cc/min to 6.247×10^{-3} cc/min with time. After the plug is heated to 40-55°C (104-131°F), the flowrate jumps to 11.729×10^{-3} cc/min, which exceeds the initial values.

Figure 6.21 illustrates the intrinsic permeabilities and hydraulic conductivities vs. cumulative time. The hydraulic conductivity decreases with time. However, it exceeds its initial value once the plug is being heated. On the other hand, the intrinsic permeability stays well under its initial value during heating (420.9×10^{-15} cm^2 vs. 634.6×10^{-15} cm^2). According to Figure 6.21, the increase in intrinsic permeability of the plug, by itself, could not cause the flowrate to exceed its initial value. The fluid (here water) has a major role in the flow rise when the plug heated. Figure 6.22 illustrates the viscosity decrease vs. temperature. The increase in flowrate, when the plug was heated, was partially caused by the plug changes, and partially by a reduction of resistance to flow of the fluid (due to the viscosity decrease).

6.5.2 Hydraulic Behavior of Plug SC-2

The flow through the plug at ambient temperatures is about 3 orders of magnitude smaller than for the SC-1 (dry plug). Figures 6.23 and 6.24 (Tables 6.9 and 6.10) show the data obtained, respectively, at 0.41-0.55 MPa (60-80 psi) and 0.66-0.69 (95-100 psi), both at ambient temperatures.

Studying the flow through the fresh plug SC-2 introduced problems that were negligible or absent during testing of SC-1. Flowrates are extremely low. Dealing with such small flows makes the results less certain, and once flow gets very small, the application of Darcy's Law becomes highly questionable (Freeze and Cherry, 1979, p. 72).

Atmospheric pressure variations and evaporation rate in the laboratory are two environmental factors that are thought to influence the flow through SC-2 (or any fresh plug at ambient temperatures). Atmospheric pressure variation is thought to be responsible for the occurrence of the "negative flow". Negative flow stands for the travel of water from the water collecting unit (pipet) to the bottom reservoir of the cement permeameter (Figure 6.25). This phenomenon usually occurs when atmospheric pressure in the laboratory rises (during nights, when room pressure builds up because the door remains closed). The atmospheric pressure rise is thought to push down the water column in the pipet. Figure 6.26 shows typical data obtained (for SC-2 at 49-55°C and .75 MPa injecting pressure). The decrease in the water level in the pipet causes a cyclic trend for the data. This phenomenon may be explained by some type of driving mechanism, such as capillary action due to incomplete saturation of the plug (especially, bottom of plug), or due to room pressure variations.

Table 6.7 Results for Sample SC-1 at Ambient and Elevated Temperatures (Linear Regression Forced through the Origin)

Temperature of Cement °C (°F)	Injecting Pressure MPa (psi)	Flowrate cc/min	R^2	Hydraulic Conductivity cm/min	95% Confidence Interval cc/min	Instrinsic Permeability cm^2 (Darcy)
22 ± 2 (71 ± 3.8)	0.52 (75)	9.548×10^{-3}	.999	3.889×10^{-6}	9.385×10^{-3} - 9.711×10^{-3}	634.6×10^{-15} (64.29×10^{-6})
22 ± 2 (71 ± 3.8)	0.55 (80)	7.655×10^{-3}	.997	3.118×10^{-6}	7.422×10^{-3} - 7.888×10^{-3}	508.8×10^{-15} (51.55×10^{-6})
22 ± 2 (71 ± 3.8)	0.57 (82)	6.247×10^{-3}	.999	2.322×10^{-6}	6.201×10^{-3} 6.294×10^{-3}	378.8×10^{-15} (38.38×10^{-6})
40 - 55 (104 - 131)	0.55 (80)	11.72×10^{-3}	.999	4.47×10^{-6}	11.449×10^{-3} 12.000×10^{-3}	420.9×10^{-15} (42.64×10^{-6})

Table 6.8 Results for Sample SC-1 at Ambient and Elevated Temperatures (Best Fit Line)

Temperature of Cement °C (°F)	Injecting Pressure MPa (psi)	Flowrate cc/min	Hydraulic Conductivity cm/min	Instrinsic Permeability cm^2 (Darcy)
22 ± 2 (71 ± 3.8)	0.52 (75)	9.318×10^{-3}	3.817×10^{-6}	622.7×10^{-15} (63.09×10^{-6})
22 ± 2 (71 ± 3.8)	0.55 (80)	7.000×10^{-3}	2.688×10^{-6}	438.6×10^{-15} (44.44×10^{-6})
22 ± 2 (71 ± 3.8)	0.57 (82)	5.527×10^{-3}	2.122×10^{-6}	346.3×10^{-15} (35.09×10^{-6})
40 - 55 (104 - 131)	0.55 (80)	11.36×10^{-3}	4.32×10^{-6}	407.7×10^{-15} (41.3×10^{-6})

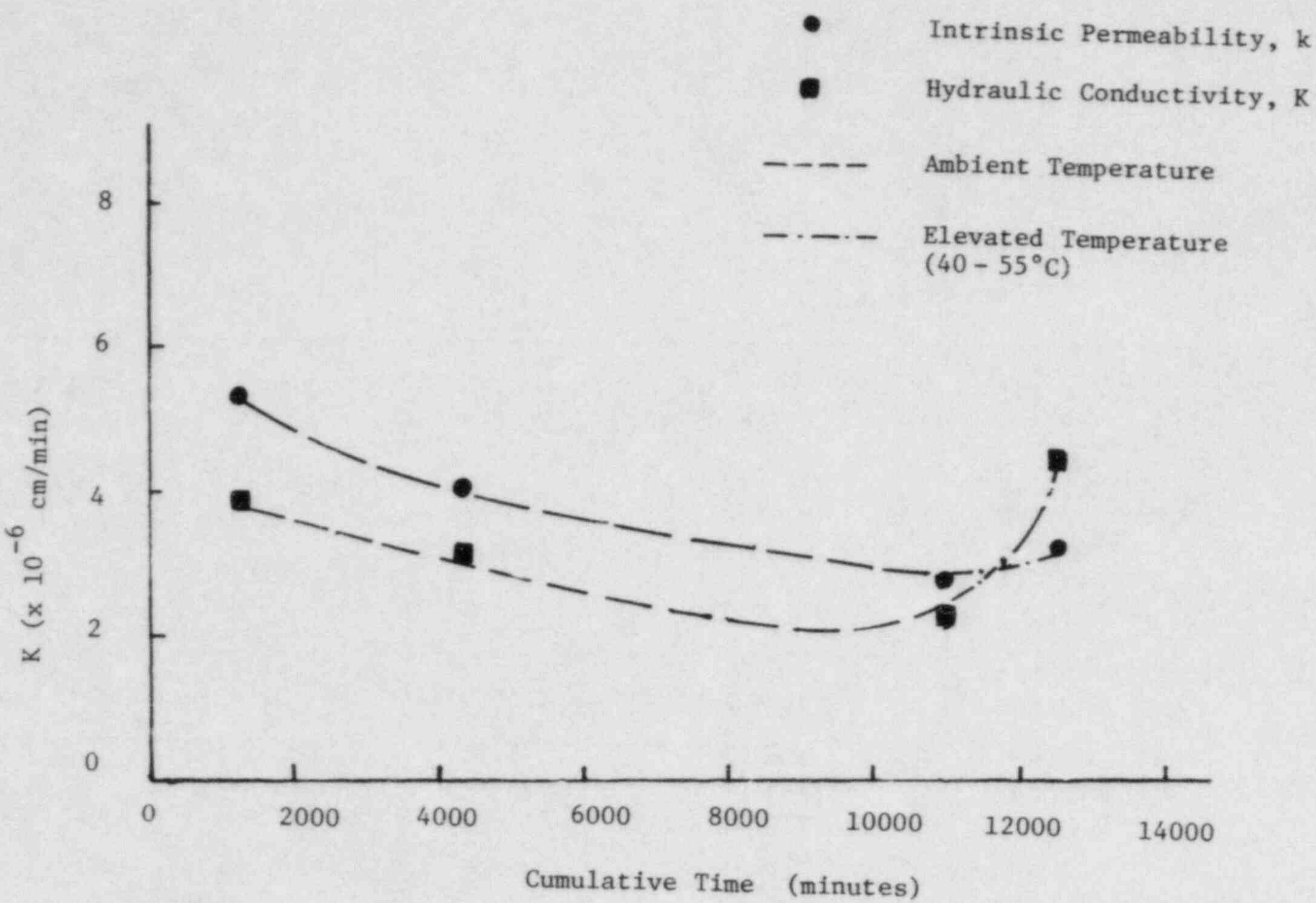

Figure 6.21 Hydraulic conductivity (K) and intrinsic permeability (k) of cement plug SC-1 as a function of time.

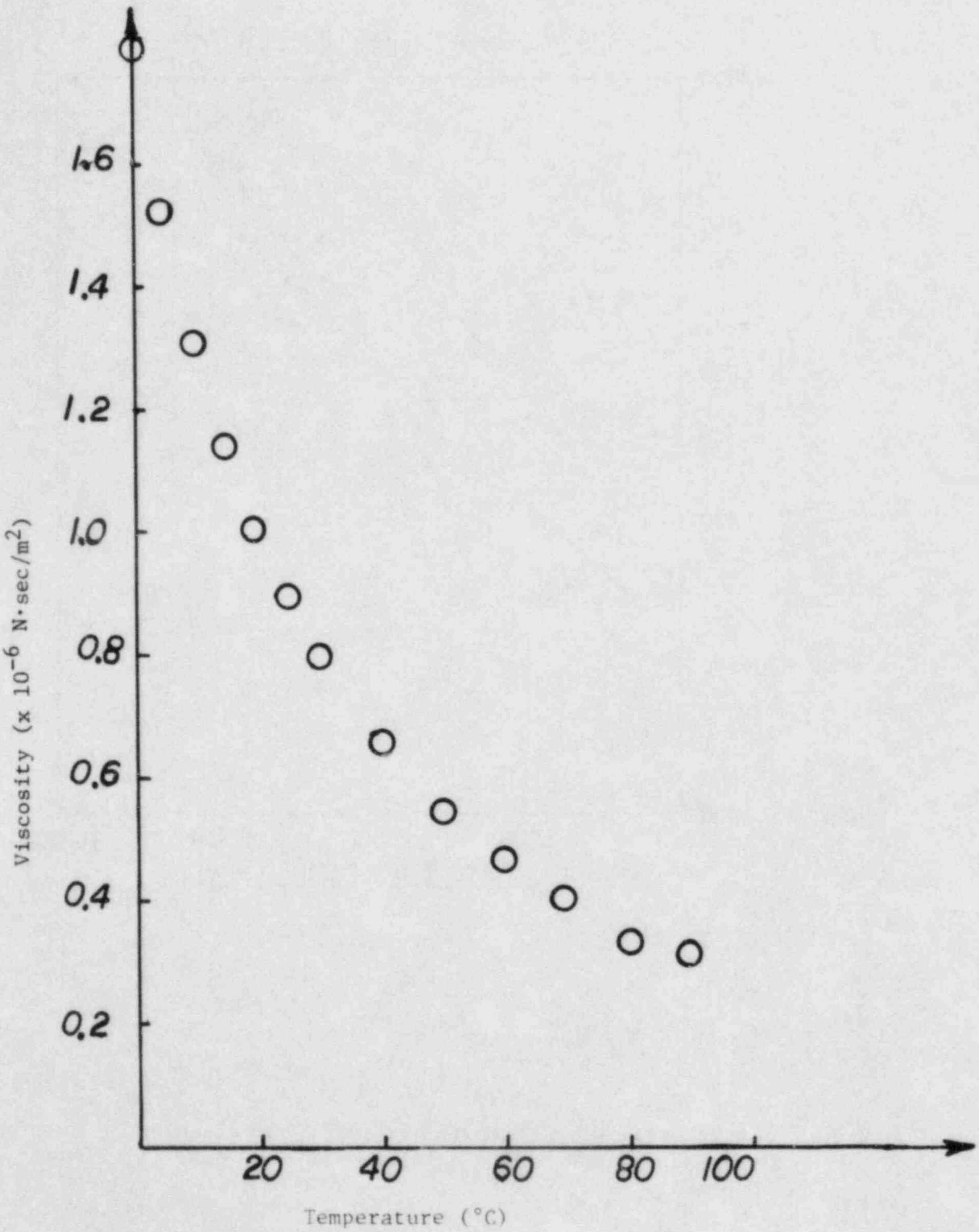

Figure 6.22 Water viscosity as a function of temperature (data from Vennard and Stroed, 1975, p. 705).

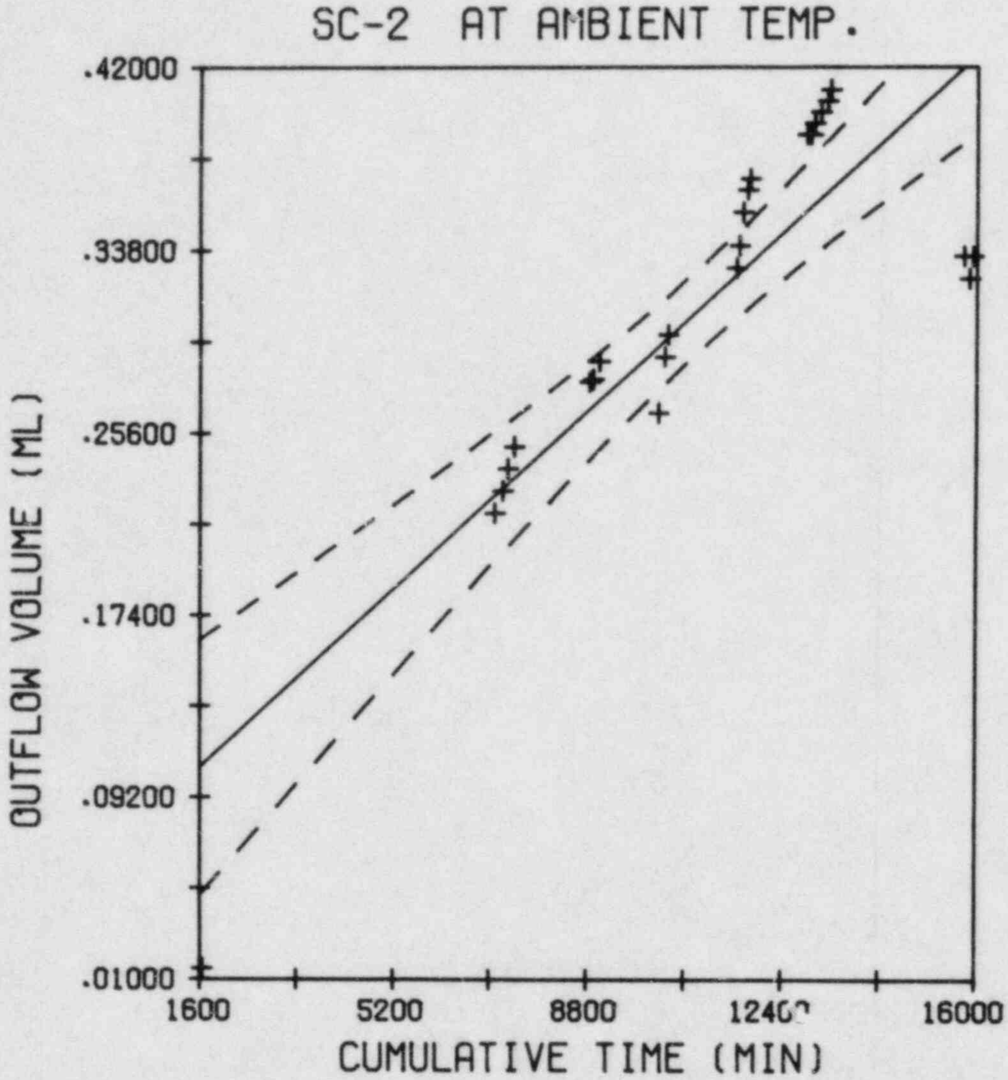

Figure 6.23 Water outflow vs. time for sample SC-2 at ambient temperature and 0.41 - 0.55 MPa (60 - 80 psi) injecting pressure.

+ : volume of water at given time (measurements)

———————— : best-fit straight line

- - - - - - - - : 95% confidence interval

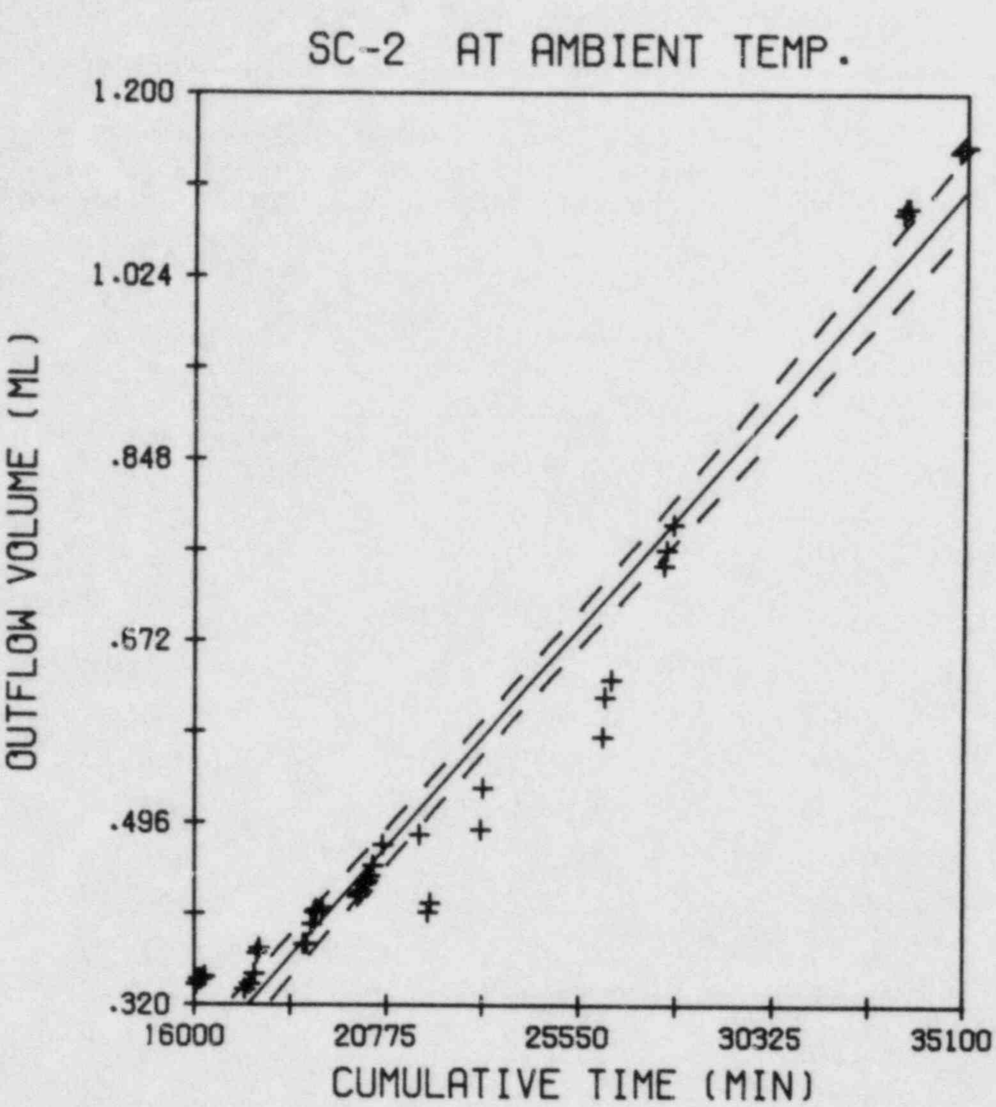

Figure 6.24 Water outflow vs. time for sample SC-2 at ambient temperature and 0.66 - 0.69 MPa (95 - 100 psi) injecting pressure.

+ : volume of water at given time

------------- : best fitted line

- - - - - - - : 95% confidence interval

Table 6.9 Data obtained from SC-2 at ambient temperature (22 ± 2°C or 71 ± 3.6°F) and .41 - .55 MPa (60 - 80 psi) injecting pressure. (γ = 9.7842 KN/m^3, μ = 0.9578 x 10^{-3} $N \cdot sec/m^2$, L = 10.67 cm)

Volume Outflow (cm^3)	Cumulative time (min)	Injecting Pressure MPa (psi)
0.015	1645	70
0.220	7105	"
0.230	7255	"
0.240	7345	"
0.250	7462	"
0.279	8845	"
0.280	8905	80
0.288	9025	70
0.265	10,105	"
0.290	10,225	"
0.300	10,285	60
0.330	11,549	105
0.340	11,605	90
0.355	11,670	60
0.365	11,750	"
0.370	11,790	"
0.390	12,850	"
0.390	12,925	"
0.395	12,985	"
0.400	13,105	"
0.405	13,230	"
0.410	13,285	"
0.335	15,760	"
0.325	15,865	"
0.335	15,925	55

Table 6.10 Data obtained from SC-2 at ambient temperature (22 ± 2°C or 71 ± 3.6°F) and .62 - .69 MPa (95 - 100 psi) injecting pressure. (γ = 9.7842 KN/m^3, μ = 0.9578 x 10^{-3} N·sec/m^2, L = 10.67 cm)

Volume Outflow (cm^3)	Cumulative time (min)	Injecting Pressure MPa (psi)
0.340	16,045	95
0.345	16,105	97
0.345	16,165	98
0.347	16,265	99
0.335	17,245	99
0.340	17,365	99
0.350	17,485	100
0.370	17,545	"
0.375	17,605	"
0.379	18,715	"
0.379	18,805	"
0.398	18,925	"
0.410	18,995	"
0.412	19,045	"
0.414	19,185	"
0.425	20,065	"
0.427	20,125	"
0.430	20,185	"
0.437	20,245	"
0.440	20,305	"
0.440	20,330	"
0.445	20,365	"
0.455	20,440	"
0.475	20,680	"
0.485	21,595	"
0.410	21,805	"
0.419	21,865	"
0.490	23,125	"
0.530	23,185	"

Table 6.10 Data obtained from SC-1 at ambient temperature (22 ± 2°C or 71 ± 3.6°F) and .66 - .69 MPa (95 - 100 psi) injecting pressure. (γ = 9.7842 KN/m^3, $\mu = 0.9578 \times 10^{-3}$ $N \cdot sec/m^2$, L = 10.67 cm)--Continued

Volume Outflow (cm^3)	Cumulative time (min)	Injecting Pressure MPa (psi)
0.580	26,125	"
0.618	26,175	"
0.635	26,335	"
0.745	27,625	"
0.760	27,685	"
0.785	27,850	"
1.085	33,503	"
1.090	33,563	"
1.090	33,625	"
1.145	34,905	"
1.147	34,970	"
1.150	35,035	"
1.150	35,095	"

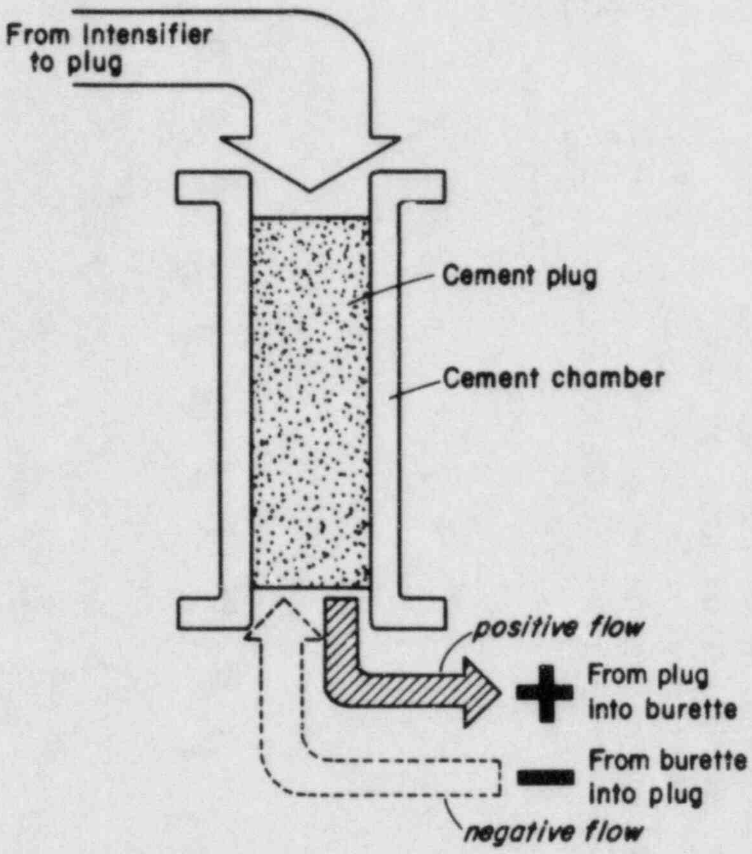

Figure 6.25 Negative flow through the cement plug.

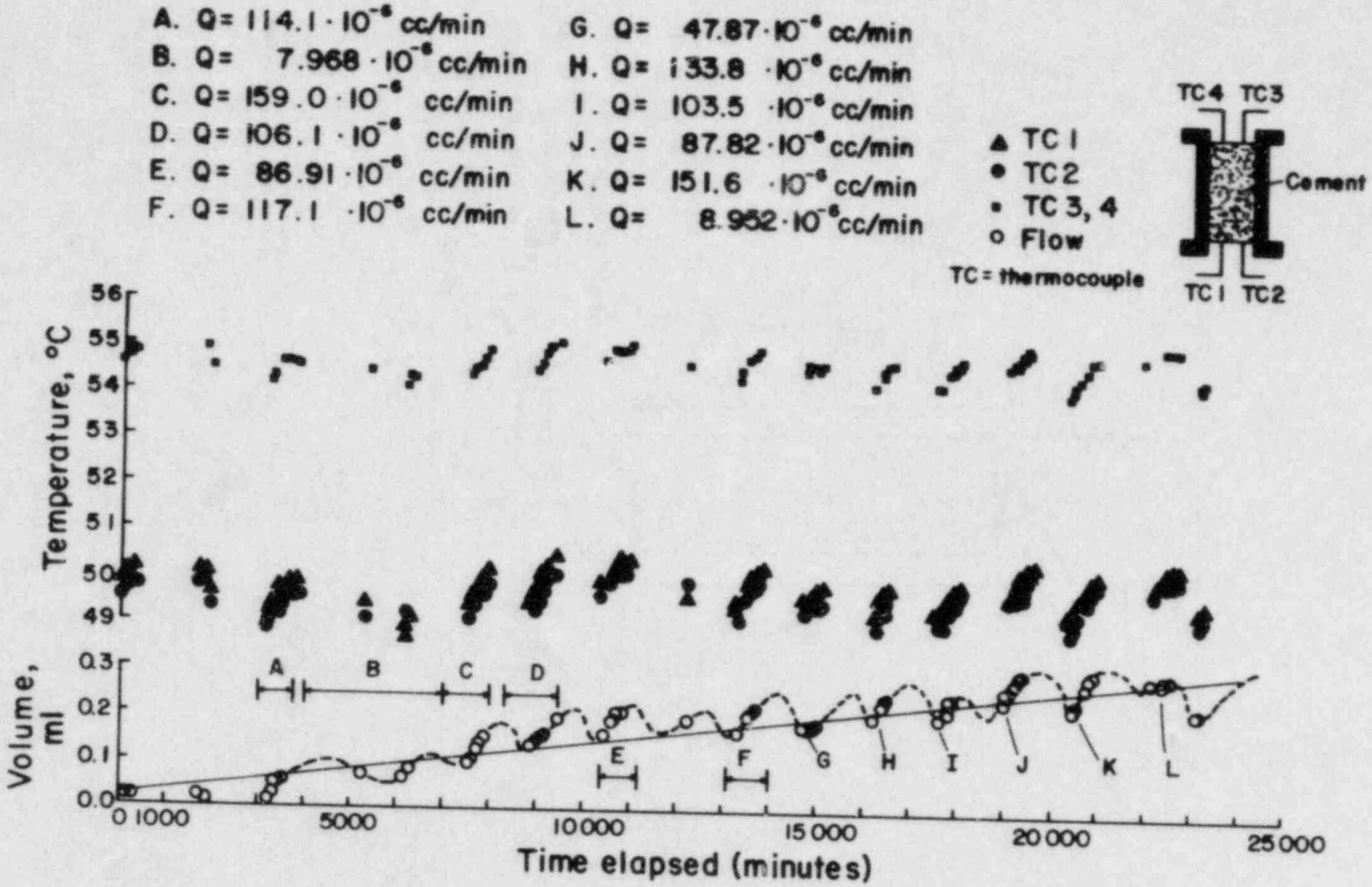

Figure 6.26 Cyclic trend of plot of outflow volume Q vs. time with negative flow dominant.

The rise-and-drop trend of the water level in the outflow collecting pipet is very similar to the cyclic trend of the atmospheric pressure in the laboratory (Figure 6.27 - compare to Figure 6.26). A sensitive pressure transducer recorded the variations of water level in an identical water collecting pipet. An automatic data acquisition system recorded the voltage of the transducer (which is linearly proportional to the water level in the pipet) every 30 minutes (Figure 6.28). The variations in the voltage (e.g. water level) for a typical day are illustrated in Figure 6.29. This figure is similar to the variation in the atmospheric pressure; e.g. the decrease in the water level coincided with the increase in the atmospheric pressure. Since the water had no place to go, it is thought that it might have been pushed down.

The second environmental factor considered is the evaporation of water from the measuring pipet. The evaporation rate is found to be of the same order of magnitude as the flow through fresh plugs at ambient temperatures (8.057×10^{-6} cc/min). Figure 6.30 shows a plot of the evaporation measurements (Table 6.10). Values computed for the outflow volume of fresh plugs were all corrected for the evaporation.

The application of heat has increased the flow through the plug SC-2. Experiments conducted on the plug SC-2 at 40-43°C and 1.15 MPa injecting pressure and at 49-55°C and .75 MPa injecting pressure are the only two exceptions observed. The reason can be related to negative flow occurring during these tests. Figures 6.31 and 6.32 show the plots obtained for these two (Tables 6.11 and 6.12). Note the scatter in the data. Generally, tests on this plug (at elevated temperatures) have shown that one can minimize the negative flow by maintaining the injecting pressure above 2.0 MPa (290 psi). This might not be true for flow testing at ambient temperature (usually higher injection pressure is then required). Figures 6.33 through 6.37 illustrate plots for the data obtained from SC-2 at elevated temperatures (Tables 6.13 through 6.17). Tables 6.18 and 6.19 contain the calculated values related to hydraulic behavior of this plug.

The direct conclusion that can be reached by the study of these tables is that the hydraulic conductivities and intrinsic permeabilities increase with temperature. Figures 6.38 and 6.39,* respectively, show the hydraulic conductivities and intrinsic permeabilities vs. temperature.

6.5.3 Hydraulic Behavior of Plug SC-3

This sample is the first of its kind for which flow is against gravity, i.e. water is injected at the bottom and flows upward. Flowrates obtained for this sample are smaller than for the SC-2 plug. Negative

---

*Although these figures might suggest a minimum at about 40°C, data obtained subsequent to completion of this report suggest that values given at 22°C are too high.

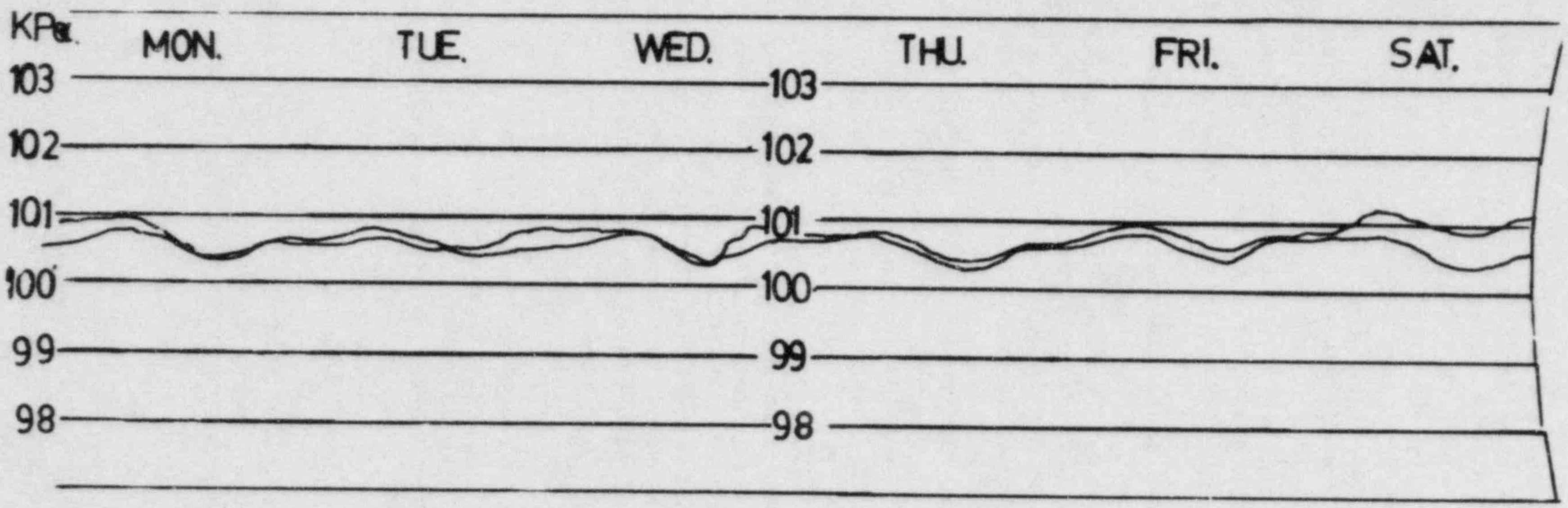

Figure 6.27 Atmospheric pressure in the laboratory for a typical two-week period.

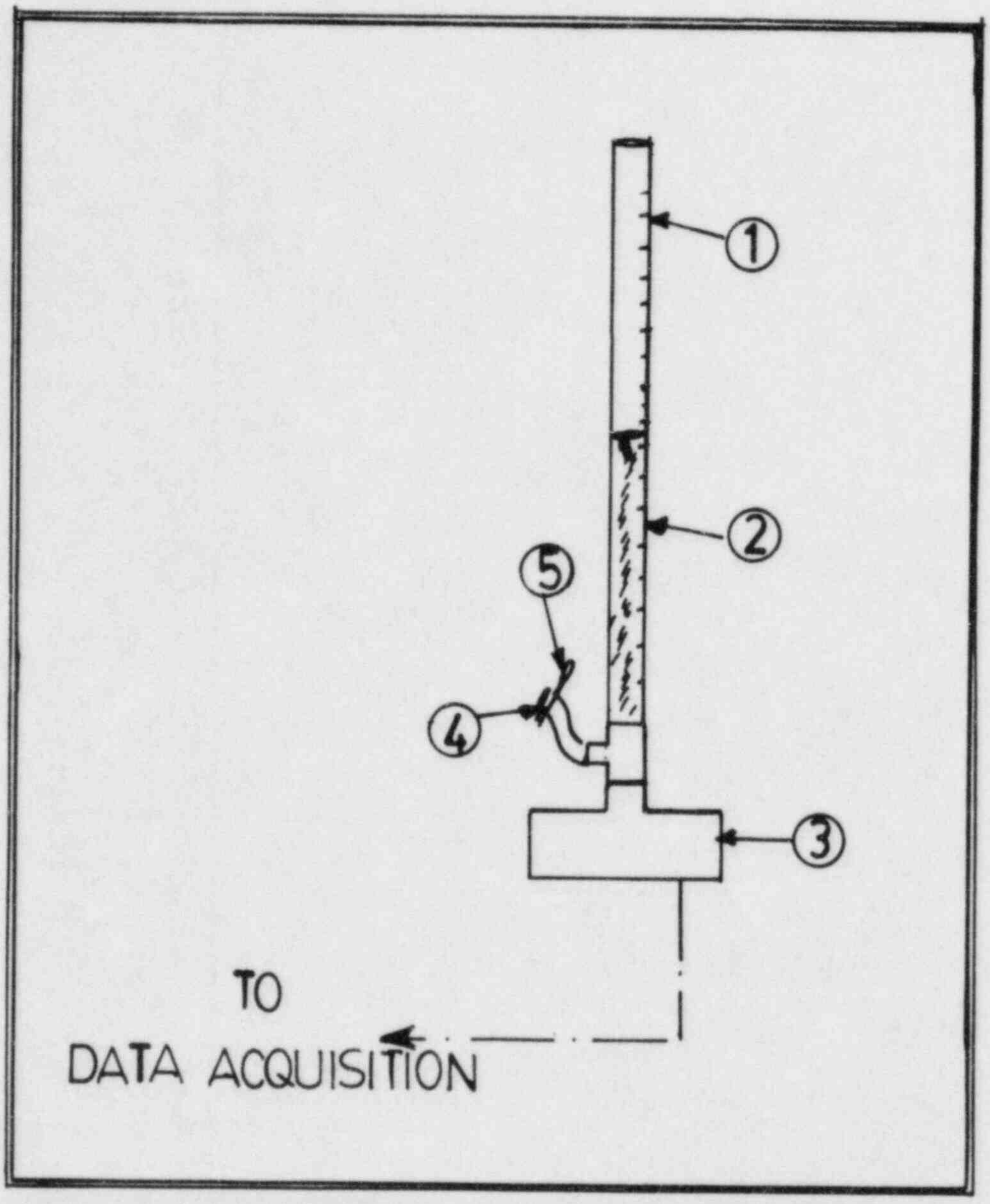

1. Pipet
2. Water
3. Pressure transducer
4. Tygon hose
5. Clip

Figure 6.28 Schematic of system used to record the decrease in water level as atmospheric temperature is increased.

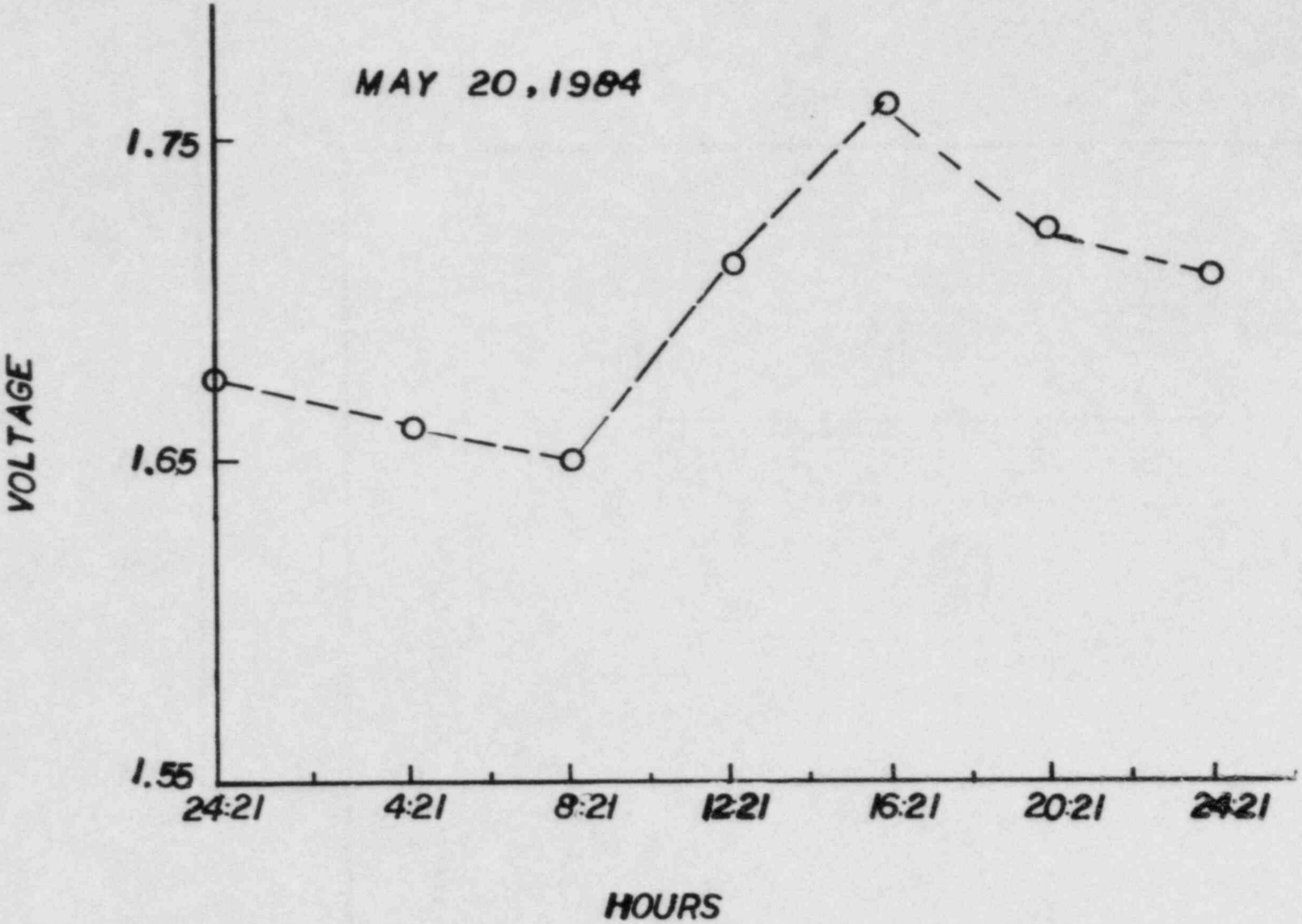

Figure 6.29 Variation in voltage (water level) with time.

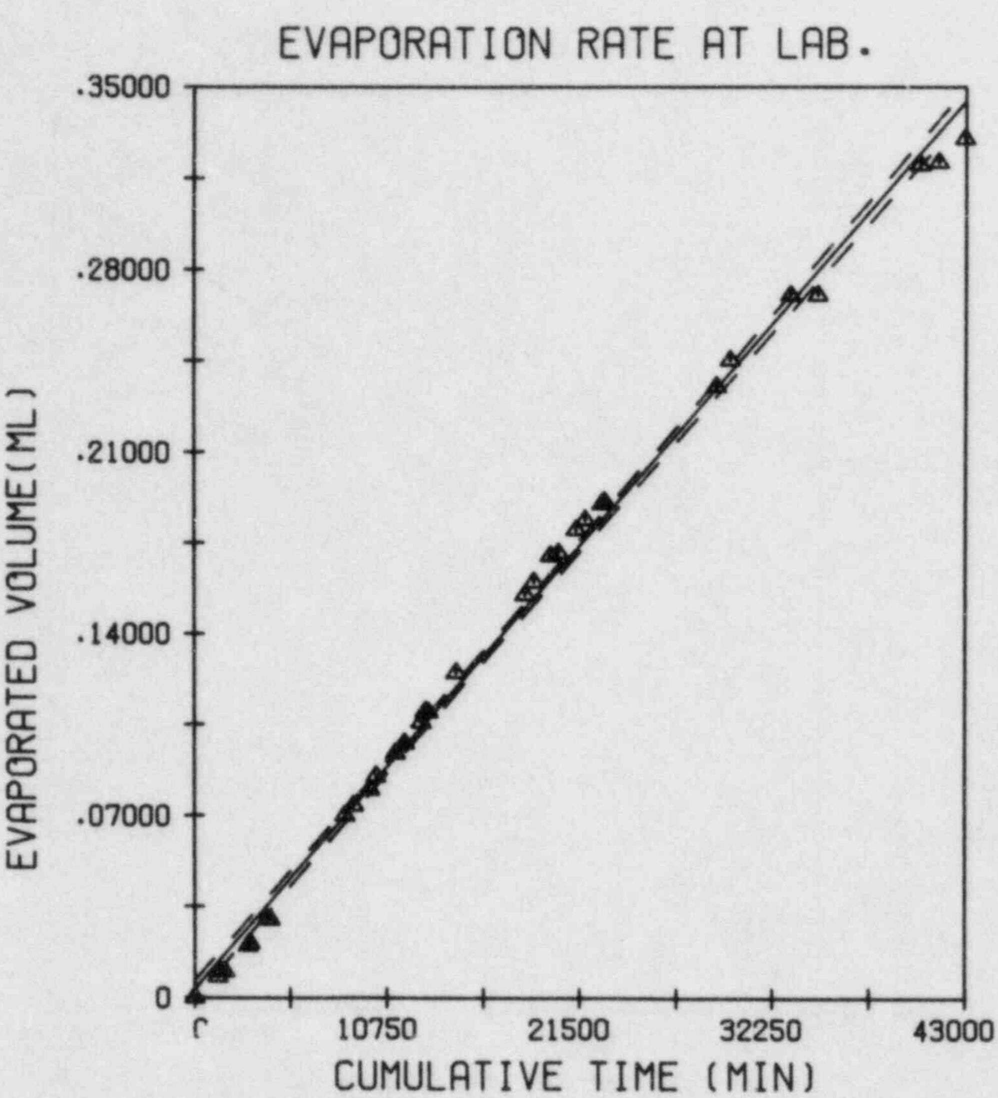

Figure 6.30 Water evaporation in the laboratory.

Δ : volume of water evaporated from the reference pipet (measurements)

———————— : best-fit straight line

- - - - - - - : 95% confidence interval

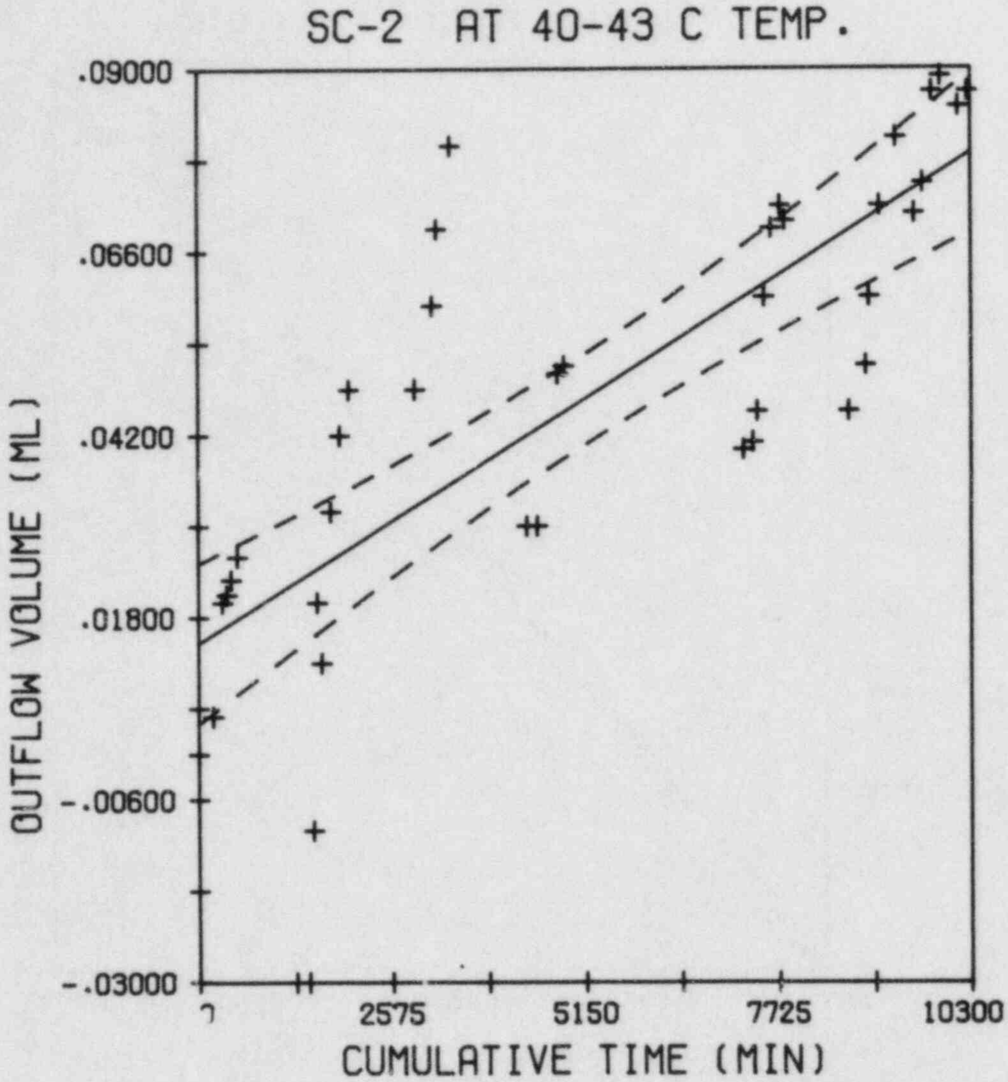

Figure 6.31 Water outflow vs. time for sample SC-2 at 40 - 43°C and 1.15 MPa (167 psi) injecting pressure.

+ : volume of water at given time (measurements)

———————— : best-fit straight line

- - - - - - - - : 95% confidence interval

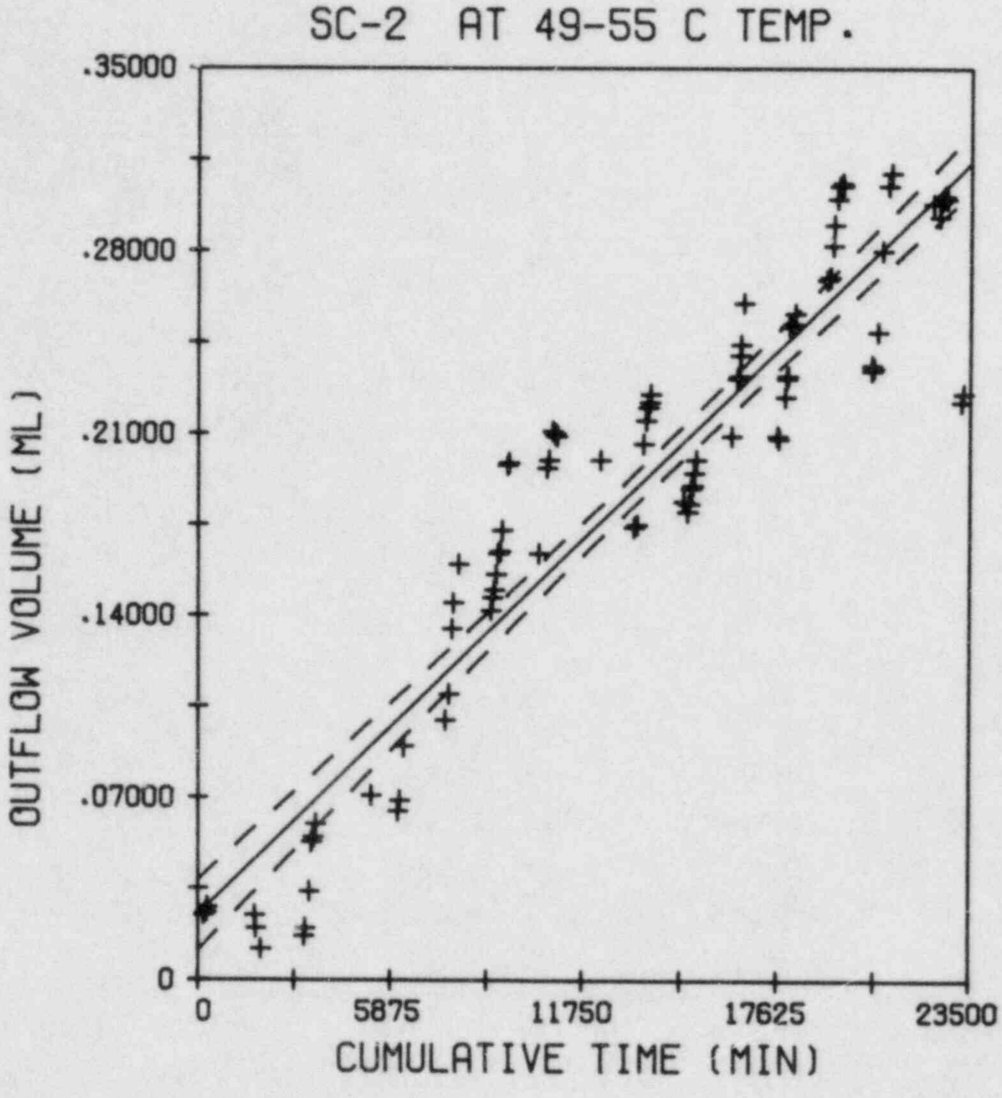

Figure 6.32 Water outflow vs. time for sample SC-2 at 49 - 55°C and 0.75 MPa (109 psi) injecting pressure.

+ : volume of water at given time (measurements)

———————— : best-fit straight line

- - - - - - - : 95% confidence interval

Table 6.11 Data obtained from sample SC-2 at 40-43°C (104-109°F) and injecting pressure of 1.15 MPa (167 psi). (γ = 9.7218 KN/m^3, $\mu = 0.6318 \times 10^{-3}$ $N \cdot sec/m^2$, L = 10.67 cm)

Cumulative Volume (cc)	Cumulative Time (min)	°C at Thermocouples Bottom TC1	TC2	Top TC3 & TC4	Injection Pressure (MPa)
0.0	0	39.9	39.5	42.2	1.15
0.005	195	40.1	39.6	42.4	"
0.02	315	40.1	39.7	42.4	"
0.021	375	40.2	39.8	43.4	"
0.023	435	40.2	39.8	42.4	"
0.026	518	40.4	40.0	42.6	"
-0.03	1455	39.9	39.5	42.3	"
-0.01	1515	40.1	39.6	42.4	"
0.02	1575	40.1	39.7	42.4	"
0.012	1635	40.2	39.8	42.4	"
0.032	1755	40.3	39.9	42.5	"
0.042	1875	40.4	40.0	42.6	"
0.048	1995	40.4	40.0	42.6	"
0.048	2880	40.1	39.7	42.3	"
0.059	3105	40.3	39.8	42.5	"
0.069	3165	40.4	39.9	42.5	"
0.080	3345	40.6	40.2	42.7	"
0.030	4375	40.1	39.7	42.4	"
0.030	4505	40.2	39.8	42.4	"
0.050	4770	40.3	39.9	42.5	"
0.051	4855	40.3	39.9	42.5	"
0.040	7255	39.7	39.3	42.1	"
0.041	7375	39.9	39.4	42.3	"
0.045	7435	39.9	39.5	42.3	"
0.060	7525	40.0	39.5	42.3	"
0.069	7615	40.1	39.6	42.3	"
0.072	7735	40.2	39.7	42.4	"
0.070	7795	40.2	39.7	42.4	"
0.045	8665	39.9	39.5	42.2	"
0.051	8895	40.0	39.6	42.3	"

Table 6.11 Data obtained from sample SC-2 at 40-43°C (104-109°F) and injecting pressure of 1.15 MPa (167 psi). (γ = 9.7218 KN/m^3, $\mu = 0.6318 \times 10^{-3}$ $N \cdot sec/m^2$, L = 10.67 cm)--Continued

Cumulative Volume (cc)	Cumulative Time (min)	°C at Thermocouples Bottom TC1	TC2	Top TC3 & TC4	Injection Pressure (MPa)
0.060	8935	40.1	39.6	42.3	1.15
0.072	9075	40.3	39.8	42.5	"
0.081	9295	-	-	-	"
0.071	9535	40.4	39.9	42.5	"
0.075	9655	40.4	40.0	42.6	"
0.087	9775	40.6	40.2	42.7	"
0.089	9895	40.2	40.2	42.8	"
0.085	10135	40.3	39.9	42.5	"
0.087	10255	40.3	39.9	42.5	"

Table 6.12 Data obtained from sample SC-2 at 49-55°C (120-131°F) and injecting pressure of .75 MPa (109 psi). (γ = 9.6796 KN/m^3, μ = 0.5308 x 10^{-3} $N \cdot sec/m^2$, L = 10.67 cm)

Cumulative Volume (cc)	Cumulative Time (min)	°C at Thermocouples Bottom TC1	TC2	Top TC3 & TC4
0.000		49.8	49.5	54.6
0.025	180	50.0	49.7	54.7
0.026	263	50.1	49.8	54.8
0.028	295	50.1	49.8	54.8
0.025	1750	50.1	49.8	54.9
0.020	1783	50.1	49.8	54.9
-	negative flow			
0.012	1937	49.6	49.3	54.5
0.017	3238	49.2	48.9	54.2
0.020	3282	49.3	49.0	54.3
0.034	3397	49.5	49.3	54.5
0.053	3477	49.7	49.4	54.6
0.055	3537	49.7	49.5	54.6
0.060	3612	49.8	49.5	54.6
0.060	3657	49.8	49.5	54.6
0.071	5307	49.4	49.1	54.4
0.065	6117	49.0	48.7	54.1
0.069	6177	49.2	48.9	54.3
0.090	6297	49.4	49.1	54.4
0.100	7557	49.4	49.1	54.4
0.110	7677	49.6	49.3	54.5
0.135	7767	49.8	49.6	54.6
0.145	7812	49.9	49.6	54.7
0.160	7964	50.1	49.8	54.9
0.142	8957	49.6	49.3	54.5
0.147	8997	49.7	49.4	54.5
0.150	9057	49.8	49.5	54.6
0.156	9117	49.9	49.7	54.8
0.164	9177	50.1	49.0	54.8
0.165	9237	50.2	49.9	54.9

Table 6.12 Data obtained from sample SC-2 at 49-55°C (120-131°F) and injecting pressure of .75 MPa (109 psi). (γ = 9.6796 KN/m^3, μ = 0.5308 x 10^{-3} N·sec/m^2, L = 10.67 cm)--Continued

Cumulative Volume (cc)	Cumulative Time (min)	°C at Thermocouples Bottom TC1	TC2	Top TC3 & TC4
0.173	9297	50.2	50.0	55.0
0.198	9462	50.4	50.1	55.1
0.199	9507	-	-	-
0.164	10,429	49.9	49.6	54.7
0.197	10,662	50.1	49.9	54.9
0.200	10,726	50.2	50.0	54.9
0.211	10,827	50.3	50.0	54.9
0.210	10,902	50.3	50.0	54.9
0.209	10,962	50.3	50.0	55.0
0.200	12,282	49.9	49.6	54.6
0.174	13,305	49.4	49.1	54.3
0.175	13,395	49.5	49.5	54.5
0.206	13,584	49.9	49.6	54.7
0.215	13,654	50.0	49.7	54.8
0.220	13,711	50.1	49.8	54.9
0.222	13,755	50.1	49.9	54.9
0.225	13,788	50.2	49.9	54.9
0.184	14,790	49.6	49.3	54.5
0.180	14,910	49.7	49.4	54.6
0.183	14,961	49.7	49.4	54.6
0.189	15,015	49.6	49.4	54.6
0.190	15,060	49.7	49.4	54.6
0.195	15,109	49.7	49.4	54.5
0.200	15,165	49.8	49.5	54.6
0.209	16,225	49.2	49.0	54.2
0.231	16,399	49.6	49.3	54.5
0.232	16,455	49.6	49.3	54.4
0.240	16,485	49.7	49.6	54.6
0.244	16,501	49.7	49.5	54.6
0.260	16,590	-	-	-

Table 6.12 Data obtained from sample SC-2 at 49-55°C (120-131°F) and injecting pressure of .75 MPa (109 psi). (γ = 9.6796 KN/m^3, $\mu = 0.5308 \times 10^{-3}$ $N \cdot sec/m^2$, L = 10.67 cm)--Continued

Cumulative Volume (cc)	Cumulative Time (min)	°C at Thermocouples Bottom TC1	TC2	Top TC3 & TC4
0.209	17,625	49.3	49.0	54.2
0.208	17,661	49.3	49.0	54.2
0.224	17,854	49.6	49.3	54.5
0.231	17,894	49.6	49.4	54.5
0.232	17,933	49.7	49.4	54.5
0.251	17,993	49.7	49.5	54.6
0.252	18,073	49.8	49.6	54.6
0.256	18,149	49.9	49.7	54.7
0.269	19,122	49.6	49.6	54.6
0.270	19,212	49.6	49.6	54.6
0.282	19,302	50.0	49.7	54.7
0.290	19,332	50.0	49.8	54.8
0.300	19,431	50.1	49.9	54.8
0.305	19,486	50.2	49.9	54.9
0.306	19,576	50.3	50.1	55.0
0.305	19,601	50.3	50.0	54.9
0.234	20,501	49.2	48.9	54.1
0.235	20,551	49.3	49.0	54.2
0.236	20,501	49.4	49.1	54.3
0.249	20,665	49.6	49.3	54.4
0.280	20,806	49.8	49.6	54.6
0.305	20,975	50.0	49.8	54.8
0.310	21,070	50.1	49.9	54.8
0.298	22,330	50.0	49.8	54.8
0.293	22,522	50.3	50.0	55.0
0.299	22,579	50.3	50.1	55.0
0.300	22,629	50.3	50.1	55.0
0.301	22,689	50.3	50.0	55.0
0.300	22,749	50.3	50.1	55.0

Table 6.12 Data obtained from sample SC-2 at 49-55°C (120-131°F) and injecting pressure of .75 MPa (109 psi). (γ = 9.6796 KN/m^3, μ = 0.5308 x 10^{-3} N·sec/m^2, L = 10.67 cm)--Continued

Cumulative Volume (cc)	Cumulative Time (min)	°C at Thermocouples Bottom TC1	TC2	Top TC3 & TC4
0.300	22,794	50.3	50.1	55.0
0.222	23,229	49.4	49.1	54.3
0.225	23,289	49.5	49.3	54.4

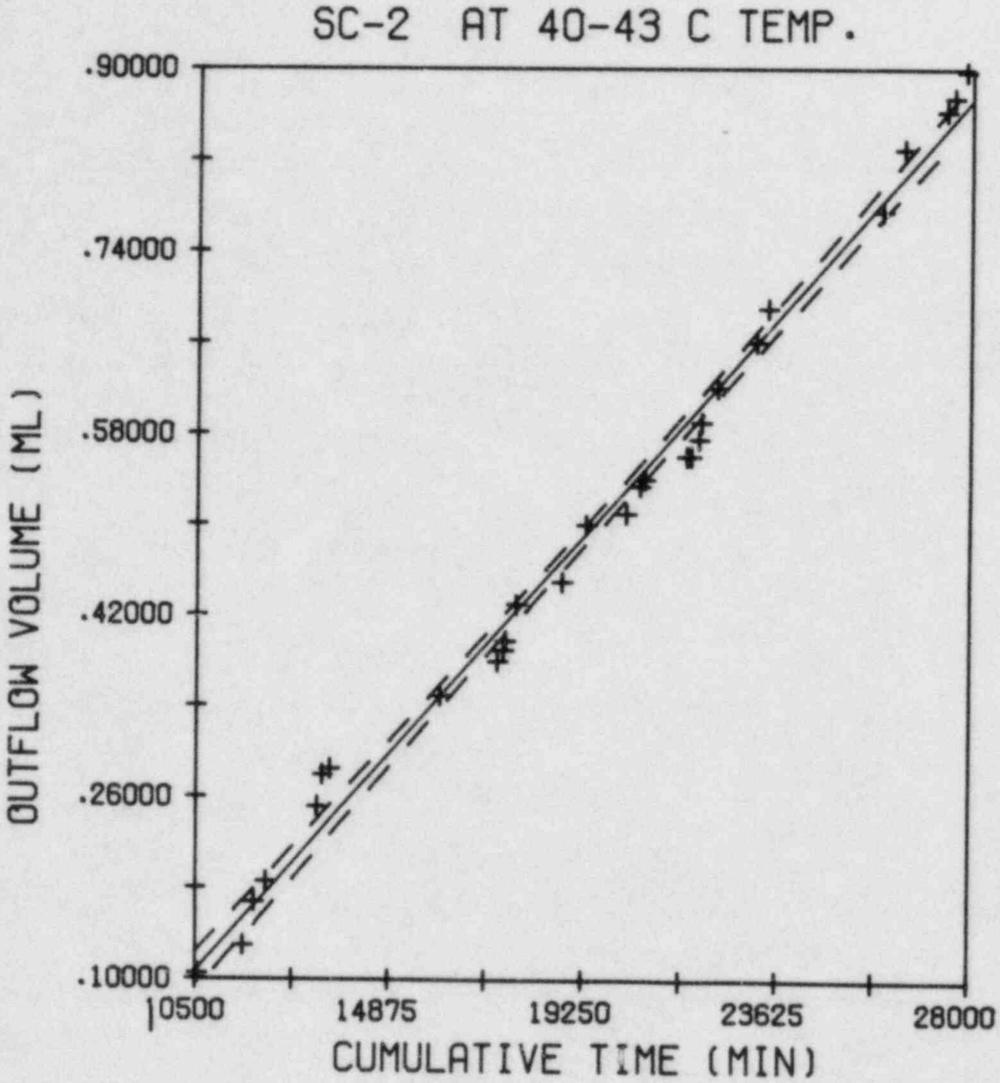

Figure 6.33 Water outflow vs. time for sample SC-2 at 40 - 43°C and 3.35 MPa (486 psi) injecting pressure.

+ : volume of water at given time (measurements)

——————— : best-fit straight line

- - - - - - - : 95% confidence interval

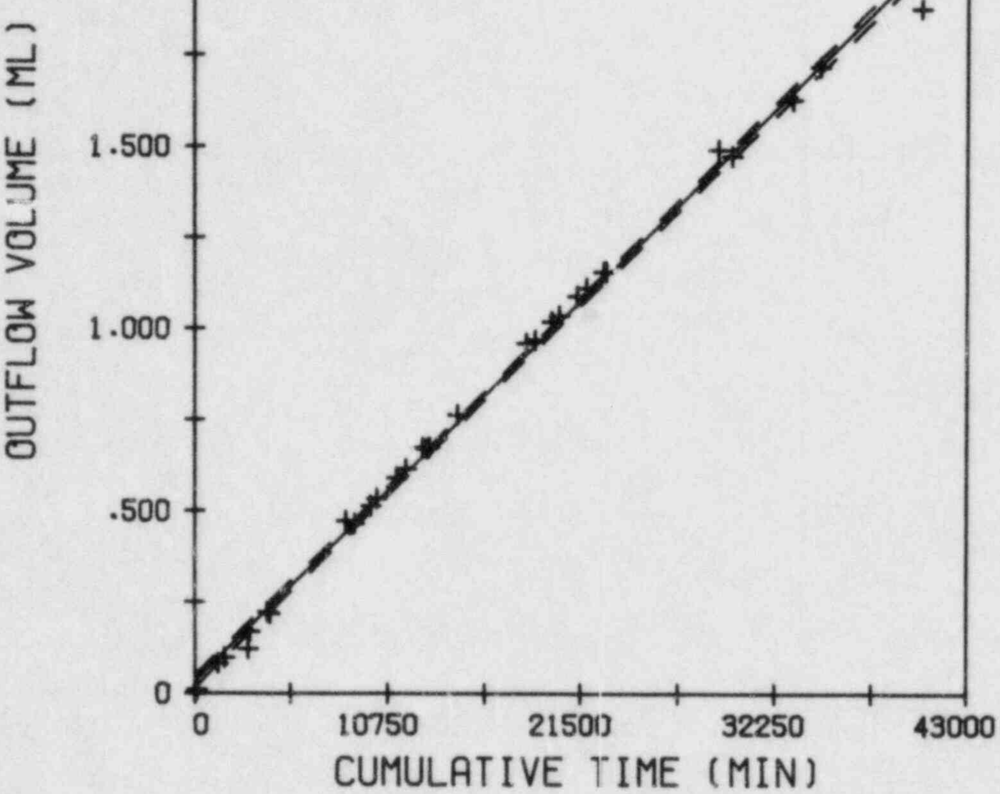

Figure 6.34 Water outflow vs. time for sample SC-2 at 49 - 50°C and 2.0 MPa (290 psi) injecting pressure.

+ : volume of water at given time (measurements)

———————— : best-fit straight line

- - - - - - - - : 95% confidence interval

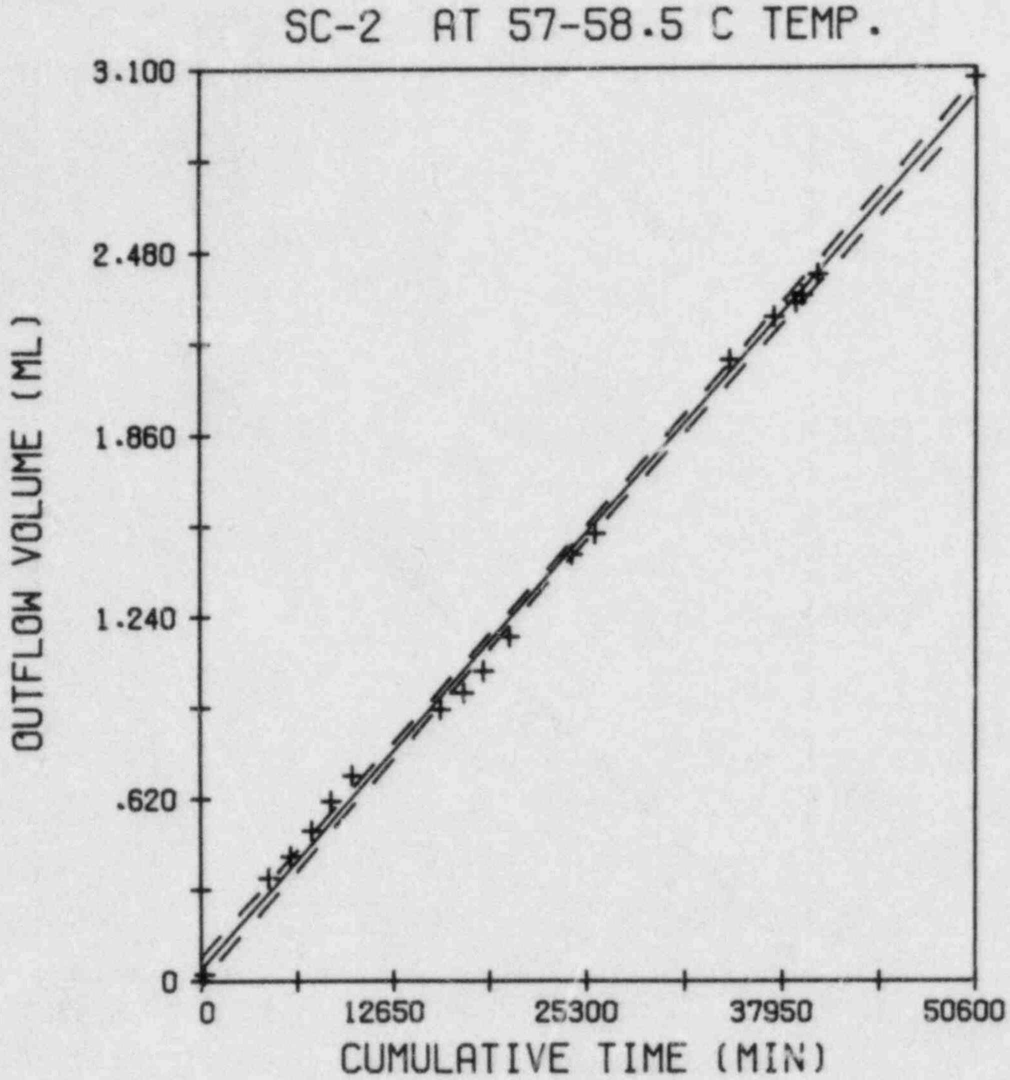

Figure 6.35 Water outflow vs. time for sample SC-2 at 57 - 58.5°C and 2.0 MPa (290 psi) injecting pressure.

+ : volume of water at given time (measurements)

———————— : best-fit straight line

- - - - - - - - : 95% confidence interval

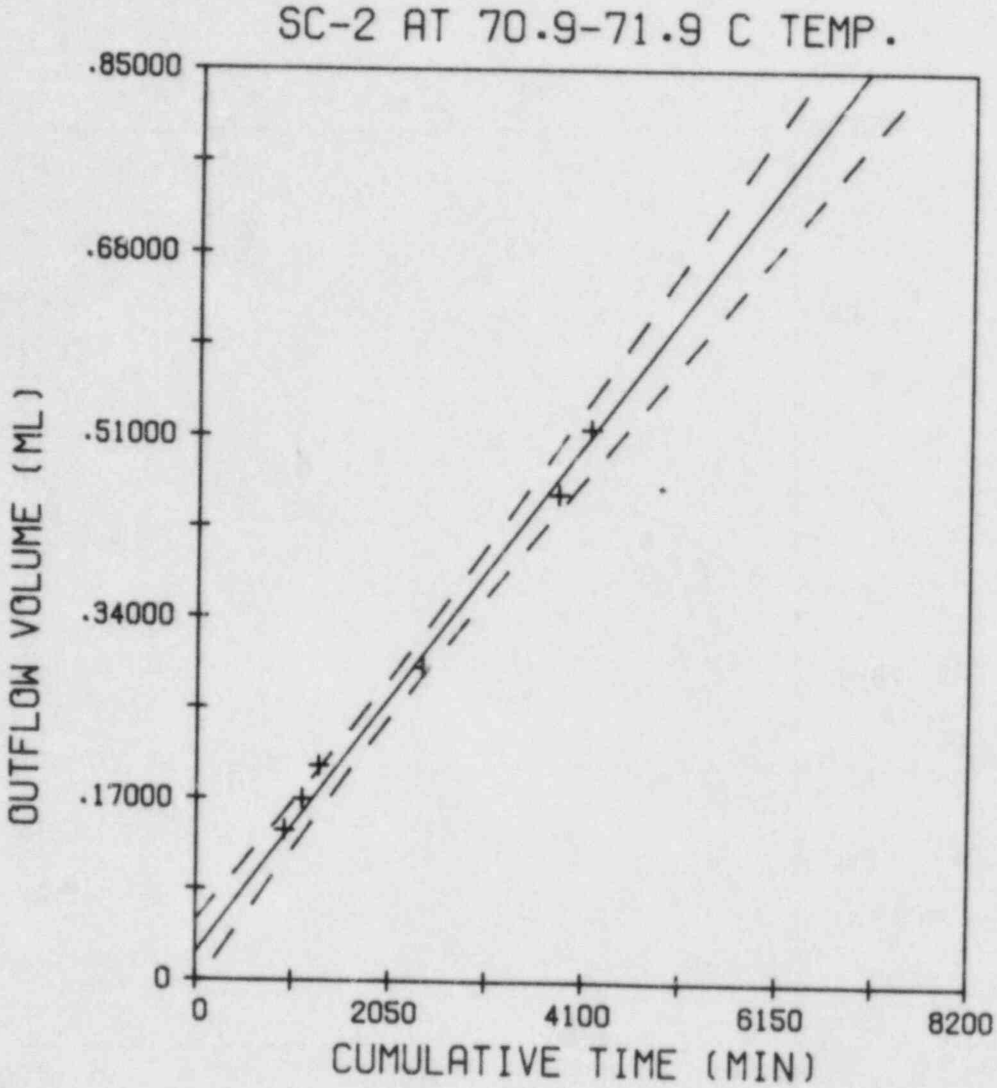

Figure 6.36 Water outflow vs. time for sample SC-2 at 70.9 - 71.9°C and 2.0 MPa (290 psi) injecting pressure.

+ : volume of water at given time (measurements)

———————— : best-fit straight line

- - - - - - - : 95% confidence interval

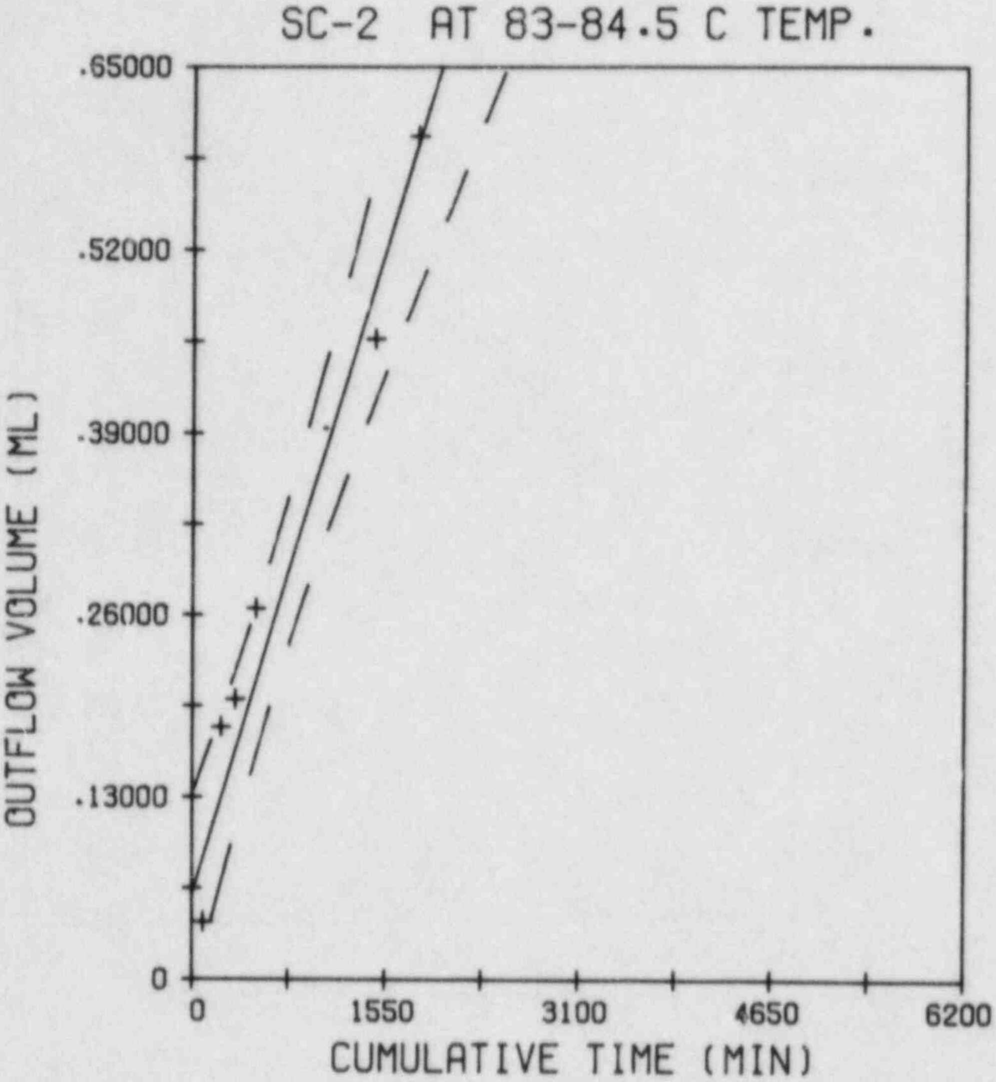

Figure 6.37 Water outflow vs. time for sample SC-2 at 83 - 84°C and 2.0 MPa (290 psi) injecting pressure.

+ : volume of water at given time (measurements)

———————— : best-fit straight line

- - - - - - - - : 95% confidence interval

Table 6.13. Data obtained from sample SC-2 at 40-43°C (104-109°F) abd injecting pressure of 3.35 MPa (486 psi). (γ = 9.7218 KN/m^3, $\mu = 0.6318 \times 10^{-3}$ $N \cdot sec/m^2$, L = 10.67 cm)

Cumulative Volume (cc)	Cumulative Time (min)	°C at Thermocouples Bottom TC1	TC2	Top TC3 & TC4	Injection Pressure (MPa)
0.105	10555	40.1	40.1	42.6	3.35
0.130	11575	40.9	40.1	42.8	"
0.168	11815	41.5	41.1	43.2	"
0.186	12085	41.5	41.2	43.3	"
0.252	13255	41.9	41.6	43.7	"
0.280	13375	42.2	41.8	43.9	"
0.285	13555	42.1	41.8	43.9	"
0.350	16045	41.7	41.3	43.6	"
0.380	17335	41.5	41.1	43.5	"
0.390	17470	41.6	41.2	43.5	"
0.398	17515	41.6	41.2	43.5	"
0.430	17755	41.8	41.4	43.7	"
0.450	18775	41.8	41.4	43.6	"
0.500	19300	42.1	41.8	43.9	"
0.510	20185	41.9	41.5	43.7	"
0.534	20500	42.0	41.7	43.9	"
0.540	20590	42.1	41.7	43.9	"
0.560	21553	42.0	41.7	43.9	"
0.560	21643	42.0	41.6	43.8	"
0.575	21823	42.1	41.7	43.8	"
0.590	21883	42.1	41.8	43.9	"
0.620	22243	42.3	42.0	44.1	"
0.660	23113	42.8	41.9	43.9	"
0.690	23383	42.4	42.1	44.2	"
0.775	25963	41.7	41.3	43.6	"
0.830	26443	42.1	41.7	43.8	"
0.863	27403	42.0	41.7	43.7	"
0.875	27583	42.1	41.8	43.9	"
0.898	27853	42.3	41.9	44.0	"

Table 6.14 Data obtained from sample SC-2 at 49-50°C (120-122°F) and Injecting Pressure of 2.0 MPa (290 psi). (γ = 9.629 KN/m^3, μ = 0.547 x 10^{-3} N·sec/m^2, L = 10.67)

Volume Through the Cement (cc)	Cumulative Time (min)	Temperature (°C) at Thermocouples Bottom TC1	TC2	Top TC3	TC4
0	0	49.4	49.6	49.8	49.8
0.01	100	49.4	49.6	49.8	49.9
0.083	1294	49.4	49.6	49.8	49.9
0.082	1388	49.4	49.6	49.8	49.8
0.099	1682	49.4	49.7	50.0	50.1
0.123	3004	49.4	49.6	49.8	49.9
0.170	3109	49.4	49.6	49.9	49.9
0.223	4080	49.3	49.5	49.7	49.7
0.220	4224	49.3	49.5	49.7	49.8
0.473	8400	49.4	49.6	49.7	49.8
0.466	8884	49.4	49.6	49.8	49.9
0.514	9822	49.4	49.6	49.7	49.8
0.535	10,176	49.4	49.6	49.8	49.8
0.535	10,254	49.4	49.6	49.8	49.8
0.592	11,257	49.3	49.5	49.6	49.7
0.616	11,778	49.4	49.6	49.8	49.8
0.674	12,704	49.4	49.5	49.6	49.7
0.672	12,944	49.5	49.6	49.8	49.8
0.675	13,074	49.5	49.6	49.8	49.8
0.765	14,629	49.5	49.7	49.9	49.9
0.960	18,504	49.4	49.5	49.7	49.7
0.970	18,974	49.5	49.7	49.8	49.8
1.02	19,884	49.4	49.5	49.6	49.6
1.036	20,334	49.4	49.7	49.8	49.9
1.089	21,319	49.4	49.6	49.7	49.7
1.112	21,839	49.5	49.8	49.8	49.8
1.155	22,782	49.3	49.4	49.7	49.7
1.156	22,926	49.4	49.7	49.8	49.8
1.489	29,109	49.5	49.6	49.8	49.8
1.472	29,874	49.3	49.5	49.7	49.7

Table 6.14 Data obtained from sample SC-2 at 49-50°C (120-122°F) and Injecting Pressure of 2.0 MPa (290 psi). (γ = 9.629 KN/m^3, μ = 0.547 x 10^{-3} N·sec/m^2, L = 10.67)--Continued

Volume Through the Cement (cc)	Cumulative Time (min)	Temperature (°C) at Thermocouples Bottom TC1	TC2	Top TC3	TC4
1.625	33,249	49.4	49.6	49.7	49.8
1.715	34,764	49.4	49.6	49.7	49.8
1.875	40,464	49.4	49.5	49.7	49.7
2.041	41,489	49.3	49.5	49.6	49.7
2.114	42,954	49.4	49.5	49.7	49.7

Table 6.15 Data obtained from sample SC-2 at 57-58.5°C (135-137°F) and Injecting Pressure of 2.0 MPa (290 psi). (γ = 9.6514 KN/m^3, $\mu = 0.4822 \times 10^{-3}$ $N \cdot sec/m^2$, L = 10.67)

Outflow Volume (cc)	Cumulative Time (min)	Temperature (°C) at Thermocouples				Ambient Temp. (°C)
		Bottom		Top		
		TC1	TC2	TC3	TC4	
0		57.7	57.9	58.1	58.1	21.9
0.023	223	57.6	57.8	58.0	58.0	22.5
0.352	4457	57.5	57.7	57.9	57.9	22.2
0.425	5867	57.7	58.1	58.2	58.2	22.0
0.513	7257	57.5	58.0	58.0	58.0	21.6
0.614	8563	57.4	57.8	57.6	57.8	-
0.700	10,008	57.5	58.8	57.9	57.9	-
0.926	15,811	57.5	57.8	57.8	57.9	22.4
0.983	17,347	57.6	57.9	58.0	58.0	22.4
1.057	18,619	57.6	58.6	58.0	58.0	22.0
1.174	20,333	57.6	59.6	58.0	58.0	22.8
1.453	24,400	57.5	60.1	57.9	57.9	21.4
1.523	25,857	57.6	57.8	58.0	58.0	23.0
2.111	34,504	57.7	57.9	58.1	58.1	22.9
2.256	37,397	57.8	58.0	58.2	58.2	23.2
2.303	38,829	57.6	58.0	58.2	58.2	23.5
2.328	39,252	57.8	58.0	58.2	58.2	24.0
2.399	40,267	57.9	57.9	58.1	58.2	23.2
3.067	50,510	57.6	57.8	58.0	58.1	22.4

Table 6.16 Data obtained from sample SC-2 at 70.9-71.9°C (160-161°F) and Injecting Pressure of 2.0 MPa (290 psi). (γ = 9.589 KN/m^3, $\mu = 0.404 \times 10^{-3}$ $N \cdot sec/m^2$, L = 10.67)

Outflow Volume (cc)	Cumulative Time (min)	Temperature (°C) at Thermocouples Bottom TC1	TC2	Top TC3	TC4	Ambient Temp. (°C)
0		70.9	71.2	71.6	71.6	22.4
0.141	945	70.9	71.2	71.5	71.6	22.3
0.170	1130	70.9	71.2	71.5	71.6	22.9
0.201	1307	71.0	71.3	71.5	71.7	23.4
0.294	2400	71.0	71.3	71.6	71.7	23.2
0.456	3822	71.0	71.3	71.6	71.7	23.2
0.517	4150	71.1	71.4	71.7	71.8	23.7
0.548	4320	71.1	71.5	71.8	71.9	23.6
0.838	8156	71.0	71.4	71.6	71.6	23.1

Table 6.17 Data obtained from sample SC-2 at 83-84.5°C (181-184°F) and Injecting Pressure of 2.0 MPa (290 psi). (γ = 9.5044 KN/m^3, μ = 0.3384 x 10^{-3} N·sec/m^2, L = 10.67)

Outflow Volume (cc)	Cumulative Time (min)	Temperature (°C) at Thermocouples: Bottom TC1	Bottom TC2	Top TC3	Top TC4	Ambient Temp. (°C)
0	0	83.2	83.5	83.9	84.0	23
0.041	90	83.2	83.6	84.0	84.1	23.2
0.180	228	83.3	83.6	84.1	84.1	23.5
0.200	344	83.3	83.7	84.1	84.2	23.8
0.265	510	83.5	83.9	84.3	84.4	23.7
0.457	1460	83.3	83.7	84.1	84.1	23.8
0.601	1800	83.4	83.8	84.2	84.3	24.1

Table 6.18 Results for Sample SC-2 at Ambient and Elevated Temperatures (Linear Regression Forced through the Origin)

Temperature of Cement °C (°F)	Injecting Pressure MPa (psi)	Flowrate cc/min	R^2	Hydraulic Conductivity cm/min	95% Confidence Interval cc/min	Instrinsic Permeability cm^2 (Darcy)
22 ± 2 (71 ± 3.8)	0.41 - 0.55 (60 - 80)	28.123×10^{-6}	.978	12.07×10^{-9}	26.356×10^{-6} - 29.891×10^{-6}	1969×10^{-18} (199.5×10^{-9})
22 ± 2 (71 ± 3.8)	0.66 - 0.69 (95 - 100)	26.019×10^{-6}	.961	8.001×10^{-9}	24.357×10^{-6} - 27.68×10^{-6}	1305×10^{-18} (132.3×10^{-9})
40 - 43 (104 - 109)	1.15 (167)	8.162×10^{-6}	.870	1.453×10^{-9}	7.127×10^{-6} - 9.196×10^{-6}	157.4×10^{-18} (15.94×10^{-9})
40 - 43 (104 - 109)	3.35 (486)	26.731×10^{-6}	.971	1.634×10^{-9}	24.955×10^{-6} - 28.507×10^{-6}	176.9×10^{-18} (17.93×10^{-9})
49 - 50 (120 - 122)	2.0 (290)	49.764×10^{-6}	.998	5.077×10^{-9}	49.156×10^{-6} - 50.373×10^{-6}	477.7×10^{-18} (48.40×10^{-9})
49 - 55 (120 - 131)	0.75 (109)	13.80×10^{-6}	.977	3.75×10^{-9}	13.558×10^{-6} - 14.245×10^{-6}	342.8×10^{-18} (34.73×10^{-9})
57 - 58.5 (135 - 137)	2.0 (290)	59.977×10^{-6}	.999	6.095×10^{-9}	58.956×10^{-6} - 60.00×10^{-6}	507.5×10^{-18} (51.42×10^{-9})
70.9 - 71.9 (160 - 161)	2.0 (290)	113.573×10^{-6}	.988	11.47×10^{-9}	103.393×10^{-6} - 123.753×10^{-6}	805.2×10^{-18} (81.58×10^{-9})
83 - 84.5 (181 - 184)	2.0 (290)	343.831×10^{-6}	.962	34.41×10^{-9}	275.125×10^{-6} - 412.547×10^{-6}	2042×10^{-18} (206.9×10^{-9})

Table 6.19 Results for Sample SC-2 at Ambient and Elevated Temperatures (Best Fit Line)

Temperature of Cement °C (°F)	Injecting Pressure MPa (psi)	Flowrate cc/min	Hydraulic Conductivity cm/min	Instrinsic Permeability cm^2 (Darcy)
22 ± 2 (71 ± 3.8)	0.41 - 0.55 (60 - 80)	32.6×10^{-6}	13.99×10^{-9}	2283×10^{-18} (231.3×10^{-9})
22 ± 2 (71 ± 3.8)	0.66 - 0.69 (95 - 100)	25.9×10^{-6}	7.941×10^{-9}	1296×10^{-18} (131.3×10^{-9})
40 - 43 (104 - 109)	1.15 (167)	6.498×10^{-6}	1.157×10^{-9}	125.3×10^{-18} (12.69×10^{-9})
40 - 43 (104 - 109)	3.35 (486)	43.79×10^{-6}	2.676×10^{-9}	289.8×10^{-18} (29.37×10^{-9})
49 - 55 (120 - 131)	0.75 (109)	12.31×10^{-6}	3.346×10^{-9}	305.8×10^{-18} (30.98×10^{-9})
49 - 50 (120 - 122)	2.0 (290)	48.46×10^{-6}	4.944×10^{-9}	465.2×10^{-18} (47.13×10^{-9})
57 - 58 (135 - 137)	2.0 (290)	58.77×10^{-6}	5.972×10^{-9}	497.3×10^{-18} (50.38×10^{-9})
70.9 - 71.9 (160 - 161)	2.0 (290)	102.8×10^{-6}	10.38×10^{-9}	728.8×10^{-18} (73.84×10^{-9})
83 - 84.5 (181 - 184)	2.0 (290)	297.4×10^{-6}	29.76×10^{-9}	1766×10^{-18} (178.9×10^{-9})

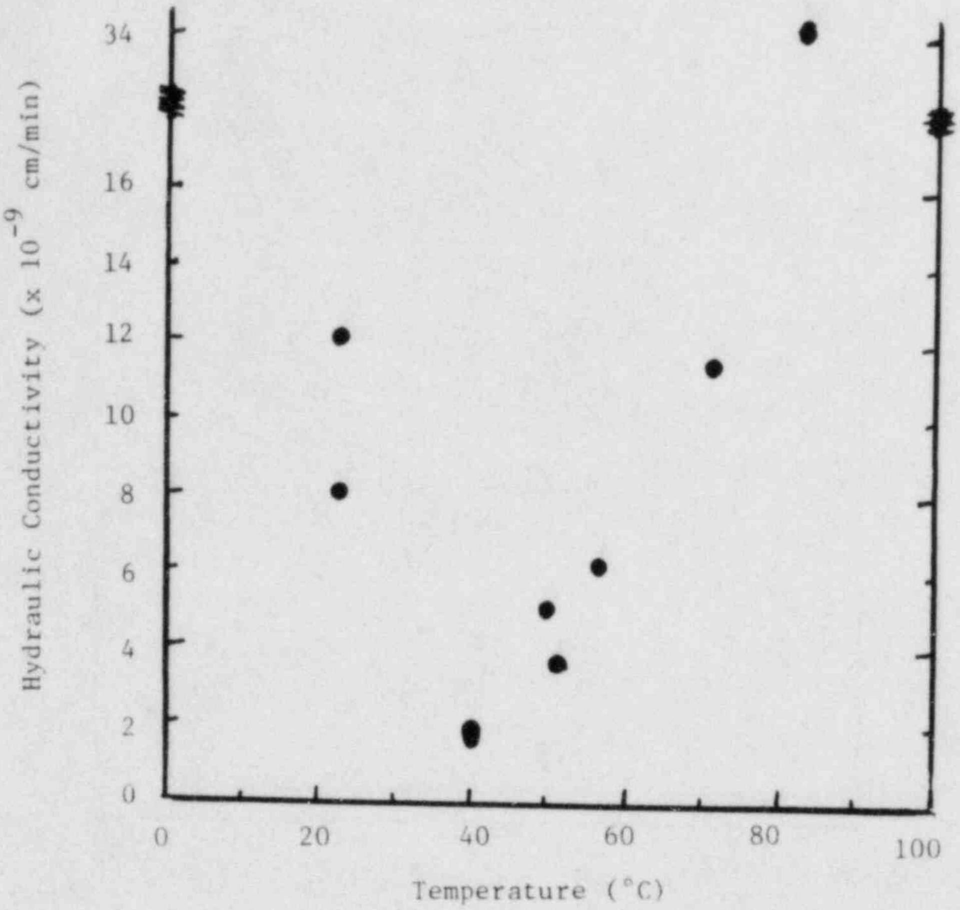

Figure 6.38 Hydraulic conductivity vs. temperature for sample SC-2. (Data at 21°C are probably incorrect, too high.)

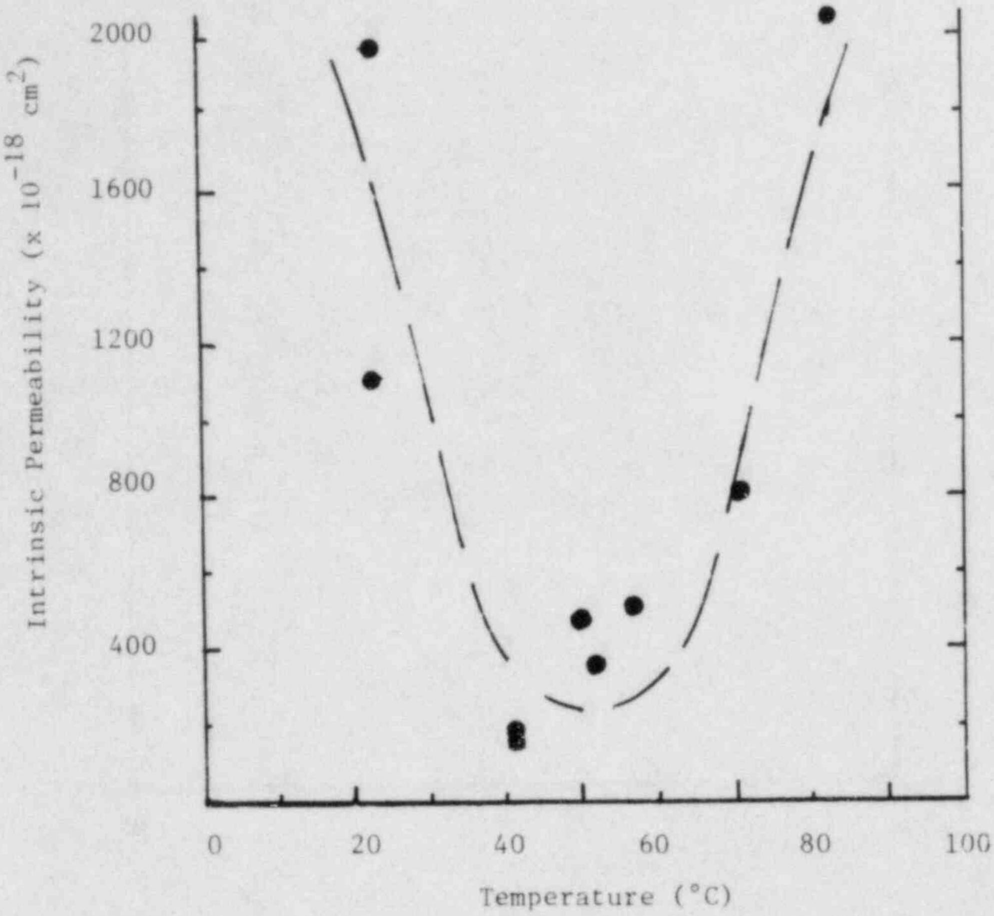

Figure 6.39 Intrinsic permeability vs. temperature for cement plug SC-2. (Data shown at 21°C are probably incorrect, too high.)

flow, however, is dominant throughout all tests. Hydraulic conductivity computed for this sample, with flow in direction of gravity forces, is 2.309×10^{-9} cm/min, which is lower than the values obtained for the plug SC-2 at ambient temperature. This could be due to time-dependency of the plug itself. Flow testing against the gravity forces exhibited an even lower flow (9.49×10^{-10} cm/min). More tests are needed to verify this fact. Figures 6.40 and 6.41 illustrates the plot of outflow volume vs. cumulative time for this plug (Tables 6.20 through 6.23).

6.6 Discussion

Studying the flow through cement plugs is very complex because of the time-dependency of cement itself (during saturation). Negative flow and low flowrates complicate the study of performance of fresh plugs at ambient temperatures. However, temperature seems to increase the permeabilities of both dry and fresh plugs; this increases the accuracy of the testing.

Dry cement plugs exhibit higher flows than the fresh plugs. Cement shrinkage and cracks due to dehydration of the cement may be major factors for the high flows. It is thought drying and consequent shrinkage provide the injected water with a low resistance pathway along the steel/plug interface. Improvement in the water flow (with time) has been noted in this research and by others (Daemen et al., 1983, p. 147). During push-out tests of cement plugs in rock boreholes the shrinkage of dry plugs in rock boreholes also has been reported. Many dry plugs can be easily pushed out by the pressure of a finger (Daemen et al., 1983, pp. 223-224). Conclusions drawn from this study are compatible with these observations.

Fresh plugs have very low permeability at ambient temperatures (22 ± 2°C or 71 ± 3.8°F). The low flows can easily be affected by environmental factors such as evaporation rate in the laboratory or variations of atmospheric pressure. Evaporation can be accounted for in calculations involved in flow studies. Negative flow induced by variations of atmospheric pressure is a dominant factor in the decrease in accuracy of experiments conducted at ambient temperatures and injecting pressure of less than 2.0 MPa (300 psi). The problem of negative flow can be alleviated by increasing the injecting pressure. However, the increase in the pressure has its own disadvantage: Injected water with pressures higher than the strength of individual grains (α bonding strength) of cement can cause displacements and permanent opening of pores, which in turn, induces higher permeabilities.

The hydraulic conductivity obtained by South (1983, pp. 71-73) for cement plug system 1 is in the order of 6.0×10^{-9} cm/min. He tested a cement cylinder with 3.80 cm in diameter and 3.35 cm in length in a Ruska liquid permeameter (at 1 atm. and ambient temperature of 21 ± 2°C). Adisoma and Daemen (1985) report values of 1×10^{-9} to 7×10^{-9} darcy for the intrinsic permeabilities.

The results obtained by this study confirm values obtained by others (all in the order of 10^{-9} cc/min or 10^{-9} darcy for fresh plugs). Long-

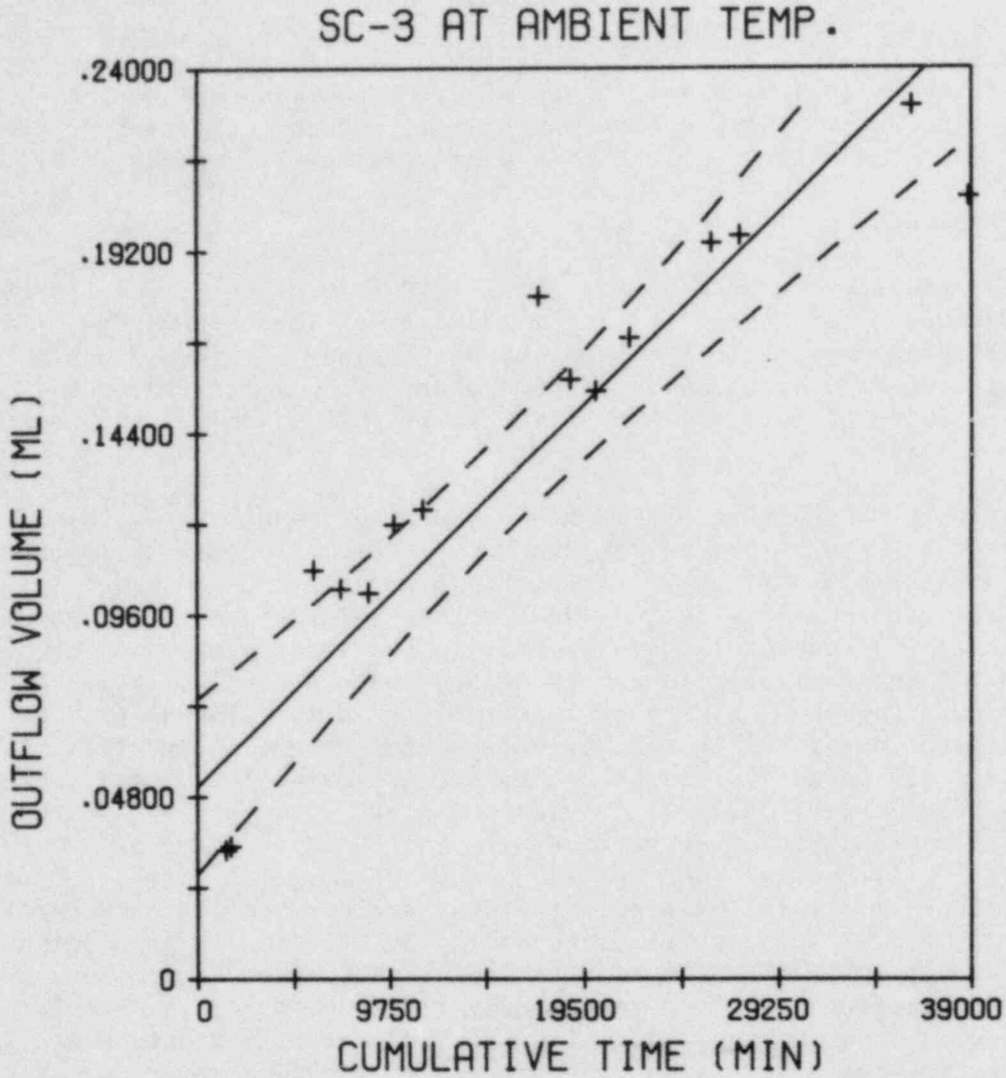

Figure 6.40 Water outflow vs. time for sample SC-3 at ambient temperature and 2.0 MPa (290 psi) injecting pressure.

+ : volume of water at given time (measurements)

———————— : best-fit straight line

- - - - - - - : 95% confidence interval

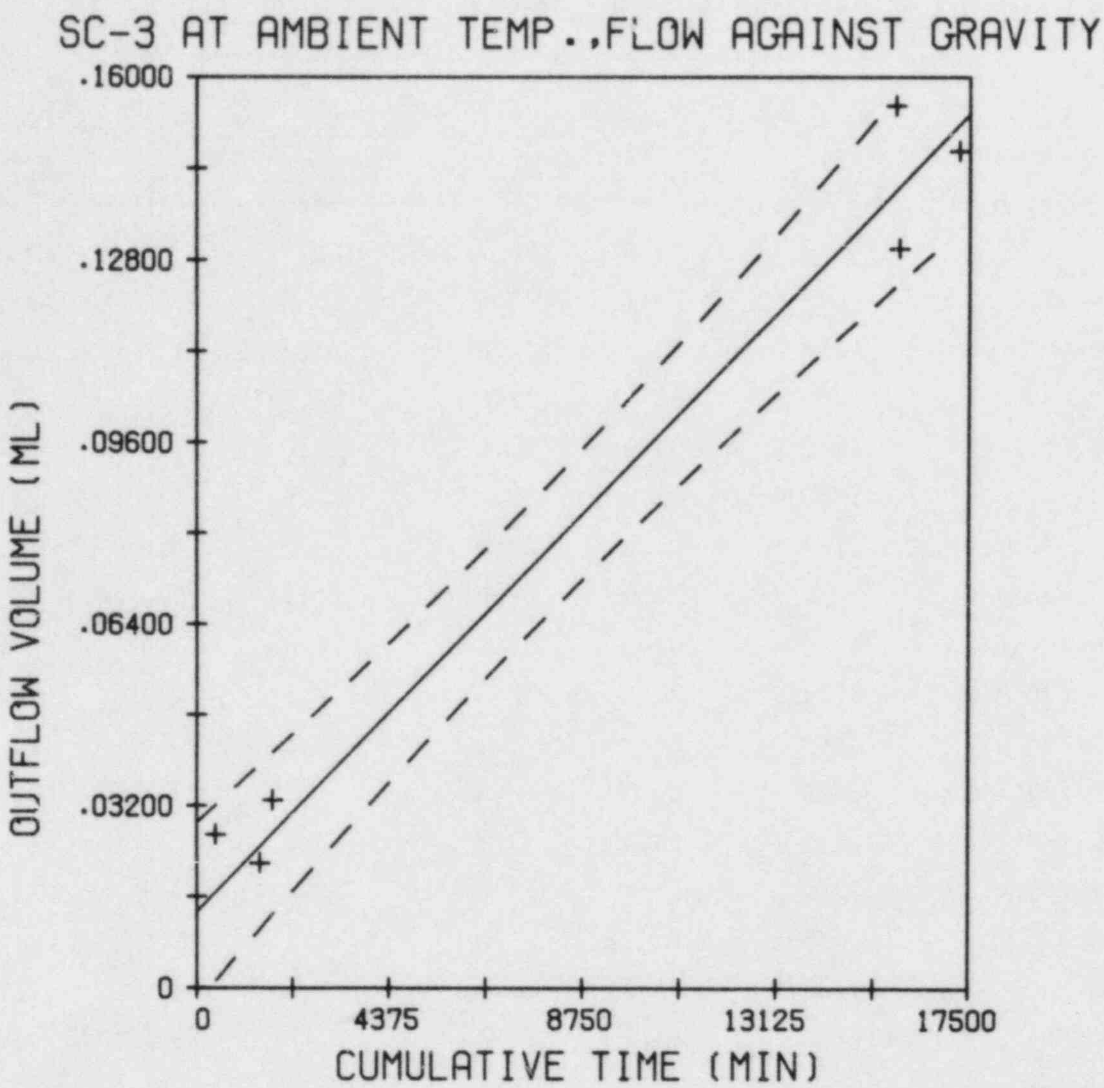

Figure 6.41 Water outflow vs. time for sample SC-3 at ambient temperature and 2.0 MPa (290 psi) injecting pressure. "Flow is against the gravity force."

+ : volume of water at given time (measurements)

———————— : best-fit straight line

- - - - - - - : 95% confidence interval

Table 6.20 Data Obtained from Sample SC-3 at Ambient Temperature (22 ± 2°C or 71 ± 3.8°F) and Injecting Pressure of 2.0 MPa (290 psi). (γ = 9.7842 KN/m^3, μ = 0.9578 x 10^{-3} $N \cdot sec/m^2$, L = 9.94)

Outflow Volume (cc)	Cumulative Time (min)	Temperature (°C) at Thermocouples Bottom TC1	TC2	Top TC3	TC4	Ambient Temp. (°C)
0	0	22.7	22.7	22.7	23.4	23.8
0.01	95	23.1	23.1	23.0	23.3	23.3
0.048	1288	22.6	22.6	22.5	22.9	22.7
0.049	1383	22.8	22.8	22.7	23.0	22.9
0.06	1680	23.0	23.0	22.8	22.8	22.7
0.108	3000	22.9	22.8	22.9	22.9	22.9
0.106	3117	23.0	23.0	23.0	23.2	23.1
0.128	4080	22.0	22.0	21.9	22.3	22.5
0.120	4220	22.3	22.3	22.3	22.6	22.5
0.270	8394	22.2	22.2	22.1	22.4	22.3
0.264	8882	23.2	23.1	23.1	23.4	23.4
0.279	9822	23.3	22.2	22.2	22.7	22.8
0.299	10,175	23.0	23.0	23.0	23.1	23.2
0.299	10,250	23.1	23.1	23.1	23.3	23.2
0.325	11,255	22.2	22.2	22.2	22.6	22.8
0.340	11,773	22.8	22.8	22.7	22.8	22.4
0.364	12,702	22.7	22.7	22.7	23.2	23.1
0.374	12,942	23.6	23.6	23.6	23.8	23.7
0.377	13,070	23.7	23.7	23.7	24.1	24.1
0.430	14,628	23.5	23.5	23.5	23.4	23.0
0.523	18,500	23.0	23.0	23.0	23.6	23.5
0.511	18,971	23.3	23.3	23.3	23.5	23.0
0.53	19,883	22.7	22.6	22.7	23.3	23.1
0.533	20,330	22.8	22.8	22.8	22.9	22.4
0.548	21,317	21.7	21.7	21.6	21.9	21.6
0.565	21,857	22.8	22.8	22.7	22.9	22.6
0.570	22,780	21.9	21.9	21.9	21.9	22.8
0.573	22,922	22.4	22.4	22.3	22.6	22.2
0.726	29,105	22.5	22.5	22.5	22.6	22.2

Table 6.20 Data Obtained from Sample SC-3 at Ambient Temperature (22 ± 2°C or 71 ± 3.8°F) and Injecting Pressure of 2.0 MPa (290 psi). (γ = 9.7842 KN/m^3, $\mu = 0.9578 \times 10^{-3}$ $N \cdot sec/m^2$, L = 9.94)--Continued

Outflow Volume (cc)	Cumulative Time (min)	Temperature (°C) at Thermocouples Bottom TC1	TC2	Top TC3	TC4	Ambient Temp. (°C)
0.683	29,870	21.8	21.8	21.7	21.9	21.5
0.763	33,245	22.4	22.4	22.4	22.6	22.1
0.756	34,825	22.5	22.5	22.4	22.7	22.4
0.907	41,495	21.7	21.7	21.6	21.5	21.6
0.881	42,950	21.7	21.7	21.6	22.1	21.7

Table 6.21 Data Obtained from Sample SC-3 at Ambient Temperature (22 ± 2°C or 71 ± 3.8°F) and Injecting Pressure of 2.0 MPa (290 psi). (γ = 9.7842 KN/m^3, μ = 0.9578 x 10^{-3} $N \cdot sec/m^2$, L = 9.94)

Outflow Volume (cc)	Cumulative Time (min)	Temperature (°C) at Thermocouples				Ambient Temp. (°C)
		Bottom		Top		
		TC1	TC2	TC3	TC4	
0	0	22.9	22.9	22.9	23.1	23.5
0.027	427	23.7	23.7	23.7	23.7	24.0
0.022	1440	22.9	22.9	22.9	22.8	23.2
0.033	1730	23.5	23.5	23.5	23.4	23.6
0.186	11,686	22.4	22.4	22.3	22.4	22.5
0.155	15,835	22.2	21.9	21.9	21.9	22.2
0.130	15,910	22.4	22.4	22.3	22.3	22.1
0.147	17,273	22.4	22.3	22.3	22.3	22.5

Table 6.22 Results for Sample SC-3 at Ambient Temperatures (Linear Regression Forced through the Origin)

Temperature of Cement °C (°F)	Injecting Pressure MPa (psi)	Flowrate cc/min	R^2	Hydraulic Conductivity cm/min	95% Confidence Interval cc/min	Instrinsic Permeability cm^2 (Darcy)
22 ± 2 (71 ± 3.8)	2.0 (290)	24.064×10^{-6}	.986	2.309×10^{-9}	23.059×10^{-6} - 25.069×10^{-6}	376.8×10^{-18} (38.17×10^{-9})
22 ± 2 (71 ± 3.8)	2.0* 290	9.889×10^{-6}	.926	$.949 \times 10^{-9}$ -	9.436×10^{-6} - 12.342×10^{-6}	154.8×10^{-18} 15.69×10^{-9}

*Flow against gravity.

Table 6.23 Results for Sample SC-3 at Ambient Temperatures (Best Fit Line)

Temperature of Cement °C (°F)	Injecting Pressure MPa (psi)	Flowrate cc/min	Hydraulic Conductivity cm/min	Instrinsic Permeability cm^2 (Darcy)
22 ± 2 (71 ± 3.8)	2.0 (290)	21.46×10^{-6}	2.059×10^{-9}	336×10^{-18} (34.04×10^{-9})
22 ± 2 (71 ± 3.8)	2.0* (290)	8.683×10^{-6}	0.833×10^{-9}	136×10^{-18} (13.77×10^{-9})

*Flow against gravity.

term tests have shown that the plug behavior is time-dependent. As the plug ages (while being saturated), it becomes less permeable. The increase in the flow through fresh plugs with increasing temperature is another conclusion that might be drawn. By studying the thermal expansion coefficients of stainless steel (304) and neat cement (respectively 9.6×10^{-6} in/in/°F and 10.3×10^{-6} in/in/°F between 32-212°F) one can conclude that the increase in flowrate with temperature does not result from widening of the gap between two media (Neville, 1981, p. 492; Inco, 1968, pp. 44-47). However, it is essential to study the effect of differential thermal expansion on cement/steel interface by means of a strain gage. The increasing trend of permeability is thought to be modeled by a power (nonlinear) relation.

The study of permeability when the injected water flows against gravity is another experiment initiated. However, more testing is needed to draw conclusions. The value obtained from this type of model shows an even smaller hydraulic conductivity for the cement plug. However, there are some doubts whether to relate this lower hydraulic conductivity to gravity or to the time dependency of the cement itself.

The last comment to be made is the question of whether or not heating can induce a permanent increase in flowrate of cement plugs (permanent deterioration). Future research should answer this question.

6.7 Future Work

Studying the behavior of cement plugs at "steady-state" conditions requires long-term tests. The plugs being studied need to be saturated. The transient pulse method is an attempt to overcome the time limitations. This test is much faster and gives more results for hydraulic behavior of cement plugs. This method not only gives the hydraulic conductivity but also the specific storage of the cement plug.

A transient pulse chamber has been constructed at the University of Arizona Machine Shop. Sealing problems in the system need to be remedied before testing can start.

The construction of a water bath capable of holding and heating two samples with diameters of 15.24 cm (6 in) and lengths of 30.48 cm (1 in) is completed. Electrical installations for the laboratory remain to be completed. The control panel, monitoring gages, and pressurizing system in conjunction with the water path are ready for operation.

Two more cement permeameters are under construction. Many cement plugs have been cured in mild steel, and will be tested to study the influence of cement-steel liner interaction on flowrates.

A radial permeameter (South, 1983, p. 77) has been loaded with a Pomona basalt core with a rock bridge. The rock is under constant water pressure for saturation. Obtaining the hydraulic conductivity of basalt rock is to establish a datum for evaluation of performance of cement plugs.

6.8 Conclusions

The application of cement permeameters to study the hydraulic behavior of cement plugs has been successful. Dry plugs exhibit larger hydraulic conductivities than fresh plugs. Negative flow and evaporation are two environmental factors that reduce the accuracy of flow tests of fresh plugs. Fresh plugs seem to permit more water to pass through them when being heated. More tests are needed to draw more definite conclusions.

6.9 References

Adisoma, G. and J.J.K. Daemen, 1985, "The Effect of Dynamic Loading on Cement Borehole Plug Performance," Topical Report, Prepared for Division of Health, Siting and Waste Management, U.S. Nuclear Regulatory Commission, by the Department of Mining and Geological Engineering, University of Arizona, Tucson.

American Petroleum Institute, 1977, APF Standard No. RP-10B.

Daemen, J.J.K., J.C. Stormont, N.I. Colburn, D.L. South, S.A. Dischler, K. Fuenkajorn, W.B. Greer, G.S. Adisoma, D.E. Miles, B. Kousari, and J. Bertuca, 1983, "Rock Mass Sealing - Experimental Assessment of Borehole Plug Performance, Annual Report, June 1982 - May 1983," NUREG/CR-3473, Prepared for Division of Health, Siting and Waste Management, U.S. Nuclear Regulatory Commission, by the Department of Mining and Geological Engineering, University of Arizona, Tucson.

Davis, S.W. and R. DeWiest, 1966, Hydrogeology, John Wiley & Sons, New York, 463 pp.

Freeze, R.A. and J.A. Cherry, 1979, Groundwater, Prentice-Hall, Inc., Englewood, NJ, 604 pp.

INCO, 1968, Properties of Some Metals and Alloys, The International Nickel Company, Inc., New York.

Neville, A.M., 1981, Properties of Concrete, Pitman, London, 779 pp.

South, D.L., 1983, "Laboratory Studies of Fluid Flow through Borehole Seals", Ph.D. Dissertation, University of Arizona, Tucson, Department of Mining and Geological Engineering.

Vennard, J.K. and R.L. Street, 1975, Elementary Fluid Mechanics, John Wiley & Sons, Inc., New York, 742 pp.

CHAPTER SEVEN

SIZE EFFECTS ON CEMENT BOREHOLE PLUG PERFORMANCE

7.1 Introduction

Most of the sealing studies performed as part of this contract have been performed on relatively small diameter boreholes (typically 1" to 4"). Because the properties of both rock and sealing materials (e.g. cement) are size-dependent, this introduces uncertainty in the extrapolation of the results to larger size plugs. An assessment of the uncertainty involved will be made on the basis of results obtained from experiments on larger diameter boreholes. To test sealing scale effects, the University of Arizona will be conducting laboratory permeability tests on boreholes in irregular blocks in order to test the influence of size effects on the performance of borehole seals. The boreholes in the blocks are available because they were drilled for core used in other tests.

Campbell-Allen et al. (1972) have studied the moisture loss of cement cured in metal discs with inside diameters of 2.54 cm (1 in), 5.08 cm (2 in), 10.16 cm (4 in), 15.24 cm (6 in) and 20.32 cm (8 in). Water-cement ratios of 0.4 - 0.8 were used in these metal discs. They concluded that any extrapolation from laboratory-sized specimens to concrete members up to 6 m thick becomes less reliable as measurements have to be continued over periods of some years even for specimens only 20 cm (7.87 in) thick. Therefore, it is reasonable to use test specimens with dimensions of the same order as the actual body or construction to be simulated. The main reason of the size effect studies is to try to make an extrapolation for more realistic field size borehole diameters, and possibly for large cement masses, as the problem becomes more significant when large masses of cement are used under conditions of elevated temperature.

All experimental work done to date on this contract has been on borehole plugs ranging from 2.54 to 10.16 cm (1 - 4 in) in diameter. The work described in this chapter involves the testing of blocks with borehole diameters of 15.80 - 19.69 cm (6.25 - 7.75 in). System 1 Cement* plugs with length to diameter ratios of 1.0 will be poured into these boreholes in order to determine whether larger borehole size will influence the sealing performance (the hydraulic conductivity) of the cement.

---

*Material specifications are given in Daemen et al. (1983, Chapter 7).

7.2 Rock Samples

The blocks are from the Pomona member of the Columbia Plateau Basalt. They have 15.80 - 19.69 cm (6.25 - 7.75 in) diameter holes remaining from the cores drilled out for other projects on this contract (Figures 7.1 and 7.2).

7.3 Cement Plug Preparation

20.32 cm (8 in) long System 1 cement plugs have been cured in a PVC pipe and in a borehole in a rock block. Both plugs have a diameter of 19.69 cm (7.75 in). The length of the PVC pipe is 54.61 cm (21.5 in). The block has a borehole length of 71.12 cm (28 in).

The cement has been poured into the PVC pipe on March 12, 1984, at a room temperature of 25°C (77°F) to gain some experience prior to pouring the cement into the rock sample having a similar diameter. On March 19, 1984, cement has been poured into the block borehole at a room temperature of 23.3°C (74°F).

The cement has been prepared by mixing 555 g of Ideal Type A Portland cement (from Tijeras Canyon, New Mexico), 249 ml of distilled water and 3 ml of D47 additive in a blender (according to API specification 10-B, API, 1977). Then, all mixes have been combined and mixed into one 4000 ml beaker, and poured into the PVC pipe and block borehole.

Water was poured on the cement plugs after six hours of curing to keep them saturated. After seven days of curing, a saturated sponge was placed underneath the cement plugs to prevent drying.

A 2.54 cm (1 in) thick PVC plate placed 11.43 cm (4.5 in) from the bottom of the PVC pipe and 8.83 cm (3.5 in) from the bottom of the block borehole supports the plug.

7.4 Cement Curing Temperature Measurements

The curing temperatures of the cement poured into the PVC pipe and into the block borehole have been measured by temperature transducers connected to a temperature indicator by means of wires. The 5-volt exciter (Part No. AAV-000-00) of the temperature indicator has been manufactured by Central Electronics, University Instrument Shop. The output connector (Part No. DM-4105) of the temperature indicator has been manufactured by Datel Intersil, Inc. The temperature indicators (LM 335A) have been manufactured by National Semiconductor, Inc. (Figure 7.3).

Three temperature sensing transducers are connected to a temperature indicator with wires through the center of the bottom PVC disc prior to pouring cement into the PVC pipe and the block borehole. The first transducer is located 2.54 cm (1 in) from the bottom of the PVC disc on the hole axis (the bottom transducer); the second one 2.54 cm (1 in) from the hole wall and 8.89 cm (3.5 in) from the bottom (the middle transducer); and the third one 10.16 cm (4 in) from the bottom on the hole axis (the top transducer).

Figure 7.1 Pomona basalt block with a 15.88 cm (6.25 in) diameter axial hole.

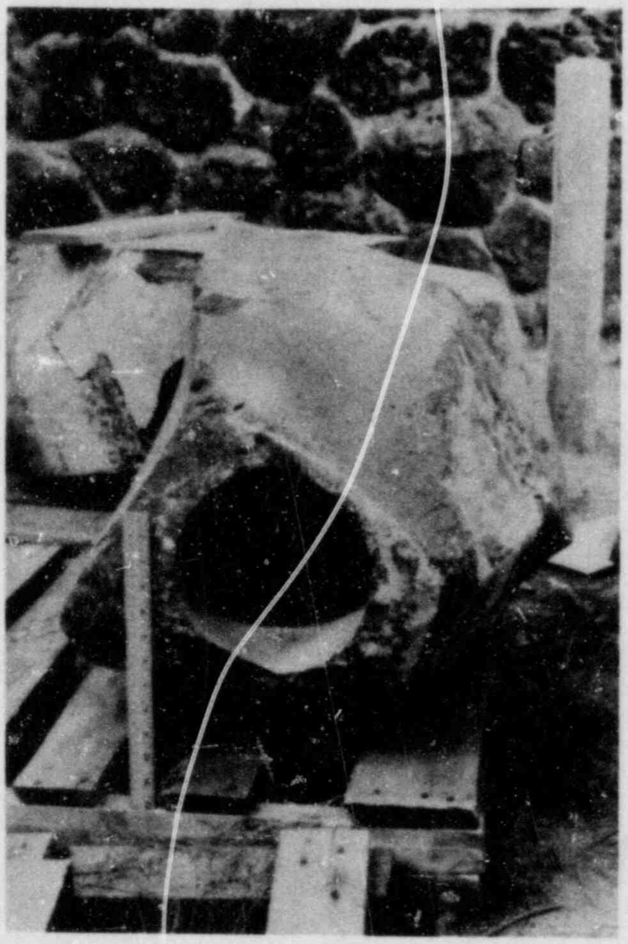

Figure 7.2 Pomona basalt block with a 19.69 cm (7.75 in) diameter axial hole.

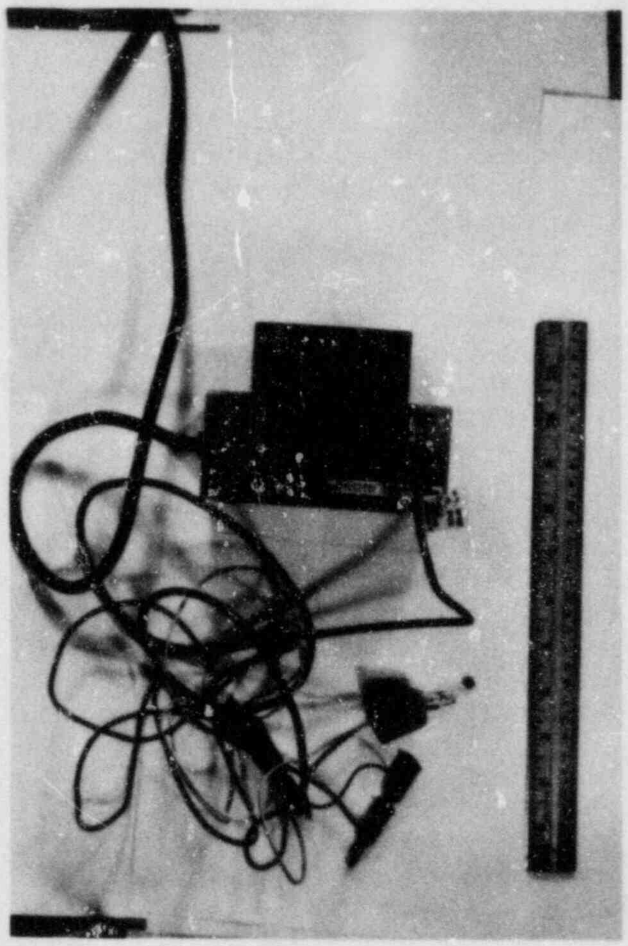

Figure 7.3 Temperature sensing transducers connected to a temperature indicator used to measure the curing temperature of cement.

The temperature transducers used to measure the curing temperature of cement in the PVC pipe have been calibrated in water at a room temperature of 25°C (77°F) and at 0°C. Those used in the block borehole have been calibrated in water at 0°C and at 96.8°C. A linear relation was assumed between true temperature and reading. Tables 7.1 and 7.2 show the calibration of digital readouts obtained from the transducers placed in the PVC pipe and the block borehole for cement curing temperature measurements.

Tables 7.3 and 7.4 show the temperatures measured by the bottom, middle and top transducers vs. the time (min) passed after the cement was poured into the PVC pipe and the block borehole. The highest curing temperatures (read by the top transducers) were 87.8°C (190°F) in the PVC pipe and 62.8°C (145°F) in the basalt borehole.

7.5 Permeability Tests

The objective of the permeability test is to determine experimentally the influence of larger plug size on hydraulic conductivity and indirectly to determine the effect of a more damaged hole wall possibly present in larger hole diameters.

7.5.1 Equipment and Laboratory Set-Up

The laboratory set-up for permeability tests is shown in Figures 7.4 and 7.5. The system consists of a nitrogen tank, a bladder accumulator, a pressure gage, a flowmeter, a packer, a steel frame, and an outflow collection system.

7.5.1.1 Bladder Accumulator

The bladder accumulator is used to maintain a constant water injection pressure up to 20.69 MPa (3000 psi) while injecting water through the cement plugs. It is a Hydrodyne VR 30-60 type, manufactured by EMG Accumulators, Inc., and has a water capacity of 1892.80 cc (2 pt) and gas volume of 938.22 cc (60 cu in).

7.5.1.2 Pressure Gage

The pressure gage used is a WIKA 213.40 type liquid filled gage with a diameter of 10.16 cm (4 in). It has a pressure rating of up to 4.14 MPa (600 psi). It measures the injection pressure coming from the bladder accumulator.

7.5.1.3 Flowmeters

The flowmeters used are Gilmont flowmeters, types K-3232-20 and K-3232-21. Type K-3232-20 can withstand pressures up to 4.14 MPa (600 psi) and has a flow rate between 0.002 - 1.1 cc/min. Type K-3232-21 has a pressure rating up to 3.45 MPa (500 psi) and a flow rate between 0.01 - 4.0 cc/min.

Table 7.1 Temperature Transducer Calibration. Assumed linear relation between temperature y and temperature indicator readout: $y = mx + b$.

Temperature Sensor	Freezing Water Temperature (y_1)	Digital Readout (x_1)	Room Temperature (y_2)	Digital Readout (x_2)	m °F/Unit x (°C/Unit x)	b °F (°C)
Bottom	32°F (0°C)	270.75	77°F (25°C)	294.6	1.887 (1.0482)	-478.8 (-283.8)
Middle	32°F (0°C)	269.45	77°F (25°C)	294.1	1.826 (1.0142)	-459.9 (-273.3)
Top	32°F (0°C)	268.85	77°F (25°C)	293.3	1.841 (1.023)	-462.8 (-274.9)

Table 7.2 Temperature Transducer Calibration for the Block. Assumed linear relation between temperature y and temperature indicator readout: $y = mx + b$.

Temperature Sensor	Freezing Water Temperature (y_1) (°F)	Digital Readout (x_1)	Boiling Water Temperature (y_2) (°F)	Digital Readout (x_2)	m (°F/Unit x)	b (°F)
Bottom	32	197.3	206	249.1	3.359	-630.75
Middle	32	269.3	206	364.5	1.828	-460.20
Top	32	260.5	206	345.7	2.042	499.92

Table 7.3 Cement Temperature During Curing. Temperatures measured at three locations in a 19.7 cm (7.75 in) diameter, 20.3 cm (8 in) long cement plug poured in PVC pipe. Time measured in minutes after pouring plug.

Time (minutes)	Temperatures (°F)		
	Bottom Transducer	Middle Transducer	Top Transducer
0	91.26	91.92	91.53
31	90.89	91.37	95.53
69	90.32	90.46	95.16
115	89.75	90.46	95.16
150	89.00	88.63	90.42
210	89.00	88.45	89.87
270	92.40	91.17	96.45
340	101.64	104.15	104.41
357	107.68	105.80	110.12
362	109.38	107.44	111.78
372	112.77	110.73	115.64
382	116.74	114.56	119.88
392	120.51	117.12	124.11
407	125.80	122.59	129.63
422	132.21	128.99	136.26
438	140.51	137.93	145.10
448	145.99	143.05	150.81
458	149.76	148.71	156.70
468	157.50	154.18	161.30
478	161.27	158.93	166.27
488	164.10	162.22	171.43
498	169.00	166.42	174.74
508	171.84	170.44	178.97
518	175.42	172.63	182.47
528	177.50	175.18	185.42
538	179.39	176.83	187.26
548	181.27	178.29	188.36
558	182.03	179.02	189.47
568	182.78	179.38	189.83

Table 7.3 Cement Temperature During Curing. Temperatures measured at three locations in a 19.7 cm (7.75 in) diameter, 20.3 cm (8 in) long cement plug poured in PVC pipe. Time measured in minutes after pouring plug.--Continued

Time (minutes)	Temperatures (°F) Bottom Transducer	Middle Transducer	Top Transducer
578	179.57	175.91	185.60
598	177.31	173.72	183.39
618	175.23	171.17	179.89
1198	100.70	98.86	101.47
1236	98.25	96.66	98.71
1256	96.92	95.57	97.42
1285	95.41	94.11	95.76
1341	92.77	91.55	92.81
1404	90.32	89.54	90.24
1561	85.41	84.61	85.45
1638	83.90	83.15	83.79

Table 7.4 Cement Temperature During Curing. Temperatures measured at three locations in a 19.7 cm (7.75 in) diameter, 20.3 cm (8 in) long cement plug poured in block. Time measured in minutes after pouring plug.

Time (minutes)	Temperatures (°F) Bottom Transducer	Middle Transducer	Top Transducer
1	92.78	97.16	100.63
27	92.10	93.32	100.84
63	89.42	89.66	97.57
90	87.40	87.47	94.71
115	85.05	86.00	92.26
148	83.04	84.54	89.40
185	81.69	83.26	87.56
223	80.69	82.53	86.54
253	80.01	82.35	86.34
283	82.03	83.26	87.56
313	84.05	84.73	89.81
343	88.75	87.65	93.89
390	95.80	94.42	102.67
420	102.52	100.08	110.03
450	109.91	106.11	118.19
490	120.66	114.52	129.42
511	125.70	119.09	135.34
526	128.38	121.84	128.61
540	131.74	124.94	144.54
570	133.42	127.14	144.54
586	133.42	127.68	144.74
597	133.42	127.68	144.74
611	133.09	127.32	144.13
621	132.41	126.95	143.41
634	131.74	126.41	142.70
1130	91.44	92.77	96.75
1426	84.72	86.74	89.81
1556	82.03	85.28	87.97
1625	80.35	84.00	86.54

Table 7.4 Cement Temperature During Curing. Temperatures measured at three locations in a 19.7 cm (7.75 in) diameter, 20.3 cm (8 in) long cement plug poured in block. Time measured in minutes after pouring plug.--Continued

Time (minutes)	Temperatures (°F) Bottom Transducer	Middle Transducer	Top Transducer
1729	79.34	83.08	85.73
2763	74.30	77.96	80.42
2820	73.97	77.96	80.00

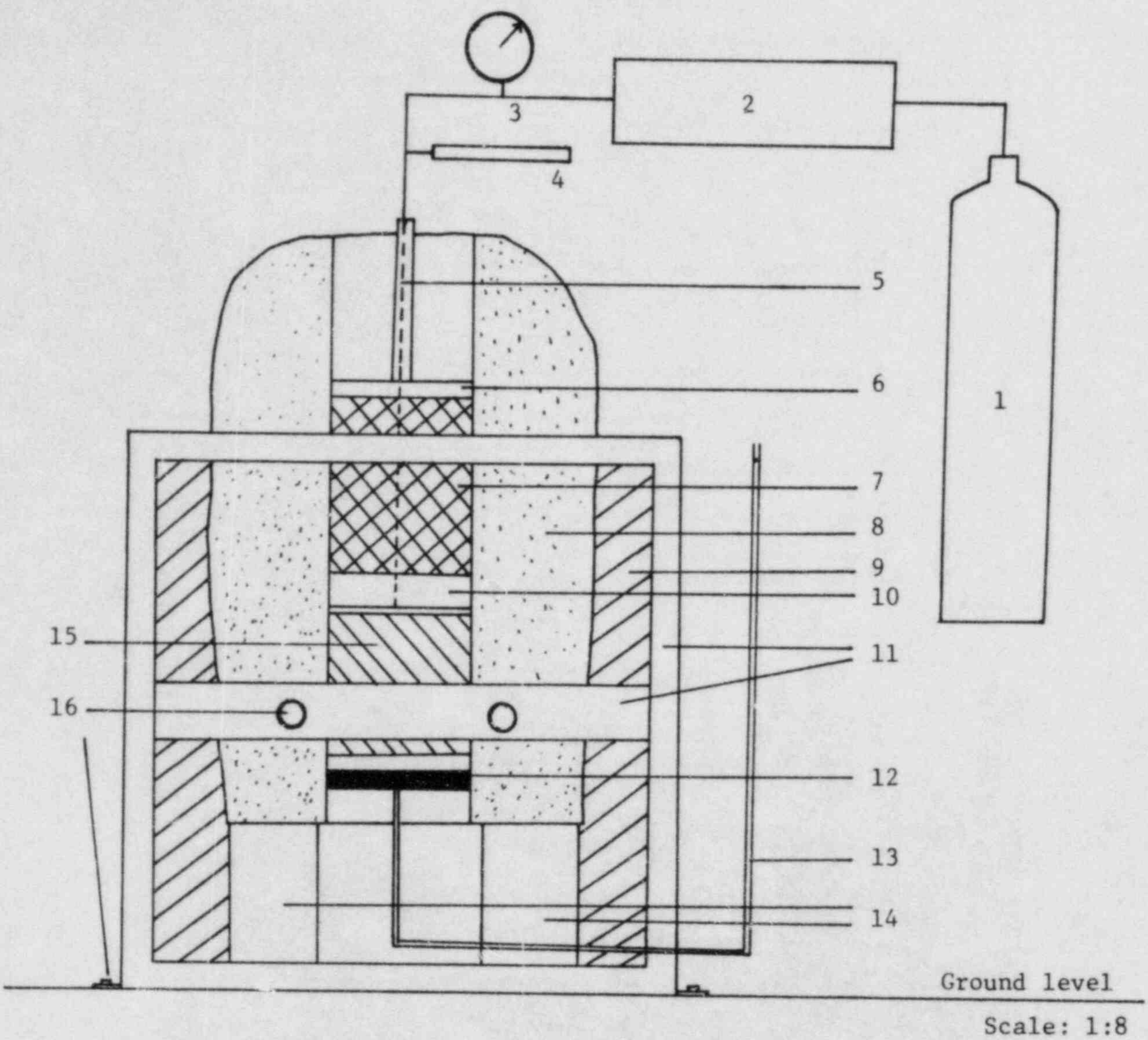

1. Nitrogen tank
2. Bladder accumulator
3. Pressure gage
4. Flowmeter
5. Center rod of packer
6. Upper end plate of packer
7. Packer (rubber)
8. Rock block
9. Cement fill
10. Lower end plate of packer
11. Steel frame
12. Bottom PVC disc
13. Recaptured flow
14. Wooden supports
15. Cement plug
16. Bolts

Figure 7.4 Laboratory set-up for permeability tests on a cement plug poured in a borehole in a Pomona basalt block.

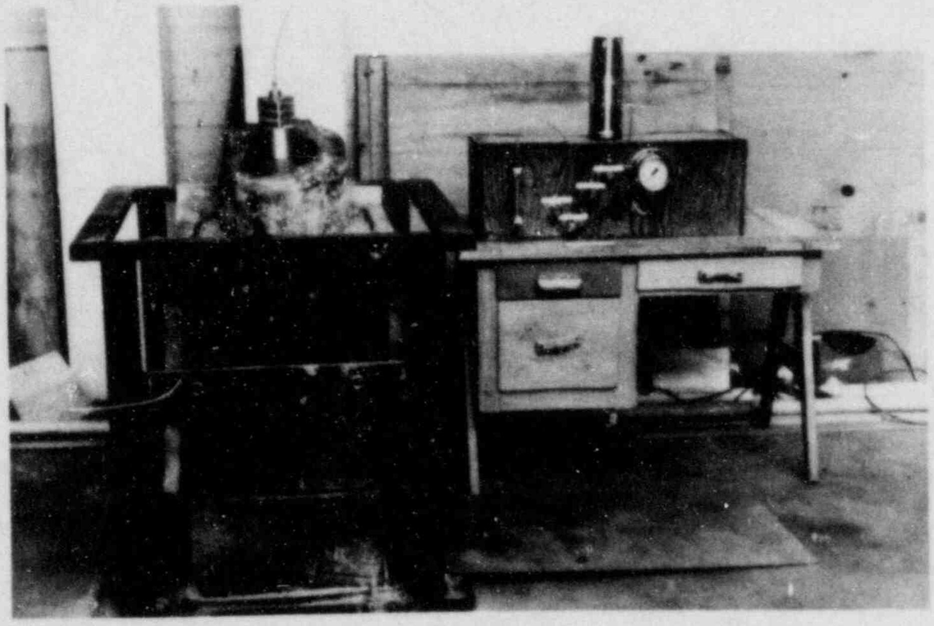

Figure 7.5 Laboratory set-up for permeability tests of cement plug in rock (Pomona basalt) block.

The K-3232-20 and K-3232-21 types of flowmeters will be used interchangeably depending on the water flow rate actually measured.

7.5.1.4 Mechanically Expandable Packers

Two packers having diameters of 19.05 cm (7.5 in) and 15.24 cm (6 in) will be placed in the borehole to test the performance of cement plugs.

The packers (rubbers) expand when they are torqued to seal the borehole and force the flow through the cement plug (Figures 7.6 and 7.7).

7.5.1.4.1 Testing of the 19.05 cm (7.5 in) Packer. The 19.05 cm (7.5 in) packer has been tested in a steel pipe to determine the contact pressure along the packer-hole contact when the packer is torqued. The steel pipe has an inside diameter of 19.60 cm (7.72 in), an outside diameter of 22.1 cm (8.70 in) and length of 57.25 cm (22.50 in). Two longitudinal and two tangential strain gages, each set placed 180° from each other, were installed on the walls of the steel pipe 40.96 cm (16.13 in) from the bottom (where the expansion of the packer rubbers took place). The strains were measured by means of a strain indicator (Figure 7.8).

The contact pressure was calculated from the measured tangential and longitudinal strains at different torques according to the formula derived from Jaeger and Cook (1979, Section 5.11), for zero outside radial stress:

$$P_i = \frac{\dfrac{E}{1 - \nu^2}\left[\varepsilon_t + \nu\varepsilon_\ell\right]}{\dfrac{2R_1^2}{R_2^2 - R_1^2}} \qquad (7.1)$$

where P_i = contact pressure (insid[illegible] stress)

E = Young's modulus of st[illegible]

ε_t = induced tangential strain

ε_ℓ = induced longitudinal strain

ν = Poisson's ratio of steel pipe

R_1 = inside radius of steel pipe

R_2 = outside radius of steel pipe

Table 7.5 shows the contact pressures generated at different torque loads. The average values of tangential and longitudinal strains were taken to calculate the contact pressure corresponding to different torques.

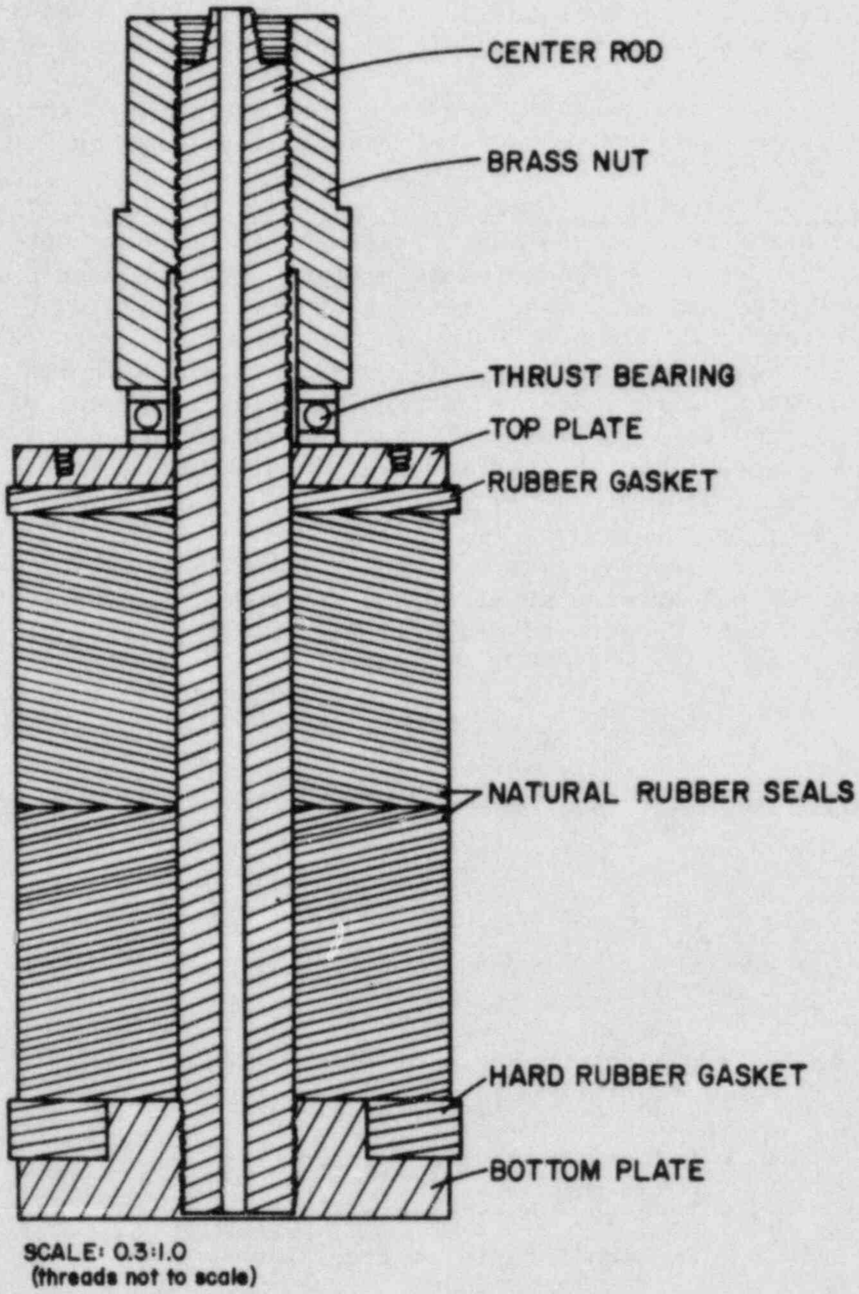

Figure 7.6 Cross-sectional view of the components of a mechanically expandable packer.

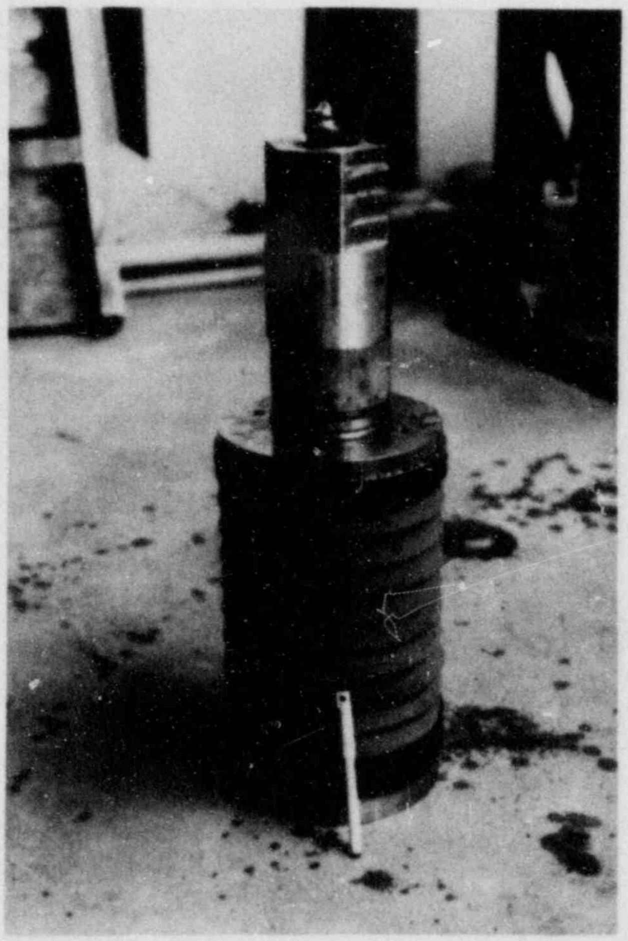

Figure 7.7 The 19.05 cm (7.5 in) mechanically expandable packer.

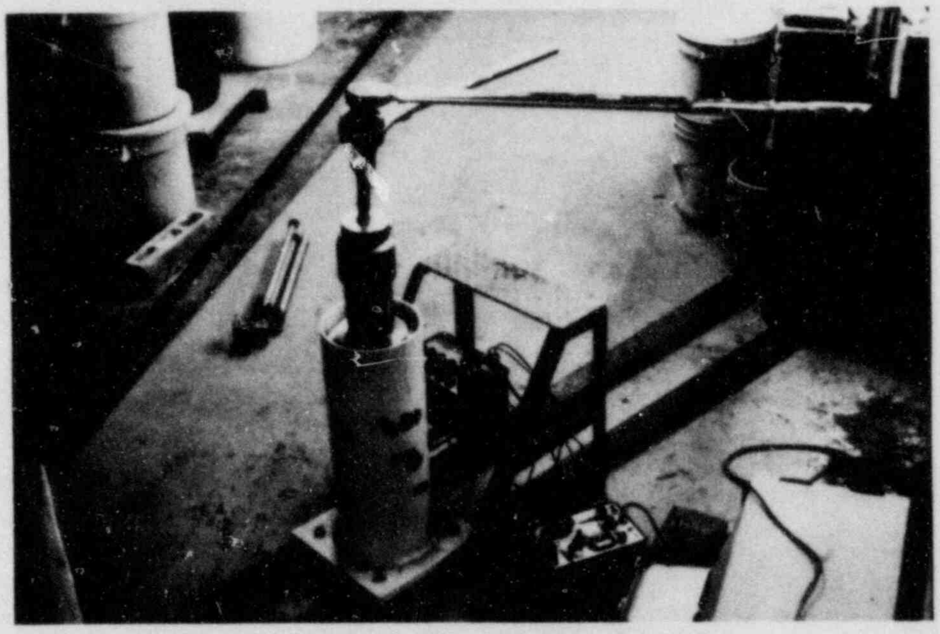

Figure 7.8 Testing of the 19.05 cm (7.5 in) packer. The packer was torqued to determine the contact pressure at the hole-wall contact by means of two longitudinal and two tangential strain gages with each set placed 180° from each other.

Table 7.5 Pipe Strain and Contact Pressure as a Function of Applied Torque

Applied Torque (ft-lb)	Measured Tangential Strain (μ in/in) 1	Measured Tangential Strain (μ in/in) 2	Measured Longitudinal Strain (μ in/in) 1	Measured Longitudinal Strain (μ in/in) 2	Internal Pressure (P_i) MPa (psi)
0	0	0	0	0	0
200	60	61	-19	-20	1.60 (232.17)
300	86	87	-27	-28	2.29 (332.38)
400	126	131	-40	-39	3.42 (495.31)
500	164	169	-50	-51	4.43 (642.55)
600	200	207	-63	-63	5.41 (783.89)
700	218	226	-69	-67	5.90 (855.98)
800	235	244	-72	-72	6.38 (925.00)
900	299	310	-91	-92	8.11 (1176.10)
1000	337	350	-104	-104	9.14 (1325.80)
1100	363	376	-113	-112	9.83 (1425.50)
1200	405	418	-123	-125	10.96 (1589.00)

Figure 7.9 shows a typical linear regression plot which gives the best fit for contact pressure vs. applied torque, with a 95% confidence band around the regression line.

The torque required to keep the packer in place for various values of the water injection pressure has been found by equating F_1 and F_2:

$$F_1 = \frac{\pi D^2}{4} \times P_t \tag{7.2}$$

$$F_2 = P_i \times \pi D \times \mu \times L \tag{7.3}$$

where F_1 = upward force exerted by injection pressure

F_2 = downward reaction force exerted by the packer

D = internal diameter of steel pipe

P_t = water injection pressure

P_i = contact pressure along packer

μ = coefficient of friction between steel pipe walls and packer rubbers

L = length of the packer rubbers (see Figure 7.10).

Table 7.6 shows the factor of safety for keeping the packer in place as a function of contact pressure and water 'njection pressure of 4.14 MPa (600 psi).

7.5.1.5 Steel Frame

A steel frame has been built to hold a basalt block with a 19.69 cm (7.75 in) diameter hole vertically, and to stabilize it when torqued. To increase the stability of the block, the space between the steel frame and the block has been filled with concrete. Bolts have been tightened against the block through the frame.

7.5.1.6 Water Outflow Collection System

A burette with a precision of 0.01 cc is used to measure the outflow through the cement plug. A similar burette is used to monitor the evaporation rate.

7.5.2 Permeability Test of the 19.69 cm (7.75 in) Block

After the cement plug was cured underwater for seven days, it was discovered that the water level above the plug dropped from 10.16 cm (4 in) to 2.54 cm (1 in). The water loss was due to a fracture dipping

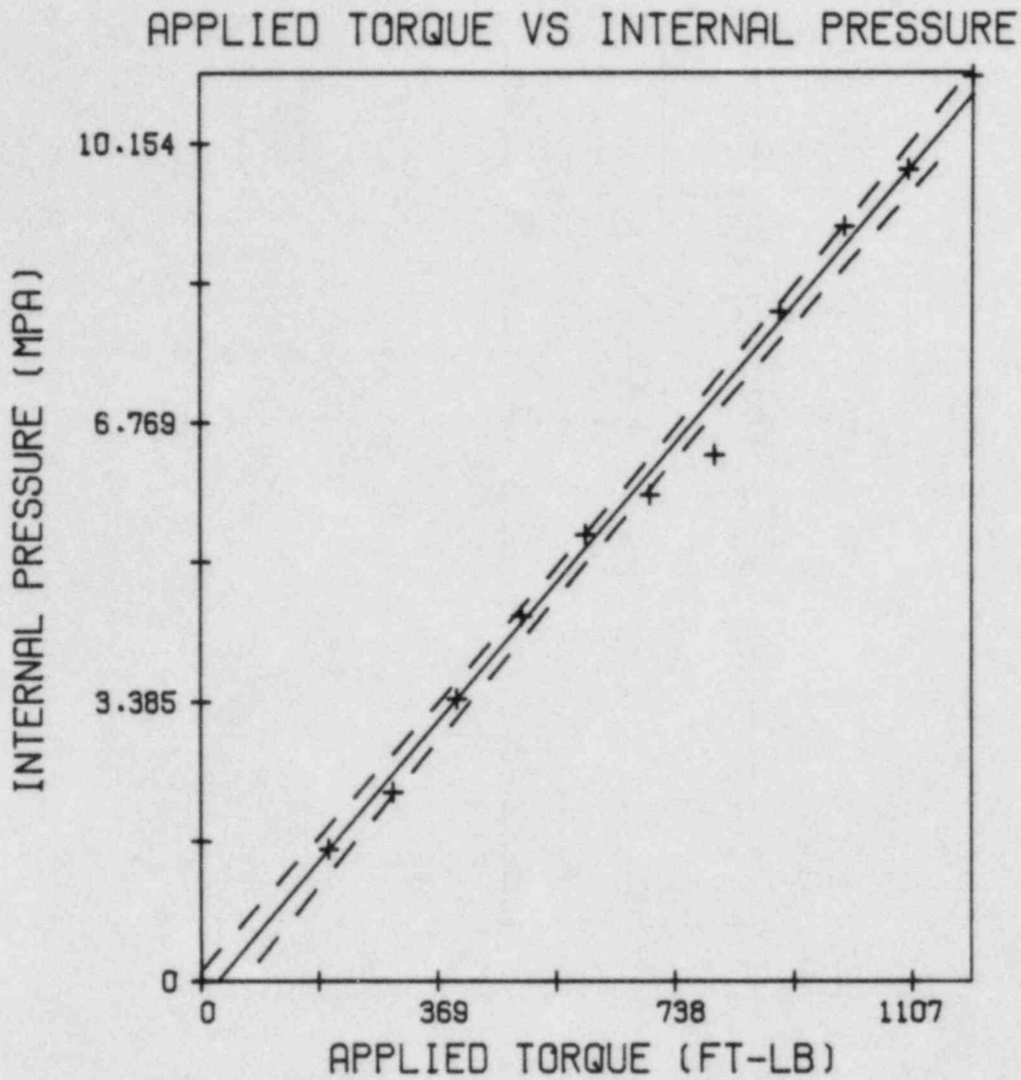

Figure 7.9 Linear regression plot for contact pressure vs. applied torque with a 95% confidence band around the regression line. The plot shown is for testing a steel pipe with a 19.69 cm (7.75 in) inside diameter and 1.25 cm wall thickness.

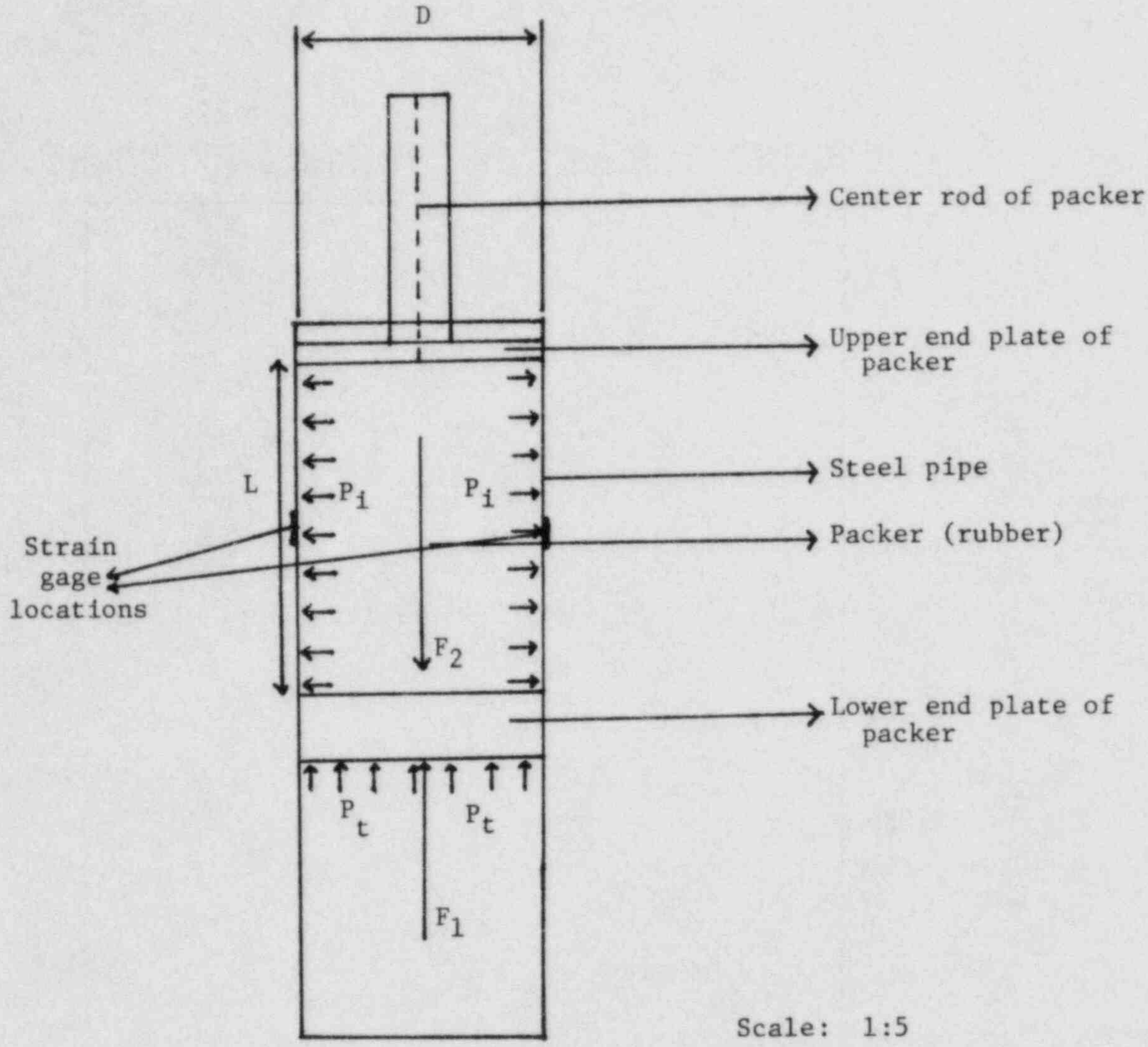

Figure 7.10 Schematic illustration of force distribution applied to and by packer.

F_1: resultant of water injection pressure P_t

F_2: resultant packer reaction force generated by friction along packer-wall contact area.

P_i: contact pressure along packer-hole contact.

Table 7.6 Factor of Safety as a Function of Contact Pressure (P_i) and Water Injection Pressure (P_t) of 4.14 MPa (600 psi).

Applied Torque (ft-lb)	Contact Pressure (P_i) MPa (psi)	Upward Force (F_1) (lb_f)	Downward Reaction Force (F_2) (lb_f)	Factor of Safety
0	0	26507.19	0	0
200	1.6 (232.17)	"	43763.01	1.65
300	2.29 (332.38)	"	62652.15	2.36
400	3.42 (495.31)	"	93363.74	3.52
500	4.43 (642.55)	"	121117.82	4.57
600	5.41 (783.89)	"	147759.78	5.57
700	5.90 (855.98)	"	161348.43	6.09
800	6.38 (925.00)	"	174358.39	6.58
900	8.11 (1176.10)	"	221689.63	8.36
1000	9.14 (1325.80)	"	249907.41	9.43
1100	9.83 (1425.50)	"	268700.42	10.14
1200	10.96 (1589.00)	"	299519.44	11.30

approximately 15° and running through the entire length of the block. The fracture (not visible before the cement was poured) probably was opened up by the expansion of the curing cement.

Figure 7.11 shows the dripping of water through the fracture. The picture was taken from the bottom of the block.

Table 7.7 shows the flow rate (outflow per unit time) of the fracture vs. time (minutes) passed after the borehole was filled with water. The fluctuation of the flow rate values might be due to a change in the fracture aperture, or due to fluctuations in head.

7.6 Future Work

Work planned for the immediate future is to apply about 0.69 MP (100 psi) vertical stress to the fracture in the block with an axial hole of 19.69 cm (7.75 in) in order to perform a study of the influence of a small confining pressure on the hydraulic conductivity of the crack.

Effects of size on curing temperature of cement and cement expansion will be studied by pouring cement into steel pipes having inside diameters of 2.54 cm (1 in), 5.72 cm (2.25 in), 10.80 cm (4.25 in), 15.88 cm (6.25 in) and 19.69 cm (7.75 in). Curing temperature of cement poured into the steel pipes will be measured by temperature sensing transducers connected to a temperature indicator. The cement expansion will be measured by two 90° strain rosettes connected to the HP data acquisition system.

Flow tests will be conducted on Pomona basalt blocks with 15.88 cm (6.25 in) and 19.69 cm (7.75 in) diameter axial holes. Simple steel frames to torque these blocks up to 200 ft-lb and to hold them vertically are being designed.

7.7 Discussion of Results and Conclusions

It deserves considerable attention that a joint or hairline fracture in a basalt block has been opened up by swelling of an expansive cement during curing of the cement. The basalt block has been inspected carefully prior to testing, and no cracks were apparent along the borehole wall to the unaided eye. Even though the present testing conditions are extremely conservative, in that the block is entirely unconfined and unstressed, this observation does point out that a swelling sealing material can easily enhance the hydraulic conductivity of the rock surrounding the sealed opening, especially if the rock is jointed or fractured, with some of the fractures running approximately normal to the tangential stress, or if the state of stress is highly anisotropic. A preliminary evaluation of the influence of fractures in the rock around seals in shafts, tunnels, and boreholes has been made by Kelsall et al., 1982, and in our last annual report (Daemen et al., 1983, Chapter 10). A simplified analysis procedure that allows a rapid assessment of the likelihood of joints, fractures or other discontinuities to open up under the influence of an internal pressure in a circular hole has been developed by Daemen (1983).

Figure 7.11 Dripping of water through the fracture in the block with a 19.69 cm (7.75 in) diameter axial hole.

Table 7.7 Flow Rate of the Fracture as a Function of Time. Time measured in minutes after pouring water of 36.67 cm (14.4 in) height above the plug.

Time (minutes)	Flow Rate (cc/min)
23	8.4
56	17.57
63	10.35
83	3.62
101	16.10
121	12.08
138	11.37
362	7.55
380	6.71
411	0.78
1185	0.68
1217	1.51
1314	0.25
1356	0.58
1801	0.38
2571	0.78
2805	0.41
3206	0.86
3299	1.04
4102	0.72
4766	3.49

7.8 References

American Petroleum Institute, 1977, Testing Oil-Well Cements and Cement Additives, Spec-10B, Twentieth Edition, American Petroleum Institute, Dallas, TX, April.

Campbell-Allen, D., J.L. Kass, and J.R. Booker, 1972, Size Effects in Drying and Shrinkage of Concrete, Research Report No. R189, by the School of Civil Engineering, Sydney University, Australia.

Daemen, J.J.K., 1983, "Slip Zones for Discontinuities Parallel to Circular Tunnels or Shafts," Int. J. Rock Mech. Min. Sci. & Geomech. Abstr., Vol. 20, no. 3, pp. 135-148.

Daemen, J.J.K., D.L. South, W.B. Greer, J.C. Stormont, S.A. Dischler, G.S. Adisoma, N.I. Colburn, K. Fuenkajorn, D.E. Miles, B. Kousari, and J. Bertuca, 1983, "Annual Report, Rock Mass Sealing, June 1, 1982 - May 31, 1983," prepared for the U.S. Nuclear Regulatory Commission, Division of Health, Siting and Waste Management, by the Department of Mining and Geological Engineering, University of Arizona, Tucson.

Jaeger, J.C. and N.G.W. Cook, 1979, Fundamentals of Rock Mechanics, Third Edition, Chapman and Hall, London, John Wiley and Sons, Inc., New York.

Kelsall, P.C., J.B. Case, and C.R. Chabaness, 1982, "A Preliminary Evaluation of the Rock Mass Disturbance Resulting from Shaft, Tunnel or Borehole Excavation," Technical Report ONWI-411, prepared by D'Appolonia Consulting Engineers, Inc., for Office of Nuclear Waste Isolation, Battelle Memorial Institute, Columbus, Ohio, November.

CHAPTER EIGHT

CEMENT SWELLING EXPERIMENTS

8.1 Introduction

This chapter describes ongoing experiments to evaluate the expansive stresses generated by Cement System 1 (e.g. Daemen et al., 1983, Section 6.4.2, p. 143). The measurements are made on six steel pipes with the same lengths and different wall thicknesses into which cement plugs have been poured. The strain induced on the steel pipes and the temperature of the cement are monitored continuously with an automatic data logger. The cement is kept saturated by maintaining a thin film of water on top of it. The testing is performed under atmospheric pressure and at a temperature of 22 ± 2°C.

8.2 Equipment and Procedures

Steel pipes with cement plugs and strain gages are shown in Figure 8.1. Table 8.1 shows the dimensions of the six pipes. The wall thickness is approximately the same for two pipes each (tolerance of 0.05 cm).

Two strain gages are installed circumferentially in the middle of each pipe. Each strain gage is connected to a data logger using a 1/4 bridge configuration. Cement is mixed according to API Standards (American Petroleum Institute specifications, 1977) and poured into each pipe. One semiconductor thermistor temperature sensor with specification of 10 Kohms at 25°C is inserted into each pipe (Figure 8.1). Logging and processing induced strain and temperature of the cement was done by HP3054DL automatic data logger, consisting of an HP3497A data logger for instrumentation and HP85B controller.

8.3 Results

The results are presented in Figures 8.2 through 8.5. Immediately after cement was poured into the pipes, the recorded temperature for each pipe was 31°C. After two hours the temperature of the pipe gradually decreased to room temperature (22 ± 1°C). The temperature of the cement increased for each pipe to 29°C after two hours. After 25 hours the temperature for each pipe became stable. and uniformly constant (22 ± 1°C). The temperature log for each pipe is shown in Figure 8.2.

The expansive stress generated by the cement can be calculated from the measured circumferential strains according to two formulas derived from Jaeger and Cook (1979, Section 5.11).

$$P = \frac{E\ \varepsilon}{2R_1^{\,2}/(R_2^{\,2} - R_1^{\,2})} \qquad (8.1)$$

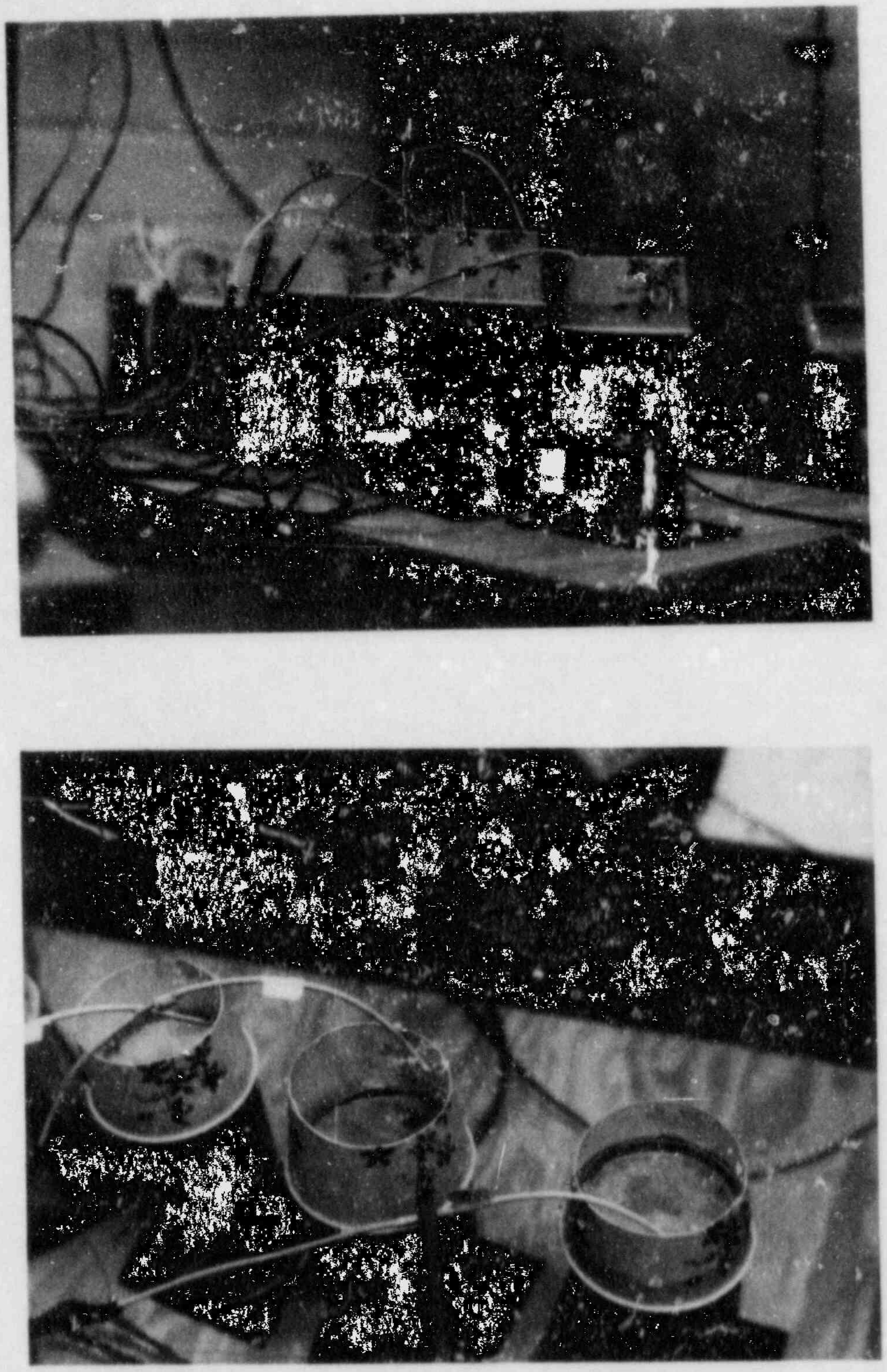

Figure 8.1 Steel pipes filled with Cement System 1 for swelling pressure measurements. Top: inserted temperature probe connection in cement. Bottom: strain gages with twisted wires.

Table 8.1 Cement Expansion Data - Cement System 1*

Pipe	Plug Length (cm)	Outside Diameter (cm)	Inside Diameter (cm)	Wall Thickness (cm)
1	12.3	6.88	6.525	0.175
2	12.2	7.210	6.370	0.420
3	12.2	6.85	6.490	0.177
4	12.3	7.070	6.445	0.310
5	12.3	7.075	6.430	0.315
6	12.8	7.200	6.350	0.425

*Cement System 1: Ideal type A cement, 50% water, 10% D53 (expansive agent), 1% D65 (dispersent). Provided by Dowell (Daemen et al., 1983, Ch. 9).

NOTE: All pipes are 13 cm long.

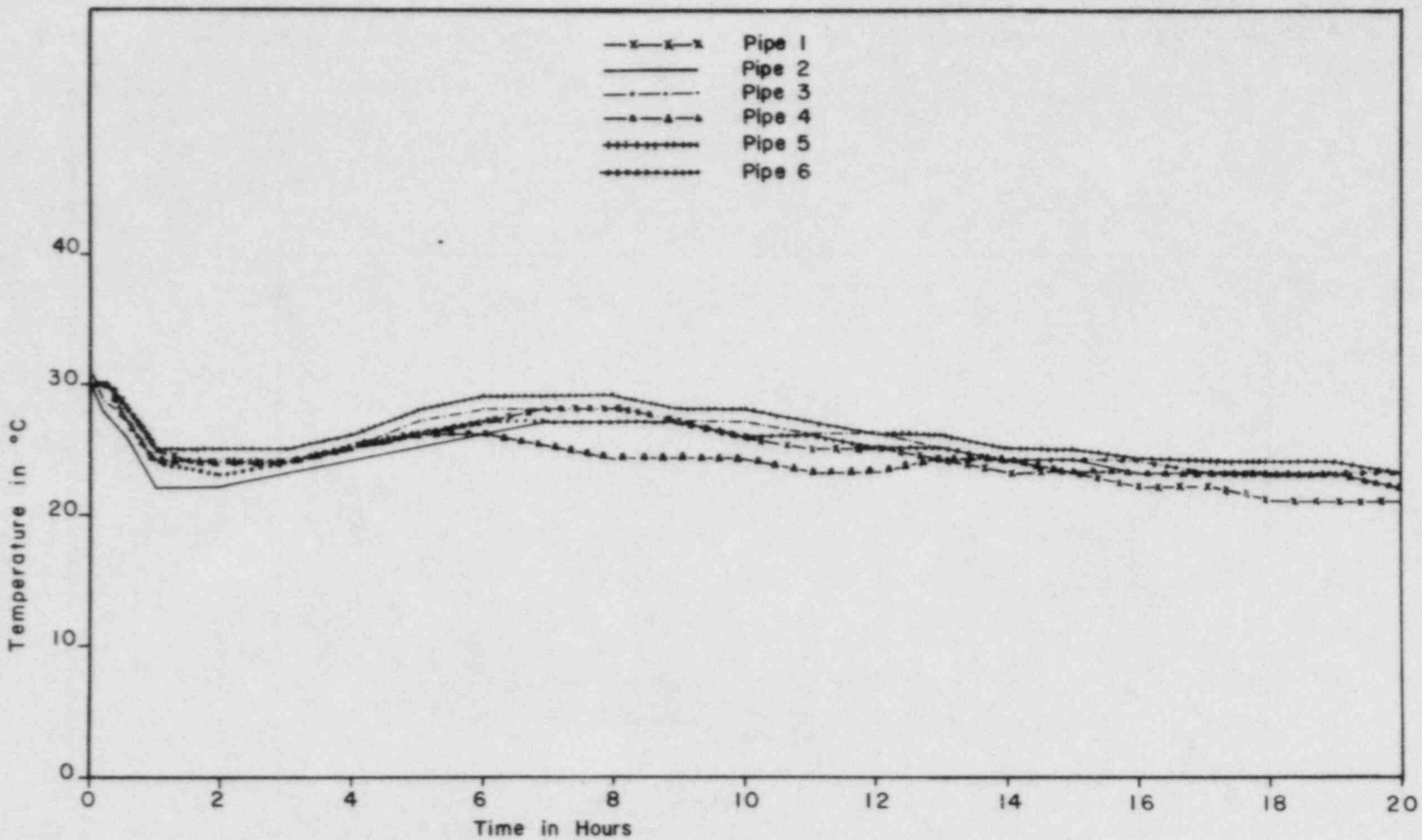

Figure 8.2 Cement temperature measured in each pipe since pouring cement.

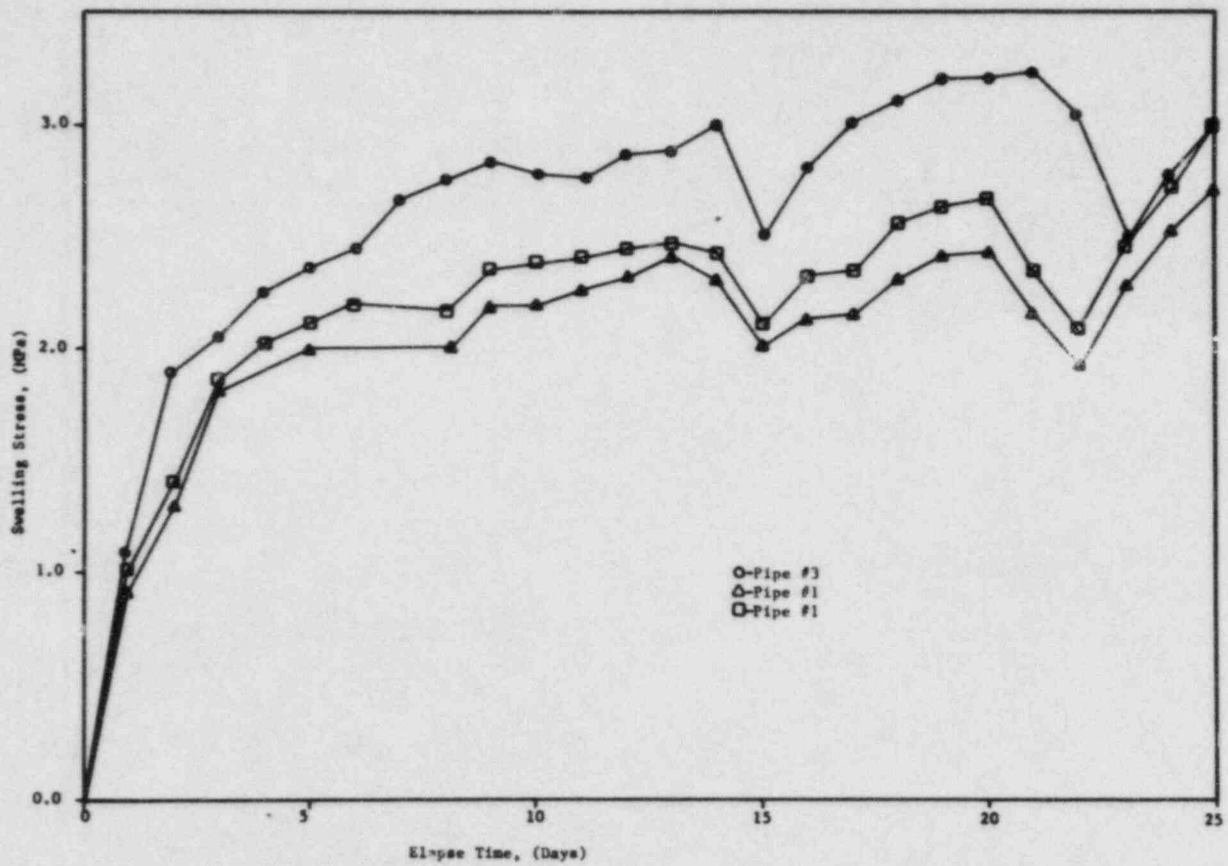

Figure 8.3 Swelling pressure for pipes 3 and 1. Radial stress calculated from circumferential strain measured on steel pipes filled with Cement System 1 in a saturated condition. Time measured since pouring cement. For pipe #1, top line: Eq. (8.2); lower line: Eq. (8.1).

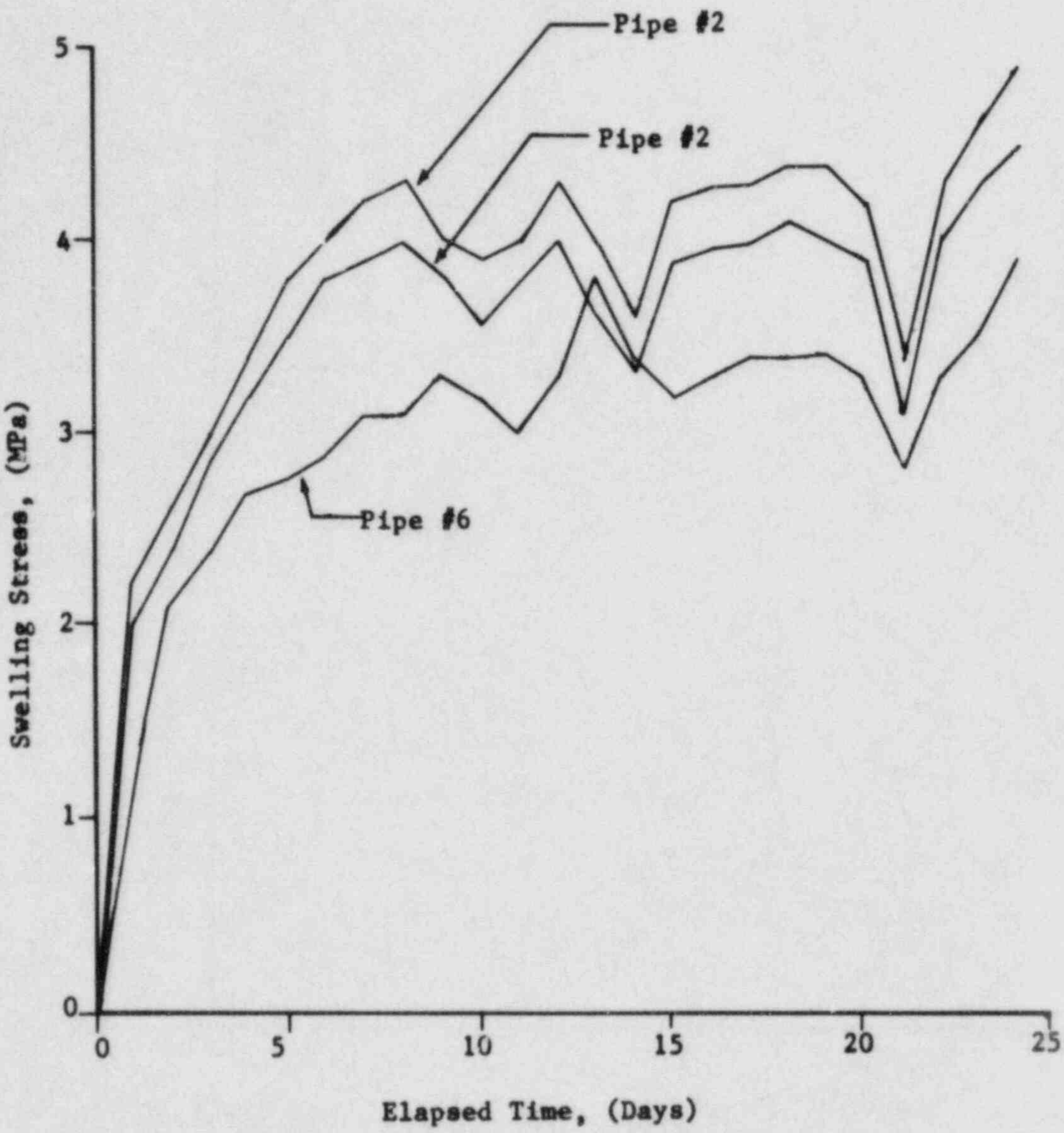

Figure 8.4 Swelling pressure for pipes 2 and 6. Radial stress calculated from circumferential strain measured on steel pipes filled with Cement System 1 in a saturated condition. Time measured since pouring cement. For pipe #2, top line: Eq. (8.2); lower line: Eq. (8.1).

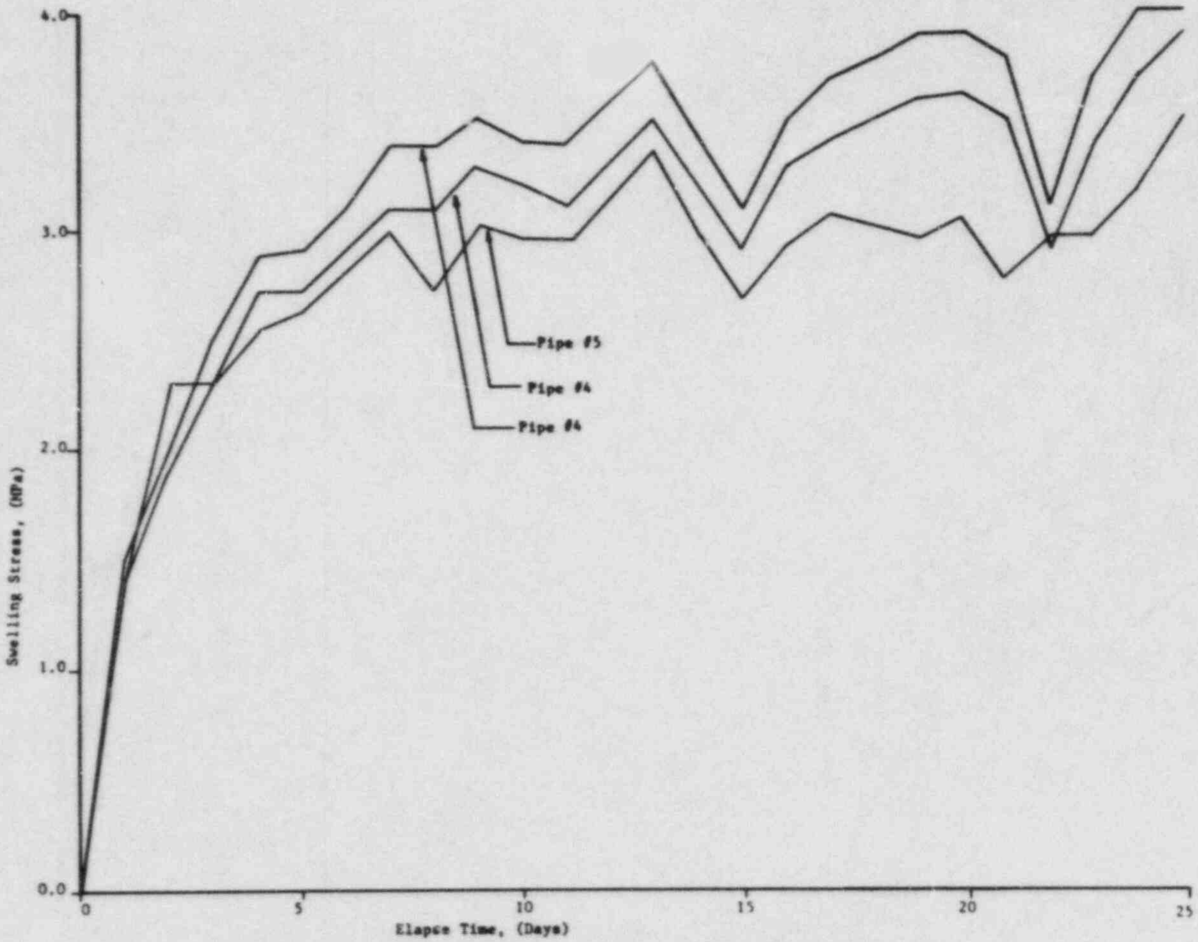

Figure 8.5 Swelling pressure for pipes 5 and 4. Radial stress calculated from circumferential strain measured on steel pipes filled with Cement System 1 in a saturated condition. Time measured since pouring cement. For pipe #4, top line: Eq. (8.2); lower line: Eq. (8.1).

$$P = \frac{E\ \varepsilon}{2R_1^2/(R_2^2 - R_1^2)\cdot(1 - \nu^2)} \tag{8.2}$$

where P = expansive stress
E = Young's modulus of steel pipe
ε = measured strain
R_1 = inside radius
R_2 = outside radius
ν = Poisson's ratio of steel pipe.

Equation (8.1) assumes a plane stress condition (i.e. no longitudinal stress in the pipe), (8.2) a plane strain condition. It is probable that the correct situation is bounded by these two extreme conditions, which are fairly close to each other for the conditions used here.

The calculated stresses vs. time for each set of pipes with the same wall thickness are shown in Figure 8.3 through 8.5. Each graph shows the stresses generated by cement computed according to Eq. (8.1). The expansive stress calculated according to Eq. (8.2) is graphed for only one of the pipes, because the stress values computed from Eq. (8.2) always are about 8% higher than the stress values calculated from Eq. (8.1). The stress fluctuates with the low and high values of repeated cycles coinciding for all pipes, and being very close for identical pipes. The difference in stresses generated by two pipes with the same wall thickness could be explained by the variable characteristics of Cement System 1 and by differences in wall thickness (0.05 cm difference). This experiment will be carried on for an indefinite period of time.

8.4 References

American Petroleum Institute, 1977, "Specification RP-10B, Testing Oil Cements and Cement Additives," Twentieth Edition, API, Dallas, TX, April.

Daemen, J.J.K., D.L. South, W.B. Greer, J.C. Stormont, S.A. Dischler, G.S. Adisoma, N.I. Colburn, K. Fuenkajorn, D.E. Miles, B. Kousari, and J. Bertucca, 1983, "Annual Report, Rock Mass Sealing, June 1, 1982 - May 31, 1983," NUREG/CR-3473, prepared for U.S. Nuclear Regulatory Commission, Division of Helath, Siting and Waste Management, by Department of Mining and Engineering, University of Arizona, Tucson.

Jaeger, J.C. and N.G.W. Cook, 1979, Fundamentals of Rock Mechanics, Third Edition, Chapman and Hall.

CHAPTER NINE

PUSH-OUT STRENGTH OF DRIED AND RESATURATED CEMENT PLUGS

9.1 Introduction

The work described in this chapter involves evaluation of the strength of push-out experiment samples which have been stored in a dry environment (70 - 80°F and 40 - 50% relative humidity). The performance of young cement plugs in initial push-out experiments was studied and analyzed by Stormont and Daemen (1983). A common observation in all these samples is that if they are allowed to dry out, they show significant shrinkage and drastic strength reduction after moderately long periods of time (e.g. more than 150 days). This type of deterioration of aged borehole plugs might be similar to that of in-situ drying under influence of heat generated by wastes.

A number of samples are being kept under water in a saturation tank. They are tested periodically in order to assess long-term effects of a dry-wet sequence on their strength performance. Some of the dried-out samples are kept in a standard concrete curing room (100% relative humidity and 80°F). These samples also are being evaluated periodically.

9.2 Test System

A new system for data recording has been designed and built. Electromechanical instruments are used in conjunction with a triple input graphic recorder to obtain continuous data from the push-out experiment. A continuous record is produced in which the applied load, top displacement, and bottom displacement are recorded. The old set-up which included dial gages and manual data recording is still used to check the continuous data recording system.

The top and bottom displacement are measured with two linear variable differential transformers (LVDT) (Figures 9.1 and 9.2). These instruments produce an electrical output differential voltage proportional to the displacement of a separate movable core. These LVDTs have a resolution of a thousandth of an inch. The linearity, a measure of instrument error, is about 0.25% of the full range of +/- 1.0 inches. Axial load is measured with a Terrametrics compression load cell which has a capacity of 10,000 lbs. Combined instrument error (nonlinearity and hysteresis) is 2-7% of full range. The signal output from load cell and LVDTs are recorded on a Hewlett-Packard X-Y1-Y2 recorder with different sensitivity ranges. The top displacement is also measured manually with a Sarrett dial gage which has a resolution of 0.001 inch and error limit of .001 inch. A soil test compression machine with dial indicator applies the load. The machine has a 60,000 lbs capacity with 100 lbs resolution. The machine is calibrated annually by a firm with calibration equipment traceable to the National Bureau of Standards.

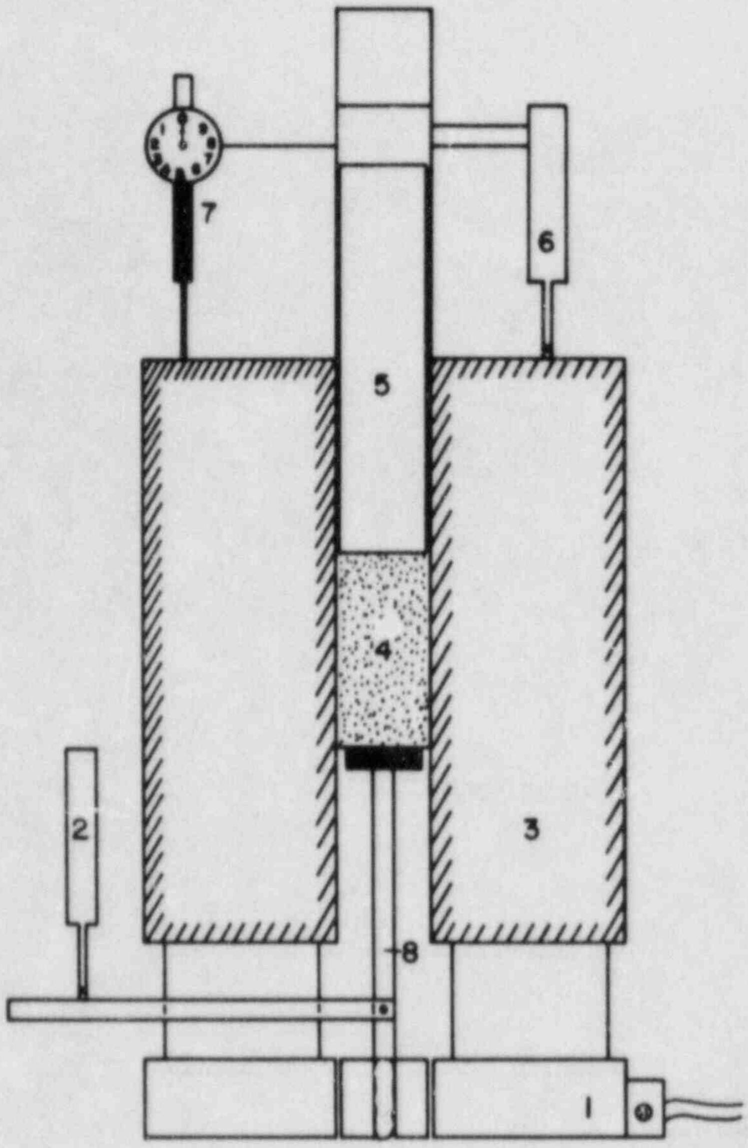

1 - Load cell
2 - Bottom LVDT
3 - Rock sample
4 - Plug
5 - Axial bar
6 - Top LVDT
7 - Dial indicator
8 - Section for bottom displacement transfer

Figure 9.1 Schematic drawing of push-out test equipment and instrumentation set-up.

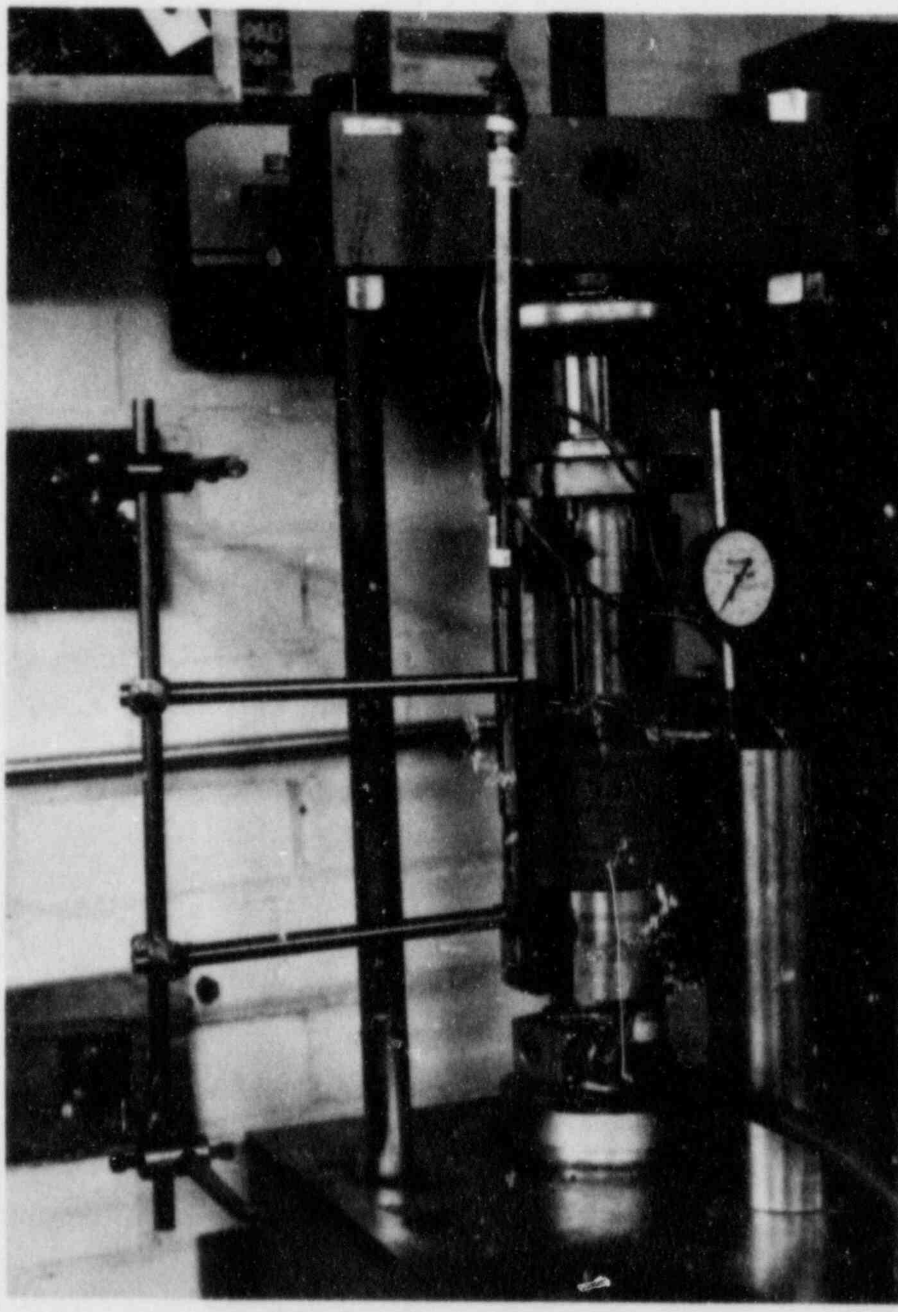

Figure 9.2 New equipment and instrumentation set-up for typical push-out test. Background: compression tester machine; bottom: load cell; top: LVDTs. Behind the LVDTs: axial bar. Foreground: top displacement dial gage. Left: frame for holding the LVDTs.

A schematic view of the new push-out experimental set-up is shown in Figure 9.1. A cylindrical steel bar transmits the axial load. Two circular jackets around the axial bar with horizontal arms are used to measure top displacement with a dial indicator and LVDT. A steel platen with inside diameter of 2 inches and thickness of 2 inches lies underneath the sample. The platen has a slit on one side to allow downward movement of the horizontal arm of the bottom vertical bar. The bottom vertical bar rests on top of a spring located in the center hole of the load cell. The top end of the vertical bar is forced in contact with the bottom end of the plug by the spring. The bottom LVDT positioned on the arm of the bottom vertical bar measures the bottom displacement.

9.3 Test Procedure

Load cell and top and bottom LVDTs are calibrated before each experiment. The load cell is calibrated with a soil test compression machine. The LVDTs are calibrated with a precision displacement dial indicator. The position of the plug in the borehole is measured independently both before and after the test. The test set-up is shown in Figures 9.1 and 9.2. Before the test start-up, the recorder is activated and the no load position of each instrument is recorded. When the load is applied, the operator reads and records the applied load and the top displacement at small load intervals (200 lbs). After the test is completed, these data points are entered on the graph generated by the continuous data recording system.

9.4 Results

A number of push-out tests have been performed on cement plugs that have been allowed to dry out and then have been resaturated by storing them in a concrete curing room or in a water tank. Considerable strength increases have been observed for all resaturated plugs in comparison with the strength of dried plugs, but initial strength (predrying) has never been recovered. Tables 9.1 and 9.2 list the history of the samples tested, their resaturation period, wet and dry cycling, dimension and strengths. Strength recovery ranges from insignificant (3%) to substantial (80%). The plugs resaturated under water showed lesser recovery than plugs which were resaturated in a concrete curing room. Only a very small recovery took place for the one plug which dried out much longer than the others. The results are very variable and no clear trend can be established. Comparison of the results is further complicated by the fact that all the plugs have previously been loaded to failure, a procedure which is likely to have induced at least some permanent damage.

Four samples (Nos. 3, 7, 14, and 15) with hole diameter of four inches and plug lengths from one to four inches fractured during curing. The fractures are most likely caused by cement expansion during resaturation (Figure 9.3). This type of fracture also has been observed during testing of young cement plugs of samples which had diameters of 4 inches and lengths of 2 to 4 inches. Figure 9.4 shows two of the samples which fractured during resaturation.

Table 9.1 History of Samples Stored in Water Tank

Sample ID	Reference	Dimensions Diameter x Length (in x in)	Days in Dry Room	Days in Wet Room	Initial Failure Load (lbs)	Second Failure Load (lbs)	Days in Wet Room	Third Failure Load (lbs)	% Strength Recovery
3	CG4-4:S1	4 x 4	241	407	31,000	Fractured*	-	-	-
4	HB2-2:S2	2 x 2	205	109	10,000	2860	Curing	-	29%
7	HB4-4:S3	4 x 4	234	360	27,500	Fractured*	-	-	-
10	HB2-2:S3	2 x 2	234	360	4000	**	Curing	-	-
11	CG2-2:S1	2 x 2	248	109	13,500	2500	Curing	-	18%
12	HB2-1:S1	2 x 1	248	109	6750	2800	Curing	-	41%
13	CG2-1:S3	2 x 1	255	374	3900	**	Curing	-	-
16	CG1-1:S3	1 x 1	178	360	7500	**	Curing	-	-
18	HB2-2:S1	2 x 2	457	203	11,200	400	Curing	-	3%
19	HB4-1:S3	4 x 1	234	399	8900	3900	Curing	-	43%
21	CG4-2:S3	4 x 2	241	394	13,400	3000	Curing	-	22%
22	HB1-2:S1	1 x 2	222	52	9500	1100	163	3200	11%
23	HB1-1:S2	1 x 1	82	52	4800	400	163	1350	8%
24	HB2-1:S3	2 x 1	174	52	4800	400	Curing	-	8%

*Samples were fractured during curing under water.

**Because of plug position in the borehole, these samples were not tested.

Table 9.2 History of Samples Stored in Concrete Curing Room

Sample ID	Reference	Dimensions Diameter x Length (in x in)	Days in Dry Room	Days in Wet Room	Initial Failure Load (lbs)	Second Failure Load (lbs)	Days in Wet Room	Percentage Strength Recovery
1	HB2-2:S1	2 x 2	248	118	1500	2500	Curing	16%
2	HB2-2:S3	2 x 2	234	96	9000	2600	Curing	29%
5	HB2-1:S2	2 x 1	205	426	4700	1100*	Curing	23%
6	CG1-2:S2	1 x 2	213	N/A	7900	N/A	Curing	-
8	CG4-2:S2	4 x 2	306	382	7700	4500	Curing	58%
9	HB2-2:S1	2 x 2	262	96	7400	4300	Curing	58%
14	HB4-2:S2	4 x 2	138	360	21,000	Fractured	Curing	-
15	HB4-1:S3	4 x 1	248	360	4400	Fractured	Curing	-
17	CG1-1:S3	1 x 1	186	Curing	3400	**	Curing	-
25	HB2-4:S1	2 x 2	179	426	7925	6300	Curing	80%
26	HB2-4:S1	2 x 4	336	426	31,500	10,400	Curing	33%

*Sample no. 5 was tested previously with failure load of 2600 lbs and 255 days of reconditioning after 2nd test.

**Sample was not tested because of problems with plug.

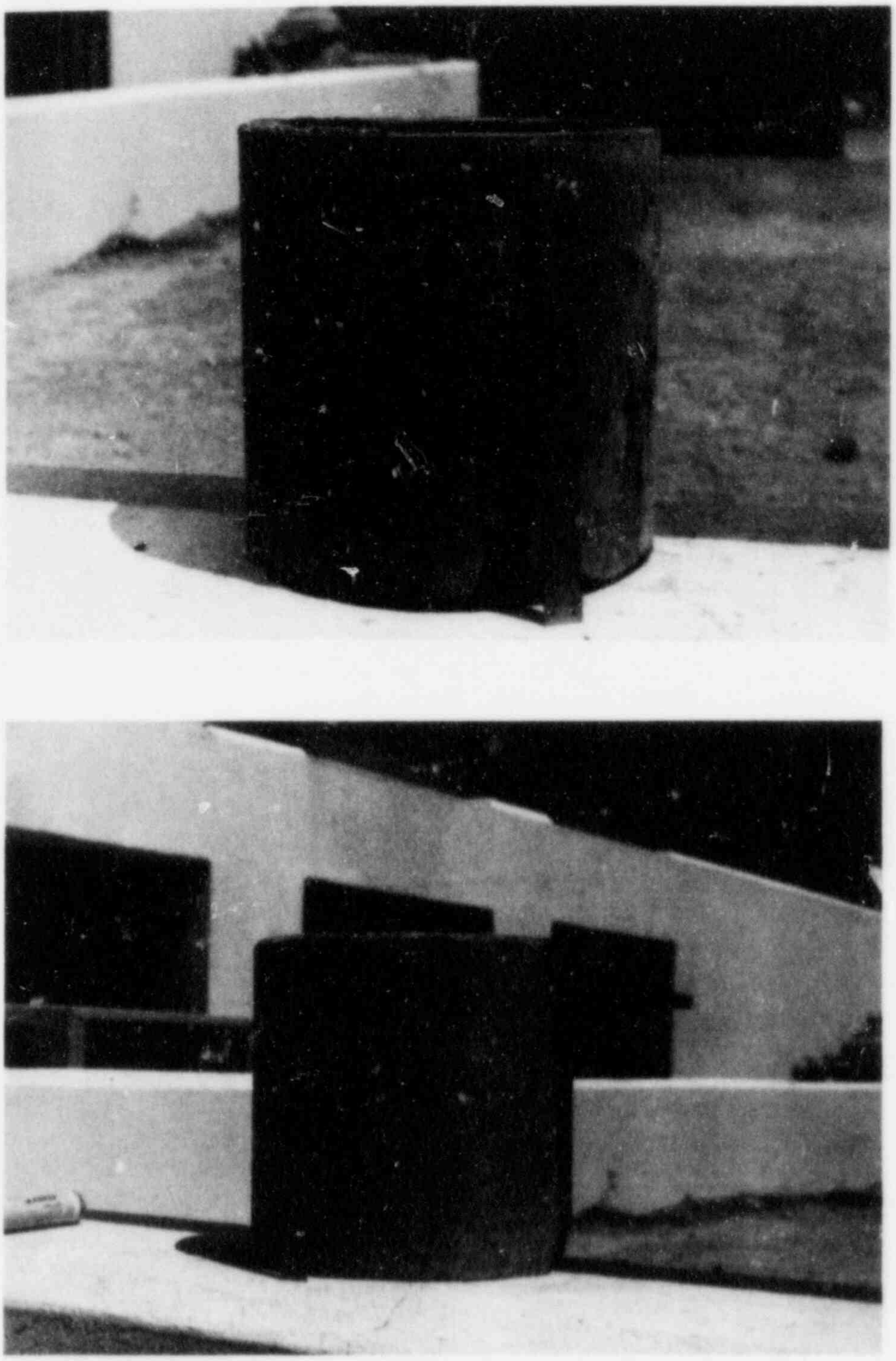

Figure 9.3 Samples fractured during saturating cement plugs. Dried-out samples with plug diameter of four inches and length of 2 inches and 4 inches. Top: sample #14, HB4-2:S2; bottom: #3, CG4-4:S2.

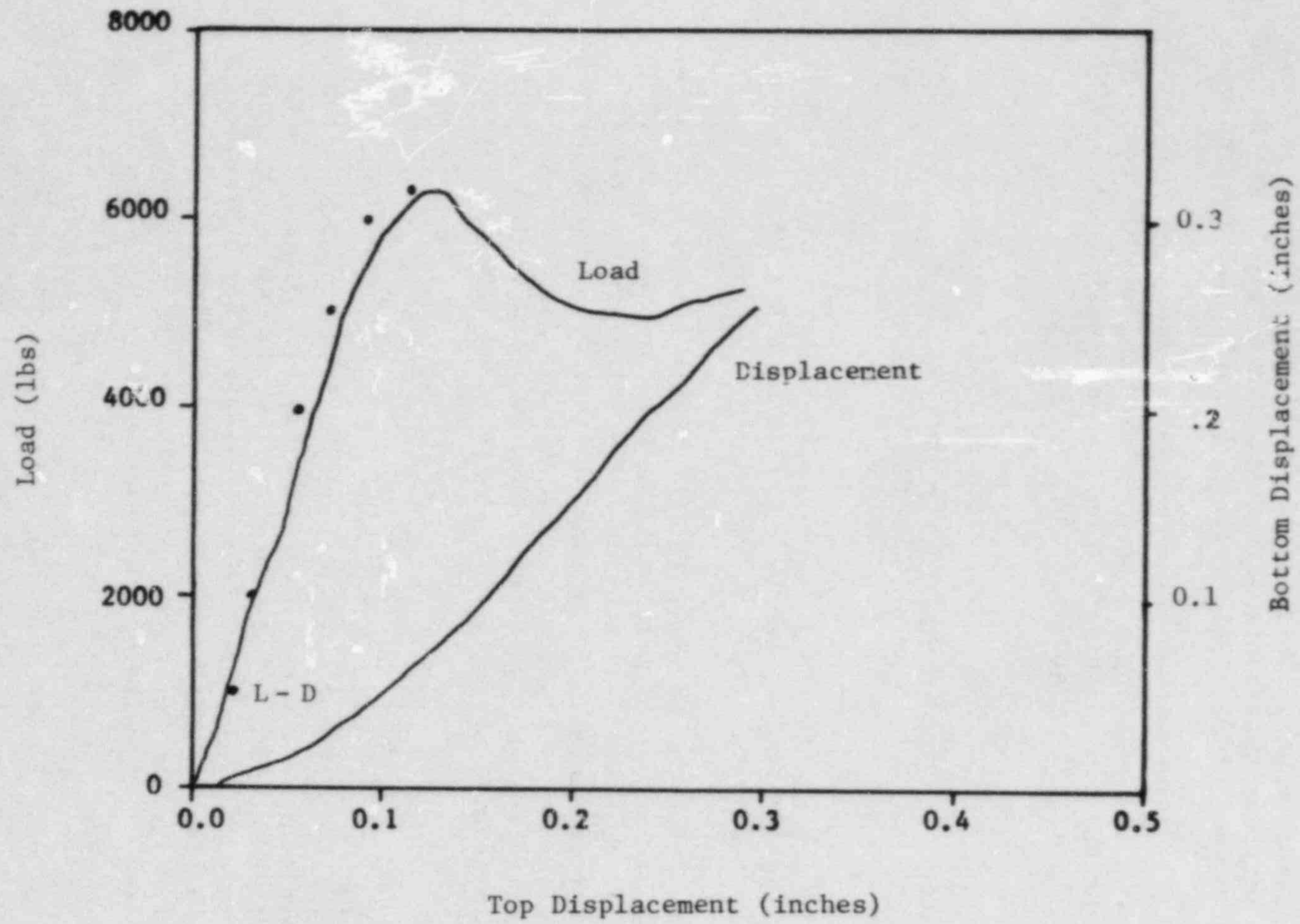

Figure 9.4 Top and bottom displacement of plug vs. axial load; sample HB2-2:S3B, No. 25; L-D: load-top displacement plot of manual test; displacement curve consists of top and bottom displacement; load curve represents load vs. top displacement and bottom displacement.

The results for each push-out test on each sample are illustrated in Figures 9.4 through 9.9. The horizontal and vertical axes of the displacement curves represent top and bottom displacements, respectively. The load curve shows the variation of plug load vs. top and bottom displacement. The dotted curve represents the data points taken with manual testing and consists of load and top displacement. The data points of the dotted curves appear to follow the load curves before and at peak strength. The reasons for the discrepancy between the manual and recorder curves are instrument error, mainly in the load cell, the small number of data points taken during manual testing, and operator error.

A relation between the swelling pressure P (internal radial stress on the cylinder) and the tensile stress S on the hole wall can be derived from Jaeger and Cook (1979, Section 5.11):

$$P = S \cdot \frac{R_2^2 - R_1^2}{R_2^2 + R_1^2} \qquad (9.1)$$

where R_1 and R_2 are the internal and external radii of the cylinder, in this case 5 cm and 7.5 cm, respectively. This equation (9.1) is represented graphically in Figure 9.19.

From the tensile strengths obtained for the basalt (Chapter 3, Table 3.1), it can be estimated that the swelling pressure must be in the range of 10 to 15 MPa, which is substantially higher than directly measured swelling pressures. It is probable that this overestimate is due to the fact that the tensile strength obtained from the ring test is an overestimate for the configuration with a swelling plug, and that a more appropriate tensile strength would be obtained from a bursting test.

9.5 References

Daemen, J.J.K., J.C. Stormont, N.I. Colburn, D.L. South, S.A. Dischler, K. Fuenkajorn, W.B. Greer, G.S. Adisoma, D.E. Miles, B. Kousari, and J. Bertuca, 1983, "Rock Mass Sealing, Annual Report, June 1, 1982 - May 31, 1983, NUREG/CR-3473, prepared for Division of Health, Siting and Waste Management, U.S. Nuclear Regulatory Commission, by the Department of Mining and Geological Engineering, University of Arizona, Tucson.

Stormont, J.C. and J.J.K. Daemen, 1983, "Axial Strength of Cement Borehole Plugs in Granite and Basalt," NUREG/CR-3594, Topical Report on Rock Mass Sealing, prepared for Division of Health, Siting and Waste Management, U.S. Nuclear Regulatory Commission, by the Department of Mining and Geological Engineering, University of Arizona, Tucson.

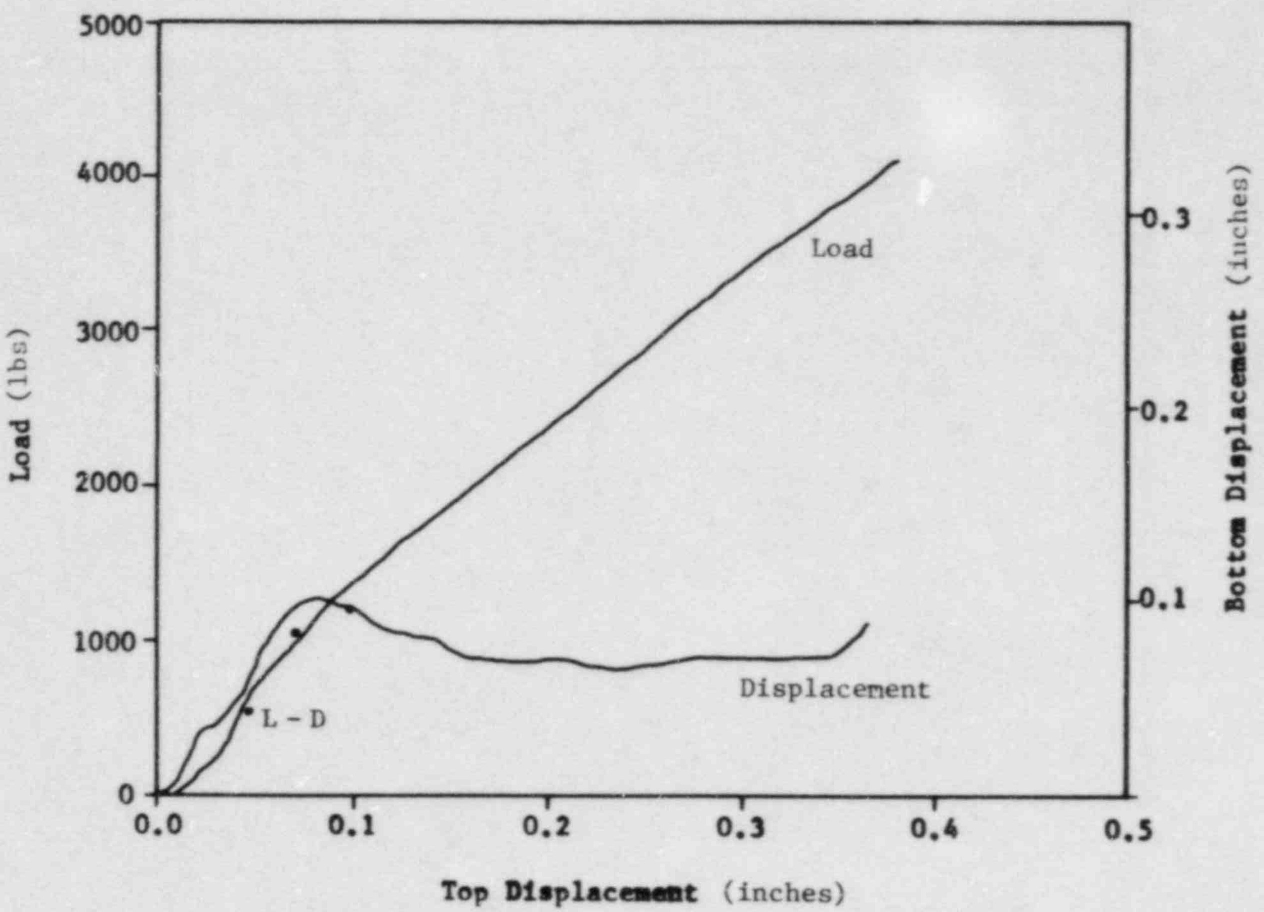

Figure 9.5 Top and bottom displacement of plug vs. axial load; sample HB2-1:S2, No. 5; L-D: load-top displacement plot of manual test; displacement curve consists of top and bottom displacement; load curve represents load vs. top displacement and bottom displacement.

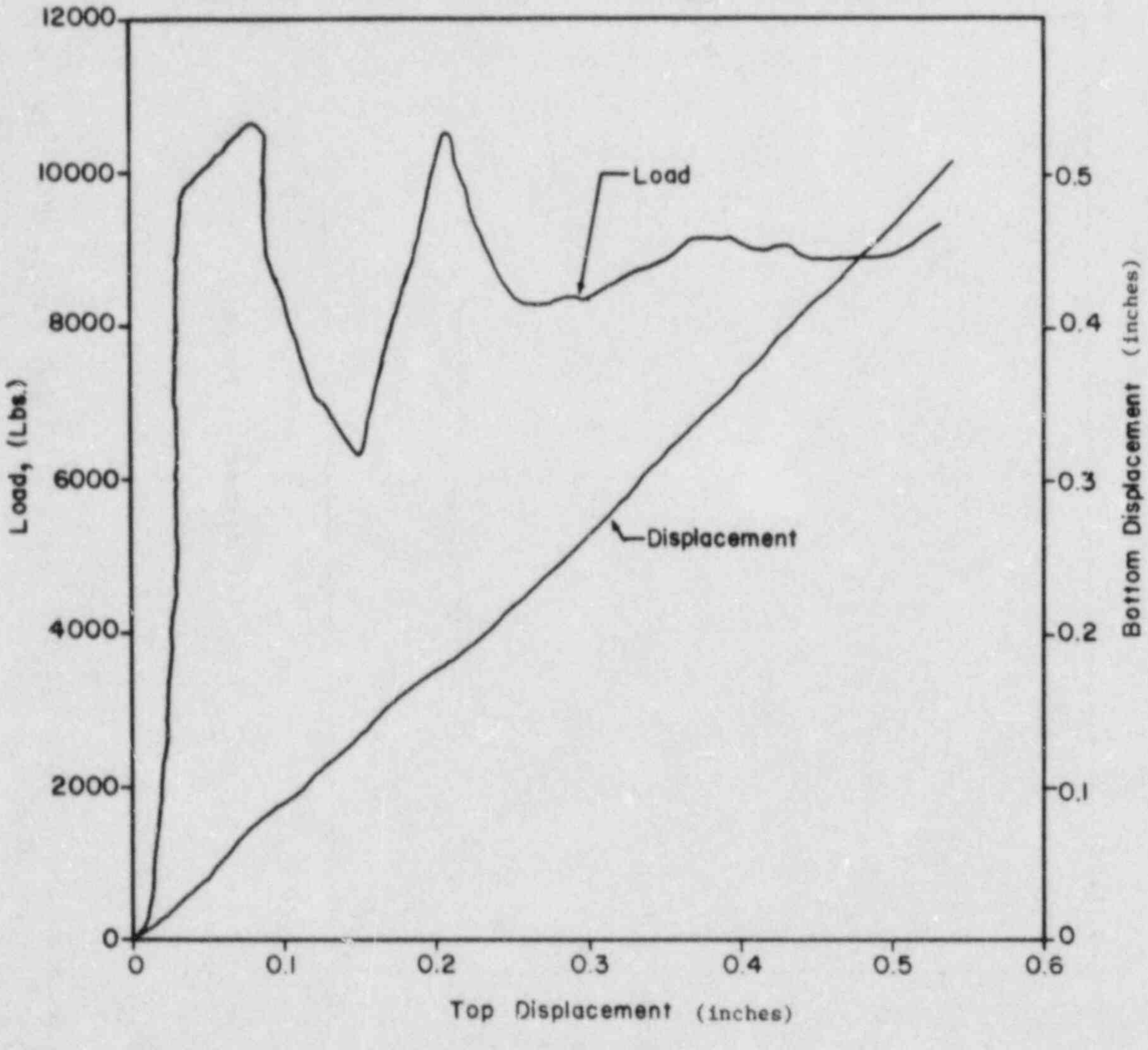

Figure 9.6 Top and bottom displacement of plug vs. axial load; sample HB2-4:S1, No. 26; L-D: load-top displacement plot of manual test; displacement curve consists of top and bottom displacement; load curve represents load vs. top displacement and bottom displacement.

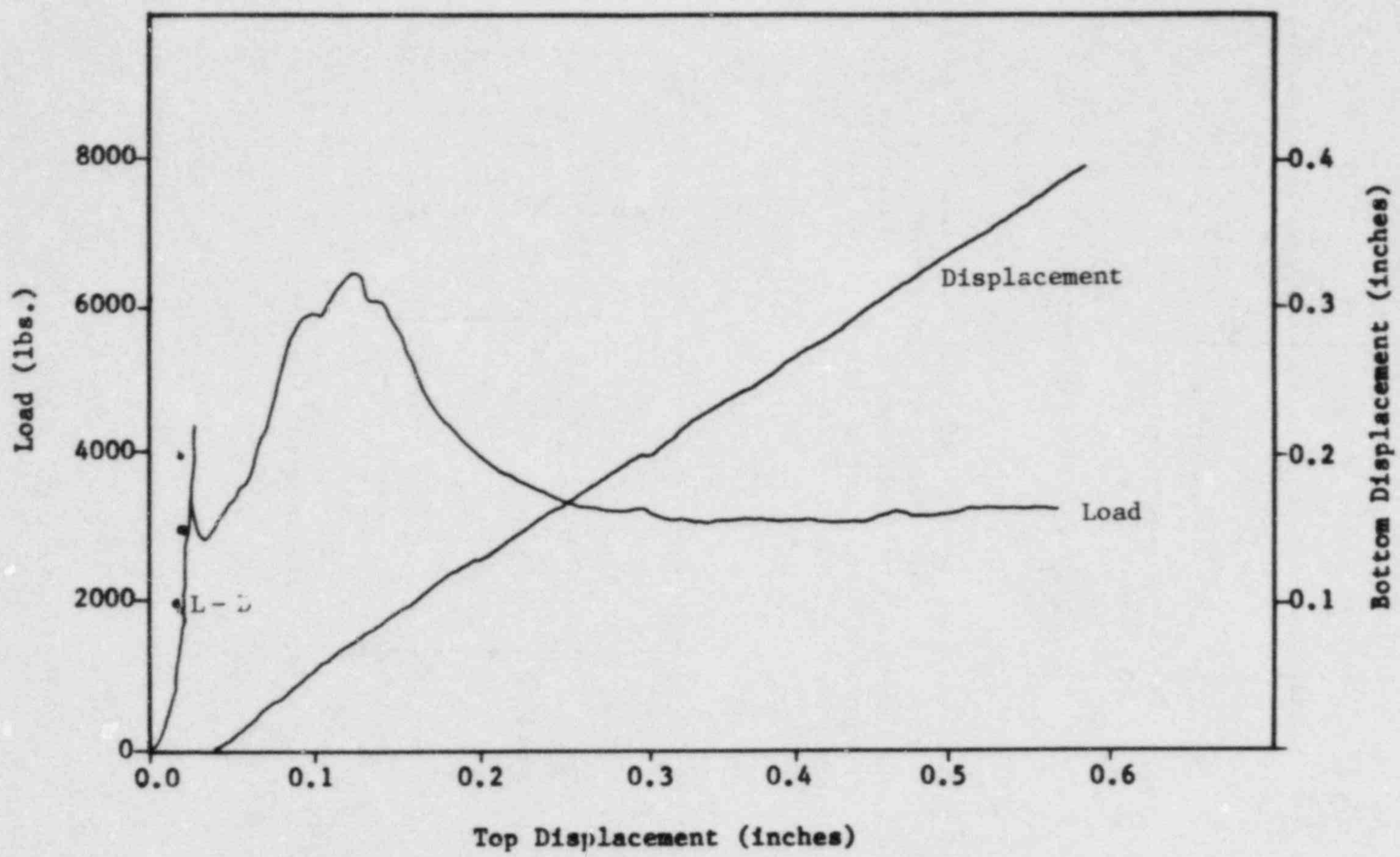

Figure 9.7 Top and bottom displacement of plug vs. axial load; sample CG4-2:S2, No. 8; L-D: load-top displacement plot of manual test; displacement curve consists of top and bottom displacement; load curve represents load vs. top displacement and bottom displacement.

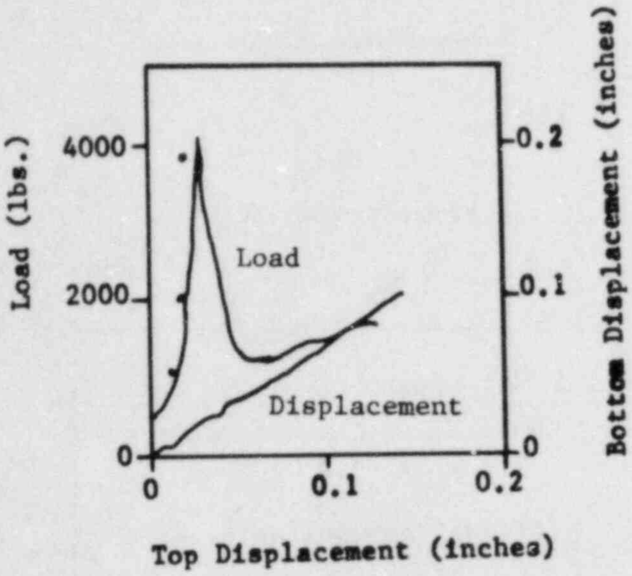

Figure 9.8 Top and bottom displacement of plug vs. axial load; sample HB4-1:S3, No. 19; L-D: load-top displacement plot of manual test; displacement curve consists of top and bottom displacement; load curve represents load vs. top displacement and bottom displacement.

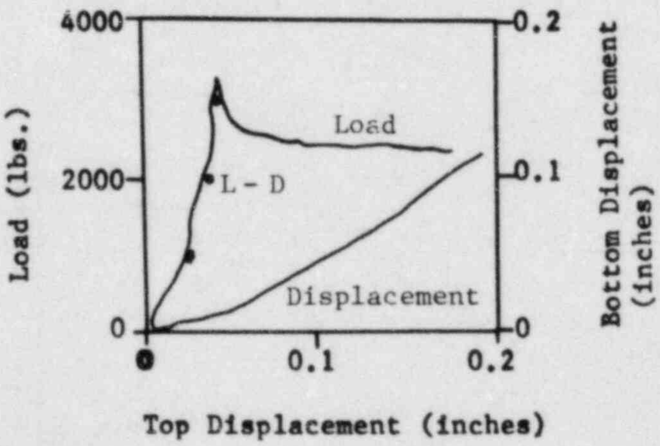

Figure 9.9 Top and bottom displacement of plug vs. axial load; sample CG4-2:S3, No. 21; L-D: load-top displacement plot of manual test; displacement curve consists of top and bottom displacement; load curve represents load vs. top displacement and bottom displacement.

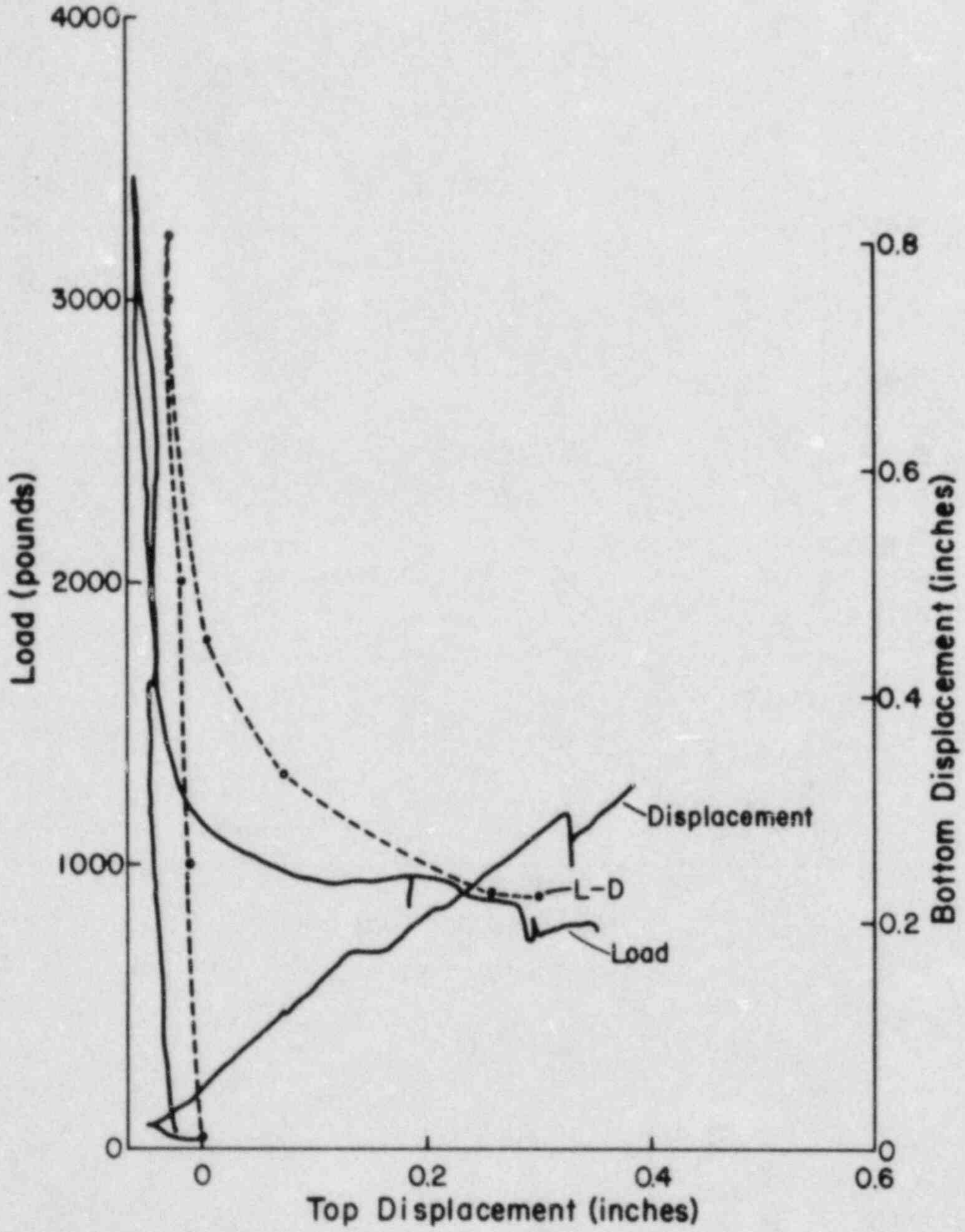

Figure 9.10 Top and bottom displacement of plug vs. axial load; sample HB1-2:S1, No. 22; L-D: load-top displacement plot of manual test; displacement curve consists of top and bottom displacement; load curve represents load vs. top displacement and bottom displacement.

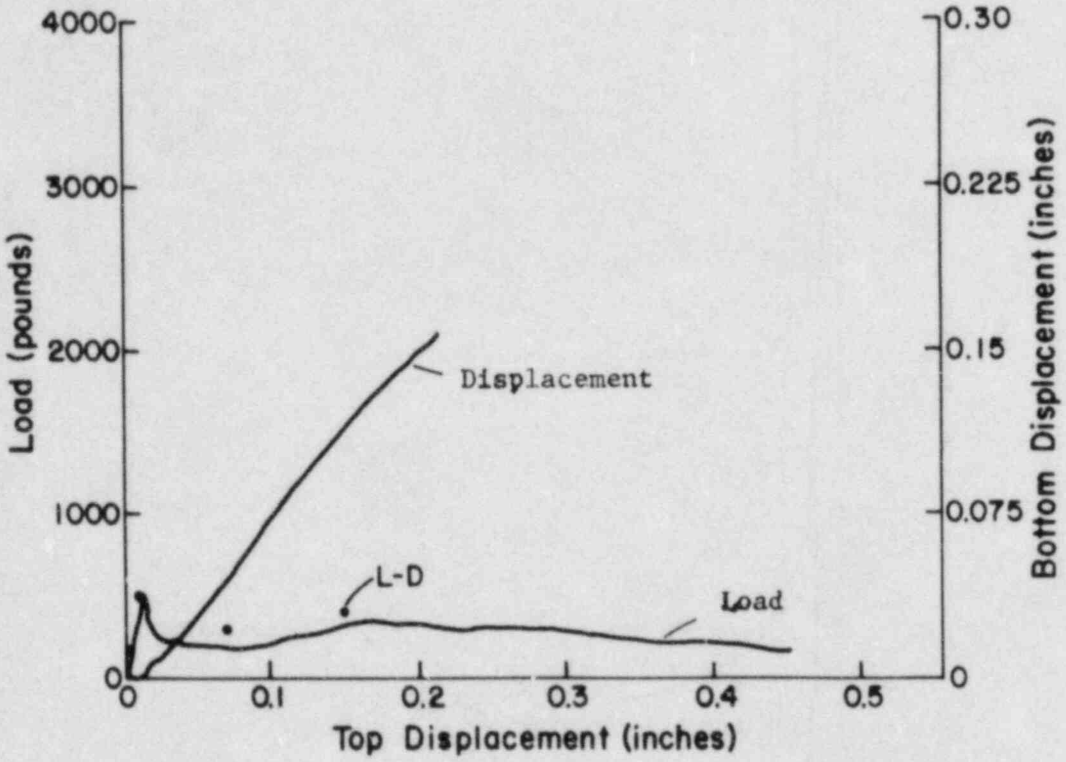

Figure 9.11 Top and bottom displacement of plug vs. axial load; sample HB2-2:S1, No. 18; L-D: load-top displacement plot of manual test; displacement curve consists of top and bottom displacement; load curve represents load vs. top displacement and bottom dis,lacement.

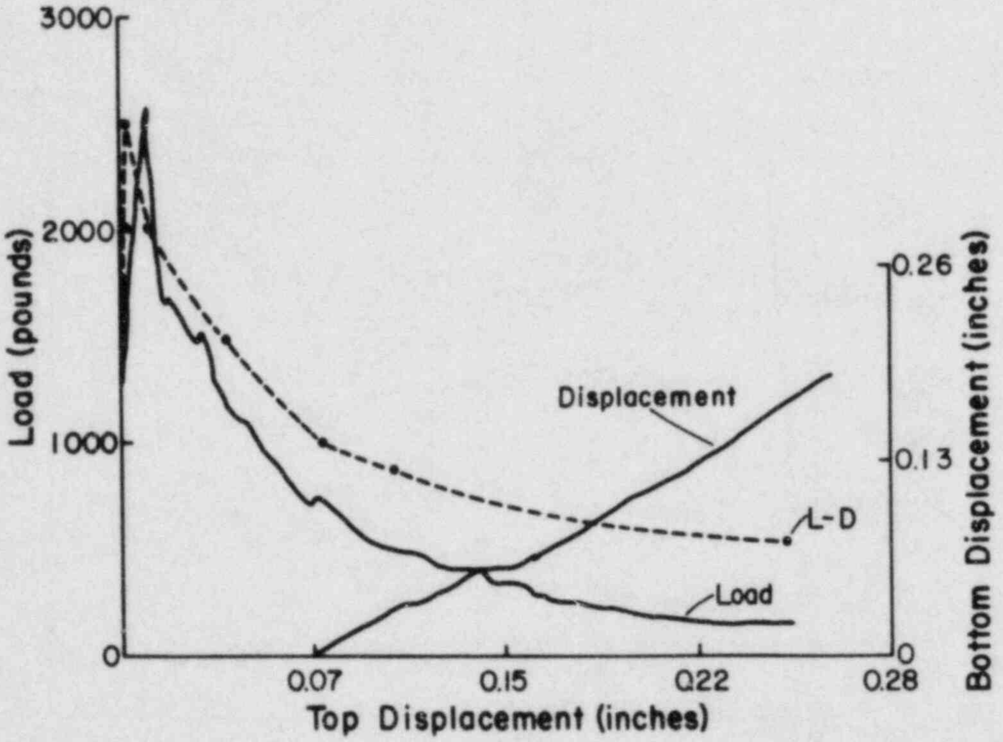

Figure 9.12 Top and bottom displacement of plug vs. axial load; sample CG2-2:S1, No. 11; L-D: load-top displacement plot of manual test; displacement curve consists of top and bottom displacement; load curve represents load vs. top displacement and bottom displacement.

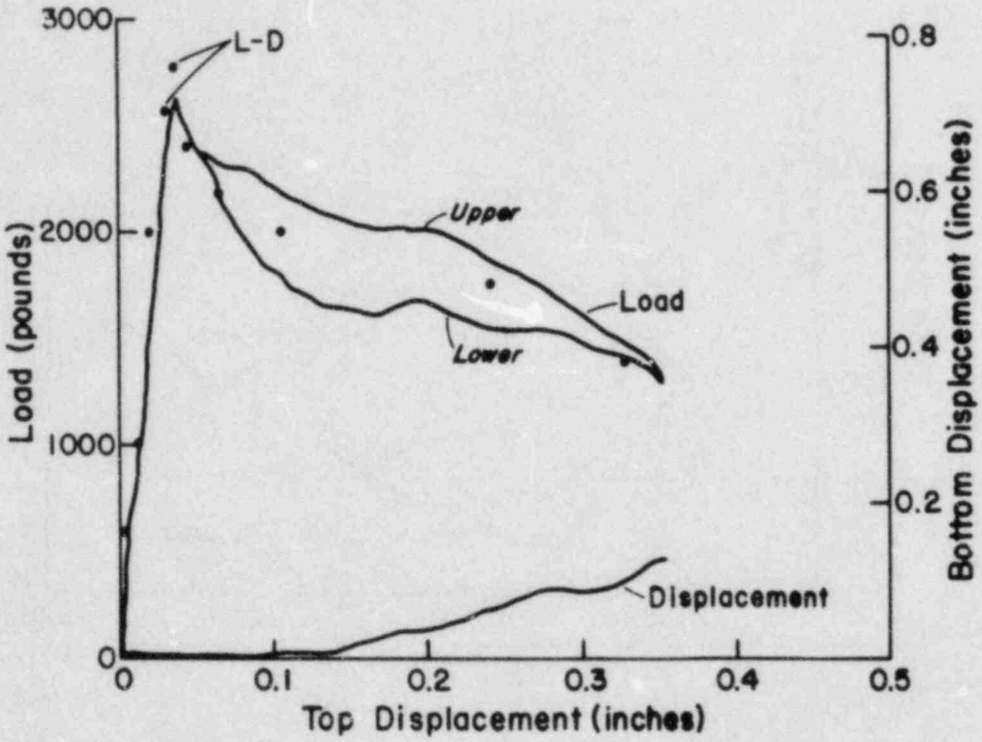

Figure 9.13 Top and bottom displacement of plug vs. axial load; sample HB2-1:S1, No. 12; L-D: load-top displacement plot of manual test; displacement curve consists of top and bottom displacement; load curve represents load vs. top displacement and bottom displacement.

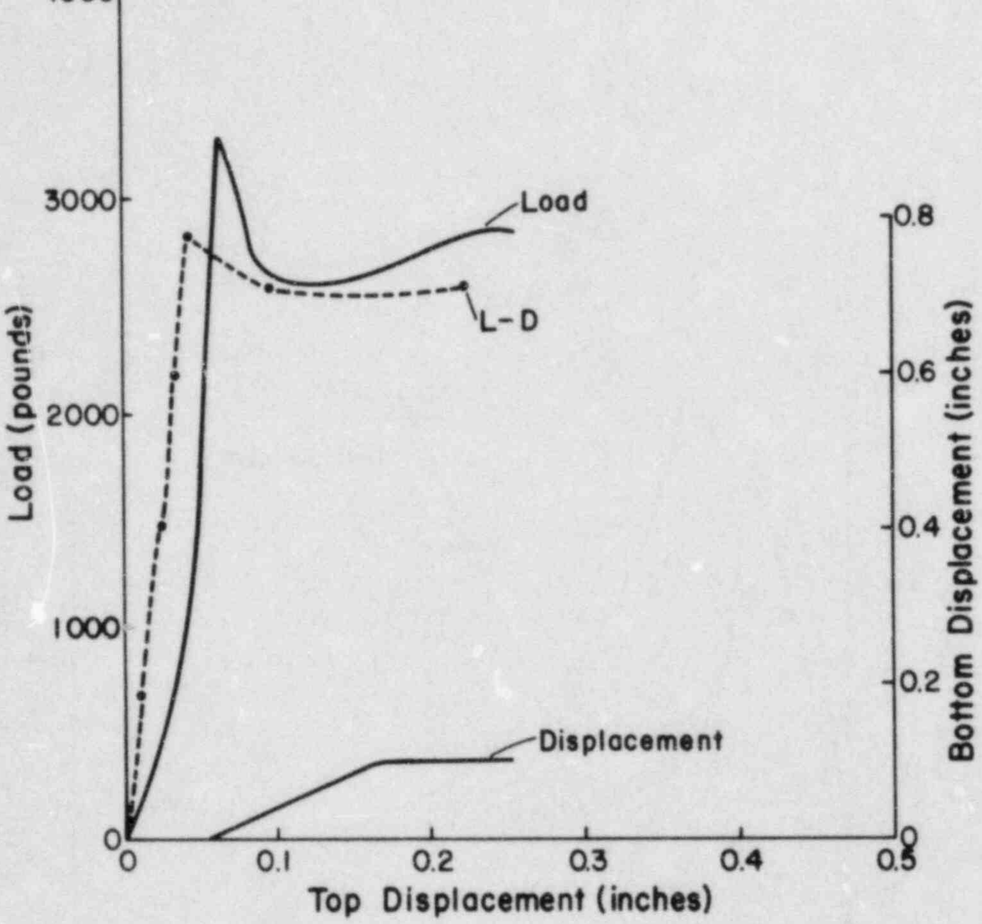

Figure 9.14 Top and bottom displacement of plug vs. axial load; sample HB2-2:S2, No. 4; L-D: load-top displacement plot of manual test; displacement curve consists of top and bottom displacement; load curve represents load vs. top displacement and bottom displacement.

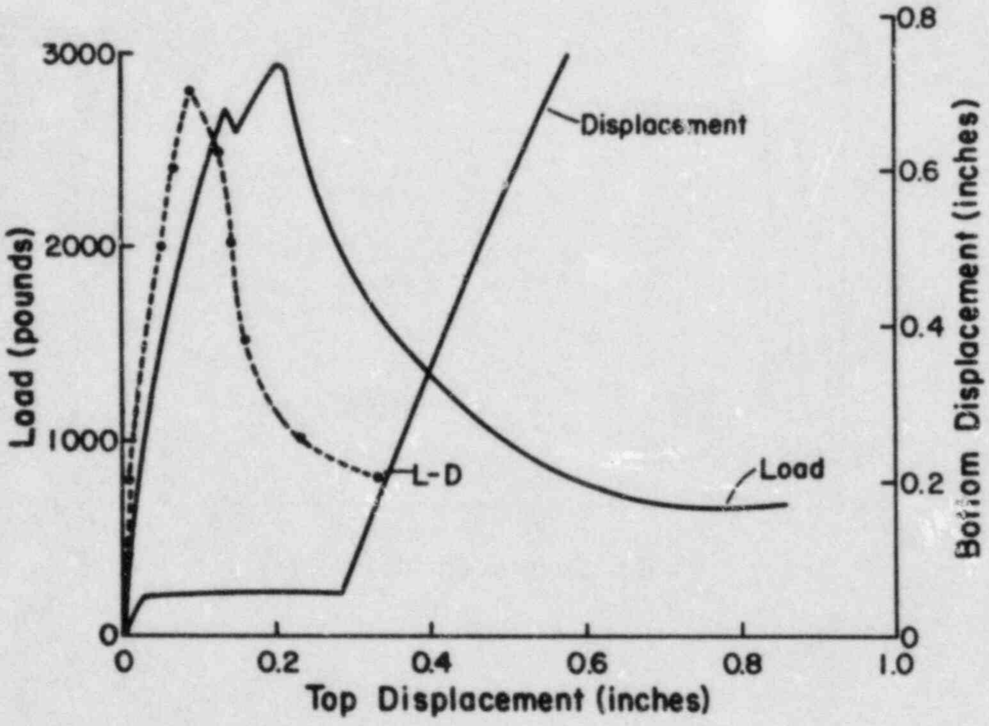

Figure 9.15 Top and bottom displacement of plug vs. axial load; sample HB2-1:S2, No. 5; L-D: load-top displacement plot of manual test; displacement curve consists of top and bottom displacement; load curve represents load vs. top displacement and bottom displacement

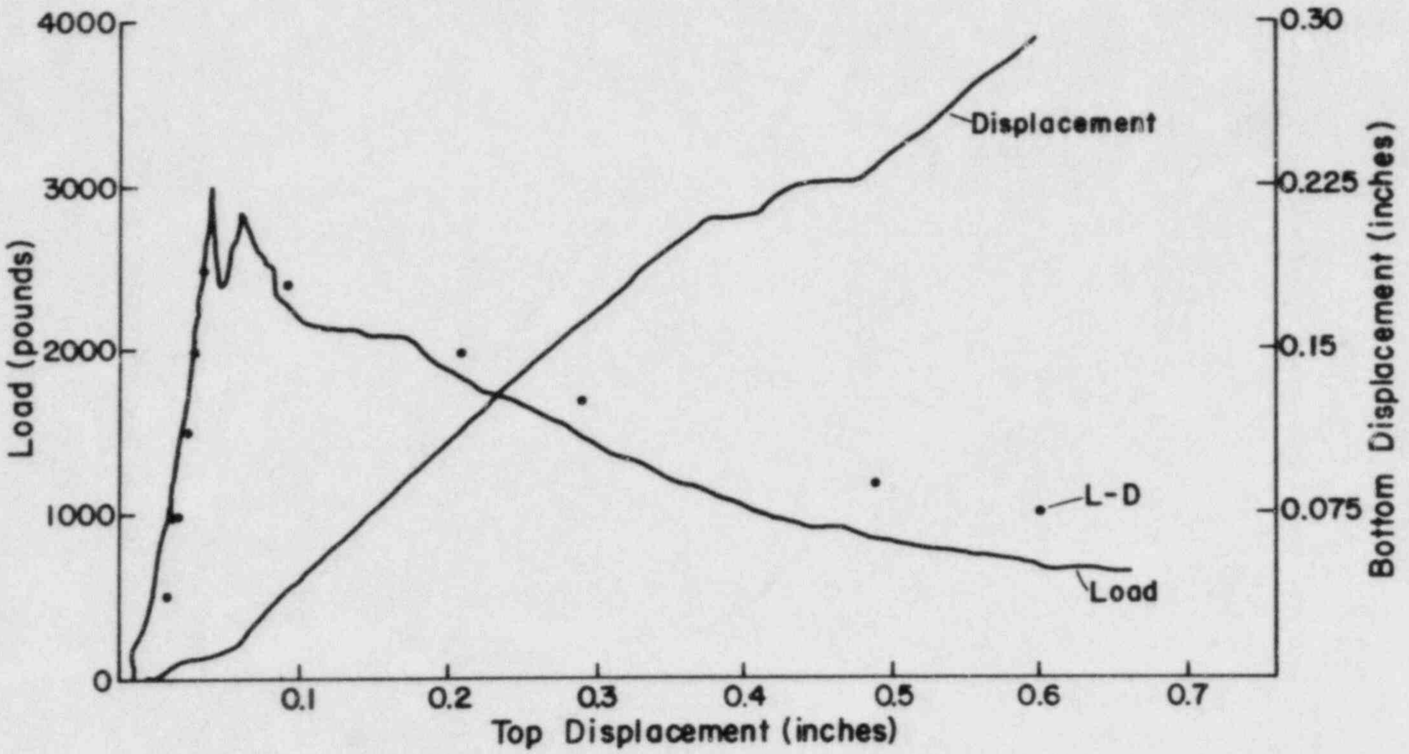

Figure 9.16 Top and bottom displacement of plug vs. axial load; sample HB2-2:S1, No. 1; L-D: load-top displacement plot of manual test; displacement curve consists of top and bottom displacement; load curve represents load vs. top displacement and bottom displacement.

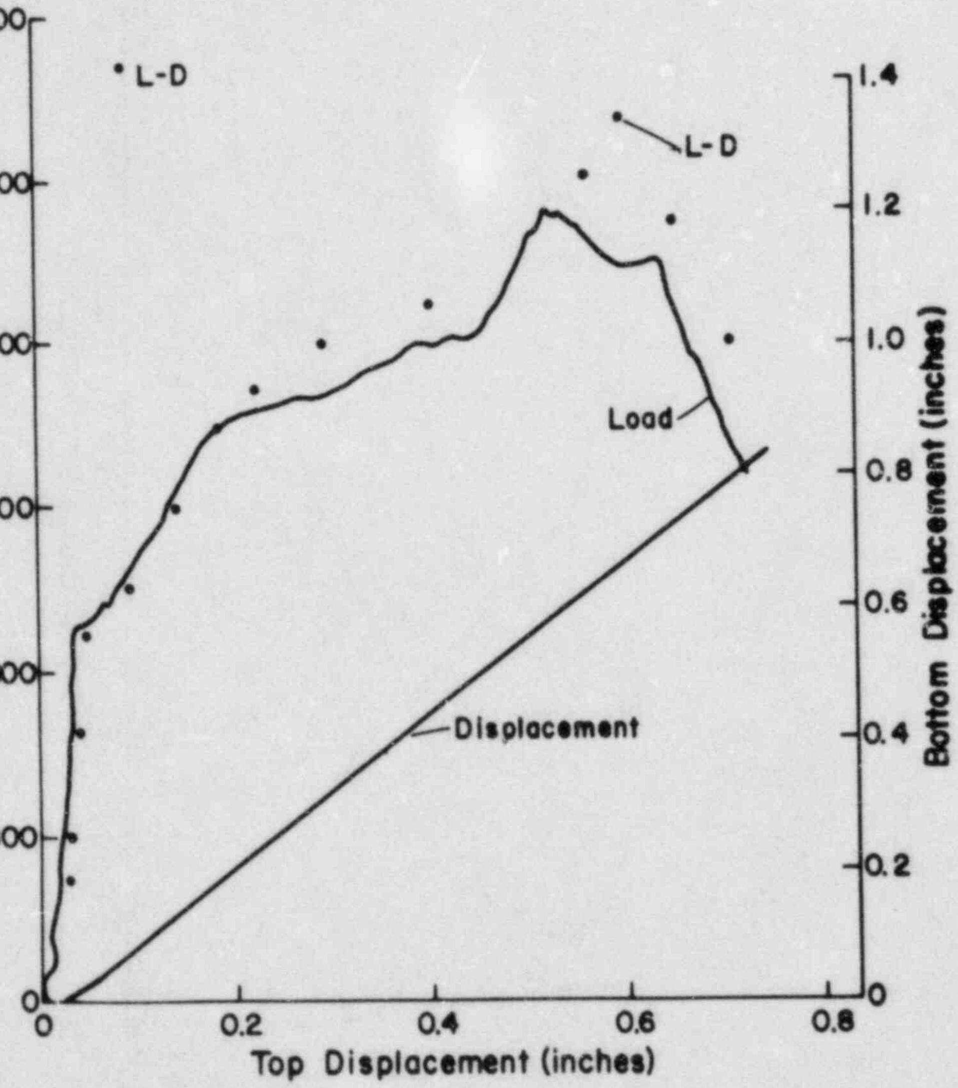

Figure 9.17 Top and bottom displacement of plug vs. axial load; sample HB2-2:S1, No. 9; L-D: load-top displacement plot of manual test; displacement curve consists of top and bottom displacement; load curve represents load vs. top displacement and bottom displacement.

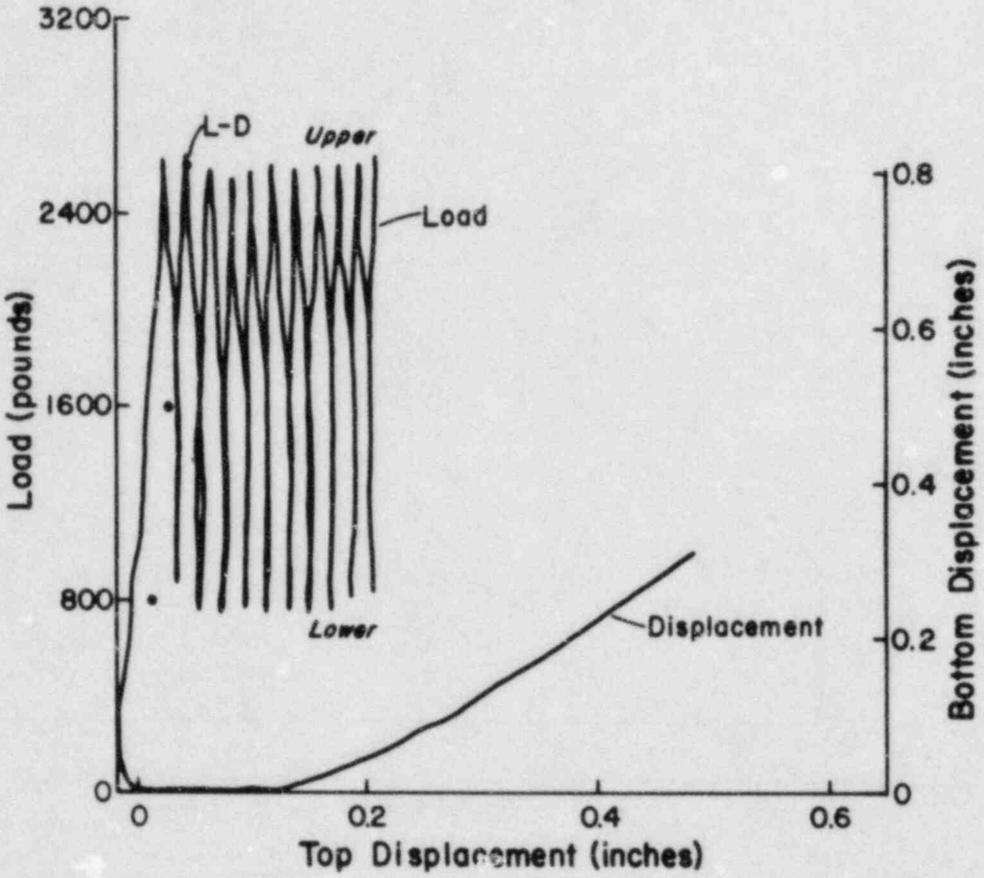

Figure 9.18 Top and bottom displacement of plug vs. axial load; sample HB2-2:S3, No. 2; L-D: load-top displacement plot of manual test; displacement curve consists of top and bottom displacement; load curve represents load vs. top displacement and bottom displacement.

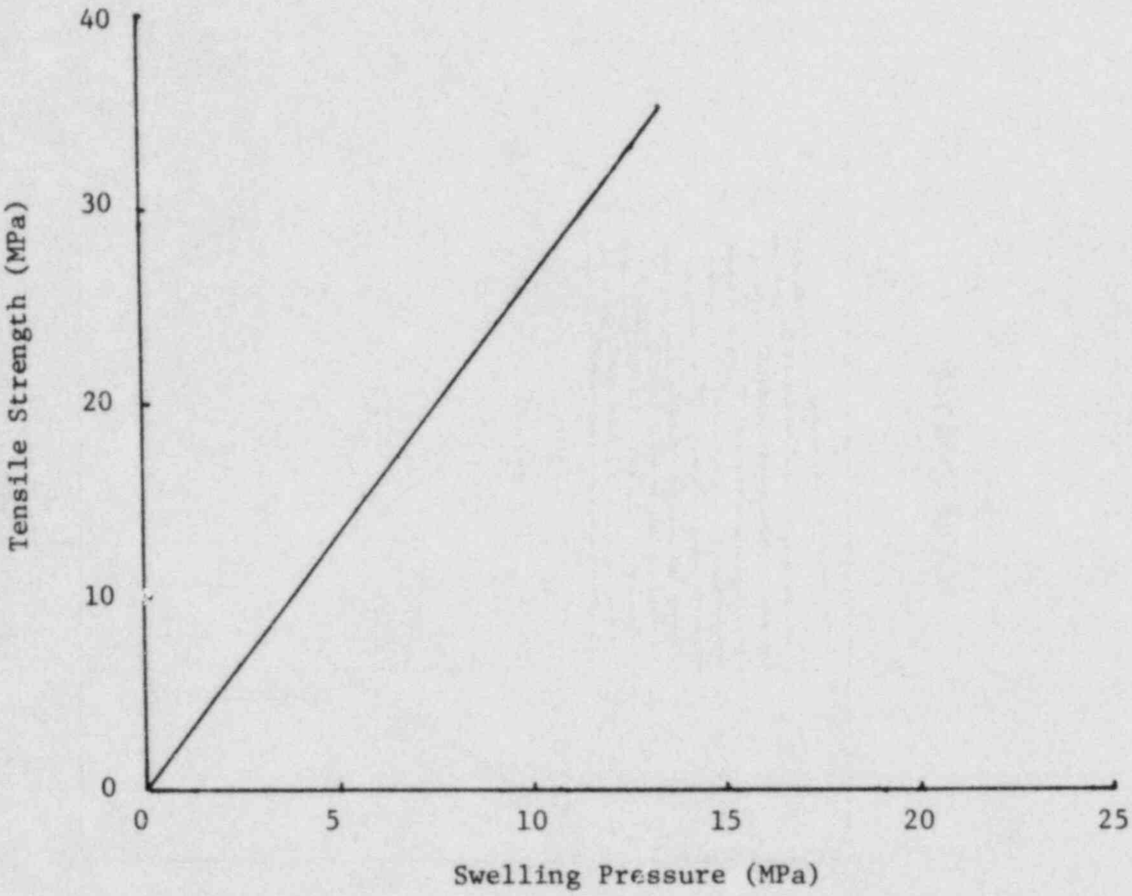

Figure 9.19 Swelling pressure required to induce tensile failure of the rock cylinder, as a function of rock tensile strength. Pomona basalt sample, 6 inch outside diameter, 4 inch internal diameter.

NRC FORM 335 (7-77) U.S. NUCLEAR REGULATORY COMMISSION

BIBLIOGRAPHIC DATA SHEET

1. REPORT NUMBER (Assigned by DDC): NUREG/CR-4174

4. TITLE AND SUBTITLE (Add Volume No., if appropriate)
Rock Mass Sealing - Experimental Assessment of Borehole Plug Performance
Annual Report, June 1983 - May 1984

2. (Leave blank)

3. RECIPIENT'S ACCESSION NO.

7. AUTHOR(S) J.J.K. Daemen, W.B. Greer, G.S. Adisoma, K. Fuenkajorn, W.D. Sawyer, Jr., A. Yazdandoost, H. Akgun, B. Kousari

5. DATE REPORT COMPLETED
MONTH: December YEAR: 1984

9. PERFORMING ORGANIZATION NAME AND MAILING ADDRESS (Include Zip Code)
Department of Mining and Geological Engineering
University of Arizona
Tucson, AZ 85721

DATE REPORT ISSUED
MONTH: March YEAR: 1985

6. (Leave blank)

8. (Leave blank)

12. SPONSORING ORGANIZATION NAME AND MAILING ADDRESS (Include Zip Code)
Division of Radiation Programs and Earth Sciences
Office of Nuclear Regulatory Research
U.S. Nuclear Regulatory Commission
Washington, DC 20555

10. PROJECT/TASK/WORK UNIT NO.

11. CONTRACT NO.
NRC-04-78-271 FIN B6627

13. TYPE OF REPORT
Technical-Annual Report

PERIOD COVERED (Inclusive dates)
June 1, 1983 - May 31, 1984

15. SUPPLEMENTARY NOTES

14. (Leave blank)

16. ABSTRACT (200 words or less) This report describes experimental borehole plugging performance assessments performed, started, or planned during June 1983 - May 1984. Results are given from field flow tests on three cement plugs installed in vertical boreholes in basalt and on one nearly horizontal cement plug. The horizontal plug and one vertical plug seal very well. Hydraulic conductivity of two vertical field plugs has been relatively high. Remedial action is described. Laboratory simulations of dynamic loading of cement plugs show no detrimental effects. Drying of cement plug, especially for months, at elevated temperatures, increases the hydraulic conductivity of the plugs severely, and reduces their bond strength along the interface.

Microscopic inspection, strength and flow tests identify the drilling-induced damaged zone in basalt. While such a damaged zone exists, and has typical features (e.g. fracture density, size, location, orientation), it is thin and not likely to be a preferential flowpath. Engineering characterization tests have been performed on seven commercial bentonites, complemented by flow tests on bentonite plugs, chemical analysis and swelling tests. Experimental designs are given for the study of size and of thermal effects on plug performance. Preliminary results are presented. Results are included from ongoing cement push-out tests and swelling measurements.

17. KEY WORDS AND DOCUMENT ANALYSIS — 17a. DESCRIPTORS

Borehole plugging	Bentonite borehole plugs	Drilling damage
Borehole sealing	Plug testing	Shaft sealing
Rock mass sealing	Seal testing	Tunnel sealing
Permeameter testing	Seal strength	Disturbed zone
Seal permeability	Rock permeability	Damaged zone
Plug permeability	Granite	
Cement borehole plugs	Basalt	

17b. IDENTIFIERS/OPEN-ENDED TERMS

18. AVAILABILITY STATEMENT
Unlimited

19. SECURITY CLASS (This report): Unclassified

20. SECURITY CLASS (This page): Unclassified

21. NO. OF PAGES

22. PRICE
S

NRC FORM 335 (7-77)

NOTICE

Availability of Reference Materials Cited in NRC Publications

Most documents cited in NRC publications will be available from one of the following sources:

1. The NRC Public Document Room, 1717 H Street, N.W.
   Washington, DC 20555

2. The NRC/GPO Sales Program, U.S. Nuclear Regulatory Commission,
   Washington, DC 20555

3. The National Technical Information Service, Springfield, VA 22161

Although the listing that follows represents the majority of documents cited in NRC publications, it is not intended to be exhaustive.

Referenced documents available for inspection and copying for a fee from the NRC Public Document Room include NRC correspondence and internal NRC memoranda; NRC Office of Inspection and Enforcement bulletins, circulars, information notices, inspection and investigation notices; Licensee Event Reports; vendor reports and correspondence; Commission papers; and applicant and licensee documents and correspondence.

The following documents in the NUREG series are available for purchase from the NRC/GPO Sales Program: formal NRC staff and contractor reports, NRC-sponsored conference proceedings, and NRC booklets and brochures. Also available are Regulatory Guides, NRC regulations in the *Code of Federal Regulations*, and *Nuclear Regulatory Commission Issuances*.

Documents available from the National Technical Information Service include NUREG series reports and technical reports prepared by other federal agencies and reports prepared by the Atomic Energy Commission, forerunner agency to the Nuclear Regulatory Commission.

Documents available from public and special technical libraries include all open literature items, such as books, journal and periodical articles, and transactions. *Federal Register* notices, federal and state legislation, and congressional reports can usually be obtained from these libraries.

Documents such as theses, dissertations, foreign reports and translations, and non-NRC conference proceedings are available for purchase from the organization sponsoring the publication cited.

Single copies of NRC draft reports are available free, to the extent of supply, upon written request to the Division of Technical Information and Document Control, U.S. Nuclear Regulatory Commission, Washington, DC 20555.

Copies of industry codes and standards used in a substantive manner in the NRC regulatory process are maintained at the NRC Library, 7920 Norfolk Avenue, Bethesda, Maryland, and are available there for reference use by the public. Codes and standards are usually copyrighted and may be purchased from the originating organization or, if they are American National Standards, from the American National Standards Institute, 1430 Broadway, New York, NY 10018.

GPO Printed copy price: $8.00

UNITED STATES
NUCLEAR REGULATORY COMMISSION
WASHINGTON, D.C. 20555

OFFICIAL BUSINESS
PENALTY FOR PRIVATE USE, $300

FOURTH CLASS MAIL
POSTAGE & FEES PAID
USNRC
WASH. D.C.
PERMIT No. G-67